Responsive Building Envelope for Grid-Interactive Efficient Buildings – Thermal Performance and Control

A Dissertation Presented for the
Doctor of Philosophy
Degree
The University of Tennessee, Knoxville

Yawen He
August 2023

Copyright © 2023 by Yawen He
All rights reserved.

ACKNOWLEDGEMENTS

I would like to express my sincere gratitude to my committee members Dr. Hongyu Zhou, Dr. Farbod Fahimi, Dr. Baoshan Huang, Dr. Shuai Li, and Dr. Som S Shrestha for their willingness to serve as committee members and provide constructive suggestions for my research.

Furthermore, I would like to thank my advisor Dr. Zhou for his dedicated support and guidance throughout this research project and thoughtful comments on this dissertation. I would also like to appreciate the valuable technical support from Dr. Fahimi on my study.

Additionally, I would like to express my appreciation to Dr. Adam Brooks, Dominic Hanna, Yucen Li, Shayan Seyfimakrani, and the undergraduate research team for their treasured assistance during the experimental research. I would like to thank Dr. Zhenglai Shen and Dr. Nima Farzadnia for their collaborative efforts on different projects.

I am also thankful to The University of Tennessee, Knoxville, and all its staff for their considerate guidance.

This research was supported by the U.S. National Science Foundation, the U.S. Department of Energy, and the startup fund provided by The University of Tennessee, Knoxville. The funding support from these institutions is greatly appreciated.

I would also like to extend my gratitude to my parents and my friends Dr. Mengying Su, Dr. Wenwen Yang, Dr. Zhixia Ding, and Dr. Min Li for their understanding and encouragement throughout my studies.

ABSTRACT

The building sector accounts for 30% of total energy consumption worldwide. Responsive building envelopes (or RBEs) are one of the approaches to achieving net-zero energy and grid-interactive efficient buildings. However, research and development of RBEs are still in the early stages of technologies, simulation, control, and design. The control strategies in prior studies did not fully explore the potential of RBEs or they obtained good performance with high design and deployment costs. A low-cost strategy that does not require knowledge of complex systems is needed, while no studies have investigated online implementations of model-free control approaches for RBEs.

To address these challenges, this dissertation describes a multidisciplinary study of the modeling, control, and design of RBEs, to understand mechanisms governing their dynamic properties and synthesis rules of multiple technologies through simulation analyses. Widely applicable mathematical models are developed that can be easily extended for multiple RBE types with validation. Computational frameworks (or co-simulation testbeds) that flexibly integrate multiple control methods and building simulation models are established with higher computation efficiency than that using commercial software during offline training. To overcome the limitations of the control strategies (e.g., rule-based control and MPC) in prior research, a novel easy-to-implement yet flexible ‘demand-based’ control strategy, and model-free online control strategies using deep reinforced learning are proposed for RBEs composed of active insulation systems (AISs). Both the physics-derived and model-free control strategies fully leverage the advantages of AISs and provide higher energy savings and thermal comfort improvement

over traditional temperature-based control methods in prior research and demand-based control. The case studies of RBEs that integrate AISs and high thermal mass or self-adaptive/active modules (e.g., evaporative cooling techniques and dynamic glazing/shading) demonstrate the superior performance of AISs in regulating thermal energy transfer to offset AC demands during the synergy. Moreover, the controller design and training implications are elaborated. The applicability assessment of promising RBE configurations is presented along with design implications based on building energy analyses in multiple scenarios. The design and control implications represent an interactive and holistic way to operate RBEs allowing energy and thermal comfort performances to be tuned for maximum efficiency.

TABLE OF CONTENTS

CHAPTER ONE Introduction 1
1.1 Background 1
1.2 Responsive building envelope 2
1.3 Literature review 6
1.3.1 Categorization of responsive building envelopes 6
1.3.2 Materials for adaptive building envelopes 21
1.3.3 Performance prediction and evaluation of buildings with responsive building envelopes 27
1.3.4 Control strategies 34
1.3.5 Automation system for responsive building envelopes 47
1.4 Problem statement 48
1.5 Research objectives and dissertation organization 51
CHAPTER TWO Model formulation 55
2.1 Model of building components with static properties 56
2.1.1 Heat conduction through walls 56
2.1.2 Heat balance within wall nodes 58
2.1.3 Heat and moisture balance of indoor air 59
2.2 Model of responsive building envelopes for active control 63
2.3 Thermal comfort 69
2.4 State-space representation and computation details 70
2.5 Model validation 74
2.6 Computational framework 77
CHAPTER THREE Demand-based control for RBE 79
3.1 Rule-based control strategies for RBE with AISs and thermal mass 80
3.1.1 Demand-based control rule 80
3.1.2 Temperature-based control rule 84
3.2 Case studies 86
3.2.1 Simulation details 86
3.2.2 Thermal behavior 89
3.2.3 Energy-saving potential 99
3.2.4 Thermal comfort performance 101
3.2.5 Operation of AIS and design implications 101
3.3 Conclusions 104
CHAPTER FOUR Model-free online reinforced learning control for RBE 107
4.1 Methods 108
4.1.1 Problem formulation 108
4.1.2 Trust Region Policy Optimization (TRPO) algorithm 120
4.1.3 Online control framework with pretraining 122
4.1.4 Case studies 127
4.2 Offline pretraining 132
4.2.1 Offline training results 132

4.2.2 Implications for controller design and offline pre-training 134
4.3 Evaluation of MFORL control 136
4.3.1 Heating season 137
4.3.2 Transitional season 142
4.3.3 Cooling season 144
4.4 Conclusions 146
CHAPTER FIVE Integration with other techniques 152
5.1 RBE with AIS and dynamic glazing/shading 152
5.1.1 Configuration and method 152
5.1.2 Model of dynamic glazing/shading 153
5.1.3 Control strategies 155
5.1.4 Thermal performance of the building with AIS and DSS 155
5.2 RBE with AIS and evaporative cooling 164
5.2.1 Configuration and method 165
5.2.2 Model of biomimetic mesoporous synthetic foam (BMSF) 169
5.2.3 Control strategies 172
5.2.4 Thermal performance of the building with AIS and evaporative cooling 172
5.3 Conclusions 183
CHAPTER SIX Conclusions and recommendations 186
6.1 Conclusions 186
6.2 Recommendations 192
REFERENCES 194
APPENDIX 220
VITA 223

LIST OF TABLES

Table 1.1 Summary of technologies for variable thermal insulation 13
Table 1.2 Typical techniques for kinetic shading systems..... 18
Table 1.3 Thermal performance of different RBEs..... 31
Table 3.1 The annual LPD (%) of the residential thermal zone in different scenarios .. 101
Table 4.1 TRPO algorithm logic 123

LIST OF FIGURES

Figure 1.1 Illustrative figure showing the different envelope thermal properties desired under various environmental conditions 5
Figure 1.2 Categories of responsive building envelope technologies 7
Figure 1.3 Variable thermal insulations (VTIs) based on: (a) active/variable vacuum; and (b) mechanical contact (Cui and Overend, 2019) 11
Figure 1.4 Schematic showing the principle of suspended particle devices (Cui and Overend, 2019) 11
Figure 1.5 Examples of adaptive ventilation: (a) the ventilated façade by Sung (Sung, 2016); (b) the meteorosensitive architectural project by Reichert et al. (Reichert, Menges and Correa, 2015); (c) the mechanically actuated façade by Biloria et al. (Biloria and Sumini, 2009) and (d)–(f) bio-inspired self-adaptive ventilated facades (Sung, 2016; Pujadas-Gispert *et al.*, 2020) 16
Figure 1.6 Schematic for dynamic glazing 16
Figure 1.7 The 'hydroceramic' concept developed by Mitrofanova et al. (E. Mitrofanova, A. Rathee, 2014) 25
Figure 1.8 Temperature-responsive materials: (a) the concept of thermo-bimetal; and (b) temperature-responsive polymers(Meng and Li, 2013) 25
Figure 1.9 Simulation of responsive building envelopes (RBEs) 31
Figure 1.10 Schematic for working mechanism of RBE composed of TES and AISs. ... 38
Figure 1.11 Design and control of RBE 40
Figure 1.12 Schematic for the architecture of MPC(Mehrizi-Sani, 2017) 43
Figure 1.13 Schematic for model-free reinforced learning control of RBE 46
Figure 1.14 Schematic for the dissertation outline 53
Figure 2.1 Schematic for normal heat exchanges within indoor and outdoor space 57
Figure 2.2 Schematic for heat exchanges with the indoor air node 60
Figure 2.3 Infiltration rate of an apartment throughout a year in San Francisco 62
Figure 2.4 Finite difference representation of an RBE layer 64
Figure 2.5 Schematic for the node scheme of synthesis of mass wall and opaque AISs. 67
Figure 2.6 Schematic for the thermal network integration of RBEs into building simulations 72
Figure 2.7 Schematic for building simulation procedure 73
Figure 2.8 (a) Isometric view of the building modeled for calibration; (b) Comparison of the simulation results between the thermal network model and EnergyPlus 76
Figure 2.9 Schematic for the versatile computational framework integrating buildings with diverse modules and control strategies 78
Figure 3.1 Control rule for building envelope with AISs and one concrete layer: (a) control rule for the interior AIS; (b) control rule for the exterior AIS 83
Figure 3.2 Illustrative figure showing the temperature-based control rule (a) without, and (b) with threshold temperature (T_{th}) 85

Figure 3.3 Simulation details for a residential thermal zone with RBE in comparison with a baseline static envelope 88
Figure 3.4 Thermal behavior of RBE in a typical heating season (January, Chicago, IL): (a) outdoor air temperature and the system output demand to reach the setpoint, $Q_{sys,dmd}$; (b) interior AIS R-value setting and indoor air, interior surface, and concrete temperatures; (c) exterior AIS R-value setting, exterior surface and concrete temperatures; (d) comparison of sensible AC load for RBE and baseline cases 90
Figure 3.5 Thermal behavior of RBE in a typical cooling season (July, Chicago, IL): (a) outdoor air temperature and the system output demand to reach the setpoint, $Q_{sys,dmd}$; (b) interior AIS RSI-value setting and indoor air, interior surface, and concrete temperatures; (c) exterior AIS RSI-value setting, exterior surface, and concrete temperatures; (d) comparison of sensible AC load for RBE and baseline cases 92
Figure 3.6 Thermal behavior of RBE in a typical transitional season (April, Chicago, IL): (a) outdoor air temperature and the system output demand to reach the setpoint, $Q_{sys,dmd}$; (b) interior AIS RSI-value setting and indoor air, interior surface, and concrete temperatures; (c) exterior AIS RSI-value setting, exterior surface and concrete temperatures; (d) comparison of sensible AC load for RBE and baseline cases 94
Figure 3.7 Comparison of RBE thermal behavior under demand-based control and temperature-based control 97
Figure 3.8 (a) Monthly energy consumption of the residential thermal zone (b) Climate classification of the six representative cities analyzed (c) Annual energy consumption compared for the static envelope baseline, RBE with temperature-based control, and RBE with demand-based control 100
Figure 3.9 (a) Whole-year time history of RSI setting for both the interior and exterior AIS for Miami, Albuquerque, and San Francisco; (b) Relative frequency density distribution of the RSI-values 102
Figure 4.1 Schematic for model-free online reinforced learning framework for RBE .. 109
Figure 4.2 Schematic for offline training framework using MFRL for the RBE 115
Figure 4.3 Schematic for ANN architecture of (a) the critic and (b) the actor 119
Figure 4.4 Schematic for online training with pretraining 126
Figure 4.5 Simulation details of the case studies 130
Figure 4.6 Control logic of simple temperature-based control for the AIS-integrated RBE 133
Figure 4.7 (a) Offline training episode reward in a typical training process (b) Comparisons of accumulated energy consumption and LPD among baseline and RBE cases under rule-based control and MFRL control by offline training 133
Figure 4.8 Thermal behavior of RBE cases and baseline in a typical heating season (February, Chicago, IL). 138
Figure 4.9 Thermal behavior of RBE cases and baseline in a typical transitional season (May, Chicago, IL) 139
Figure 4.10 Thermal behavior of RBE cases and baseline in a typical cooling season (August, Chicago, IL) 140

Figure 4.11 Comparisons among baseline and RBE cases under simple temperature-based control, demand-based control, and MFORL control in the performance of: (a) accumulated energy consumption (b) LPD..... 147
Figure 5.1 Schematic for the node scheme of synthesis of mass wall and exterior dynamic glazing/shading and interior AIS 154
Figure 5.2 Control rule for exterior dynamic shading systems..... 156
Figure 5.3 Simulation details for buildings with a baseline roof and the RBEs with DSS 157
Figure 5.4 Thermal behavior of RBE in a typical heating season (January, Chicago, IL): (a) outdoor air temperature and the system output demand to reach the setpoint, $Q_{sys,dmd}$ of the thermal zone with DSS; (b) interior AIS R-value setting and indoor air, interior surface and concrete temperatures of the thermal zone with an exterior static insulation and an interior AIS; (c) interior AIS R-value setting and indoor air, interior surface and concrete temperatures of the thermal zone with DSS and AIS; (d) comparison of sensible AC load for different RBEs and baseline cases 159
Figure 5.5 Thermal behavior of RBE in a typical cooling season (June, Chicago, IL): (a) outdoor air temperature and the system output demand to reach the setpoint, $Q_{sys,dmd}$ of the thermal zone with DSS; (b) interior AIS R-value setting and indoor air, interior surface and concrete temperatures of the thermal zone with an exterior static insulation and an interior AIS; (c) interior AIS R-value setting and indoor air, interior surface and concrete temperatures of the thermal zone with DSS and AIS; (d) comparison of sensible AC load for different RBEs and baseline cases 161
Figure 5.6 (a) Monthly energy consumption of the residential thermal zone with baseline envelope and with different RBEs (b) Monthly LPD of the residential thermal zone with baseline envelope and with different RBEs..... 163
Figure 5.7 Schematic for responsive roofs integrated with AIS and evaporative cooling techniques 166
Figure 5.8 Schematic showing BMSF (a) the wetting and evaporation mechanism; (b) sintering process and microstructure of BMSF; (c) perceived evaporation mechanism; and (d) optical micro-image showing the wetted BMSF..... 170
Figure 5.9 Thermal network model of the concrete roof covered with BMSF panel.... 170
Figure 5.10 Simulation details for buildings with a baseline roof and the ones with BMSF and AIS 173
Figure 5.11 Thermal behavior of evaporative cooling roof composed of BMSF and AIS compared with baseline in a summer week (June, Los Angeles, CA): (a) outdoor air temperature and heat flux; (b) interior AIS R-value setting and indoor air, interior surface, and exterior surface temperatures; (c) exterior surface temperatures (d) comparison of sensible AC load for baseline roof and the BMSF roof with and without AIS 176
Figure 5.12 Thermal behavior of the evaporative cooling roof composed of BMSF and AIS compared with baseline in a winter week (January, Los Angeles, CA): (a) outdoor air temperature and heat flux; (b) interior AIS R-value setting and indoor air, interior surface, and exterior surface temperatures; (c) exterior surface temperatures (d)

comparison of sensible AC load for baseline roof and the BMSF roof with and without AIS 177
Figure 5.13 Energy performance of the building installed with baseline, BMSF roof and BMSF roof with AIS: (a) Monthly mean AC load and (b) Monthly LPD 180

CHAPTER ONE
INTRODUCTION

1.1 Background

The International Energy Agency (IEA) estimates that the building sector accounts for 30% of global final energy consumption (IEA, 2022), where a substantial portion (over 60% (Ramesh, Prakash and Shukla, 2010)) is the operational energy used for space heating/cooling and lighting. Over the past decade, significant progress has been made to reduce building energy consumption including innovations in high insulation façade, daylighting, and passive ventilation (Krarti, Erickson and Hillman, 2005; Artmann, Manz and Heiselberg, 2007; Ihm, Nemri and Krarti, 2009; Sadineni, Madala and Boehm, 2011). However, despite the highly mutable and dynamic forces acting on our building stocks – i.e., from the changing climates and energies, to the occupant behaviors (Scott, Wrench and Hadley, 1994; Belzer, Scott and Sands, 1996; Frank, 2005; Holmes and Hacker, 2007; Masoso and Grobler, 2010; Wang, Chen and Ren, 2010; Yu *et al.*, 2011; Wan *et al.*, 2012), the majority of current building practices still operate the envelope as a static system. Substantial energy-saving potential may reside in solutions that transcend the building envelope's role from a simple protective space divider to a more intelligent and responsive functional assembly attuned to climate and energy optimizations (Goia *et al.*, 2010; Kirkegaard and Worre Foged, 2011; Velikov K, 2013; Bodach, Lang and Hamhaber, 2014).

To date, several passive approaches have been taken to achieve the responsive behaviors of smart building envelopes including the utilization of intrinsic material properties such as the thermoresponsive of Tbimetals and shape-memory polymers for

self-ventilation and daylighting control (Sung, 2010; Brigham, 2015; Rybkowski *et al.*, 2015). Leaps forward in high-performance envelope technology may desire more pervasive solutions that can accommodate much broader variation in conditions and performance criteria – an intelligent skin that can facilitate more complex building system communication, respond to occupant requests, and adapt and learn over time. Increasingly, building façades are being developed as complex systems of material assemblies attuned to climate and energy optimization – they are equipped with new performative materials, sensors, actuators, and artificial intelligence that support automated and dynamic functionalities of buildings, such as regulating natural daylighting, air and sound transmission, thermal transfer, and interior air quality (Velikov K, 2013). This paradigm shift from static building envelopes to more intelligent 'building skin' that can sense and respond to environmental changes provides opportunities for energy savings, improving occupant comfort, and enabling adaptations to the changing climate.

1.2 Responsive building envelope

The dynamic nature of forces and energies acting on the building structure has prompted the emergence of high-performance building skins that are interactive and responsive to the environment (Wigginton and Harris, 2002; Stec and Paassen, 2005; Biloria and Sumini, 2009; Joe *et al.*, 2013; Loonen *et al.*, 2013; Loonen, 2015). Responsive building envelopes (or RBEs) –also known as smart, environmental-adaptive, or intelligent building envelopes are one of the approaches to achieving Net-zero energy buildings (Net ZEB) (Athienitis and Brien, 2015) and grid-interactive efficient buildings (GEB), which has been an increasingly popular research topic in the past decade (Taveres-Cachat *et al.*, 2019). The core concept is to design buildings that

could express similar responses to those found in plants, or that could imitate physiological responses of homeotherm animals like sweating or shivering (Velikov K, 2013). In order to replicate such functionalities in buildings, RBEs rely on integrated technologies that are designed to enable the building to respond to a range of environmental stimuli such as temperature change, using a combination of passive, active, and/or cognitive control strategies (Biloria and Sumini, 2009). This design philosophy has a significant impact on the whole-building metabolism by enabling buildings to actively/semi-actively interact with their surrounding environment. By incorporating renewable energy harvesting systems (RES) and appropriate control strategies, it is possible to substantially improve the overall performance of the building in terms of energy/operational cost, demand-side management, and occupant comfort (Xu, Dessel and Messac, 2007; Xu and Dessel, 2008; Biloria and Sumini, 2009; Taveres-Cachat *et al.*, 2019).

The thermophysical properties of building envelopes are of great importance to reduce the energy consumption of buildings as the envelope is the main component separating indoor spaces from the outdoor environment. From an energy-saving perspective, a high-insulation level (i.e., high R-value) is desired in cold climate zones with low internal gains levels but has limited benefit during summer (Jong-Jin Kim and Jin Woo Moon, 2009). Similarly, envelopes with high insulation in hot climate zones provide marginal energy savings during transient and summer seasons (Jong-Jin Kim and Jin Woo Moon, 2009). Higher thermal mass (high C) is desired in a temperate climate when thermal storage can be beneficial to improve thermal comfort and energy efficiency. High thermal mass is beneficial for residential buildings under hot humid climates during the daytime but may increase building energy use at night (Cheng, Ng

and Givoni, 2005). For the same reason, the high thermal mass could have adverse impacts on building energy efficiency in cold climate zones (Reilly and Kinnane, 2017).

Different environmental/weather conditions with different operation and occupancy schedules may desire different 'optimal' combinations of the building envelope's thermal properties, see **Figure 1.1**. To date, explorations of the "responsive envelope" concept are mostly achieved via mechanical actuation and regulatory feedback systems (e.g., automated shading panels and louvers (Hammad and Abu-Hijleh, 2010; Lee *et al.*, 2013)) or the use of stimulus-responsive smart materials such as shape-memory polymers and thermo-bimetals for local morphing control (Sung, 2010; Rybkowski *et al.*, 2015). Drawbacks of mechanically-actuated systems include high operational energy and the need for frequent maintenance cycles (Thuot and Andersen, 2011); on the other hand, the operations of smart material envelopes are typically binary (Velikov K, 2013) – i.e., their intended performance is no longer guaranteed as soon as the real-occurring disturbances deviate from the design conditions (Loonen *et al.*, 2013). Some other existing techniques include "switchable" vacuum insulation (David K Benson, Potter and Tracy, 1994; Berge *et al.*, 2015), in which case the thermal conductivity can be adjusted by changing the enclosed vacuum level within the insulation layer. Challenges associated with dynamic vacuum insulation include the need for continuous energy input as a high vacuum level is normally required to achieve notable conductivity variation, in conjunction with its durability issue (Simmler and Brunner, 2005; Brunner and Wakili, 2014; Brunner *et al.*, 2014; Kalnæs and Jelle, 2014).

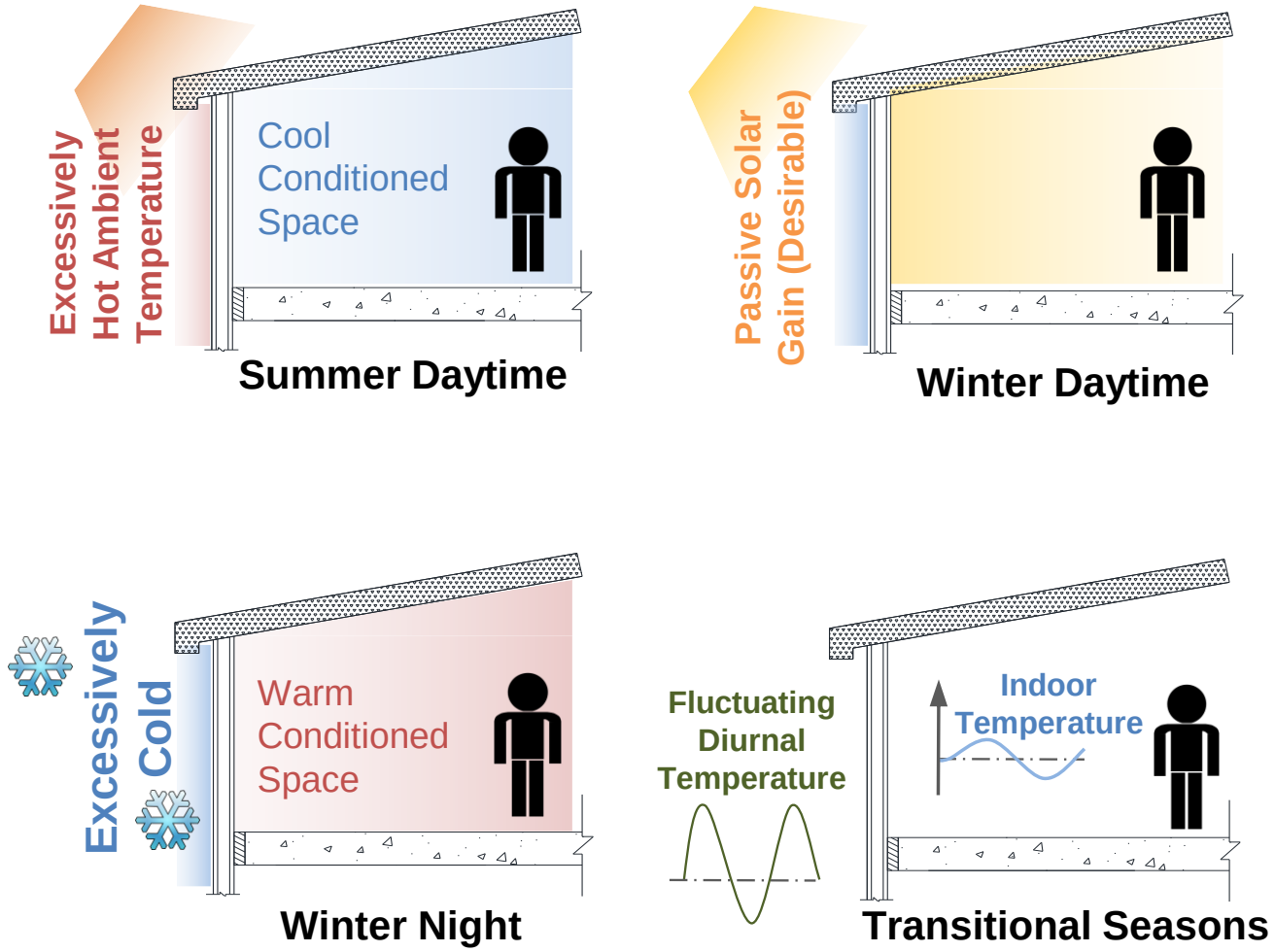


Figure 1.1 Illustrative figure showing the different envelope thermal properties desired under various environmental conditions.

1.3 Literature review

1.3.1 Categorization of responsive building envelopes

Responsive building envelopes (or RBEs) can be classified into one of the following general types, or a combination thereof, based on their thermal characteristics(with some emerging technology evolving and adding to the inventory): 1) variable thermal insulations, 2) dynamic shading, 3) controllable/adaptive ventilation, and 4) variable thermal masses, as shown in **Figure 1.2**.

1.3.1.1 Variable/Active insulations

Variable (or 'switchable') thermal insulation, in the form of an opaque panel that alternates between thermally conductive and insulated states, can be an effective means of regulating buildings' thermal environment by selectively transferring heat between the indoor and outdoor environments. To date, some pioneering work has been undertaken by researchers to develop variable insulation technologies intended for applications in the automotive and aerospace industries (Cui and Overend, 2019). The exploration of variable insulation technologies for building envelope applications is in early-stage development.

The variable thermal insulations (VTIs), i.e., dynamic or active insulation systems (Antretter and Boudreaux, 2019; Mumme and James, 2020) act as 'heat valves/ or switches' to regulate heat flow through the envelope assembly between the outdoor environment and indoor spaces. They are intended to provide beneficial heat flow into (or out of) the indoor space when desired. Based on their actuation mechanisms, VTIs may be achieved through the density transition of its thermal carrier medium, creation of an alternative heat flow path (i.e., via mechanical contact or suspended particles), or material phase change (Cui and Overend, 2019).

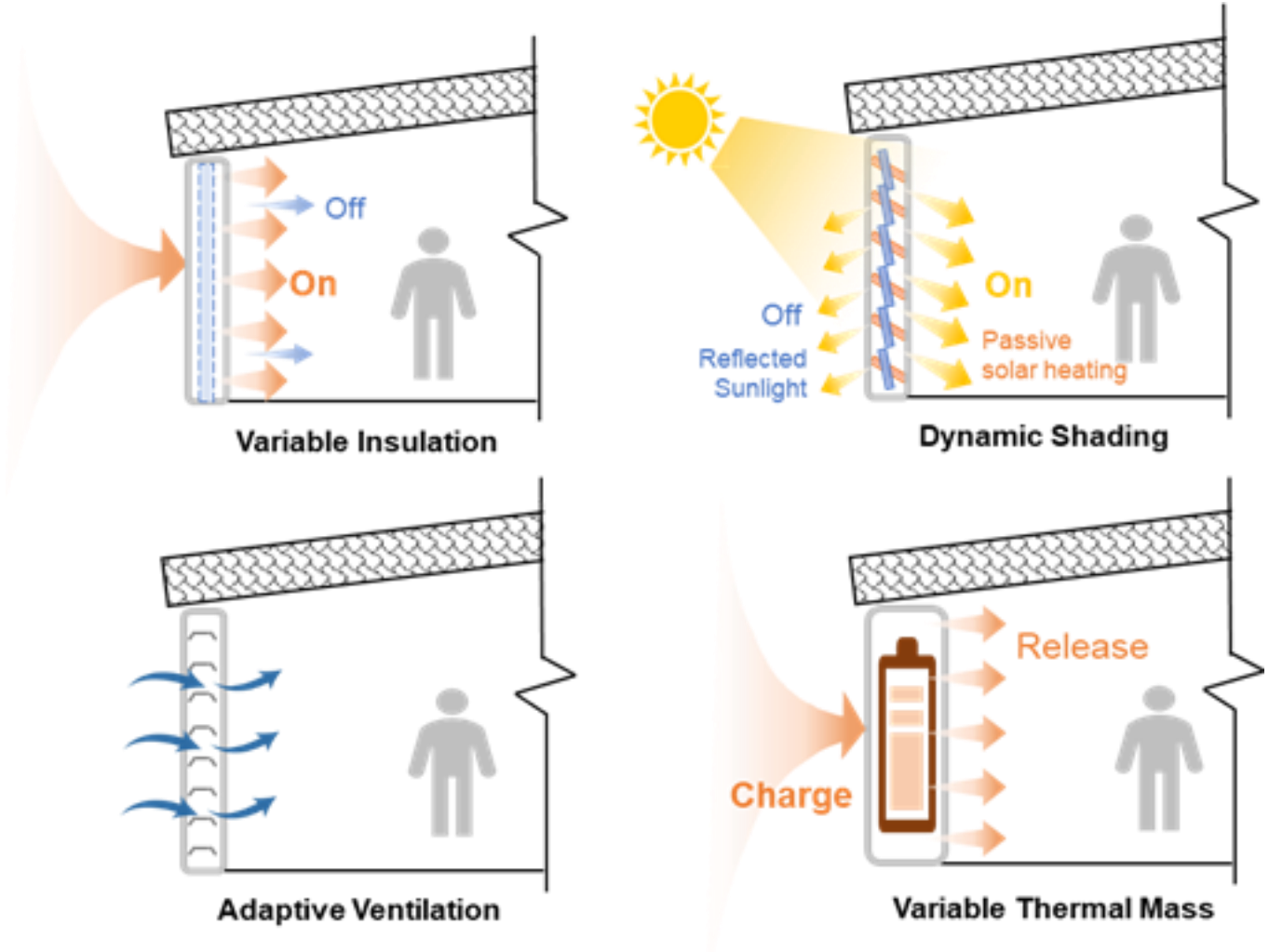


Figure 1.2 Categories of responsive building envelope technologies

Some VTIs behave like a 'binary switch' with an "on and off" mode – i.e., their thermal conductivities can change between two discrete states; whereas some other types of VTIs can gradually regulate their thermal properties based on the desired insulation levels. This is mainly achieved by responsive materials (i.e., those having tunable thermal properties (Tomko *et al.*, 2018)) or a functional assembly (e.g., active thermal bridge). The change of material thermal conductivity can be accomplished through the tuning of material micro-structures (including pore characteristics – pore shape, pore size, and porosity), chemical composition, or physical phase state.

1.3.1.1.1 Active vacuum insulation

Conductive heat transfer in the insulated material is dictated by the collision between gas molecules and solid surfaces. Depending on the mobility of gas molecules and the size of the cavity that encloses the gas phase, the heat transfer falls into three regimes: (i) the viscous regime, where heat transfer is dominated by the collisions between gas molecules, (ii) the molecular regime, where heat transfer is governed by the direct collision between the gas molecules and solid surfaces, and (iii) the transitional regime in between the first two (Yan Feng, 2005). The transition between one heat transfer regime to another is determined by the Knudsen number, which is the ratio of the mean free path (i.e. the average distance traveled between two successive collisions) to the characteristic length of the enclosure. Vacuum-based switchable thermal insulation works by alternating the heat transfer regime between the conductive viscous regime and the insulated molecular regime. This is achieved by reversibly pressurizing or evacuating the enclosure with a thermally conductive gas. The vacuum-based thermal switch typically consists of a micro-/ or nano-porous core, an impermeable seal, and a (vacuum) pump controlling the pressure inside the sealed core,

see **Figure 1.3** (a) on Page 11. In order to reduce the local Knudsen number and make it easier to achieve the pressure-sensitive molecular regime, porous filling materials such as aerogel or fumed silica (Berge *et al.*, 2015) or fabricating microscale narrow gaps (Krielaart, Vermeer and Vanapalli, 2015) are often used to artificially create small pores or gaps in the vacuum volume.

1.3.1.1.2 VTIs based on mechanical contact

Mechanical contact is perhaps one of the most intuitive means to control the heat flux across insulation panels. The switching mechanism works by bringing/ or separating two solid surfaces through mechanical contact to create conductive pathways, see **Figure 1.3** (b) on Page 11. The presence/ absence of mechanical contact causes a change in the dominant thermal transfer mechanism from gaseous convection/ conduction to solid thermal conduction. As a result, rapid alternation in the overall heat transfer rate by orders of magnitude can be achieved. A mechanical thermal switch normally consists of three basic elements: (1) two solid surfaces, (2) an actuator that separates two surfaces or brings two surfaces into contact, and (3) an enclosed cavity filled with insulative gas or compressible porous insulative materials. The movement of two surfaces can be actuated by several mechanisms including actively controlled mechanical actuators (Pflug *et al.*, 2015) and passive thermoresponsive materials (Cui and Overend, 2019). Research efforts to improve the performance of mechanical-contact based VTIs have mainly focused on the heat transfer efficiency (both insulation and conduction capability to increase the 'switching ratio') and the actuation mechanisms.

1.3.1.1.3 VTIs based on suspended-particles

The alternation in thermal conductivities of insulation panels can also be achieved through liquid based suspensions – the heat transfer rate in fluidic media can

be altered by introducing thermally conductive insoluble (typically solid) particles (Cui and Overend, 2019). Colloids, which consist of a liquid phase and microscopically dispersed suspended particles, have been used to create VTIs (Eapen *et al.*, 2010). As the size of suspended particles in colloids is reduced to the nanoscale, the colloidal fluid is known as a nanofluid. The dispersed nanoparticles in nanofluids are subjected to vigorous Brownian motion to form well-dispersed and stable two-phase (binary) or three-phase (trinary) mixtures. The effective thermal conductivities of these nanofluidic mixtures can be described by Fourier's law of heat conduction, which is a function of the thermal conductivities of the constituent phases, their volume fractions, and the spatial distributions.

In nanofluids, microscopic heat transfer mechanisms such as micro convection on the particle-liquid interface (Jang and Choi, 2004), the ballistic phonon interactions between nanoparticles (Das, Sarit K., Stephen U. Choi, Wenhua Yu, 2007), and the clustering of nanoparticles (Angayarkanni and Philip, 2015), also contribute to the heat transfer in the mixtures. Among these mechanisms, the clustering effect –i.e. the connectivity of particles, causes significant changes in the mixtures' thermal concavity by creating locally packed clusters with high internal thermal conductivity (Philip, Shima and Raj, 2008). Tunable thermal properties can be achieved by modulating the connectivity and spatial distribution of clustered nanoparticles in the base fluid, leading to alternation in effective thermal conductivity. The formation of such clustering processes can be triggered by external fields such as temperature and magnetic fields (Eapen *et al.*, 2010) – e.g., magnetite nanoparticles suspended in the fluid can align into chain-like structures when magnetic fields are applied. This process is reversible when the external magnetic field is removed, as illustrated in **Figure 1.4**.

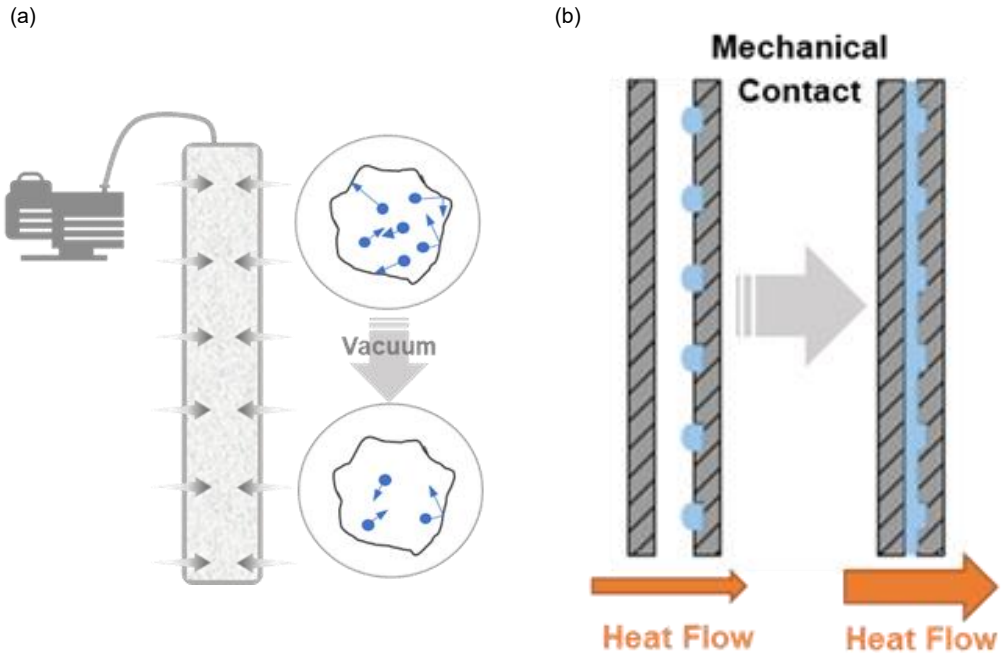


Figure 1.3 Variable thermal insulations (VTIs) based on: (a) active/variable vacuum; and (b) mechanical contact (Cui and Overend, 2019)

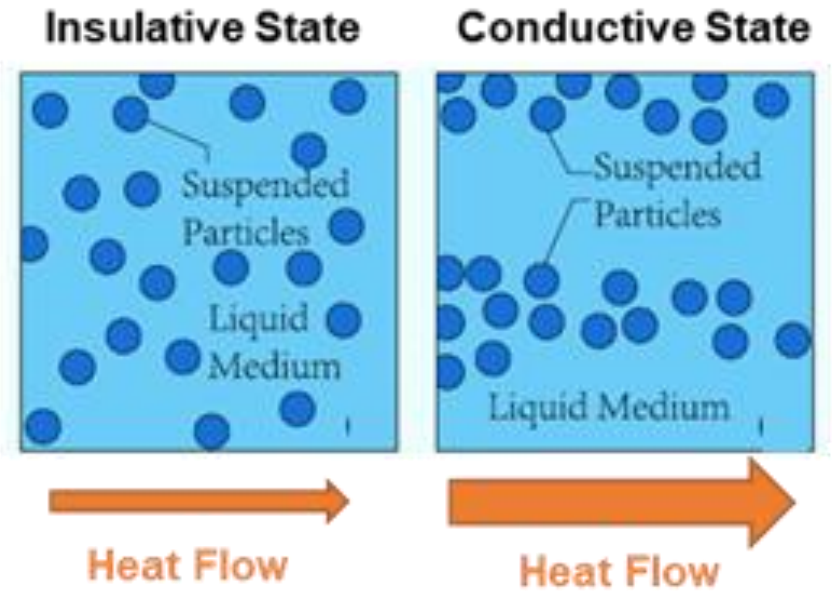


Figure 1.4 Schematic showing the principle of suspended particle devices (Cui and Overend, 2019)

1.3.1.1.4 VTIs based on material phase change

Another pathway to achieve VTI is through the phase change of thermal carrier materials. The phase of substances undergoes physical transitions most commonly between solid, liquid, and gaseous states triggered by condition changes such as temperature and pressure. During phase transitions, part of the potential energy within the materials will be converted into kinetic energy or vice versa. Such reversible conversion in the evaporation-condensation cycle enables fluids/gases to transfer much more energy during the heat transfer process, leading to highly effective thermal conductance (Zohuri, 2011). One way to achieve VTI through material phase-change is to intermittently interrupt the evaporation-condensation cycle, which will lead to an alternation in heat transfer between the conductive state where heat is mostly transported by evaporation and condensation processes, and the insulated state where the gaseous conduction or single-phase natural convection is dominant. Based on this principle, technologies known as the variable conductance heat pipe (VCHP) are developed for VTIs. A typical VCHP consists of four elements: a working fluid that undergoes phase transition during heat transfer, a sealed container consisting of an evaporator, condenser, and transport section, a wick structure, and a control unit that regulates the evaporation-condensation cycle (Faghri, 1995).

Table 1.1 summarizes several prior research on variable thermal insulation technologies (David K. Benson, Potter and Tracy, 1994; Varga, Oliveira and Afonso, 2002; Kimber, Clark and Schaefer, 2014; Loonen, Hoes and Hensen, 2014; Wu *et al.*, 2014; Park, Srubar and Krarti, 2015; Pflug *et al.*, 2015, 2018; Tomko *et al.*, 2018).

Table 1.1 Summary of technologies for variable thermal insulation

Technology	Triggering mechanism	Description	Thermal conductivity – W/mK (R-value Range - $m^2 \cdot K/W$)		Response time
			λ_{min} (R_{min})	λ_{max} (R_{max})	
Active Vacuum	Pressure/evacuate the filling material (gas) or fabricated narrow gaps	Variable pressure VIP (Berge *et al.*, 2015)	0.007	0.019	20 min
		Variable Pressure Aerogel blanket (Berge *et al.*, 2015)	0.011	0.017	Few mins
		Variable conductance insulation (David K. Benson, Potter and Tracy, 1994)	0.025(0.13)	0.2(1)	N.A.
Thermodiode / Pipe-Embedded Insulation	Control the direction of the heat flow through the diodes	Bi-directional thermo diode (Varga, Oliveira and Afonso, 2002)	0.07	0.35	Long response time
	Accelerate/impede the fluid flow or disturb thermal boundary layers	Walls change between being insulation and thermally conductive states (Krzaczek and Kowalczuk, 2011; Iffa *et al.*, 2022)	(0.03)	(0.25)	Short response time
Mechanical Contact	Bring two panels into mechanical contact or separation	Translucent element switchable U-value (Pflug *et al.*, 2015)	0.0175 (0.33)	0.075 (1.43)	Few mins
	Change the thickness of air layers	Adaptive Multilayer Wall Air layer (Kimber, Clark and Schaefer, 2014)	0.005 (0.13)	0.2 (5)	N.A.
	Roller system	Movable insulation (Pflug *et al.*, 2017)	(0.35)	(4)	N.A.
Suspended Particles	Form/break chain-like structures by external fields	Suspended particle device (Cui and Overend, 2019)	0.14-0.17	0.31-0.56	N.A.
	Direction of nanotubes	Carbon nanotubes suspension in liquid (Wu *et al.*, 2014)	0.4 (0.02)	1.2	Few secs
Phase-Change Technologies	Alternation in heat transfer between (1) evaporation and condensation processes and (2) natural convection.	Variable conductance heat pipe (VCHP) (Wu *et al.*, 2014)	N.A.	N.A.	N.A.
		Integrated flat-plate heat pipe (Wu *et al.*, 2014)	N.A.	N.A.	N.A.
		Flat-plate heat pipe with bounded wires (Wu *et al.*, 2014)			
Chemical reaction	Change micro-structure through hydration and dehydration	Bio-inspired topologically networked material (Tomko *et al.*, 2018)	0.5	1.35	Few secs

In these examples, the "on-and-off" thermal switch was achieved by changing material thermal conductivity through hydration/ dehydration (Tomko *et al.*, 2018); changing porosity; changes in materials orientation (Wu *et al.*, 2014), or alternating the overall insulation through convective heat transfer (Pflug *et al.*, 2015). Continuous thermal conductivity change was also achieved by varying the vacuum pressure of vacuum insulated panels (VIP) (Berge *et al.*, 2015). The variable thermal insulation may also be achieved through multi-layer retractable thermal insulation (the overall insulation value can be changed gradually by controlling the number of active insulation layers (Kimber, Clark and Schaefer, 2014)). **Table 1.1** also lists the thermal conductivity (or R-value) range of the VTIs achieved through different mechanisms along with a brief description of the heat transfer and triggering mechanisms.

1.3.1.2 Controllable/adaptive ventilation

Controllable/adaptive ventilation systems (Sung, 2016; Pujadas-Gispert *et al.*, 2020) can also behave as heat switches by changing the amount of airflow, and thus convective heat flow, into and out of building indoor spaces, see **Figure 1.5** on Page 16. Examples to implement adaptive ventilation as a form of responsive building envelopes include the bio-inspired ventilated facade developed by Doris Sung and Ester Pujadas-Gispert et al. (Sung, 2016; Pujadas-Gispert *et al.*, 2020), which provides building surface cooling through natural ventilation, as shown in **Figure 1.5** (a), (d)-(f) on Page 16. Inspired by the opening and closing behavior of pine cones in response to hygroscopic conditions, Reichert et al. (Reichert, Menges and Correa, 2015) developed a responsive façade component, named Meteorosensitive Architecture, which harnesses the elastic deformation of veneer composite materials to make a

tunable, humidity-responsive façade opening system, see **Figure 1.5** (b) on Page 16. An interesting feature of these concepts (or similar) is that the material acts as a sensor and actuator at the same time, which embeds the adaptive capacity as an inherent feature of the building shell. Another example of kinetic ventilation systems is the mechanically actuated adaptive façade developed by Biloria et al. (Biloria and Sumini, 2009), see **Figure 1.5** (c) on Page 16.

1.3.1.3 Dynamic glazing and dynamic shading

Dynamic glazing (Casini, 2018) with variable optical characteristics (e.g. reflectance and transmittance) modulates the amount of near-infrared radiation and visible light entering the indoor space, allowing for energy savings as well as greater thermal and visual comfort for occupants, see **Figure 1.6**. Existing techniques to achieve dynamic glazing include electrochromics (DeForest *et al.*, 2017), gasochromics (Delalat, Ranjbar and Salamati, 2016), nanocrystal in-glass composites (DeForest *et al.*, 2017), electrokinetic pixels (Casini, 2018), elastomer-deformation tunable window (Shian and Clarke, 2016), and liquid infill tunable window (Casini, 2018). For the purpose of clarity, the translucent building envelope that changes insulation (Pflug *et al.*, 2015) rather than regulating incoming radiation, is outside the scope of dynamic glazing. Dynamic glazing can operate passively or actively, depending on the materials and actuation mechanism used. Passive dynamic glazing systems are self-regulated ones responding automatically to natural stimuli such as light (photochromic) or heat (thermochroic, phase changes materials). For instance, thermochromic materials with variable reflectance (Park and Krarti, 2016; Berardi, Garai and Morselli, 2020) are triggered by outdoor temperature changes. These materials are applied as envelope coating to control the solar heat gain of buildings.

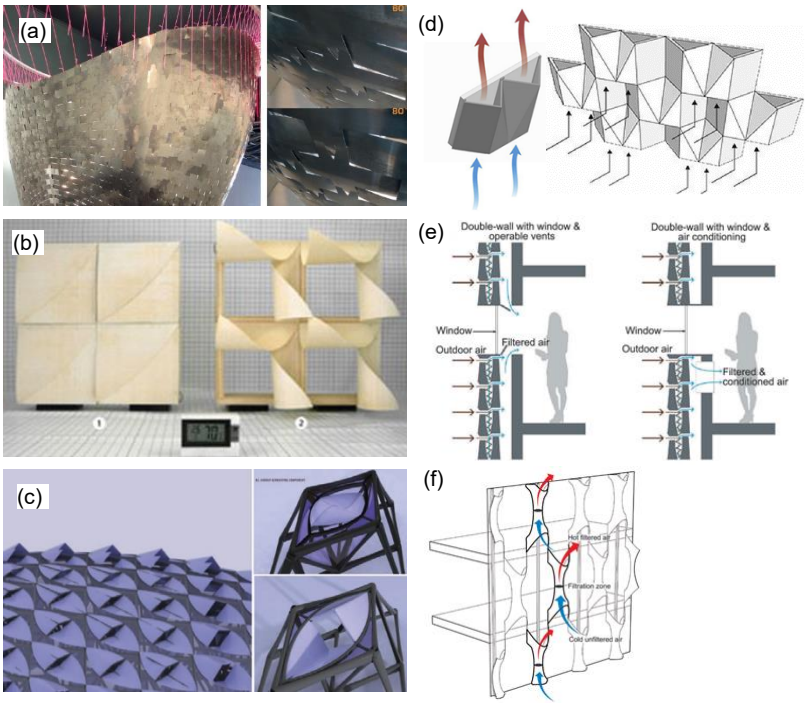


Figure 1.5 Examples of adaptive ventilation: (a) the ventilated façade by Sung (Sung, 2016); (b) the meteorosensitive architectural project by Reichert et al. (Reichert, Menges and Correa, 2015); (c) the mechanically actuated façade by Biloria et al. (Biloria and Sumini, 2009) and (d)–(f) bio-inspired self-adaptive ventilated facades (Sung, 2016; Pujadas-Gispert *et al.*, 2020)

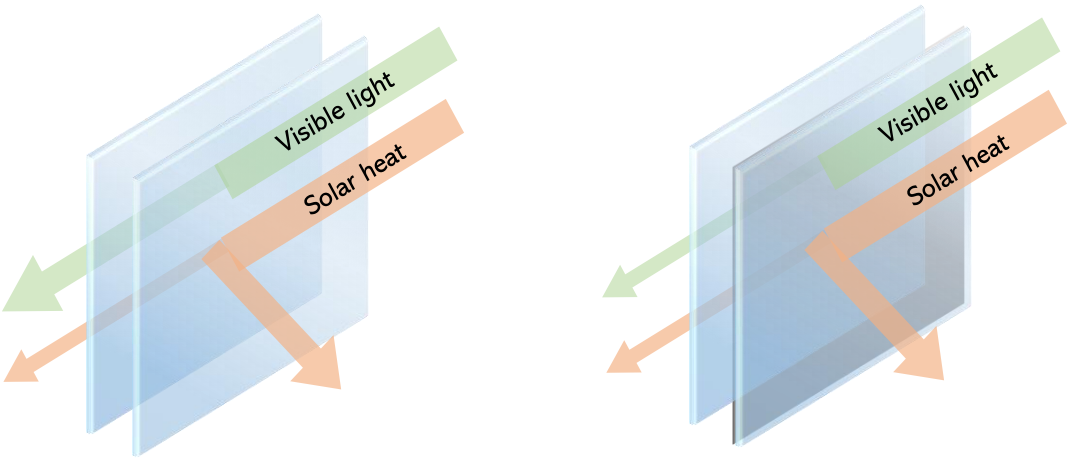


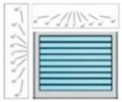
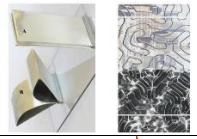
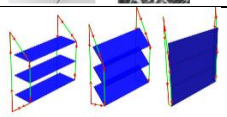
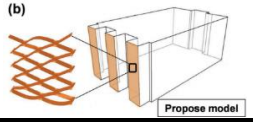
Figure 1.6 Schema6ic for dynamic glazing

On the other hand, active dynamic glazing modules are adjustable systems that can be actively controlled according to users' inputs. Some systems of this type such as electrochromic glazing respond to electrical triggers and change their optical characteristics (e.g., absorbance, reflectance, or light scattering).

Dynamic shading devices are intelligent systems automatically operated in response to outdoor or indoor parameters in favor of a high comfort level and improved energy performance. It is essentially designed to shelter a building from undesired solar radiation, which works through converting direct solar radiation into diffuse light and modulating the amounts of light penetration into the indoor space. The advancements in software and hardware provide opportunities for solar shading systems to function dynamically within their context. This development has helped dynamic shading systems respond to variable environmental parameters such as sun angles and solar insolation. The automatic response presents the key feature of dynamic shading systems – e.g., mechanically actuated shading devices have three main components: a sensor network to obtain data, a controller to determine the suitable action, and mechanical actuators to execute the response. Over recent years, a number of semi-active and passive mechanisms have also been developed for dynamic shading.

The thermal and energy performance of shading systems involves two main aspects: (i) light regulation which includes preventing glare and maintaining adequate indoor illuminance, and (ii) providing acceptable thermal environments by controlling solar heat gains accompanied with direct and diffused solar irradiations (Al-Masrani and Al-Obaidi, 2019). The modulation of solar radiation can be achieved through mechanical actuation or morphing metamaterials or kinetic devices. Some technologies to tune shading areas studied in prior research are summarized in **Table 1.2**.

Table 1.2 Typical techniques for kinetic shading systems

Technology	Motion pattern	Schematic	Description
Electric/mechanical actuation	Rotation		Louvres (Al-Masrani and Al-Obaidi, 2019)
	Translation		Roller shade (Al-Masrani and Al-Obaidi, 2019)
	Rotation+ translation/ folding		Origami structure (Tang *et al.*, 2017)
	Rotation + translation/revolving /folding/sliding		Kinetic device(Biloria and Sumini, 2009; Dewidar, K.M, Mohamed, N.M., Ashour *et al.*, 2013; Velikov K, 2013; Fraternali, De Chiara and Skelton, 2015; Pesenti *et al.*, 2015; Zawidzki, 2015)
	Deformation of dielectric elastomers		Dielectric systems composed of electro-active polymers with electric conduction features (Decker, 2013)
Deformation actuated device	Rotation + translation/revolving /folding/sliding		Shape memory alloy (SMA) actuated device (Fraternali, De Chiara and Skelton, 2015; Pesenti *et al.*, 2015)
Temperature actuated device	Rotation+ translation/folding		Self-adaptive kirigami metastructures (Tang *et al.*, 2017)

These include dynamic louvers, adaptive kiri-kirigami structures (Tang et al., 2017) that can respond to irradiance changes, kinetic shading systems, etc (Al-Masrani and Al-Obaidi, 2019). Some of the systems are self-adaptive to temperature changes (Dewidar, K.M, Mohamed, N.M., Ashour et al., 2013) while others are triggered by electric (Velikov K, 2013) or shape memory alloy (SMA) actuators (Fraternali, De Chiara and Skelton, 2015; Pesenti et al., 2015). Solar shading systems have been proven to be effective in shedding intensive solar radiation to reduce building energy consumption, especially during peak hours. In addition to energy savings, passive shading systems are also effective bioclimatic means to maintain the balance between visual and thermal demands.

1.3.1.4 Variable thermal mass

Thermal energy storage (TES) generally refers to the temporary storage of thermal energy, which can be released for later use when desired (Dincer and Rosen, 2013). Conceptually, TES behaves like a battery system, absorbing and storing undesirable thermal energy from outdoor or indoor environments and the stored energy can be released during off-peak hours or when heating or cooling is needed (see **Figure 1.2**). TES systems can be classified into three types: sensible, latent, and thermochemical (Stadler and Sterner, 2018) storage. Sensible heat storage systems store thermal energy with a change in the temperature of the storage media before and after charging. Latent heat storage systems store energy without changes in the medium temperature. Charging /discharging of TES involves changing the physical state (and the corresponding enthalpy) of the storage medium (e.g., phase change materials (PCM)). In buildings, latent heat storage systems can store and release heat with small temperature swings and low self-discharge, which are highly desirable from the thermal comfort perspective. Thermochemical heat storage

systems use reversible thermochemical reactions to store or release heat. The storage system is charged by an endothermic reaction and discharged by an exothermic reaction. Thermochemical heat storage typically has a high storage capacity per unit volume or mass of the storage medium, but controlling the reversible thermochemical reactions may be challenging (Cabeza *et al.*, 2017).

Besides the passive utilization of TES in buildings, thermal energy can also be charged/discharged actively through a thermal carrier (e.g., fluid). Active thermal storage systems are mainly characterized by forced convection heat transfer, and/or mass transfer (e.g., heat carrier fluids) in some cases (Navarro *et al.*, 2016). Examples of active TES systems in buildings include the integration of phase change material (PCM)-charged walls with active control to store solar heat collected during the daytime for overnight heating. In a study by Navarro L et al. (Navarro *et al.*, 2015), phase change materials are encapsulated in aluminum tubes and then placed inside an active prefabricated concrete slab system. During winter, the PCM is melted by passing hot air from the solar air collector and stored until heating is needed. In summer, outside air is passed through the slab at night to solidify the PCM. In addition, a recent effort by Gracia A de et al.(Gracia, 2019) tries to expand the utilization of energy stored in TES through developing kinetic configuration (e.g. rotatable polymer-PCM composite enabling movable thermal energy stored in TES.

Moreover, some RBE configurations not only store unwanted thermal energy temporarily to offset the mismatch between thermal energy availability and demand but also utilizes building envelope as a heating or cooling device by embedding heating elements or heat extraction channels (Ma, Wang and Guo, 2015). One example of this

integrated configuration is thermally activated building systems (TABS) (Lehmann, Dorer and Koschenz, 2007), where a hydronic circulation system is embedded in heavy building thermal mass (e.g. thick concrete slabs in ceilings or floors). TABS combines the advantage of radiant surface heating and cooling and the utilization of building structure as a thermal energy storage media (Ma, Wang and Guo, 2015). In addition, some other examples utilize renewable energy resources (e.g., solar energy (Xu, Dessel and Messac, 2007; Xu and Dessel, 2008)) as heat sources (or generate electricity for heating and cooling) within the variable thermal mass to charge the indoor space.

1.3.2 Materials for adaptive building envelopes

The dynamic activation in passive systems works via intrinsic properties of environmentally responsive smart materials that represent a promising pathway for the development of adaptive building envelope technologies. Building performance can be improved with the use of passive systems to reduce energy consumption, and greenhouse gas emissions (Villegas, Gutiérrez and Colorado, 2020), and provide opportunities to interact with outdoor environments. Environmentally responsive, or 'intelligent', materials play an essential role in achieving these goals. A brief discussion is provided herein to introduce some emerging materials used in architectural skins that have been explored for controlling environmental variables such as temperature, lighting, and humidity.

1.3.2.1 Humidity-sensitive materials

Hygroscopy refers to the ability of a material or physical system to absorb water from the environment or release it back. Materials that attract water or water vapor from their ambient environment are hygroscopic. This property is usually seen as a disadvantage for conventional building materials. For example, the ability of wood to absorb moisture often

leads to unwanted deformation of the materials. However, expansion and contraction in a specific direction can result from anisotropic deformation controlled by cell wall architecture through cellulose swelling and shrinkage (Ministerial and Forum, 2011). In this way, changes in the cellulose volume by humidity exchange allow movement of, for instance, the pine cone scales under hydrated/dehydration cycles (Marshall, 2015). Inspired by this principle, hygroscopic properties of materials have been explored for passive building envelope control (Ministerial and Forum, 2011; Ogwezi *et al.*, 2013). For example, laminate composite systems with specific fibers direction were reported as principal components to achieve moisture response with autonomous movement. Architectural skin with closed modules under low humidity conditions and open modules under high humidity conditions was reported in (Augustin, 2018). Chen et al. (Villegas, Gutiérrez and Colorado, 2020) fabricated a dynamic architectural surface made of a matrix of tiles elaborated with lime veneer, nylon, and plastic with hydro-sensitive capabilities due to the different porous densities of the constituent materials. In addition, synthetic superabsorbent polymers such as hydrogels have been used in dynamic envelope systems with two main approaches. The first focuses on the ability of the material to retain large amounts of water, and the second path leverages the volume change of super-absorbent polymers after hydration/desiccation. An example of the first approach is the hydroceramics proposed by Mitrofanova et al. (E. Mitrofanova, A. Rathee, 2014), which consists of a multi-cavity system that catches rainwater. The panels are made of clay and filled with hydrogel spheres. The system provides passive cooling to buildings building through rainwater harvesting by the envelope module, and the long-term storage of water and moisture release throughout the day improves thermal exchanges

between the building and the external environment as shown in **Figure 1.7** on Page 25. The second approach consists of a force generating system (I. Ayala Castro, M. Manosong, 2017). The devices are based on an acrylic piece attached to hydrophobic fabric pockets filled with sodium polyacrylate spheres with a mesh in contact with it. When the humidity goes through the mesh, the volume change of the pockets is triggered to generate movement from one side to another to allow airflow. A different system which uses the force-generating hydrogels was reported (L. Roth, 2015), where a surface made of a matrix of silicone scales was fixed by a polyacrylates composite. When the surface is in contact with water, the composites' net points swell, and the architectural scales can open and close when it shrinks. The hydration/dehydration of certain materials has also been explored to create tunable materials that have reversibly variable thermal conductivities. To that end, Hopkins et al. (Tomko *et al.*, 2018) developed topologically networked bio-inspired materials for reversible thermal conductivity switching. They propose that by varying the network topology, or crosslinked structure, of squid ring teeth-based bio-polymers through tandem repetition of DNA sequences, the thermal switching ratio can be directly programmed. This on/off ratio in thermal conductivity switching is promising in dynamic building envelopes where reversible thermal conductivity switching is desired as introduced in previous sections.

1.3.2.2 Temperature-responsive materials

Since temperature control is one of the main functional objectives of responsive building envelopes, 'temperature-responsive materials' have been widely explored for RBE applications. Hybrid shape memory materials are a class of stimulus-responsive components made of two different materials which do not have shape memory capabilities (Sun *et al.*, 2012). For example, bi-metallic shape memory strips are made of two metallic pieces with

different thermal expansion coefficients bonded by an adhesive. The system operation is based on the asymmetric stress distribution within the two laminated layers due to the expansion/contraction of each strip caused by thermal gradient differences. This phenomenon allows shape changes such as bending, triggered by direct or indirect heating. This principle has been applied to architectural surfaces with active thermal features triggered by solar irradiation as well as ambient temperature changes. An early study reports stimulus-responsive skins that utilized the behavior of thermobimetals in architecture by Sun et al. (Sun *et al.*, 2012), see **Figure 1.8** (a). Another class of temperature-responsive material is based on the use of shape memory alloys (SMA) as their active components. SMA has several features including superelasticity, shape memory effect, and high damping capacity (Liu *et al.*, 1999). The shape memory effect has been leveraged to achieve a bi-directional movement by a martensitic reversible transformation because of temperature change (i.e., warming or cooling). The use of SMA in architecture either as a dynamic system by itself or as a part of a system has shown an important improvement in performance and reducing operational energy consumption – i.e., the temperature-responsive behavior of SMA can generate passive movements that do not rely on sensors and external energy inputs. Nickel-Titanium alloy (NiTi) is the most reported SMA in responsive envelope systems because of its reliable mechanical performance (Sun *et al.*, 2012). Several responsive building envelopes which focused on heat and lighting control used NiTi SMA as an actuator or as components of the actuation mechanisms. These systems' operations are mostly based on prestressed SMA springs or wires trying to recover their original shape due to temperature change, which generates mechanical force in the process for morphing or actuation.

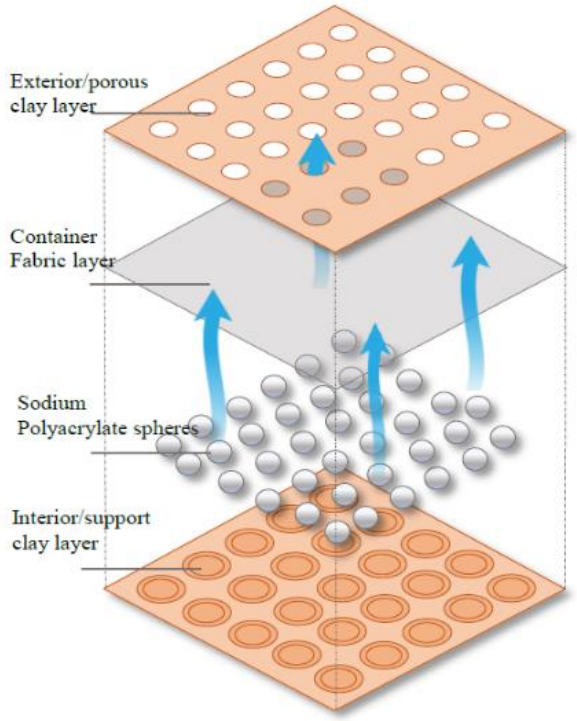


Figure 1.7 The 'hydroceramic' concept developed by Mitrofanova et al. (E. Mitrofanova, A. Rathee, 2014)

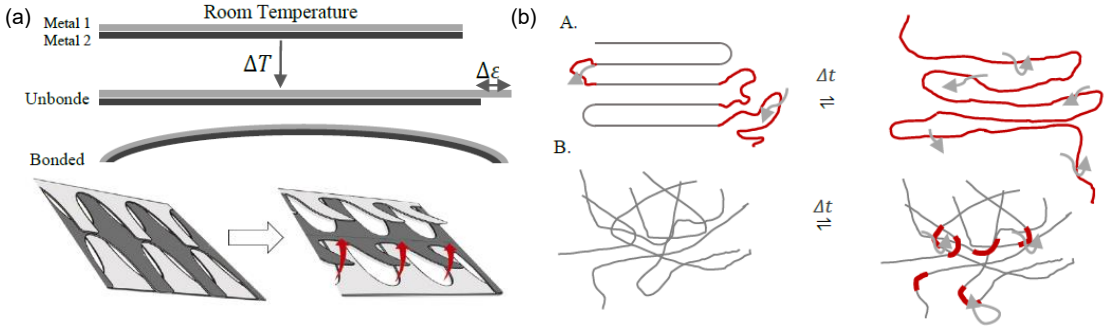


Figure 1.8 Temperature-responsive materials: (a) the concept of thermo-bimetal; and (b) temperature-responsive polymers (Meng and Li, 2013)

Shape memory polymers (SMPs) are stable polymer networks with reversible shape transitions triggered by stimuli such as temperature, pH, electricity, magnetic field, light, and ions mainly (Meng and Li, 2013). There are numerous molecular structures that can drive the shape memory effect in polymers. In the case of thermal-responsive SMPs, polymers with molecular entanglement, chemical crosslinking, crystallization, and interpenetrated network may be used. The reversible switching transitions can be crystallization and vitrification as shown in **Figure 1.8** (b). During this process, shape change or mechanical force can be generated when the material is subjected to environmental changes. Commercial temperature-responsive SMPs have been used to develop dynamic structures in architectural skins (Beites, 2013).

1.3.2.3 Electrochromic materials and passive lighting control

The change of optical properties of materials in response to electric current or temperature change has been utilized for the development of responsive building envelopes. The electrochromic effect, for instance, occurs in partially hydrated transition metal oxides (J.S.E.M. Svensson and C.G. Granqvist, 1985). Reversible electrochemical reactions facilitated by the ion extraction and insertion of metal oxides lead to changes in physical properties such as conductivity, IR absorption, and color. Electrochromic materials, in the form of thin coatings, have been widely used for building windows and façade. The system shifts from an oxide insulator state to a quasi-metallic one when an external potential is applied. The electroactive layers change their optical properties between their oxidized and reduced form because of electron flow in the system. Tungsten oxide WO_3 in its amorphous state is the most studied among the cases of electrochromic coatings. (J.S.E.M. Svensson and C.G. Granqvist, 1985). The system can be customized to

obtain different time responses as well as absorbing /reflecting rates as demonstrated by many prior studies.

By using a dielectric elastomeric layer derived from an electro-active polymer (EAP) sandwiched between two electrodes, a multilayer system was created by Krietemeyer et al. (Krietemeyer and Dyson, 2011). The dynamic behavior is triggered when an electric current goes through the laminate which rises electrostatic forces that generate a contraction of the elastomer. As a result, a dimensional change occurs going from a thick to a flat and thin plate, allowing the components to deform in predicted directions. This mechanism has been used for daylighting control, where a network made of elastomer-coated silver electrodes was developed (Decker, 2013). A bi-directional movement of the laminated components allows the transition between "on and off" modes for the passage of sunlight into the indoor space.

1.3.3 Performance prediction and evaluation of buildings with responsive building envelopes

1.3.3.1 Building performance simulation

One of the unique features of RBEs is the capability to adjust their thermal, optical, or other physical properties in a reversible way in response to variable external (climate) or internal (occupants' requirements) boundary conditions, in order to meet specific priorities – e.g., minimizing the building energy use, or maximizing the thermal comfort. The successful design of RBE is a challenging task which may consider the performance demands in diverse aspects (e.g., robustness, energy use, healthcare, and environmental impacts). RBEs are complex systems whose design typically combines multiple physical domains (thermal, luminous, air quality, etc.). Unlike traditional buildings whose energy

system is primarily comprised of the ventilation and air-conditioning (HVAC) system, the performance and design of buildings with RBEs vary largely by local climatic conditions as well as the interactions with occupants and other building equipment and subsystems. Traditional characterization methods for building envelopes, such as U-value and g-value, are based on static assumptions. Therefore, due to the intrinsic time-varying behavior of RBEs, these metrics provide limited and potentially misleading information for dynamic systems. Therefore, a more comprehensive, simulation-based approach may be used instead for whole-building performance indicators such as total primary energy use and/or indoor occupant comfort and environmental quality metrics.

Modeling and simulation can bring important insights into the mutual influence between the design and performance aspects of RBEs. However, simulation of the dynamic nature of RBEs can be significantly more complex than performance prediction of conventional static building envelope since most existing simulation tools are not developed for this purpose. Differing from the static representation of the building envelopes, the modeling and simulation of RBEs have to accurately represent the time-varying building envelope properties (or system states). Compared with the simulation-based analysis of static building envelopes, three major additional requirements for performance prediction of RBEs were identified by Loonen et al.(Loonen *et al.*, 2017):

1) Modeling the time-varying envelope properties

Building envelope specifications such as material properties or position of components need to be changeable during simulation run-time to properly account for

transient heat transfer and perhaps energy storage effects (if/when active insulation system or TES is used) in the building envelope constructions.

2) Modeling the dynamic operation of the RBE adaptation

The dynamic nature of RBEs gives rise to a strong mutual dependency between design and control/operation (Favoino, Jin and Overend, 2017; Jin, Favoino and Overend, 2017). The performance of the RBE highly depends on the control strategy (i.e., whether it is passive, semi-active, or active) chosen during building operation. Moreover, effective design and operation of a responsive building envelope system depend also on the integration with operations (e.g., occupancy, scheduling) and other building services.

3) Computation frameworks for design and control of buildings with RBEs

To perform design and control analyses, versatile Computation frameworks that can flexibly integrate diverse self-adaptive or active building components (e.g., AIS, greenery systems, TES and dynamic shading) and control strategies (e.g., physics-based and model-free approaches) with high computation efficiency are required.

For effective performance prediction of RBEs, it is essential to simultaneously consider performance indices at multiple levels, with respect to (i) time resolutions, (ii) spatial effects, and (iii) physical domains (**Figure 1.9** on Page 31). The currently available information about modeling and simulation approaches for responsive building facades and relevant issues is fragmented (Kimber, Clark and Schaefer, 2014; Park, Srubar and Krarti, 2015; Pflug *et al.*, 2015). No generic approach has been developed for the design and control of RBEs. Existing simulation platforms such as EnergyPlus (Favoino, Jin and Overend, 2017; Jin, Favoino and Overend, 2017) and IDA ICE (Claros-marfil *et al.*, 2014)

have some capability to simulate the performance of building envelopes with moveable insulation. A controllable layer can be added to the interior or exterior side of an opaque envelope layup to provide variable insulation. These materials are assumed to be massless (no thermal energy storage).

1.3.3.2 Energy-saving potential

To assess the thermal performance of the responsive envelopes and their applicability in different scenarios, scholars (Juaristi *et al.*, 2021) conducted building energy simulations and experiments to quantify the indices for different types of building with different RBE configurations. The related parameters of the cases are summarized in **Table 1.3**.

Among the various RBE concepts, active insulation systems (AISs), or sometimes also referred to as 'dynamic insulation materials (DIMs)' or adaptive opaque façade (AOF), are building envelopes with insulation materials that can actively change their thermal conductivity, which have been studied as one of the most promising RBE technologies so far to achieve building energy savings and improving occupant comfort. Early studies conducted by Krarti et al. (Park, Srubar and Krarti, 2015; Menyhart and Krarti, 2017) demonstrated that RBEs comprised of an AIS layer could lead to total energy savings ranging from 7% to 42% for residential buildings in different US climate zones. For these simulations by 3R2C models, the AIS layer was assumed to be able to change its thermal resistance (R-value) between two values, and its reaction was controlled using a simple temperature-based control approach (Park, Srubar and Krarti, 2015; Menyhart and Krarti, 2017).

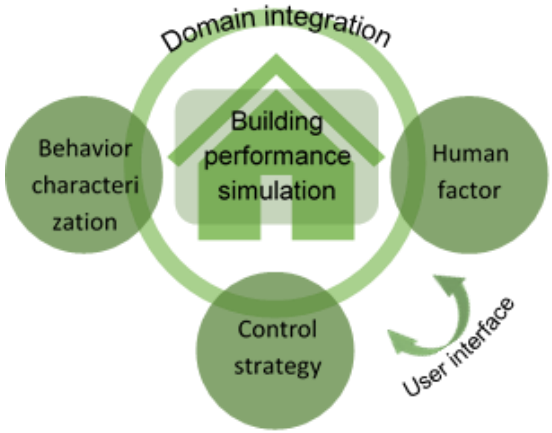


Figure 1.9 Simulation of responsive building envelopes (RBEs)

Table 1.3 Thermal performance of different RBEs

RBE configuration	Performance			Control type	Building type	Climate zone/weather condition	Data source
	short-term energy use or heat flux reduction (%)	Annual energy use reduction (%)	LPD reduction (%)				
INS +AIS+ INS	N.A.	2 ~ 45	N.A.	RBC	An office building	hot-dry, mixed-dry, mixed-humid, marine	Simulation (Rupp and Krarti, 2019)
INS +AIS+ INS		0 ~ 44	N.A.	RBC	A residential building	hot-dry, mixed-dry, mixed-humid, marine, cold	Simulation (Dehwah and Krarti, 2020)

Table 1.3 continued

RBE configuration	Performance			Control type	Building type	Climate zone/weather condition	Data source
	short-term energy use or heat flux reduction (%)	Annual energy use reduction (%)	LPD reduction (%)				
AIS + TM + AIS	N.A.	16 ~ 47	20 ~50	RBC or MPC	An office room	temperate climate	Simulation (Favoino, Jin and Overend, 2017)
AIS + TM		17.5 ~ 40	10				
TM + AIS		0 ~ 8	0 ~12.5				
TCH + TM		-11 ~ 1	N.A.	RBC	A typical living room of a residential building	Mild Temperate Climates (Cfa), Hot-summer Mediterranean Climate (Csa), Warm-summer Mediterranean Climate (Csb) and Tropical savanna climate with dry-winter	Simulation (Juaristi *et al.*, 2021)
CAC + TM		-8.1 ~ 0.4					
KC + TM		-5.4 ~ 0.3					
TM + AIS + TM		-3.1~12.4					
AIS + TM		4.4 ~ 17.5					
TCH + AIS + TM		2.7 ~15.6					
CAC +TCH + TM		-10.5 ~ -0.7					
CAC +KC + TM		-19.1 ~ -6.7					
KC + AIS + TM		12.8 ~ 34.2					
CAC+KC +AIS +TM		8.5 ~30.5					
AIS + TM	N.A.	2 ~ 12.5	N.A.	RBC	A residential building	hot-humid, hot-dry, mixed-dry, mixed-humid, marine, cold, very cold, and subarctic	Simulation (Antretter and Boudreaux, 2019)
INS+ TM + AIS		-15~ -1					
AIS + TM + AIS		5 ~ 70					

Table 1.3 continued

RBE configuration	Performance			Control type	Building type	Climate zone/weather condition	Data source
	short-term energy use or heat flux reduction (%)	Annual energy use reduction (%)	LPD reduction (%)				
AIS + PCM+ AIS	N.A.	~ 20	N.A.	RBC	A residential building	hot humid climate	Simulation (Mumme and James, 2020)
AIS + PCM+ AIS	1 ~ 48	N.A.	N.A.	RBC	A building envelope	hot-dry, marine	Simulation (Kishore *et al.*, 2021)
AIS+TES+AIS	(60)	N.A.	N.A.	Schedules	A building envelope	Temperate	Experiment (Iffa *et al.*, 2022)
CAC+AIS+CAC	44	N.A.	N.A.	Passive	A commercial building	hot humid climate	Experiment (Elsarrag, Al-Horr and Imbabi, 2012)

In addition, Shekar and Krarti (Shekar and Krarti, 2017) investigated the use of a genetic algorithm (GA) based optimization approach to determine the optimal R-value setting for AISs. It was shown that depending on the building design, operation strategies, and climatic conditions, the use of AIS with GA-optimized control may lead to 17% of annual energy savings for US office buildings. When implemented as a roofing system (Dehwah and Krarti, 2020), AIS has shown the ability to reduce up to 44% of the energy use for space cooling, especially in mild climates and under heating dominated conditions. Further, Rupp and Krarti (Rupp and Krarti, 2019) compared several 'multi-step' control strategies – as opposed to the 'two-step' control used in most prior studies, for AISs in a residential building. A parametric analysis presented by the authors showed that more energy savings can be obtained by the multi-step control strategy in mild climates with relatively fewer cooling/heating degree-days; whereas RBE with simple "on and off" switchable insulation systems (i.e., with two settings: low and high R-value) would capture most of the cooling and heating savings that advanced dynamic insulation technologies that can vary their R-value continuously.

Although comprehensive, prior research on AISs as standalone building insulation systems did not fully leverage the energy-saving potential of RBE. To this end, Juaristi et al. (Juaristi *et al.*, 2021) conducted a scoping study of over 15 RBE typologies for residential buildings situated in six different climate zones. The RBEs designed in the case studies consist of different functional components and exhibit varied behavior in different scenarios. The simulation results show that RBEs consisting of a single functional component or combinations of the components including static insulation (INS), thermochromics (TCH), automated kinetic cladding (KC), and controllable convective heat transfer of air cavities (CAC) bring marginal

energy-saving potential or even adverse effect as compared to the baseline. In contrast, RBEs composed of only active insulation system/adaptive insulation components (AIS) or combinations of AIS with other components provide up to 34.2% energy use reduction. The simulation results show that the RBE composed of an exterior AIS layer and a thermal mass layer (TM), e.g., a concrete (CONC) layer, provides higher energy savings than the one composed of an AIS layer sandwiched between two thermal mass layers. Among the 15 available topologies, the RBE composed of KC, AIS, and TM from exterior surface to interior surface attained the maximum energy savings. In addition, the pilot simulation study by Antretter et al. (Antretter and Boudreaux, 2019) and Mumme et al. (Mumme and James, 2020) combined AISs with both sensible and latent thermal energy storage (TES) layers. In their study, different RBE layouts were studied under rule-based control (RBC), where AISs were applied on the exterior, interior, or both sides of a thermal mass layer. They performed simulations via EnergyPlus on a DOE residential prototype building in eight selected climate zones. The results indicated that RBEs comprising a thermal mass layer sandwiched between two AIS layers brought up to 71% energy use reduction while providing grid flexibility potential. Similar findings were concluded from the parametric studies conducted by Favoino et al. (Favoino, Jin and Overend, 2017; Jin, Favoino and Overend, 2017) for an office room extracted from a building in a temperate climate in Shanghai – RBEs composed of a thermal mass layer sandwiched by two AISs attained maximum energy savings among all the configurations studied. All of these results indicated that AIS is effective in regulating the charging and discharging of thermal energy stored in thermal masses for effective heating/cooling load reduction. More recently, Kishore et al. (Kishore *et al.*, 2021) studied the energy performance of buildings with phase change

materials (PCM) enabled TES in combination with AIS. It was found that the PCM-AIS-integrated wall provides significantly higher energy-saving potential than the AIS-only wall or the PCM-only wall in all climates. Depending on the climate, the PCM-AIS-integrated wall could provide 15–72% reductions in annual heat gain and 7–38% reductions in annual heat loss (Kishore *et al.*, 2021). The analysis presented in their study reinforces the need to combine scalable dynamic insulations with thermal energy storage systems for building energy savings.

1.3.3.3 Thermal comfort

Favoino et al. (Favoino, Jin and Overend, 2017; Jin, Favoino and Overend, 2017) conducted parametric studies over an office room with different RBEs composed of AISs extracted from a building in a temperate climate under rule-based control and model predictive control (MPC) control. As **Table 1.3** shows, the simulation results show that the RBE composed of a thermal mass layer sandwiched by two AIS layers provides higher thermal comfort improvement with a lower long-term percentage of dissatisfied (LPD) as compared to the other configurations. Kinetic RBEs based on biomimicry morphological approaches also improve indoor thermal comfort through controlling solar heat gain with promising energy savings (Hosseini *et al.*, 2019).

1.3.3.4 Other performance indices

In addition to improving energy performance and thermal comfort, responsive envelopes are also designed to contribute to air quality, acoustic quality (Loonen *et al.*, 2015; Carlucci, 2021), visual performance, and daylighting performance improvement (Wang, Beltrán and Kim, 2012; Krietemeyer, Andow and Dyson, 2015; Amir Tabadkani , Saeed Banihashemi, 2018; Valitabar *et al.*, 2018). Tabadkani et al. (Amir Tabadkani , Saeed Banihashemi, 2018) conducted parametric studies over sun responsive building

envelope to improve daylighting performance and visual comfort; the responsive building envelope provides a 10% visual discomfort reduction and keeps an indoor glare-free environment. The air-flow-responsive kinetic envelopes and kinetic envelopes correlated to natural ventilation not only help reduce energy use and thermal discomfort, but also improve air quality and facilitate daylighting performance(Wang, Beltrán and Kim, 2012).

1.3.3.5 Promising designs

Prior studies and preliminary analyses/simulations indicate that a synergy of multiple self-adaptive or active envelope technologies presented in **Figure 1.10** (e.g., AIS, TES, dynamic shading, evaporative cooling technology, etc.) shows tremendous advantages. To achieve net-zero energy building, diverse techniques and strategies have been investigated to harvest energy from outdoor environments and reduce energy demands of indoor spaces. In response, a synthesis of TES and heat valves/switches was developed as shown in **Figure 1.10**, where the responsive building envelope consists of one TES layer sandwiched between two heat valves/switches. The TES serves as the container to store thermal energy from the ambient environment and as an energy source releasing beneficial heat flow into indoor space when desired. The TES layer can be sensible heat storage with static thermal mass (Mumme and James, 2020) or latent heat storage (e.g., phase change material (El Mankibi *et al.*, 2015)). Heat valves control heat exchange with the TES layer: the exterior heat valve suppresses adverse heat flow and harvests or even quantifies the beneficial heat flow into TES meanwhile the interior valve provides the on-demand heat flow to offset AC load with quantified heat flow and store energy from indoor space. Therefore, RBEs can control the quantity of energy released into indoor space and provide on-demand compensating heat flow to construct sustainable building environments.

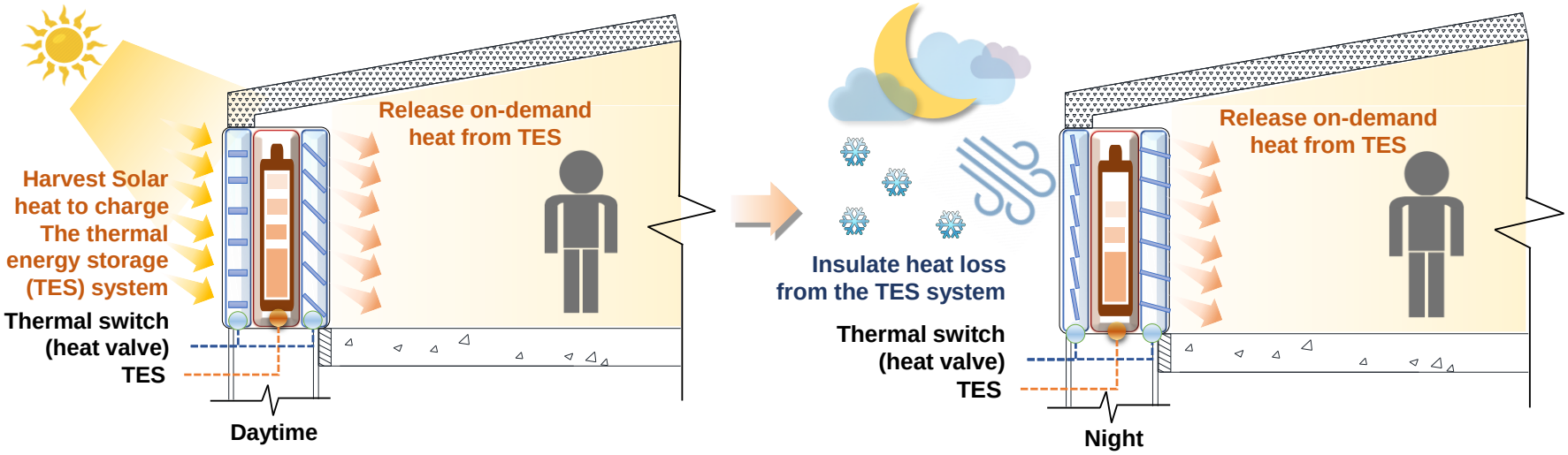


Figure 1.10 Schematic for working mechanism of RBE composed of TES and AISs.

1.3.4 Control strategies

Building control provides the link between sensed variables and actuator actions by means of certain control logic in order to obtain prescribed objectives (e.g., energy savings, improved occupant comfort, peak load shedding). **Figure 1.11** illustrates the coupled process of building control and design for responsive building envelopes.

The control of responsive building envelopes can be categorized into (i) intrinsic (passive) and (ii) extrinsic (active or semi-active) concepts (Loonen *et al.*, 2013). Passive control strategies utilize the intrinsic properties of materials or mechanisms that are automatically triggered by a stimulus (surface temperature, solar radiation, etc.). This level of intelligence is embedded in the material and the switching mechanism is activated by a variation in its internal energy. The intrinsic control is also referred to as "direct" or "open-loop" control. Materials or mechanisms having these characteristics are often tagged with 'smart' envelopes (e.g., thermochromic, photochromic, and PCMs), as no intervention from an external system/user is required.

In contrast, extrinsic control refers to the presence of an external decision-making component that is able to trigger the adaptive mechanisms according to a feedback rule. This is referred to as the feedback (or closed-loop) control type. Building envelope systems with this feature, together with its control system, are often referred to as "intelligent" envelopes (movable shading devices, kinetic facades, electro-chromic glazing, etc.). Hence, intelligent systems require a control management system to respond in an adaptive manner, consisting of sensors, processors, and actuators.

The control strategies are also classified into classical control, hard control, soft control, and other control according to the algorithms they use (Han *et al.*, 2018).

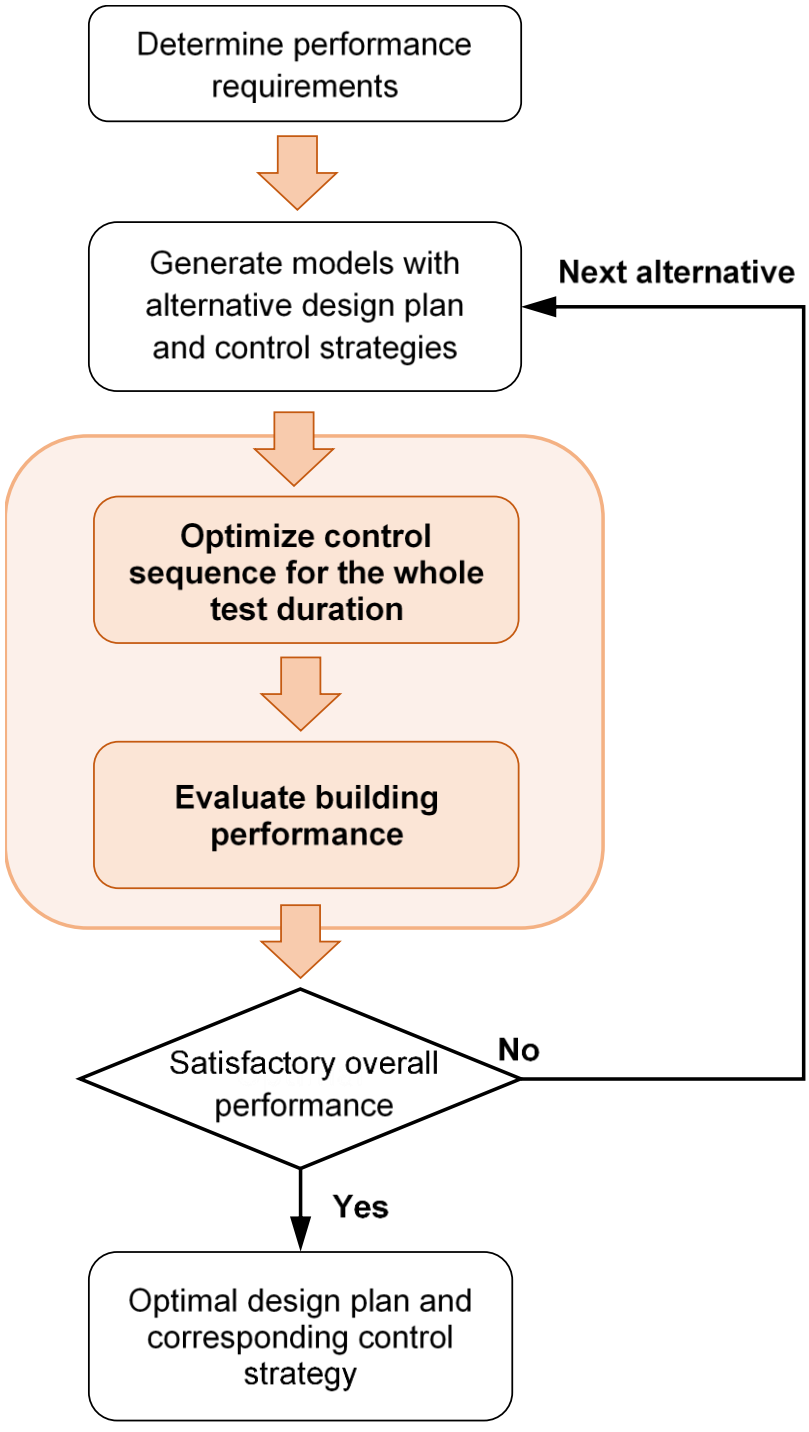


Figure 1.11 Design and control of RBE

Classical control uses a mathematical model to represent the relationships between the input and output of a system and generates control actions with rule-based controllers. The most common types of these controllers are on-and-off and PID controllers. The hard control generally includes gain scheduling, state feedback control, model predictive control (MPC), robust control, nonlinear control, and adaptive control. The soft controller uses intelligent control algorithms, e.g., ANN control and fuzzy logic control. The following sections give a brief description of the representative techniques: (i) rule-based control, (ii) model predictive control (MPC), and (iii) model-free control.

1.3.4.1 Rule-based control (RBC)

Rule-based control includes hard-coded intrinsic, hard-coded extrinsic, and time-scheduled control. Hard-coded intrinsic control refers to control options that capture the intrinsic properties of actuator materials or mechanisms – for example, for the actuation of thermo-optical properties of a fenestration system (e.g., thermochromic windows or phase-changing materials), the temperature-dependent material properties are modeled and embedded in the control algorithm. Hard-coded extrinsic control, on the other hand, can apply customized presets by the users. These typically include if-then-else statements where the user can select (i) sensor types (e.g., incident solar radiation, room temperature, heating or cooling demand, etc., or combinations thereof) and (ii) control thresholds to actuate specific adaptive technology. Time-scheduled control shares many characteristics with hard-coded extrinsic control systems but is different in the sense that control actions are predetermined as a function of time instead of being based on boundary conditions or simulation state variables.

For RBE applications, a number of studies have explored the rule-based control strategy for RBEs (Shekar and Krarti, 2017; Rupp and Krarti, 2019). Although previous research has encompassed understandings on the energy-saving potential, benefits, and costs of RBEs with AISs, existing control strategies did not fully explore the potential of AISs, particularly systems with AISs integrated with thermal mass/TES for enhanced energy savings. The majority of the research to date considered the R-value setting and HVAC operation separately (Cui *et al.*, 2022). Hence, the processes of adjusting thermal resistances of AISs and HVAC control were decoupled. While this strategy had shown satisfactory performance with AISs acting as standalone insulations for buildings, its combination with TES adds complex dynamics where the different layers of AISs (i.e., exterior or interior) may be actuated at different time slots of the day/season to allow the thermal mass layer to charge (store) and release thermal energy when desired to either reduce or shed the peak AC loads.

1.3.4.2 Model predictive control (MPC)

Model Predictive Control (MPC) is a class of building control methods that use an explicit model to predict the future response of a plant – i.e., the thermal behavior of a building component. Model predictive control (MPC) is an online control methodology, capable of utilizing system information through a well-developed model and real-time measurements to modify model parameters at each step.

The building model that is used for MPC can be an empirical model derived from tests performed in the plant, a dynamic physics-based model or a data-driven model. At each control step, MPC solves an optimization problem to calculate the control sequence for manipulated variables of the building control system (Favoino, Jin and Overend, 2017; Jin, Favoino and Overend, 2017), see **Figure 1.12**.

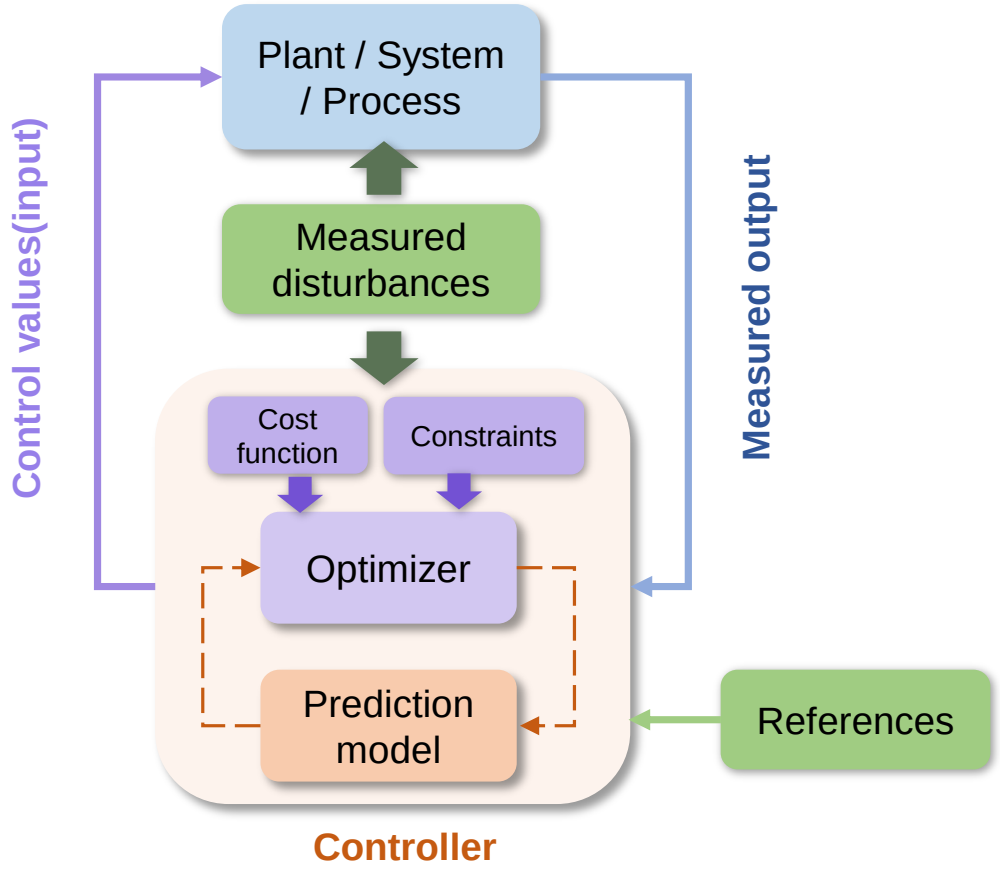


Figure 1.12 Schematic for the architecture of MPC(Mehrizi-Sani, 2017)

In terms of the RBEs integrating AIS and TES, due to the 'time-lag' effect brought by TES, a more sophisticated control strategy is required to achieve optimal performance of the system. To that end, Jin et al. (Favoino, Jin and Overend, 2017; Jin, Favoino and Overend, 2017) and Cui et al. (Cui *et al.*, 2022) explored model-predictive control (MPC) as the control strategy for AISs and AISs-thermal mass integrated building envelopes. Additionally, Sepehri et al. (Sepehri and Pavlak, 2023) investigated the annual potential benefits of jointly optimizing AIS and HVAC system controls using MPC. MPC has the advantages of being able to formulate and solve multiple optimization objectives, such as minimizing total energy consumption or operational cost (Ma, Qin and Salsbury, 2014), minimizing peak load demand (Biyik and Kahraman, 2019), and minimizing the deviation between aggregated HVAC power consumption (Bursill, O'Brien and Beausoleil-Morrison, 2020). MPC is an appropriate choice for handling the slow moving process with time delays and therefore it is well-suited for simple and small systems (Gholamzadehmir *et al.*, 2020). As an optimal control method, MPC can solve multi-objective problems (e.g. joint optimization of AIS and HVAC system operations (Sepehri and Pavlak, 2023)) based on a delicate model (e.g. white-box (Sepehri and Pavlak, 2023), grey-box (Cui *et al.*, 2022) or black-box model (Sun, Haghighat and Fung, 2020; Khalil *et al.*, 2022)) identifying the system. While effective, high-fidelity model (e.g., explicit physics-based models) formulation is challenging and time-consuming for RBEs achieving dynamic thermal properties through sophisticated mechanisms. MPC requires the formulation of modeling, data collection, expert monitoring, and deployment, which leads to higher design and deployment costs, especially for complex systems with large solution spaces (Shaikh *et al.*, 2014). Moreover, learning characteristics of the whole environment and an accurate

model might not necessarily provide better performance under dynamic conditions in real-time applications. In addition, its heavy sensitivity to model errors makes it hard to establish fixed models/rules and ensure stable performance in a changing environment with high levels of variability (Santos-Herrero, Lopez-Guede and Flores-Abascal, 2021). To overcome these challenges, adaptive controllers (Alkhatib *et al.*, 2021) can reduce the sensitivity to uncertainties occurring in system dynamics through adjusting the model parameters based the real-time feedback from the system to promote its generalization in real-world applications.

1.3.4.3 Model-free control

On the contrary, as **Figure 1.13** shows, model-free approaches provide possibilities to eliminate the labor-intensive work of model formulation and calibration (Liu and Henze, 2006) for optimization. Especially some AI-based model-free control approaches such as model-free reinforcement learning (MFRL) (Zheng and Wang, 2002) algorithms can support efficient end-to-end online learning (Wang and Hong, 2020). The controller (agent) directly learns to make optimal decisions (actions) for building control using only several monitored indices (states) among numerous available data without any mathematical model of the real system (Michailidis *et al.*, 2018). Similar to adaptive control, MFRL controller can also flexibly adjust its parameters to reduce the discrepancy between its prediction and the real-time measured results from the environment with higher robustness in response to fluctuated disturbances/uncertainties (Sutton and Barto, G., 2018). Therefore, 'plug-and-play' (Baldi *et al.*, 2015; Michailidis *et al.*, 2018) controllers may be developed using MFRL methods while drastically reducing the controller and computational complexity for intricate RBE systems with satisfactory performance (Wang and Hong, 2020).

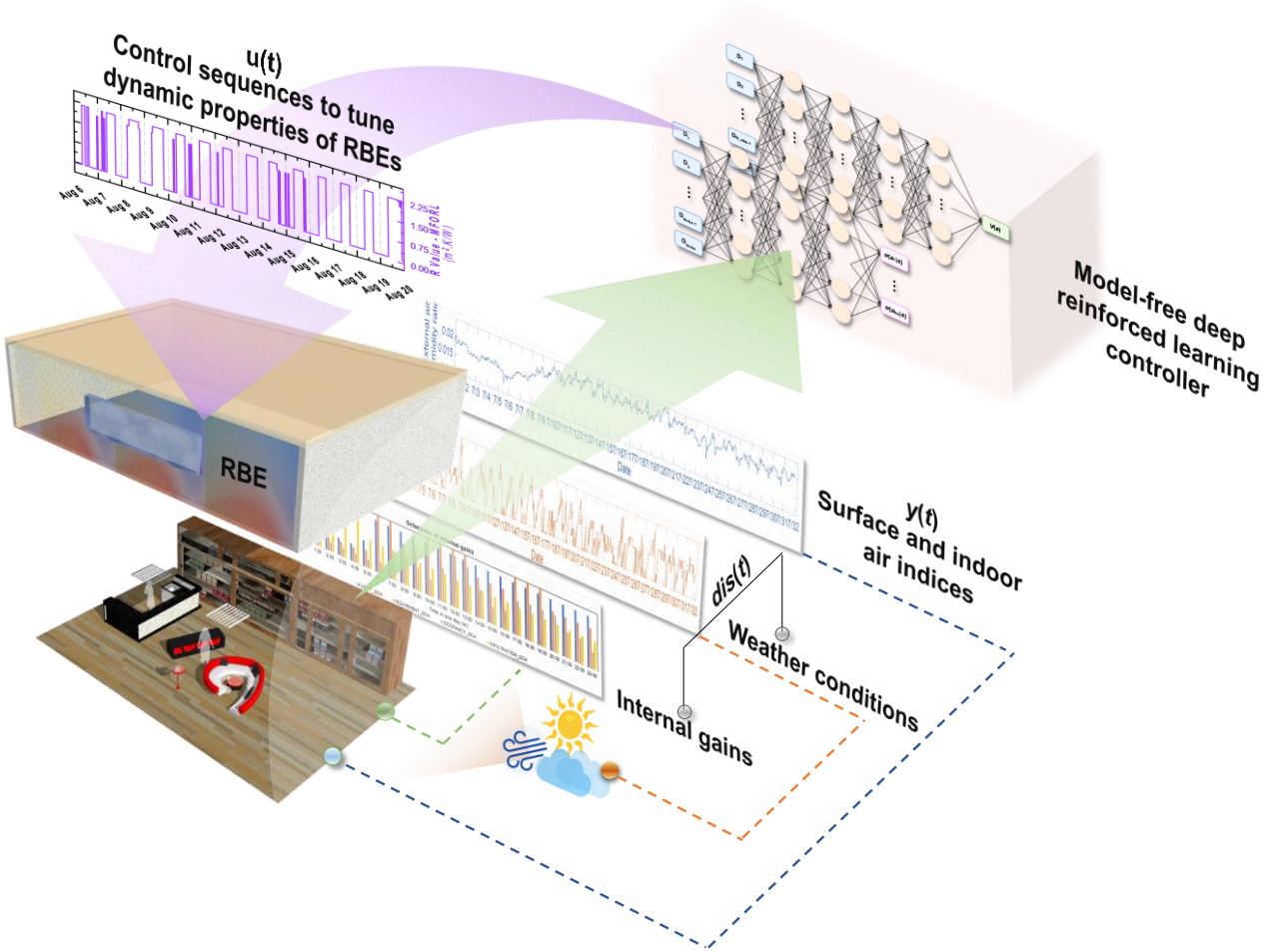


Figure 1.13 Schematic for model-free reinforced learning control of RBE

Although model-free control approaches have been applied in research for building control conducted by Yoon et al and Pinto et al (Yoon and Moon, 2019; Pinto *et al.*, 2021), no studies have investigated the potential of MFRL methods in leveraging strengths of the complex RBE systems to improve building energy performance through online learning. Furthermore, model-free controller design and training strategies for RBE systems remain very limited. Meanwhile finding pathways to attaining prominent performance using fewer data and lower training costs has been a crucial topic in this field (Wang and Hong, 2020).

In this dissertation, multiple control strategies are designed, deployed, and evaluated for buildings with RBEs. The formulation details for different control strategies are illustrated in CHAPTER THREE, CHAPTER FOUR, and CHAPTER FIVE.

1.3.5 Automation system for responsive building envelopes

The generic building automation systems (BAS) (or building management systems (BMS)/building energy management systems (BEMS)) (Trubiano, 2013) for responsive buildings encompass the building's services (e.g., lighting, energy generation and management, security, heat/cooling, ventilation, and air conditioning) and adaptive façades. Controlling the RBE as a component of the whole system is a challenging task in consideration of the performance demands in diverse aspects (e.g., robustness, energy use, healthcare, and environmental impacts), through the synergy of the three main types of hardware components, i.e., sensors, a central automation controller (CAC) and/or several local controllers for subsystems, and output devices. The sensors are used to monitor important indices (e.g., temperature, humidity, carbon

dioxide, light level and occupancy) and register events (e.g., abnormal activity, security breaches, and fire outbreaks). The CAC is a specialized computer that processes collected data and initiates the responses to external stimuli. The output devices such as relays and actuators implement the commands generated by the controller.

The BAS components communicate through pre-defined communications protocols/a specialized communications hub with integrated software provide scheduling, remote access, and a communications interface. The human-building interaction is generally achieved through dashboards or web interfaces at the workstations with access to controller to set preferences for systems operation, interact with appliances remotely and check device/sensor status. The workstation can be a panel PC with a comprehensive human machine interface (HMI), that communicates with the database through a gateway to extract and present the data collected by the sensors.

A representative BAS integrated with dynamic shading (Velikov K, 2013) monitors environmental changes and tracks inhabitant actions in different scenarios to maintain a balance between energy consumption and comfort performance by an adaptive living interface system, which provides real-time feedback and alerts users when occupant actions would promote energy savings.

1.4 Problem statement

The residential and commercial building sectors consume around 40% of the primary energy within the United States. The energy consumption in the built environment contributes to as much as 80% of demand at peak load conditions on the grid (Harris, 2019). Rather than relying solely on the generation side solutions to manage peak load, building systems can also aid in providing demand flexibility at

critical times. Developing smart envelope systems that can dynamically change their properties in response to signals can potentially lead to greater flexibility in operation and services provided to the electrical grid (Mumme and James, 2020). Ideally, the thermal properties of building envelopes should be attuned to the specific climate conditions to which they are subjected. However, due to the limitation of technologies, achieving variable insulation (i.e., variable R-value) has been the primary focus of current technology developments although there have been a few exploratory studies to investigate means to adjust/control the heat flow from and into the thermal mass of RBEs (Kishore *et al.*, 2021). The literature review shows that multiple technologies were proposed to achieve the responsive building envelope concept. However, most technologies are either conceptual or only tested as bench-scale prototypes. Some envelope designs show a high energy demand for changing their properties.

Furthermore, to date, only limited simulation tools are available that enable assessment of the effects of active insulation materials - EnergyPlus with the EMS modules has powerful capabilities to develop rule-based control algorithms for active insulation systems, but a more comprehensive simulation capacity is desired to integrate other dynamic features of the self-adaptive or responsive building envelopes using emerging novel techniques with complex mechanisms. Some knowledge gaps identified in other review work (Loonen *et al.*, 2017; Antretter and Boudreaux, 2019) and by this dissertation include:

❖ The research gaps in the research on modeling and simulation of RBE include:

- Although existing commercial simulation tools are applicable for building energy analyses of some dynamic envelopes (e.g., active insulation systems), they do not support analyses with universal availability for self-adaptive or responsive building

envelopes using emerging novel techniques with complex mechanisms with high computational efficiency.

- Existing commercial simulation tools are unavailable for flexible access to some parameters/settings desired for control of diverse novel RBE configurations. No versatile computational frameworks that can flexibly integrate multiple control strategies and building modules with high computational efficiency are available for the design and control of RBEs

❖ The knowledge gaps in the field of controlling for RBEs include:

- Traditional rule-based control strategies for AISs show limitations of overheating/overcooling effects. Although delicate controllers (e.g., MPC) with sophisticated models are effective, high design and deployment costs, especially for complex systems with large solution spaces make it hard to establish fixed models/rules and ensure high fidelity. An easy-to-implement rule-based control strategy with higher performance or a model-free control strategy without knowledge of complex systems is required for RBE systems.
- No previous studies have investigated the potential of MFRL methods in leveraging strengths of the complex RBE systems to improve building energy performance through online learning. No model-free online reinforced learning control and training frameworks (e.g., those using co-simulation testbeds) have been developed for RBE systems with high computational efficiency.
- model-free online controller design and training strategies for RBE systems remain very limited.

❖ The research on the application of diverse RBEs remains in its early stage with the following gaps to complement RBE design strategies:

- Previous research did not fully explore the potential of active insulation systems (AISs), particularly the systems with AISs integrated with high thermal mass for enhanced energy savings. AISs that can change R-value continuously with corresponding control strategies have not been thoroughly investigated.
- To date, only a limited number of studies on the performance of RBEs that integrate AISs, and self-adaptive/active functional modules (e.g., evaporative cooling techniques, dynamic glazing/shading) have been identified and further investigations are required to fully leverage the advantages of AISs.
- Design strategies are not well established for RBEs, e.g., RBE configuration design and applicability assessment of RBEs in different scenarios.

1.5 Research objectives and dissertation organization

To address these challenges, this dissertation describes a multidisciplinary study of the design, construction, and operation (control) of responsive building envelopes, with the goal of understanding mechanisms governing its dynamic properties and synthesis rules of multiple technologies/layers when desired. This will be accomplished through establishing a computational framework to design and optimize dynamic envelope properties and formulating a model-free reinforcement learning control method for autonomous performance regulation and self-adaptation. The strategy presented in this research represents an interactive and holistic way to design and operate building envelopes, allowing both energy and thermal comfort performances to be tuned for maximum efficiency. In this research, the applicability of different RBEs will be evaluated based on the energy-saving potential and thermal comfort of the various building types under different weather conditions and internal gains. Control

strategies for different RBE configurations in different scenarios will be formulated. RBE design and control implementation considerations will be discussed.

Specific research objectives of this dissertation will be obtained through the procedure outlined in **Figure 1.14** including:

- Develop widely applicable mathematical models that can be easily extended for multiple types of self-adaptive building envelopes with experimental calibration as well as responsive building envelopes with validation, in order to perform building energy analyses and AI-based offline training and learning analyses with high computational efficiency.
- Establish computational frameworks that integrate multiple control methods (e.g., rule-based control and model-free online reinforcement learning control methods) and building simulation models for the design and control of buildings with RBEs.
- Develop an easy-to-implement yet flexible rule-based control strategy with smart regulation to improve the energy and thermal comfort performance of traditional rule-based controllers for buildings with RBEs.
- Formulate a model-free online reinforced learning control framework using a co-simulation testbed for buildings with RBEs to investigate the behavior of the model-free controller within the sustainable and smart context as compared to the traditional rule-based controllers.
- Propose an efficient model-free online training and control strategy for RBEs with robust performance and high computational efficiency. Provide suggestions for model-free controller design and pretraining of RBE systems with low deployment costs (e.g., system operation, instrumentation, and maintenance).

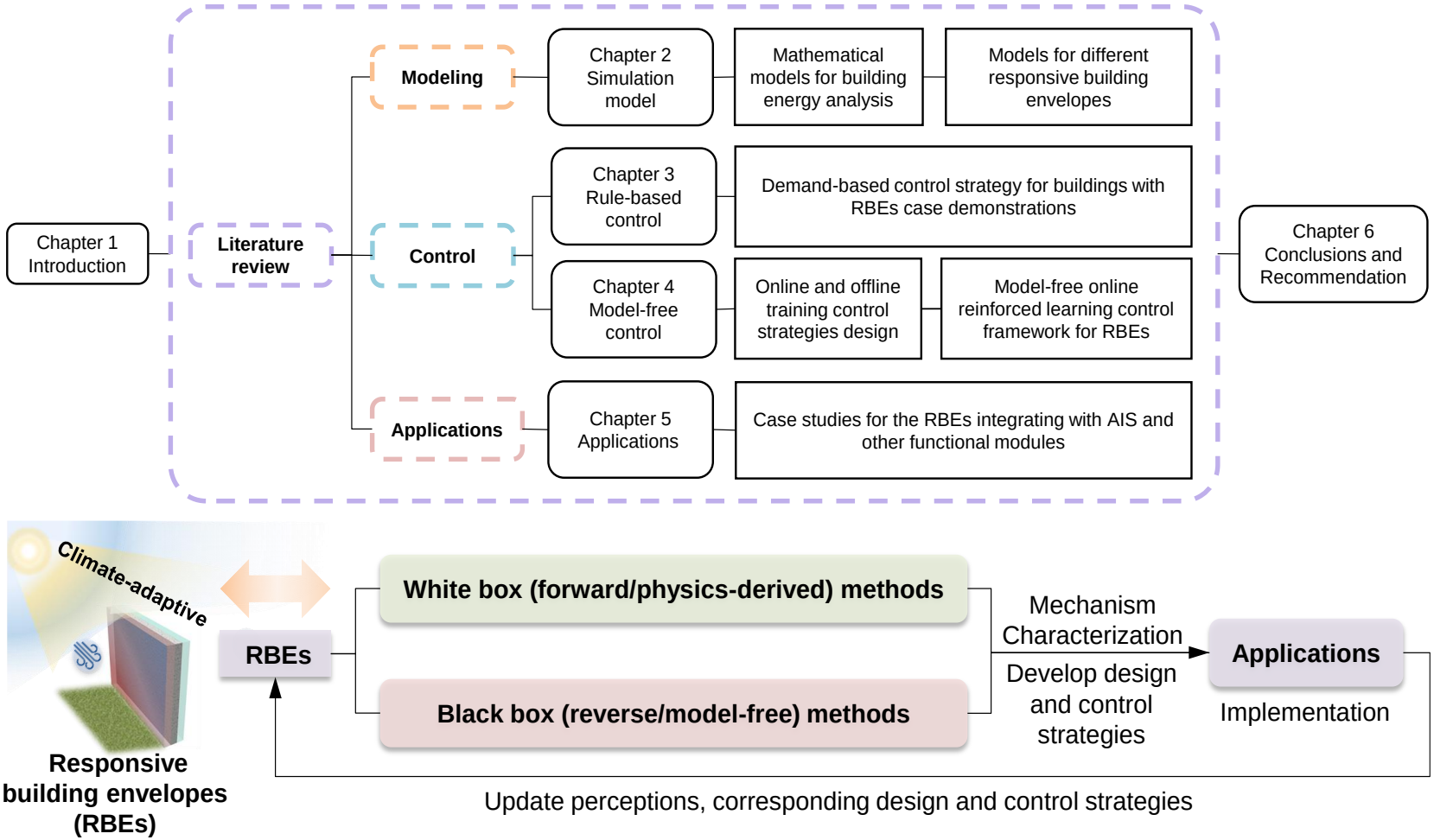


Figure 1.14 Schematic for the dissertation outline

- Characterize the underlying mechanisms governing the thermal behaviors of representative RBEs (e.g., the systems integrating AISs, evaporative cooling techniques, dynamic glazing/shading, and high thermal mass) and synthesis rules of multiple functional modules. Perform building energy analyses to quantify the energy-saving and thermal comfort performance of buildings with diverse RBEs.
- Develop design implications for RBEs, e.g., identifying requirements of variable insulation and assessing the applicability of these promising RBE configurations in diverse scenarios with multiple building types, climate conditions, and internal gains.

CHAPTER TWO
MODEL FORMULATION

To study thermal behaviors of the building with responsive building envelopes, a hydro-thermal network model based on a finite difference approach was established to perform energy analysis. **Figure 2.1** shows general forms of heat exchange and moisture balance considered in the building model. Heat exchanges with outdoor environments computed in the model include short-wave radiation, long-wave radiation, and convection applied on the surfaces. The energy balance of indoor air and interior wall surfaces, including the convective heat exchange with interior wall surfaces, air conditioner, and infiltration, long-wave and short-wave radiation from internal gains e.g., human activity, lighting, and equipment were considered for the indoor space heat exchange. The moisture balance of indoor air was also considered. Heat exchanges with glazing mainly consider radiation transmitted through windows, convective heat, short-wave and long-wave radiant interactions with indoor space, see **Figure 2.1**. The latent heat impact from self-adaptive techniques (e.g., transpiration within greenery systems or evaporative cooling roofs) was also considered when these techniques were adopted.

The model for building components with static properties and responsive envelope components eligible for active control, thermal comfort indices adopted in the analyses, and computation details are illustrated in the following sections. Section 2.1 elaborates on the model formulation for building energy systems with static properties. Section 2.2 illustrates model formulation for representative responsive building envelope components that can be modulated under active control.

2.1 Model of building components with static properties

2.1.1 Heat conduction through walls

The heat diffusion equation for any point with temperature $T(x, y, z)$ in a wall can be expressed as:

$$c_p(x,y,z)\rho(x,y,z)\frac{\partial T}{\partial t}=\left[\frac{\partial}{\partial x}\left(\lambda_x\frac{\partial T}{\partial x}\right)+\frac{\partial}{\partial y}\left(\lambda_y\frac{\partial T}{\partial y}\right)+\frac{\partial}{\partial z}\left(\lambda_z\frac{\partial T}{\partial z}\right)\right]+Q_V'''(x,y,z) \quad (2.1)$$

where t is time; c_p, ρ, and λ are the material's specific heat, density, and thermal conductivity, respectively; and $Q_V'''(x,y,z)$ is the rate of heat transferred from energy sources (e.g., solar radiant heat and latent heat). Other notations in the following equations can be found in the nomenclature in the Appendix.

For a differential control volume, Equation (2.1) is expressed as:

$$\int_V c_p(x,y,z)\rho(x,y,z)\frac{\partial T}{\partial t}dV=\int_V\left[\frac{\partial}{\partial x}\left(\lambda_x\frac{\partial T}{\partial x}\right)+\frac{\partial}{\partial y}\left(\lambda_y\frac{\partial T}{\partial y}\right)+\frac{\partial}{\partial z}\left(\lambda_z\frac{\partial T}{\partial z}\right)\right]dV+\dot{E}_V \quad (2.2)$$

where V is volume and $\dot{E}_V$ is the rate of heat transferred from energy sources/sinks in this differential control volume.

Each material layer is discretized into a number of finite volumes, where the energy balance method (Theodore L. Bergman, Frank P. Incropera, David P. DeWitt, 2011) is applied. Thus, Equation (2.2) can be rewritten as a general form for node i in a thermal network as:

$$\int_{V_i} c_p(x_i,y_i,z_i)\rho(x_i,y_i,z_i)dV_i\frac{\partial T_i}{\partial t}=H_i^{i-1}T_{i-1}+H_i^{i+1}T_{i+1}-\left(H_i^{i-1}+H_i^{i+1}\right)T_i+Q_i \quad (2.3)$$

where subscript i represents the node number; H_i^{i-1} is the heat transfer coefficient representing conduction between node i-1 and node i; Q_i is the rate of heat transfer from energy sources in the finite volume of node i.

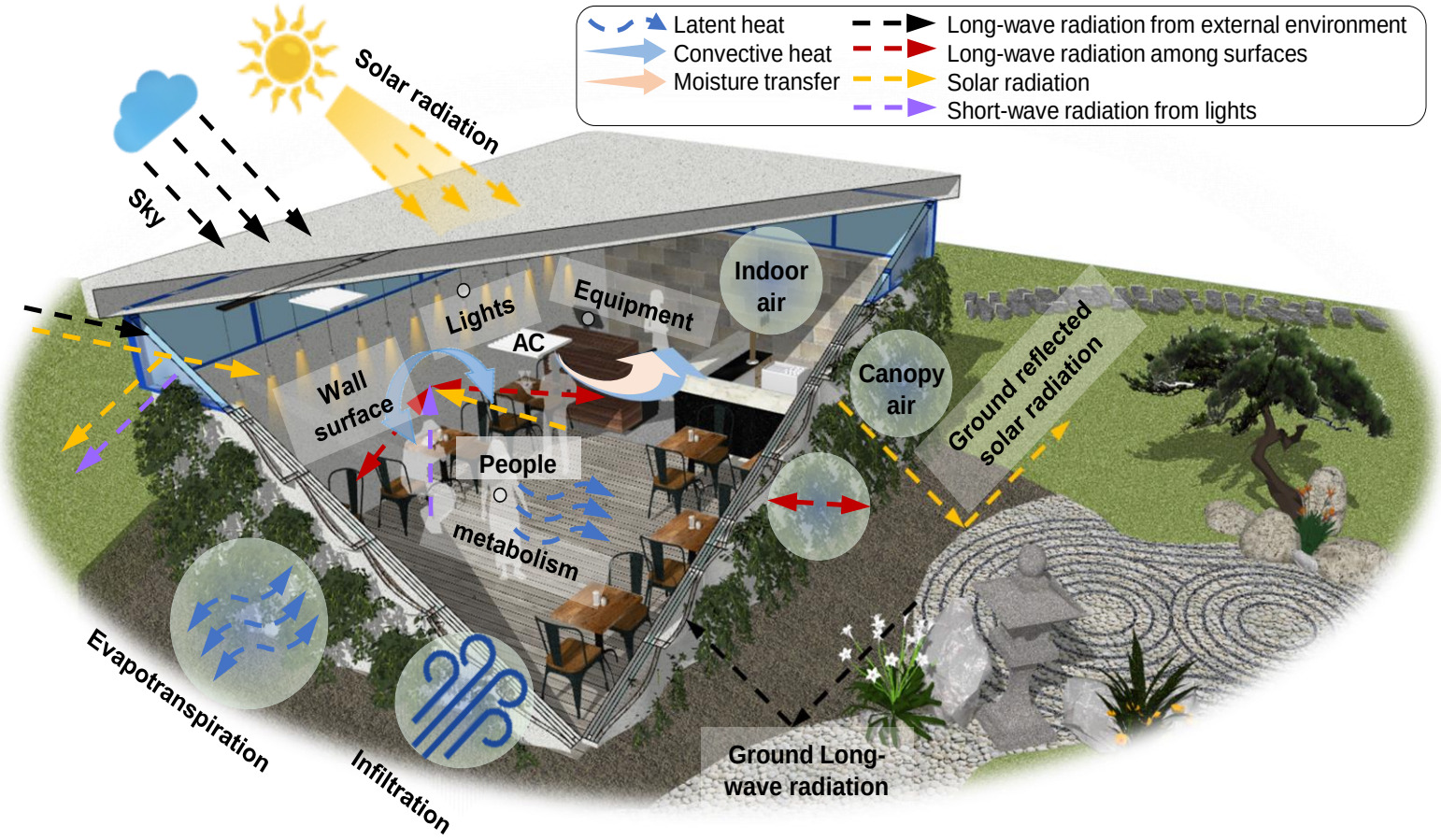


Figure 2.1 Schematic for normal heat exchanges within indoor and outdoor space

Thus, heat transfer among building components can be expressed by a nodal network of discretized wall layers and air. Wall layers include mass layers and no mass layers (e.g., ultra-lightweight components or material).

2.1.2 Heat balance within wall nodes

The heat transfer within the wall component can be expressed as one of the three node types:

(1) Exterior surface node

$$\rho_{i,w} c_{p,w} V_{i,w} \frac{dT_{i,w}}{dt} = H_{i,w}^{aw}\left(T_{aw} - T_{i,w}\right) + H_{i,w}^{i-1} T_{i-1} + H_{i,w}^{i+1} T_{i+1} - \left(H_{i,w}^{i-1} + H_{i,w}^{i+1}\right) T_{i,w} + Q_{i,sw,w} + Q_{i,lw,w} \tag{2.4}$$

$$Q_{i,sw,w} = \alpha_{i,w}(t) I_s^{\downarrow} A_{i,w} \tag{2.5}$$

$$Q_{i,lw,w} = \begin{bmatrix} F_i^{sky}\left(T_{sky,abs}^4 - T_{i,abs,w}^4\right) + F_i^{grd}\left(T_{grd,abs}^4 - T_{i,abs,w}^4\right) \\ + F_i^{air_ex}\left(T_{air_ex,abs}^4 - T_{i,abs,w}^4\right) \end{bmatrix} \cdot \sigma \varepsilon_{i,w} A_{i,w} + \sum_k \sigma \varepsilon_{i,w} F_i^k \left(T_{k,abs}^4 - T_{i,abs,w}^4\right) A_k \tag{2.6}$$

(2) Internal node

$$\rho_{i,w} c_{p,w} V_{i,w} \frac{dT_{i,w}}{dt} = H_{i,w}^{i-1} T_{i-1} + H_{i,w}^{i+1} T_{i+1} - \left(H_{i,w}^{i-1} + H_{i,w}^{i+1}\right) T_{i,w} \tag{2.7}$$

(3) Interior surface node

$$\rho_{i,w} c_{p,w} V_{i,w} \frac{dT_{i,w}}{dt} = H_{i,w}^{p}\left(T_p - T_{i,w}\right) + H_{i,w}^{i-1} T_{i-1} + H_{i,w}^{i+1} T_{i+1} - \left(H_{i,w}^{i-1} + H_{i,w}^{i+1}\right) T_{i,w} + Q_{i,sw,w} + Q_{i,lw,w} \tag{2.8}$$

$$Q_{i,sw,w} = \alpha_{i,w} I_s^{\downarrow} A_{i,w} + Q_{i,sw}^{light} \tag{2.9}$$

$$Q_{i,lw,w} = \sum_k \sigma \varepsilon_{i,w} F_i^k \left(T_{k,abs}^4 - T_{i,abs,w}^4\right) A_k + Q_{i,lw}^{people} + Q_{i,lw}^{light} + Q_{i,lw}^{equip} \tag{2.10}$$

where $H_{i,w}^{p}$ is heat transfer coefficient between air node *j* and wall node *i*; $\alpha_{i,b}$ is solar absorptance; $I_s^{\downarrow}$ is solar radiation incident; σ is Stephan-Boltzmann constant; ε is surface emissivity; F_i^k is view factor for node *i* with exterior emitting surface *k*.

2.1.3 Heat and moisture balance of indoor air

As is shown in **Figure 2.2**, the heat transfer process for indoor air includes convective heat exchange with interior wall and window surfaces, air conditioning, infiltration, and absorption of heat from internal gains $Q_{p,int}$ generated by occupant activity $Q_{p,conv}^{people}$, lighting $Q_{p,conv}^{light}$, and equipment $Q_{p,conv}^{equip}$. The heat balance of indoor air node *j* is expressed as:

$$\rho_p c_{p,p} V_p \frac{dT_p}{dt} = \sum_k H_p^k \left(T_k - T_p\right) + c_{p,p}\dot{m}_p^{sys}\left(T_{sup,p} - T_p\right) + c_{p,p}\dot{m}_p^{inf}\left(T_{air_ex} - T_p\right) + Q_{p,int} \quad (2.11)$$

$$Q_{p,int} = Q_{p,conv}^{people} + Q_{p,conv}^{light} + Q_{p,conv}^{equip} \quad (2.12)$$

where $\dot{m}_p^{sys}$ and $\dot{m}_p^{inf}$ are mass flow rate into the indoor zone for air node *p* from the air conditioner and outdoor air, respectively; $T_{sup,p}$ is the supply air temperature of air conditioner for indoor air node *p*.

The moisture balance for indoor air node *p* is:

$$\dot{W}_p = w_p^{int} + w_p^{sys} + w_p^{inf} \quad (2.13)$$

where W_p is the water mass of indoor air node *p*, w_p^{int}, w_p^{sys} and w_p^{inf} are moisture transfer rate for indoor air node *p* from internal latent heat gains, air conditioning system supply air, and infiltration.

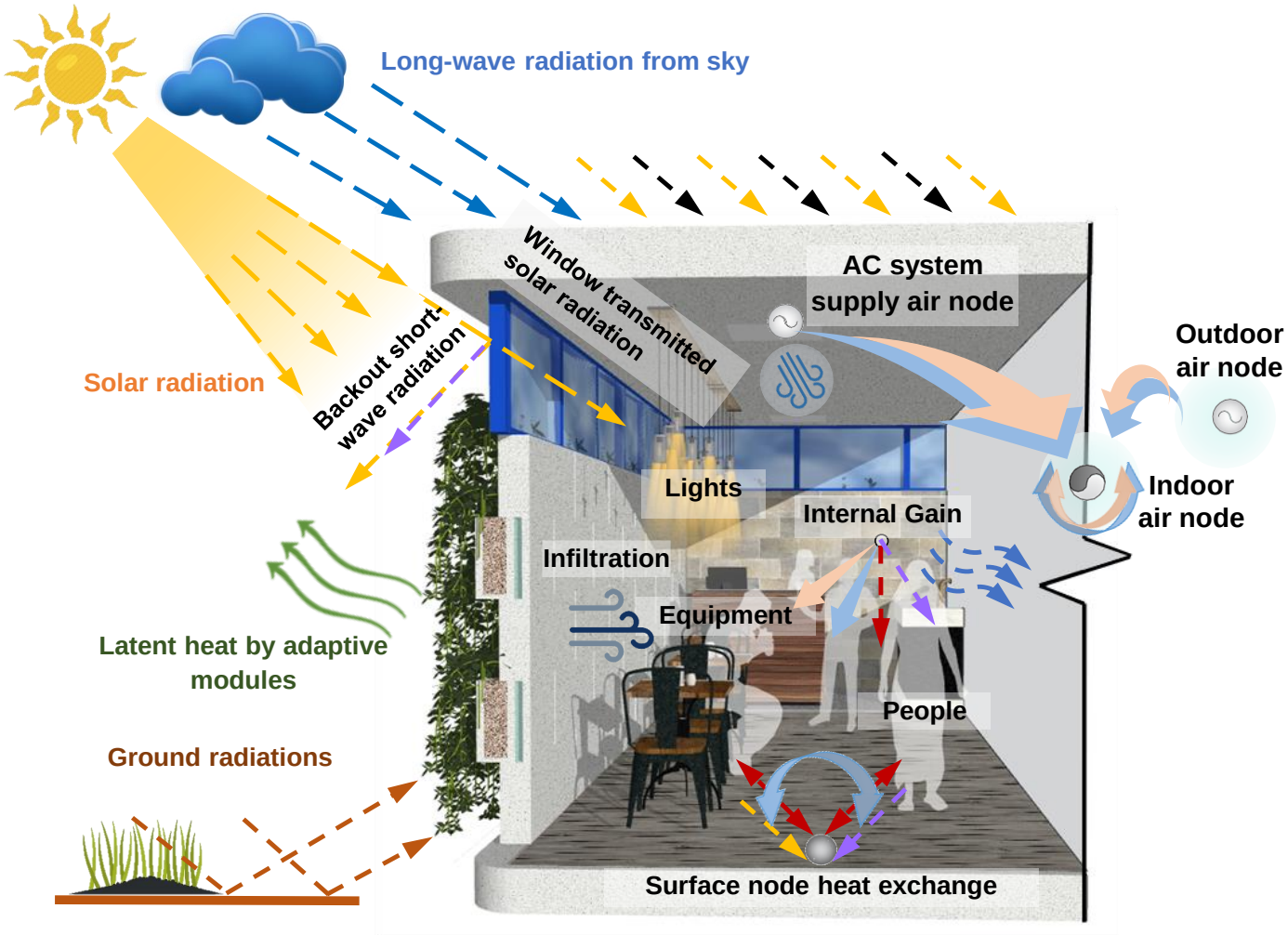


Figure 2.2 Schematic for heat exchanges with the indoor air node

For the infiltration rate estimation, several methods are available for building energy simulation (Goubran *et al.*, 2017), i.e., the design infiltration calculation method following the process proposed by ASHRAE, the seasonal design infiltration calculation method, the seasonal design infiltration simulation method using the airflow building models for the simulation software CONTAM (Dols and Polidoro, 2020) and the yearly infiltration simulation method using yearly transient airflow simulations by CONTAM. The infiltration rate can be generally estimated as a function of pressure difference across a crack or opening in the building envelope:

$$\dot{m}_p^{inf} = C_d A_{EL} \sqrt{2\Delta P \rho_{air_ex}} \tag{2.14}$$

where C_d is discharge coefficient; A_{EL} is effective leakage area; ΔP is the pressure drop across the crack or opening.

With this model, a whole-year transient simulation of the infiltration rate was performed on an apartment extracted from a building in San Francisco using CONTAM, with the results shown in **Figure 2.3**.

According to the comparisons among different methods in prior literature (Goubran *et al.*, 2017), the infiltration mass flow rates by the design methods are much higher than those obtained by yearly transient simulations. Therefore, in the DOE reference building models, a fixed infiltration rate magnitude is adopted in the simulations, which can consider the average impacts over a year (Deru *et al.*, 2011). Accordingly, fixed infiltration rate magnitudes with designated schedules varying in different scenarios are applied in the following simulation case studies.

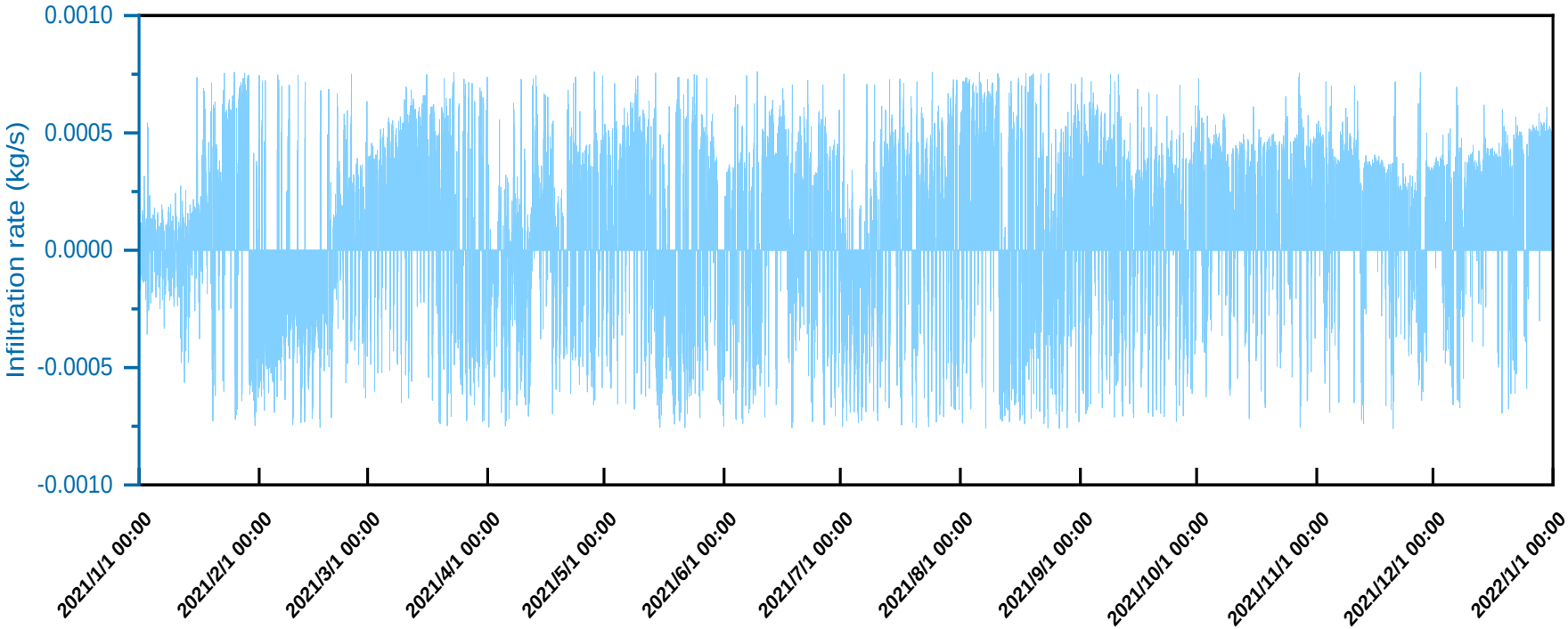


Figure 2.3 Infiltration rate of an apartment throughout a year in San Francisco

2.2 Model of responsive building envelopes for active control

In order to allow maximum flexibility in the implementation of AIS control, in this research a thermal network model based on a finite difference approach is established for building envelopes integrated with variable thermal mass and AISs. The 1-D heat transfer equation for any point with temperature *T* can be expressed as:

$$\frac{\partial(\rho h)}{\partial t} = \frac{\partial}{\partial x}\left(\lambda \frac{\partial T}{\partial x}\right) + q_v \tag{2.15}$$

$$c_p = \frac{\partial h}{\partial T} \tag{2.16}$$

where *h* is specific enthalpy; q_v is the rate of heat generated (or dissipated) within the material.

Considering material's specific heat $c_p(t,T)$ and thermal conductivity $\lambda(t)$ are variables as functions of time, Equation (2.15) can be written as:

$$\rho c_p(t,T)\frac{\partial T}{\partial t} = \lambda(t)\frac{\partial}{\partial x}\left(\frac{\partial T}{\partial x}\right) + q_v(t) \tag{2.17}$$

For a differential control volume as shown in **Figure 2.4**, Equation (2.16) is expressed as:

$$\int_V \rho c_p(t,T)\frac{\partial T}{\partial t}dV = \int_V \left[\lambda(t)\frac{\partial}{\partial x}\left(\frac{\partial T}{\partial x}\right)\right]dV + \dot{E}_V \tag{2.18}$$

$$\left[\begin{array}{l} \rho_i c_{p,i}^j \dfrac{\left(T_i^{j+1} - T_i^j\right)\Delta x_i}{\Delta t^j} \\ + f_{c_p}{}'\left(T_i^{j,j+1}\right)\rho_i \dfrac{\left(T_i^{j+1} - T_i^j\right)^2 \Delta x_i}{\Delta t^j} \end{array}\right] A = \lambda_{i-1}^j \frac{T_{i-1}^j - T_i^j}{\delta x_{i-1}} A + \lambda_i^j \frac{T_{i+1}^j - T_i^j}{\delta x_i} A + Q_i^j \tag{2.19}$$

where

$$c_p = f_{c_p}(T) \tag{2.20}$$

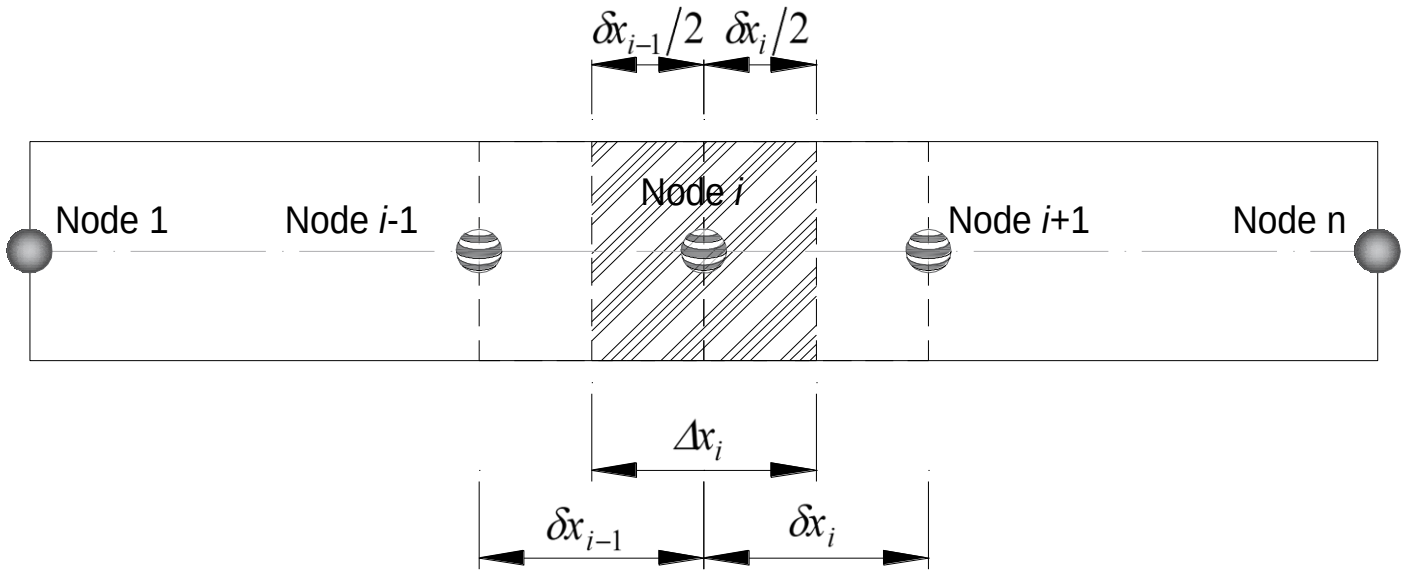


Figure 2.4 Finite difference representation of an RBE layer

Equation (2.19) can be approximated as the following equation in the scenario under a small time step or when the *h*-T relation is linear.

$$\left[\rho_i c_{p,i}^{j}\frac{\left(T_i^{j+1}-T_i^{j}\right)\Delta x_i}{\Delta t^{j}}+\frac{1}{2}\rho_i\frac{\left(c_{p,i}^{j+1}-c_{p,i}^{j}\right)\left(T_i^{j+1}-T_i^{j}\right)\Delta x_i}{\Delta t^{j}}\right]A=$$
$$\lambda_{i-1}^{j}\frac{T_{i-1}^{j}-T_i^{j}}{\delta x_{i-1}}A+\lambda_i^{j}\frac{T_{i+1}^{j}-T_i^{j}}{\delta x_i}A+Q_i^{j} \tag{2.21}$$

where subscript *i* represents the nodal number; superscript *j* represents the j^{th} time step; *A* is the surface area of the finite volume represented by node *i*; Q_i^j is the rate of heat transfer from energy sources in the finite volume of node *i* at j^{th} time step.

Each layer of the RBE can be discretized into a number of finite volumes represented by a nodal network. Thus, finite difference method can be applied:

Equation (2.21) can be further rewritten as a general form for node *i* in a thermal network as:

$$\left(C_i^j+\frac{1}{2}\Delta C_i^j\right)\left(T_i^{j+1}-T_i^{j}\right)=\left[H_{i-1,i}^{j}T_{i-1}^{j}+H_{i+1,i}^{j}T_{i+1}^{j}-\left(H_{i-1,i}^{j}+H_{i+1,i}^{j}\right)T_i^{j}+Q_i^{j}\right]\Delta t^{j} \tag{2.22}$$

where C_i^j is the thermal capacitance of node *i* at j^{th} time step; $H_{i-1,i}^{j}$ is the heat transfer coefficient representing conduction between node *i*-1 and node *i* with variable thermal properties at j^{th} time step:

$$\begin{aligned}
C_i^j &= \rho_i c_{p,i}^{j}\Delta x_i A\\
\Delta C_i^j &= \rho_i\left(c_{p,i}^{j+1}-c_{p,i}^{j}\right)\Delta x_i A\\
H_{i-1,i}^{j} &= \lambda_{i-1}^{j}\frac{A}{\delta x_{i-1}}\\
H_{i+1,i}^{j} &= \lambda_{i+1}^{j}\frac{A}{\delta x_i}
\end{aligned} \tag{2.23}$$

For an AIS with negligible thermal mass (David K. Benson, Potter and Tracy, 1994; Varga, Oliveira and Afonso, 2002; Kimber, Clark and Schaefer, 2014; Loonen,

Hoes and Hensen, 2014; Wu *et al.*, 2014; Park, Srubar and Krarti, 2015; Pflug *et al.*, 2015, 2018; Tomko *et al.*, 2018), it can be represented by a 'no-mass layer' consisting of two nodes – one capture the convective and radiant heat transfer from the exterior environment, while another connected to the internal nodes for conduction. Thus, the AIS with negligible thermal mass in a thermal network may be represented as:

$$\left(H_{i-1,i}^{j}+H_{i+1,i}^{j}\right)T_{i}^{j}=H_{i+1,i}^{j}\,T_{i+1}^{j}+H_{i-1,i}^{j}\,T_{i-1}^{j}+Q_{i}^{j} \tag{2.24}$$

where the time-varying heat transfer coefficient $H_{k,i}^{j}$ between node *k* and node *i* with variable insulation at time t^{j} can be adjusted to regulate the amount of heat flow into indoor space. In different AIS designs, the heat transfer coefficient can either be idealized as a binary function where its insulation value 'switches' between two values (Equation (2.25)) or gradually in response to the environmental stimuli (Equation (2.26)):

$$H_{k,i}^{j}=f_{binary}\left(t^{j},T^{j},Q^{j}\right)=\begin{cases}H_{high} & \text{criterion 1}\\ H_{low} & \text{criterion 2}\end{cases} \tag{2.25}$$

$$H_{k,i}^{j}=f_{continous}\left(t^{j},T^{j},Q^{j}\right) \tag{2.26}$$

As **Figure 2.5** shows, a representative RBE layout is a high thermal mass concrete layer sandwiched between two active insulation (or AIS) layers, to allow for load shifting capabilities. In this configuration, the thermal resistances (R-values) of the exterior and interior AISs can be separately controlled (Antretter and Boudreaux, 2019). During the heating season, the thermal resistance of the external AIS layer can be lowered when the exterior air temperature is higher than the temperature of the thermal mass to allow the thermal mass to be 'charged'; otherwise, the exterior AIS is switched to 'insulative' mode to minimize heat loss of the concrete thermal mass.

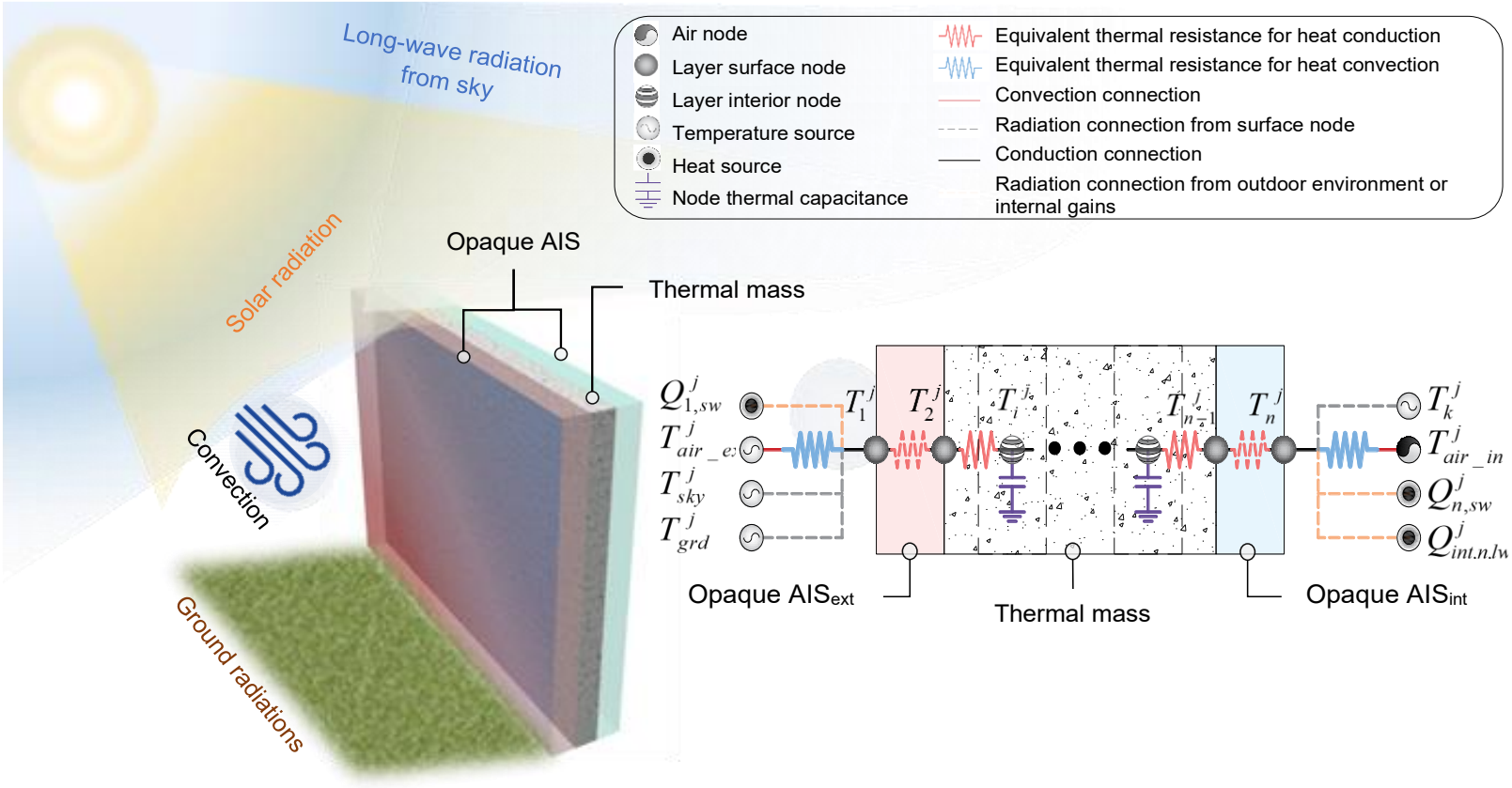


Figure 2.5 Schematic for the node scheme of synthesis of mass wall and opaque AISs

For a given moment when heating is needed and the temperature of the thermal mass is higher than that of the interior air, the thermal conductivity of interior AIS can be increased to offset the AC system demand. The same logic applies to the cooling season to discharge/precool the thermal mass when outdoor air temperatures are lower than the thermal mass while utilizing the 'precooled' thermal mass to reduce cooling loads. This design has been proven more effective than other layouts in previous studies (Jin, Favoino and Overend, 2017; Antretter and Boudreaux, 2019). Since this RBE layout combines the benefits of active insulation (AIS) and thermal energy storage (TES), it is also referred as to TES-AIS integrated RBE (Mumme and James, 2020; Kishore *et al.*, 2021).

Details of the control logic will be elaborated in CHAPTER THREE. A representative nodal scheme for the responsive building envelope with the synthesis of the mass wall (mass layer) and the AISs (no-mass layer) is presented in **Figure 2.5**.

For this configuration with dynamic properties, considering the heat flow from short-wave radiation $Q_{1,sw}^{j}$, long-wave radiation $Q_{1,lw}^{j}$ and convection acting on the exterior AIS (opaque, no solar transmission), Equation (2.24) can be rewritten as:

$$\left(H_{air_ex,1}^{j}+H_{2,1}^{j}\right)T_{1}^{j}=H_{2,1}^{j}T_{2}^{j}+H_{air_ex,1}^{j}\,T_{air_ex}^{j}+Q_{1,sw}^{j}+Q_{1,lw}^{j} \tag{2.27}$$

$$Q_{1,sw}^{j}=\alpha_{1}I_{s,1}^{\downarrow,j}A_{1} \tag{2.28}$$

$$Q_{1,lw}^{j}=\left\{\begin{array}{l}F_{1}^{sky}\left[\left(T_{sky,abs}^{j}\right)^{4}-\left(T_{1,abs}^{j}\right)^{4}\right]+F_{1}^{grd}\left[\left(T_{grd,abs}^{j}\right)^{4}-\left(T_{1,abs}^{j}\right)^{4}\right]\\ +F_{1}^{air_ex}\left[\left(T_{air_ex,abs}^{j}\right)^{4}-\left(T_{1,abs}^{j}\right)^{4}\right]\end{array}\right\}\\ \cdot\sigma\varepsilon_{1}A_{1}+\sum_{k}\sigma\varepsilon_{1}F_{1}^{k}\left[\left(T_{k,abs}^{j}\right)^{4}-\left(T_{1,abs}^{j}\right)^{4}\right]A_{k} \tag{2.29}$$

where $H_{2,1}^{j}$ is heat transfer coefficient at j^{th} time step between node 1 (exterior surface of AIS) and node 2 (exterior surface of the concrete layer) – $H_{2,1}^{j}$ is a time variant

determined by the control sequence; α_1 is constant solar absorptance of exterior active insulation surface. F_1^k is the view factor for node 1 with exterior emitting surface *k* – i.e., wall or window surfaces.

The interior surface node considers short-wave radiation from lighting ($Q^j_{light,n,sw}$), and long-wave radiation from occupant activities, lighting, and equipment ($Q^j_{people,n,lw}$, $Q^j_{light,n,lw}$, $Q^j_{equip,n,lw}$). Thus, the heat balance equation for interior surface nodes can be expressed as:

$$\left(H^j_{n-1,n} + H^j_{air_in,n}\right)T^j_n = H^j_{n-1,n}T^j_{n-1} + H^j_{air_in,n}T^j_{air_in} + Q^j_{n,sw} + Q^j_{n,lw} \tag{2.30}$$

$$Q^j_{n,sw} = \alpha_n I^{\downarrow,j}_{s,n} A_n + Q^j_{light,n,sw} \tag{2.31}$$

$$Q^j_{n,lw} = \sum_k \sigma\varepsilon_n F^k_n \left[\left(T^j_{k,abs}\right)^4 - \left(T^j_{n,abs}\right)^4\right]A_k + Q^j_{people,n,lw} + Q^j_{light,n,lw} + Q^j_{equip,n,lw} \tag{2.32}$$

The heat balance equation for the thermal node at the AIS-concrete interface and the internal nodes within the concrete wall layer follows the formulation of typical mass walls as:

$$C^j_i T^{j+1}_i = C^j_i T^j_i + \left[H^j_{i-1,i}\,T^j_{i-1} + H^j_{i+1,i}\,T^j_{i+1} - \left(H^j_{i-1,i} + H^j_{i+1,i}\right)T^j_i + Q^j_i\right]\Delta t^j \tag{2.33}$$

2.3 Thermal comfort

Thermal comfort indices i.e., the Predicted Mean Vote (PMV) and Predicted Percentage of Dissatisfied (PPD) based on Frager's model (ISO, 2005) were used to evaluate the thermal comfort-time performance of buildings. PMV predicts the mean value of the votes of a large group of people considering the influence of indoor environments (humidity, air temperature, velocity, and mean radiant temperature) and human metabolism, while PPD gives a quantitative prediction for the percentage of thermally dissatisfied occupants shown as the following function of PMV:

$$PPD = 100 - 95e^{-0.03353PMV^4 - 0.2179PMV^2} \tag{2.34}$$

The Long-term Percentage of Dissatisfied (LPD) reflects occupants' long-term thermal comfort (Carlucci, 2013) defined by the following equation:

$$LPD(p, PPD) = \frac{\sum_{n=1}^{N}\sum_{r=1}^{R}\left(p_r^j \cdot PPD_r^j \cdot \Delta t^j\right)}{\sum_{j=1}^{N}\sum_{r=1}^{R}\left(PPD_r^j \cdot \Delta t^j\right)} \tag{2.35}$$

where p_r^j is the occupation rate at j^{th} time step for r^{th} zone; PPD_r^j is the percentage of dissatisfied; Δt^j is time step duration. This normalized index gives an overall impression of the building's thermal comfort performance for all the occupants over the whole time. Frager's model was used to calculate PPD for LPD computation.

2.4 State-space representation and computation details

The whole building simulation model is the network assembling of all the wall layer nodes and air nodes, based on heat and moisture balance equations. The state-space representation (Kim and Braun, 2015) of the thermal network can then be written as:

$$\begin{aligned} &\tilde{C} = \begin{bmatrix} \tilde{C}_L & 0 \\ 0 & \tilde{C}_A \end{bmatrix}; \tilde{M} = \begin{bmatrix} \tilde{M}_L & 0 \\ 0 & \tilde{M}_A \end{bmatrix}; \vec{T} = \begin{bmatrix} \vec{T}_L \\ \vec{T}_A \end{bmatrix} \\ &\tilde{H} = \begin{bmatrix} \tilde{H}_{LL} & \tilde{H}_{LA} \\ \tilde{H}_{AL} & \tilde{H}_{AA} \end{bmatrix}; \vec{Q} = \begin{bmatrix} \vec{Q}_L \\ \vec{Q}_A \end{bmatrix} \end{aligned} \tag{2.36}$$

$$\tilde{C}\tilde{M}\dot{\vec{T}} = \tilde{H}\vec{T} + \vec{Q} \tag{2.37}$$

The building's thermal behavior is solved by the discrete state space model through discretization of time:

$$\vec{T}_{n+1} = \left(E + \Delta t \tilde{C}^{-1} \tilde{M}^{-1} \tilde{H}\right) \vec{T}_n + \Delta t \tilde{C}^{-1} \tilde{M}^{-1} \vec{Q} \tag{2.38}$$

where $\tilde{C}$ is the thermal capacitance matrix; $\tilde{M}$ is the modification matrix for surface nodes; $\tilde{H}$ is the heat transfer matrix; E is identical matrix; $\vec{T}$ is the node temperature vector; $\vec{Q}$ is the rate of heat exchange for nodes from different sources. Subscript L refers to thermal nodes representing wall, window, foliage, and soil; subscript A refers to air nodes (zone air or canopy air). As **Figure 2.6** presents, the 3-D heat transfer process and moisture balance of buildings with multiple thermal zone can be represented by assembling a nodal network that represents the interactions among all the wall layer nodes, air nodes and diverse disturbances (e.g., changes in outdoor environment and internal gains) that represented by temperature and heat source nodes. With these efficient nodal schemes, the thermal networks can flexibly integrate diverse RBE modules (e.g., AIS, dynamic glazing/shading, greenery systems, PCM, evaporative foam panels) into building energy simulations with promising computational performance.

The general building simulation procedure using thermal network models are presented in **Figure 2.7**. In the heat balance equation, long-wave radiation is linearized using the same method performed in reference (Deardorff, 1978). Simple glazing system model (Berkeley *et al.*, 2019) was used for windows in this building model, in which the window layer is a no-mass layer. Models in reference (Berkeley *et al.*, 2019) were adopted for calculating internal gains from occupants, lighting, and equipment. For each time step, heat balance and moisture balance were computed separately.

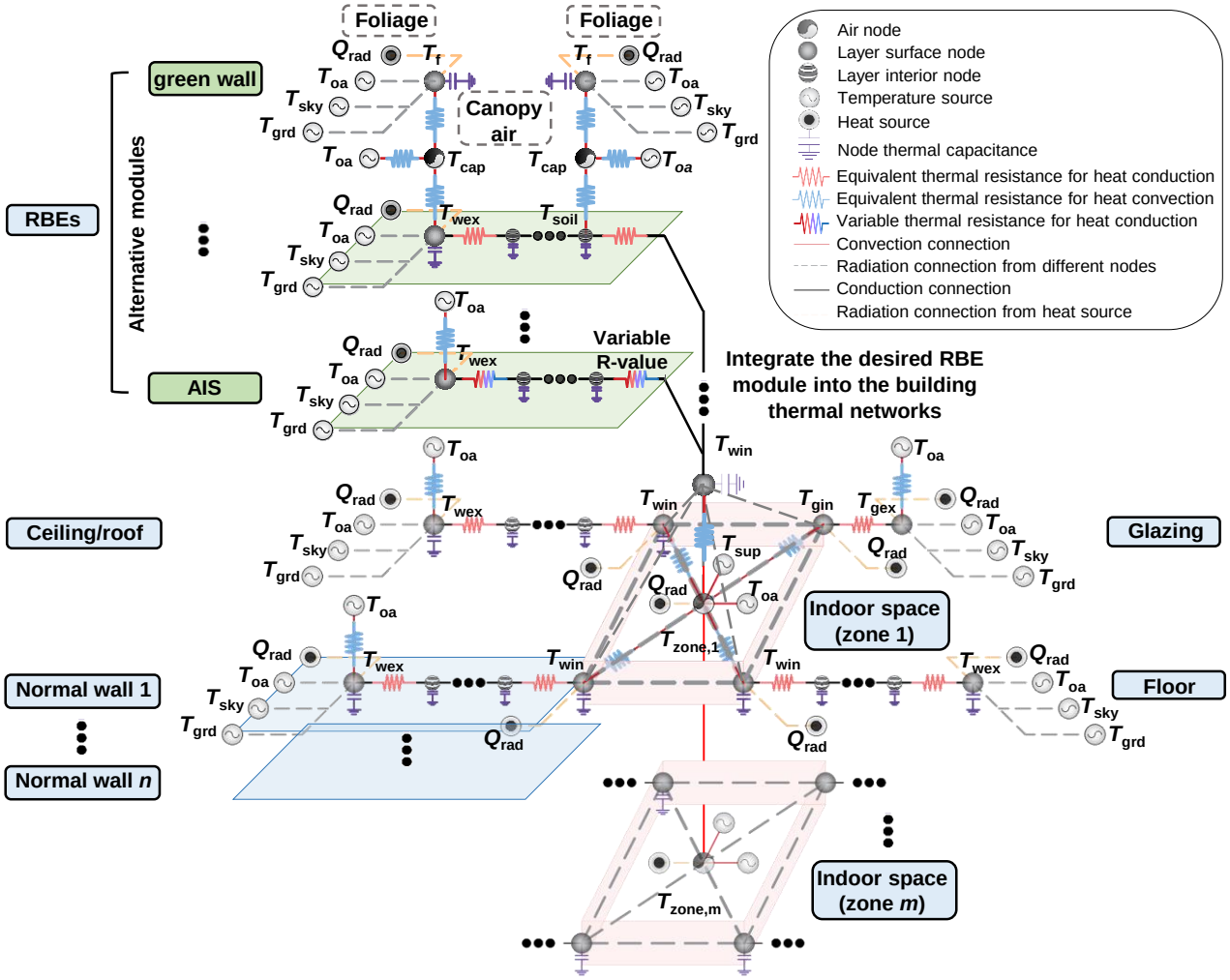


Figure 2.6 Schematic for the thermal network integration of RBEs into building simulations

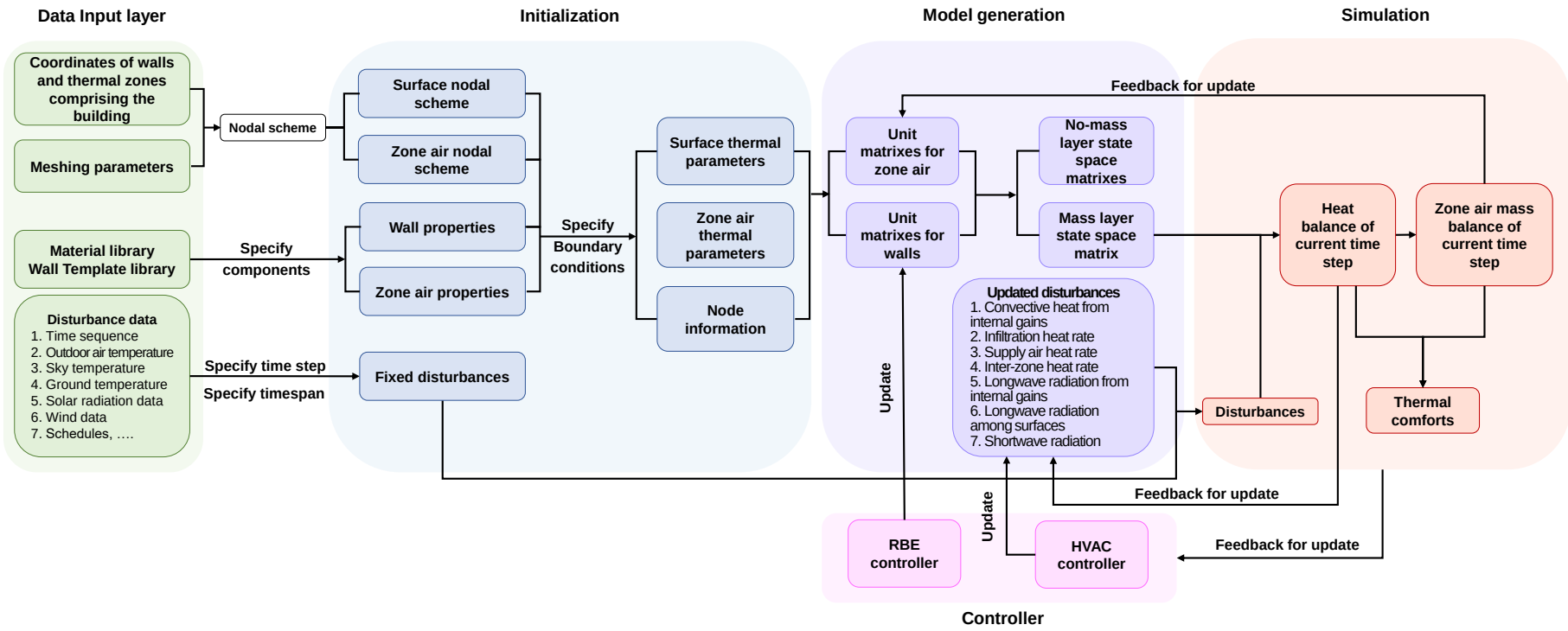


Figure 2.7 Schematic for building simulation procedure

2.5 Model validation

To validate the thermal network model for the whole-building energy analysis with the RBE, simulations were performed on a single-zone house as shown in **Figure 2.8** and the results were compared to those obtained from EnergyPlus simulations.

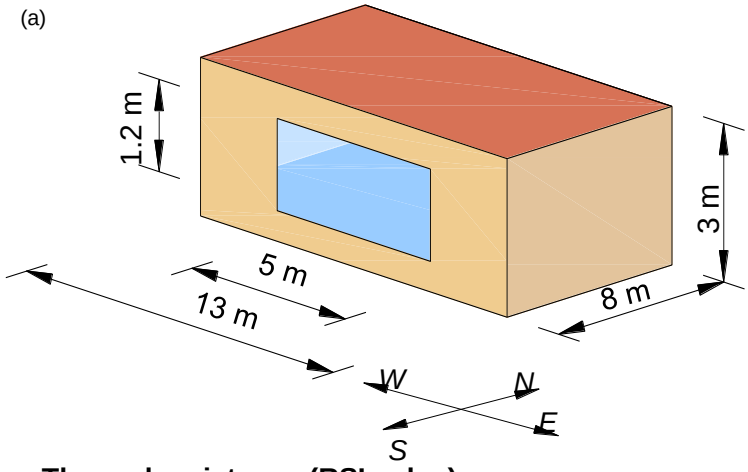
The house has an RBE with a 15% window ratio on its south exterior walls, floor, and roof. The dimension of the single-room building is 13 m (L) × 8m (W) ×3.05 m (H). The RBE consists of a 100-mm thick concrete layer sandwiched between two opaque AIS layers with (R_{low} =0.01 Km^2/W and R_{high} =1.5 Km^2/W). The RSI-values of other exterior walls, floor, and roof are enlisted in **Figure 2.8** according to ASHRAE 90.1. Typical meteorological year 3 (TMY3) weather data of San Francisco is used for the simulation. The U-value of the glazing is 2.0 $W/(K\ m^2)$. The window solar heat gain coefficient (SHGC) is 0.1, which is compliant with ASHRAE-90.1 (ASHRAE, 2019) and within the available range according to NFRC (Council, 2013). The solar absorptance of all the walls was 0.7 and the surface emissivity of all the walls was 0.9, which are commonly used (Berkeley L, Ridge OAK, Ut-battelle MBY, For A, Energy S, Or D, 2019). The indoor air temperature was controlled by a constant air volume (CAV) HVAC system with dual setpoints of 21.1-23.9℃. The selection of this neutral band is based on prior research (ADVANCED RESEARCH PROJECTS AGENCY – ENERGY (ARPA-E) U.S. DEPARTMENT OF ENERGY, 2014). The other simulation details are enlisted in **Figure 2.8** (a).

For the thermal network model, the heat balance of indoor air considers convective heat exchange with interior wall and window surfaces, air conditioning, infiltration, and absorption of heat from internal gains generated by occupant activity, lighting, and equipment. The influence of air conditioning, infiltration, and human

activity on the moisture balance of indoor air was also considered whereas the influence of moisture on wall thermal properties was neglected. The 3-D heat transfer process of a thermal zone was represented by assembling a nodal network that represents the interactions among all the wall layer nodes and air nodes following a general approach proposed by Kim et al. (Kim and Braun, 2015). Detailed formulations for the building envelope, interior partitions, and indoor air represented by a nodal network for a single-zone building can be found in the previous work of the authors (He *et al.*, 2020). In numerical computation, long-wave radiation is linearized using the same method as detailed in (Deardorff, 1978). Simple glazing system model (Berkeley *et al.*, 2019) was used for windows in this building model, where the window layer is assumed as a no-mass layer. At each time step, the heat balance and moisture balance of indoor air were computed separately.

Figure 2.8 (b) presents the outdoor air temperature, RSI-value settings of the exterior and interior AISs, and the simulated surface temperatures, as well as the indoor air temperature obtained by both the thermal network and EnergyPlus models. It can be seen that the simulation results match closely. The CV-RMSE (coefficient of variation of the root mean square error) and NMBE (normalized mean bias error) of energy consumption (district heating or cooling) are calculated at 3.6% and 1.5%, respectively, which are both well under the ASHRAE Guideline 14 (Monetti *et al.*, 2015) (i.e., <30% CV-RMSE and <10% NMBE for hourly data), indicating acceptable accuracy of the thermal network model.

(a)



Thermal resistance (RSI-value)
Roof: 2.4 (K·m^2)/W
Exterior wall: 1.5 (K·m^2)/W
Floor: 4.6 (K·m^2)/W

Equipment
Amplitude: 5.38 W/m^2
Lights
Amplitude: 3.88 W/m^2
People
Amplitude: 2.5 people
Infiltration
Amplitude: 0.000302 m^3/s per unit envelope area

CAV system
Supply air mass rate
Heating: 0.13 m^3/s
Cooling: 0.2 m^3/s

(b)

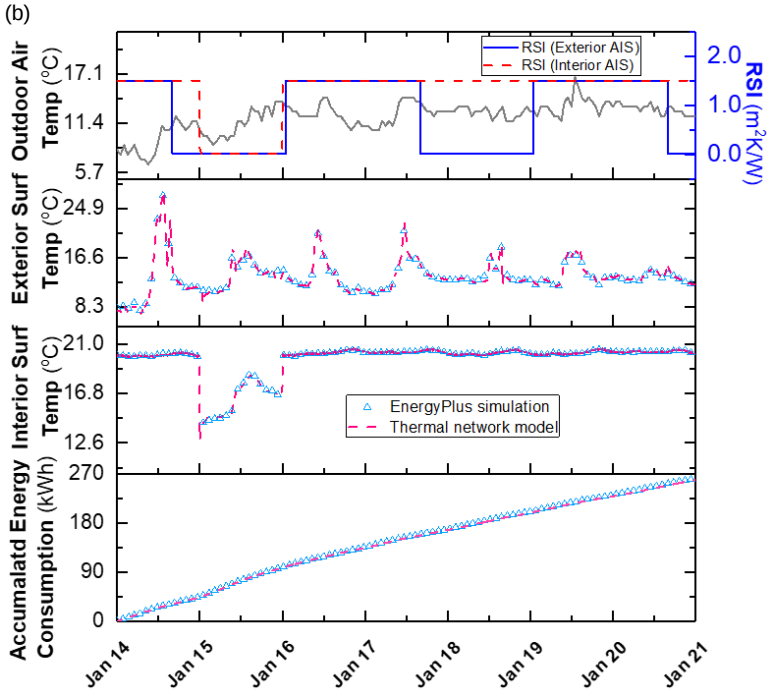


Figure 2.8 (a) Isometric view of the building modeled for calibration; (b) Comparison of the simulation results between the thermal network model and EnergyPlus

2.6 Computational framework

To identify the underlying mechanisms that RBEs work in different scenarios for design and control implications (e.g., applicability of diverse RBE types) to fully leverage the advantages of RBEs and construct smart and sustainable built environments, building energy analyses with multiple RBEs using different control strategies are required. To this end, a versatile computational framework that enables flexible integration of buildings with diverse functional modules and control strategies was developed in this dissertation displayed in **Figure 2.9**, which can be deployed for building/infrastructure energy analyses, validation/experimental calibration, offline training, and online training and control/co-simulation implementation. This framework mainly comprises four components, i.e., the control panel available for white box (forward/physics-derived) and black box (reverse/model-free) control strategies, the physical system/plant to be controlled, the panel for initialization and parameter settings and the data exchange layer or co-simulation platform when online training and control or validation/experimental calibration is applied. The physical system/plant can be a real system or represented by commercial software (e.g., EnergyPlus) or thermal network models coded by MATLAB that can be easily extended for multiple functional building/infrastructure components with high computational efficiency. To perform building energy analyses, the whole computational framework is initialized with parameter settings, including assigning building/infrastructure configurations with geometric parameters, corresponding material properties, schedules of occupancy, lighting and equipment, importing weather data, configuring controller settings of responsive modules and HVAC, and computation settings (e.g., nodal scheme generation, initial conditions, thermal comfort models, evaporation/transpiration models, parallel computation, co-simulation, data processing/export, online/offline training and calibration).

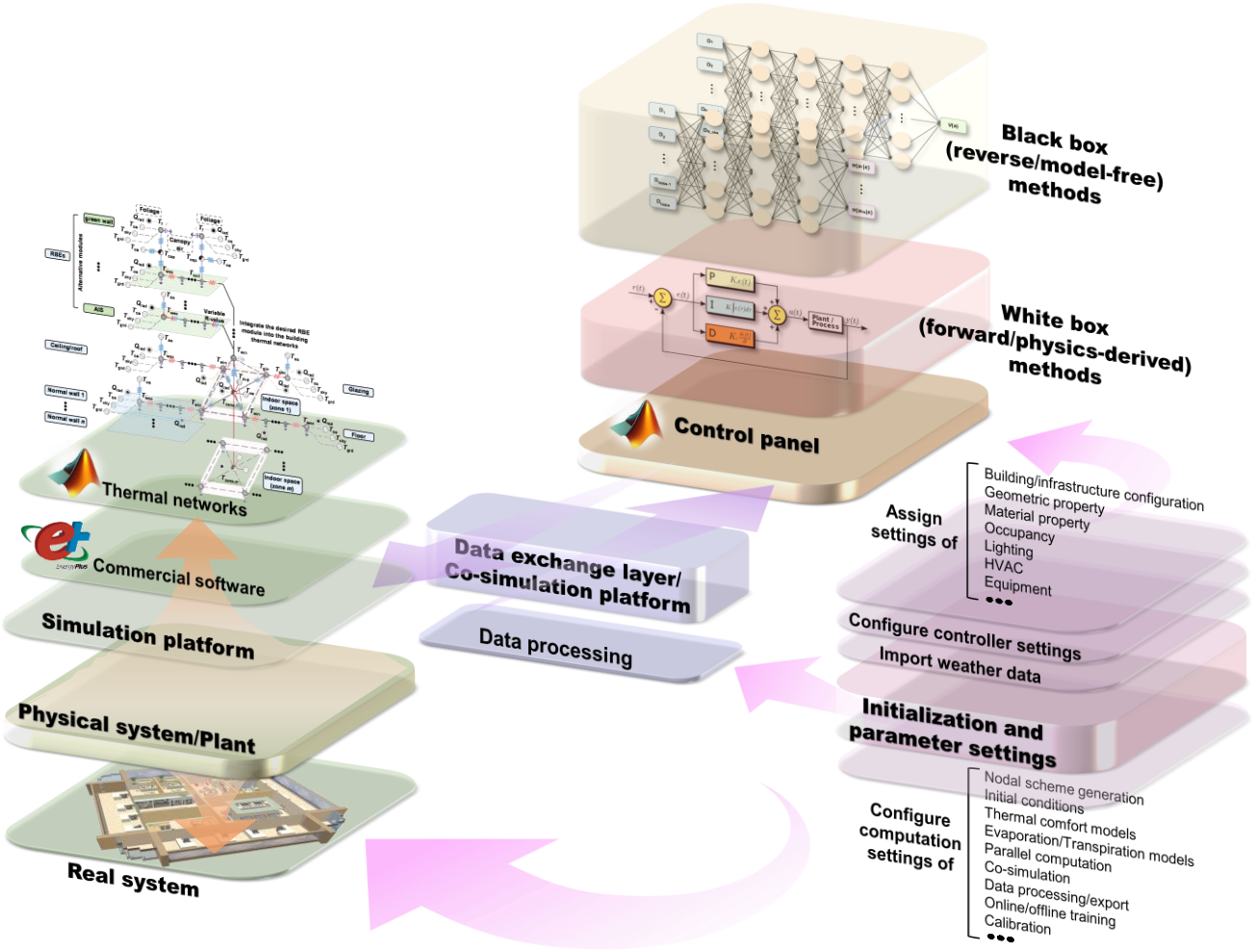


Figure 2.9 Schematic for the versatile computational framework integrating buildings with diverse modules and control strategies

CHAPTER THREE
DEMAND-BASED CONTROL FOR RBE

Although it has been well demonstrated that responsive building envelope (RBE) has tremendous potential to improve the building's energy performance by dynamically providing passive cooling/heating to reduce energy consumption, there is still a significant gap in formulating the control strategy of such systems. In particular, for RBEs that integrate active insulation systems (AISs) and high thermal mass, the formulation of optimal control rules for such systems is challenging. To address these challenges, in this chapter, an easy-to-implement yet flexible 'demand-based' control rule is formulated based on demand analysis to project the 'desired' thermal resistance of the AIS layers such that it beneficially utilizes the heat storage or precooling of the thermal mass to reduce AC load. In this study, a thermal network model described in CHAPTER TWO is established for RBEs with integrated AIS and high thermal mass to perform whole building energy simulations. A residential thermal zone having RBE exterior walls is analyzed in six (6) climate zones – i.e., Miami, Phoenix, San Francisco, Albuquerque, Chicago, and Minneapolis, to quantify the thermal performance, energy-saving potential, and thermal comfort improvement of high thermal mass-AIS integrated RBE with demand-based control. The performance of the newly developed demand-based control strategy is compared with temperature-based controllers. Some design and implementation considerations are discussed.

3.1 Rule-based control strategies for RBE with AISs and thermal mass

3.1.1 Demand-based control rule

In this section, an easy-to-implement yet flexible 'demand-based' control rule is formulated for the high thermal mass-AIS integrated RBEs to beneficially utilize the heat storage or precooling of the thermal mass to reduce AC load. Since the sensible AC load for a thermal zone is mainly attributed to: (1) the convective heat exchange between indoor air with interior walls and window surfaces, (2) infiltration, and (3) internal gains from occupant activity, lighting, and equipment (Berkeley *et al.*, 2019), the control rule for AIS is formulated based on the AC demand approximated from estimated internal gains, infiltration, as well as measured surface temperatures and air temperatures. For simplicity, the control rule formulation is based on a single thermal zone while it can be extended to a multi-zone scenario via distributed control strategies with a decentralized law (Moroşan *et al.*, 2010; Li and Zhang, 2021). More detailed control formulation for a multi-zone building with RBEs is worth further investigation and is beyond the scope of this study. The heat balance of the zone air for a single thermal zone is:

$$C_{air_in}^{j}\frac{\Delta T_{air_in}^{j}}{\Delta t^{j}} = Q_{air_in,int}^{j} + Q_{air_in,inf}^{j} + \sum_{i}^{N_{surfaces}} H_{i,air_in}^{j}\left(T_{i}^{j} - T_{air_in}^{j}\right) + Q_{sys}^{j} \qquad (3.1)$$

where $C_{air_in}^{j}$ is the thermal capacitance of the indoor air node at the j^{th} time step; H_{i,air_in}^{j} is the heat transfer coefficient between surface node *i* and the indoor air node; $N_{surfaces}$ is the number of wall surfaces; Q_{sys}^{j} is the HVAC system output; $Q_{air_in,int}^{j}$ and $Q_{air_in,inf}^{j}$ are convective heat gain from internal loads and infiltration, which can be expressed as (Berkeley *et al.*, 2019):

$$Q^j_{air_in,int} = Q^j_{people,air_in,conv} + Q^j_{light,air_in,conv} + Q^j_{equip,air_in,conv} \tag{3.2}$$

$$Q^j_{air_in,inf} = c_{p,air_in}\Delta m^j_{air_in,inf}\left(T^j_{air_ex} - T^j_{air_in}\right) \tag{3.3}$$

For each control step *j*, for a time interval Δt^j, the system output demand $Q^j_{sys}(T^j_{set})$ to reach the setpoint T^j_{set} can be written as:

$$Q^j_{sys,dmd}(T^j_{set}) = C^j_{air_in}\frac{T^j_{set} - T^j_{air_in}}{\Delta t^j} - \sum_m^{N_{surface}} H^j_{m,air_in}\left(T^j_m - T^j_{air_in}\right) - Q^j_{air_in,int} - Q^j_{air_in,inf} \tag{3.4}$$

If one of the exterior surfaces is an RBE. Under cooling mode, when the thermal mass (concrete) has a lower temperature than the indoor air ($T^j_{n-1} < T^j_{air_in}$), we suppose that all or a portion of the system output demand to reach the setpoint $Q^j_{sys,dmd}(T^j_{set})$ is compensated by the beneficial heat flow from the RBE, Equation (3.4) becomes:

$$\begin{aligned} Q^j_{sys,dmd}(T^j_{set}) + H^j_{n,air_in}\left(T^j_n - T^j_{air_in}\right) = C^j_{air_in}\frac{T^j_{set} - T^j_{air_in}}{\Delta t^j} - \sum_m^{N_{surface}-1} H^j_{m,air_in}\left(T^j_m - T^j_{air_in}\right) \\ - Q^j_{air_in,int} - Q^j_{air_in,inf} \end{aligned} \tag{3.5}$$

where T^j_n is the interior surface temperature of the RBE; H^j_{n,air_in} is the heat transfer coefficient between the RBE interior surface and the indoor air. In an ideal case when all of $Q^j_{sys,dmd}$ can be supplied by the desired convective heat transfer from the RBE – i.e., $Q^j_{sys,dmd} = 0$, and consider the heat balance of the RBE interior surface node:

$$H^j_{n,air_in}\left(T^j_n - T^j_{air_in}\right) = \frac{A_n}{R^j_{n-1,n}}\left(T^j_{n-1} - T^j_n\right) + Q^j_{n,sw} + Q^j_{n,lw} \tag{3.6}$$

where T^j_{n-1} is temperature at the concrete interior AIS interface; A_n is the interior surface area. Equation (3.5) becomes:

$$\frac{A_n}{R^j_{n-1,n}\Big|_{Q^j_{sys,dmd}=0}}\left(T^j_{n-1}-T^j_n\right)=C^j_{air_in}\frac{T^j_{set}-T^j_{air_in}}{\Delta t^j}-\sum_m^{N_{other}}H^j_{m,air_in}\left(T^j_m-T^j_{air_in}\right)$$
$$-Q^j_{air_in,int}-Q^j_{air_in,inf}-Q^j_{n,sw}-Q^j_{n,lw} \tag{3.7}$$

$R^j_{n-1,n}\Big|_{Q^j_{sys,dmd}=0}$ is the desired thermal insulation level of the interior AIS to achieve $Q^j_{sys,dmd}=0$. Rewriting Equation (3.7) and considering the physical limits of the AIS thermal resistance, we have:

$$R^j_{n-1,n}\Big|_{Q^j_{sys,dmd}=0}=\max\left[\frac{T^j_{n-1}-T^j_n}{\left(Q^j_{RBE,des}-Q^j_{n,sw}-Q^j_{n,lw}\right)/A_n},R_{low}\right] \tag{3.8}$$

where $Q^j_{RBE,des}$ is the ideal (desired) heat flow from AIS to offset HVAC load, which can be written as:

$$Q^j_{RBE,des}=C^j_{air_in}\frac{T^j_{set}-T^j_{air_in}}{\Delta t^j}-\sum_m^{N_{other}}H^j_{m,air_in}\left(T^j_m-T^j_{air_in}\right)-Q^j_{air_in,int}-Q^j_{air_in,inf} \tag{3.9}$$

where R_{low} is the lowest thermal resistance of AIS limited by its materials and design.

When $T^j_{n-1}>T^j_{air_in}$ and under cooling mode, the R-value of interior AIS is set to R_{high} to minimize the undesired heat flow from the thermal mass layer to indoor space, see **Figure 3.1**. Similarly, under heating mode and when the thermal mass layer can provide beneficial heat flow to the indoor space ($T^j_{n-1}>T^j_{air_in}$), the thermal resistance of interior AIS can be calculated using Equation (3.8), otherwise ($T^j_{n-1}<T^j_{air_in}$) the thermal resistance of interior AIS will be set to R_{high}. The detailed control sequence is shown in **Figure 3.1**.

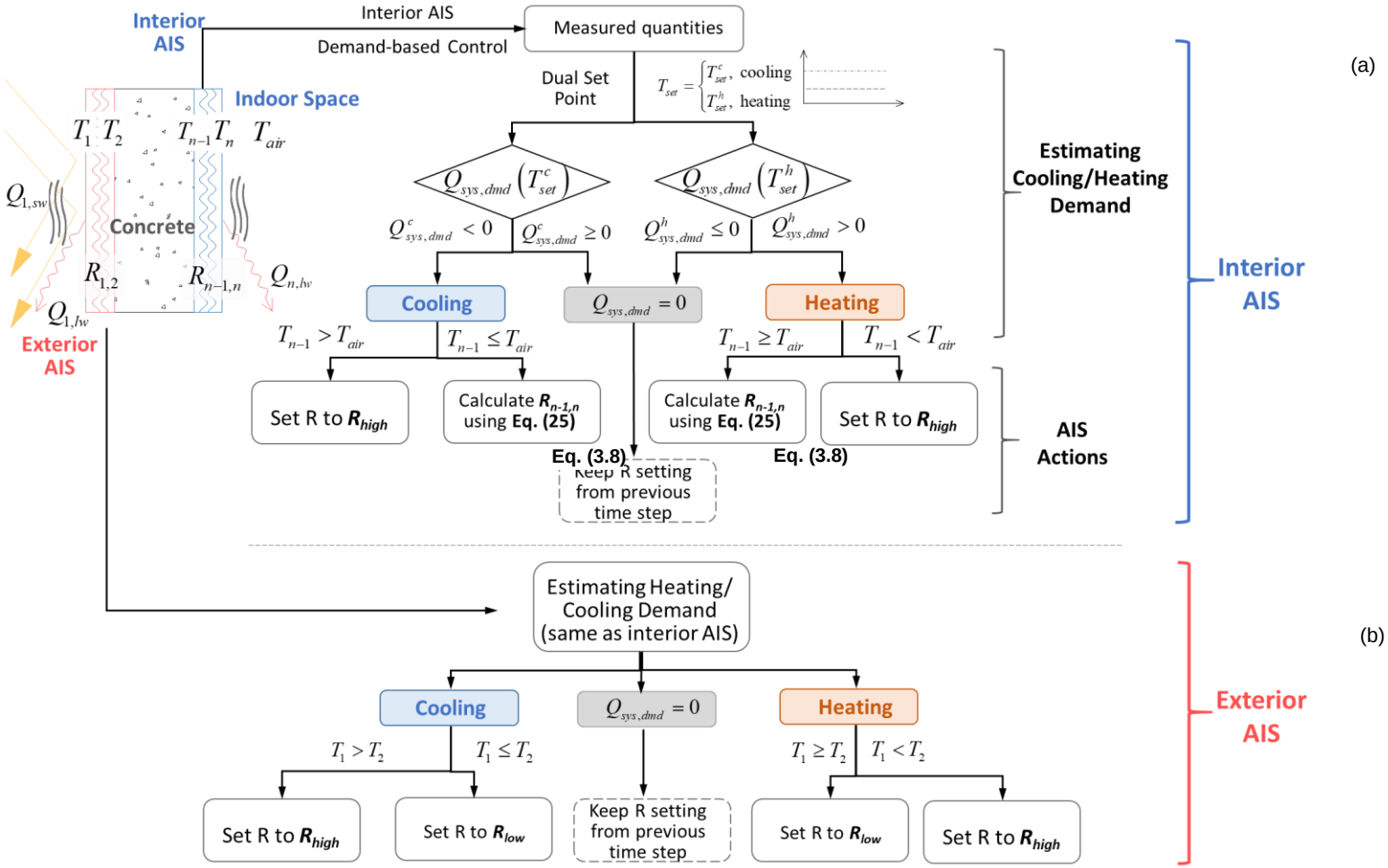


Figure 3.1 Control rule for building envelope with AISs and one concrete layer: (a) control rule for the interior AIS; (b) control rule for the exterior AIS

The proposed control sequence will enable the RBE to provide on-demand heat flow to help reach a specific indoor air setpoint while minimizing AC demand. To achieve this, AISs with continuously adjustable thermal resistances (e.g., variable pressure VIP (Berge et al., 2015) and adaptive multi-layer insulation (Kimber, Clark and Schaefer, 2014)) may provide benefit over the 'two-step' control (RSI-value can be switched only between R_{high} and R_{low}) (Rupp and Krarti, 2019). The thermal resistance setting of exterior AIS is dictated by the 'charging/discharging' needs of the thermal mass layer – i.e., under cooling mode, when the concrete temperature T_2^j is greater than the exterior AIS surface temperature T_1^j, the thermal resistance of exterior AIS $R_{1,2}^j$ is set to R_{low}; otherwise $R_{1,2}^j$ is set to R_{high}. Likewise, under heating mode, if $T_2^j < T_1^j$, $R_{1,2}^j$ is set to R_{low}; otherwise $R_{1,2}^j$ is set to R_{high}, see **Figure 3.1**.

3.1.2 Temperature-based control rule

To testify the performance of the proposed demand-based control method for RBEs, typical temperature-based control rules similar to previous work (Kishore *et al.*, 2021) are also applied for comparison. In particular, the temperature-based control rule shown as the block diagram in **Figure 3.2**, is applied to the interior and exterior AISs. It was found in the previous work (Kishore *et al.*, 2021) that during transitional seasons, temperature-based control rules without a secondary temperature constraint tend to cause overcooling/overheating, especially in the case of AIS working together with a thermal mass.

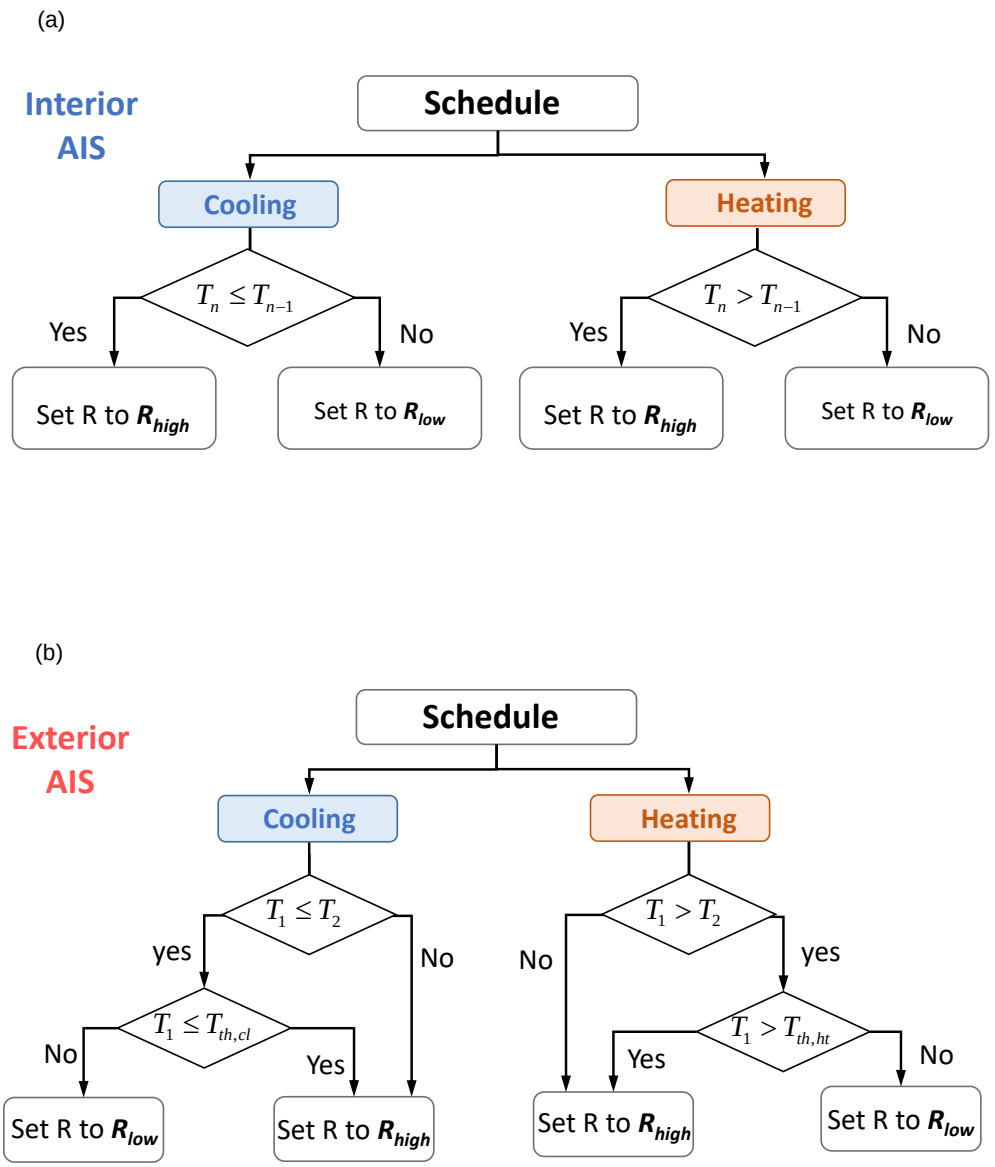


Figure 3.2 Illustrative figure showing the temperature-based control rule (a) without, and (b) with threshold temperature (T_{th})

For the control logic for interior AIS^{b}_{int} presented in **Figure 3.2** (a): (1) Under heating mode, when the interior concrete surface temperature is higher than the interior surface temperature, the R-value of AIS^{b}_{int} is set to R_{min} to facilitate heat flow to charge the concrete thermal mass; otherwise R-value of AIS^{b}_{int} is set to R_{max}. (2) Under cooling mode, when the interior concrete surface temperature is lower than the interior surface temperature R-value of AIS^{b}_{int} is set to R_{min} to help to dissipate the undesirable heat stored in the concrete layer, and vice versa.

As shown in **Figure 3.2** (b), for the exterior AIS^{b}_{ext} (1) Under heating mode, when the exterior surface temperature is higher than the exterior concrete surface temperature and exterior surface temperature is lower than the secondary temperature constraint $T_{th,ht}$ in case of overheating effect, the R-value of AIS^{b}_{ext}, is set to R_{min} to facilitate heat flow to charge the concrete thermal mass; otherwise R-value of AIS^{b}_{ext} is set to R_{max}. (2) Under cooling mode, when the exterior surface temperature is lower than the exterior concrete surface temperature and exterior surface temperature is higher than the secondary temperature constraint $T_{th,cl}$ in case of overcooling effect, the R-value of AIS^{b}_{ext} is set to R_{min} to help to dissipate the undesirable heat stored in the concrete layer to the outdoor environment, otherwise, the R-value of AIS^{b}_{ext} is set to R_{max}.

3.2 Case studies

3.2.1 Simulation details

To study the thermal behavior and energy-saving potential of the RBE, the thermal network model as described in CHAPTER TWO is implemented to model a single 13 m (L) × 8m (W) ×3.05 m (H) exterior thermal zone extracted from an intermediate floor of an apartment

building. The exterior wall exposed to the outdoor environment is assumed to be either RBE or an ASHRAE-90.1 compliant standard wall in the baseline case for comparison. All internal walls are assumed to be adiabatic (Jin, Favoino and Overend, 2017). The window-to-wall ratio is 15% for the exterior wall. Some other wall properties (e.g., window U-value, window SHGC, solar absorptance, and surface emissivity of walls) and simulation parameters considered include occupant activities, lighting, equipment schedules, and infiltration level as listed in **Figure 3.3.** RBEs described in CHAPTER TWO are used for the case study – i.e., a concrete (thermal mass) layer sandwiched between two opaque AISs as shown in CHAPTER TWO. The RSI-value range of exterior or interior AIS is assumed to be R_{low} (0.1 Km^2/W) to R_{high} based on the thermal resistance range reported in prior literature (Menyhart and Krarti, 2017; ASHRAE, 2019; Mumme and James, 2020; Juaristi *et al.*, 2021). To provide comparisons of the thermal behavior and energy performance of RBE as compared to the static baseline, a baseline exterior wall is designed with the same layout as RBE where a concrete mass layer is sandwiched between two rigid foam insulation panels with the same overall thermal mass and thermal resistance (or the upper limit for RBE with AISs) as the RBE cases. The thermal resistance of the baseline wall (static) and the R_{high} of RBE are set based on the RSI-value enlisted in **Figure 3.3** for different climate zones in accordance with ASHRAE 90.1. The indoor air temperature was controlled by HVAC with dual setpoints of 21.1-23.9. For the simulation, it is also assumed that the long-wave absorptance and long-wave emissivity are the same for all wall surfaces. Typical meteorological year 3 (TMY3) weather data of 6 representative climate zones (Miami, Phoenix, San Francisco, Albuquerque, Chicago and Minneapolis) were used for the simulation.

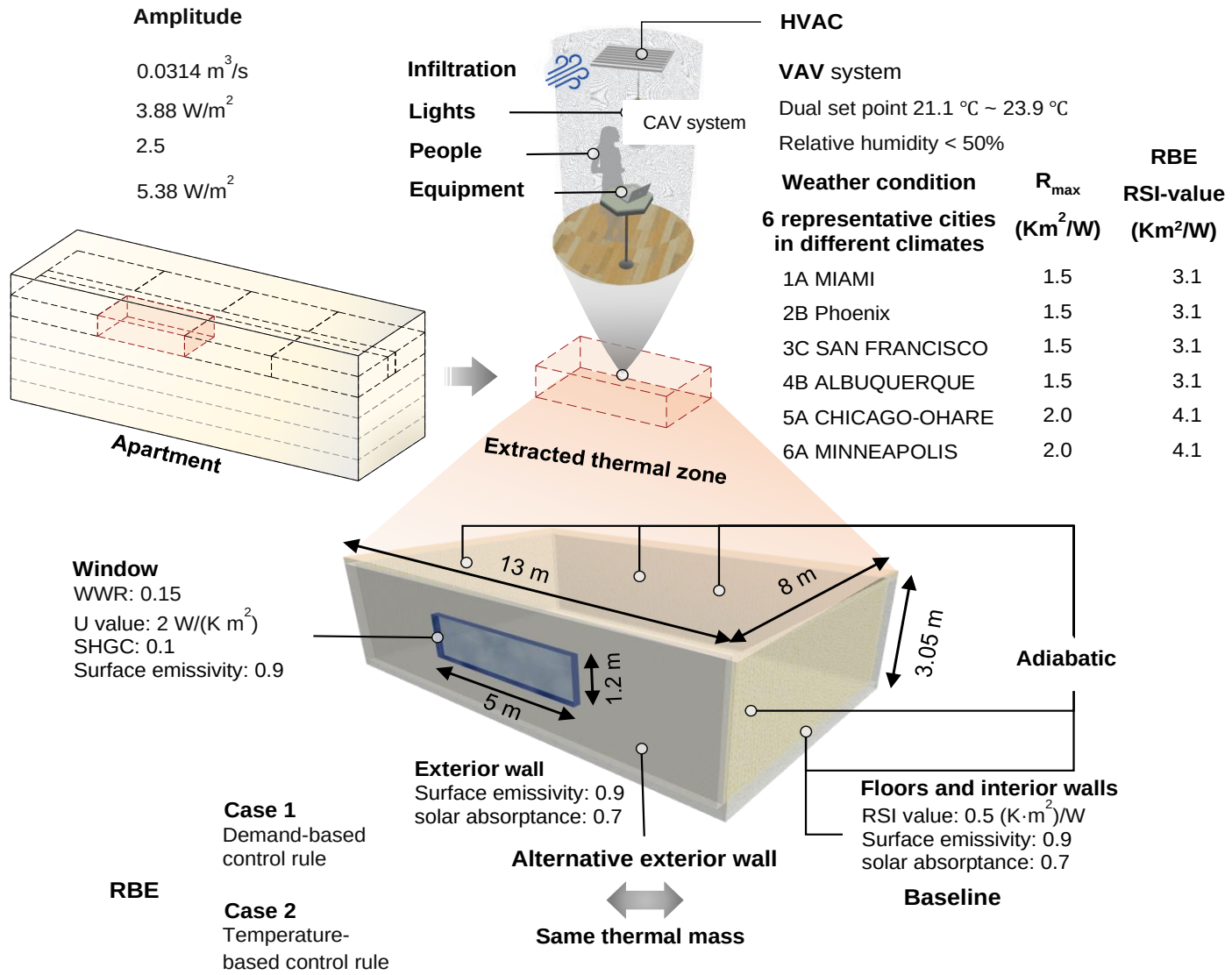


Figure 3.3 Simulation details for a residential thermal zone with RBE in comparison with a baseline static envelope

The Predicted Mean Vote (PMV) and Predicted Percentage of Dissatisfied (PPD) based on Frager's model (ISO, 2005) are used to evaluate the thermal comfort-time performance of the building. The Long-term Percentage of Dissatisfied (LPD) is used to assess occupants' long-term thermal comfort (Carlucci, 2013).

3.2.2 Thermal behavior

3.2.2.1. Heating season

Figure 3.4 shows the thermal behavior of the RBE during heating seasons. Seven days' (January 3rd–10th) data in Chicago, IL (ASHRAE climate zone 5A) are arbitrarily chosen to illustrate the thermal behavior and AIS operations of the RBE during the heating season. **Figure 3.4** (a) shows the outdoor air temperature and estimated system output demand $Q_{sys,dmd}^{j}$ to reach the setpoint, as calculated using Equation (3.4) and according to the flowchart shown in **Figure 3.1**. During the winter months, the AC is in heating mode during most days. **Figure 3.4** (b) shows that the temperature of concrete thermal mass is always lower than the indoor air temperature during this period, the interior AIS therefore remains at high thermal resistance mode (R_{high}) to minimize the heat loss from the indoor space. As shown in **Figure 3.4** (c), when the exterior surface temperature is higher than the concrete temperature, the thermal resistance (RSI-value) of the exterior AIS is set to R_{low} to allow beneficial heat flow to charge/heat the concrete thermal mass. Otherwise, the RSI-value of the exterior AIS is set to R_{high} to minimize the heat loss from the concrete. This dynamic behavior of exterior AIS helps to maintain a relatively low temperature difference between the concrete layer and the interior surface, thus reducing the heat loss.

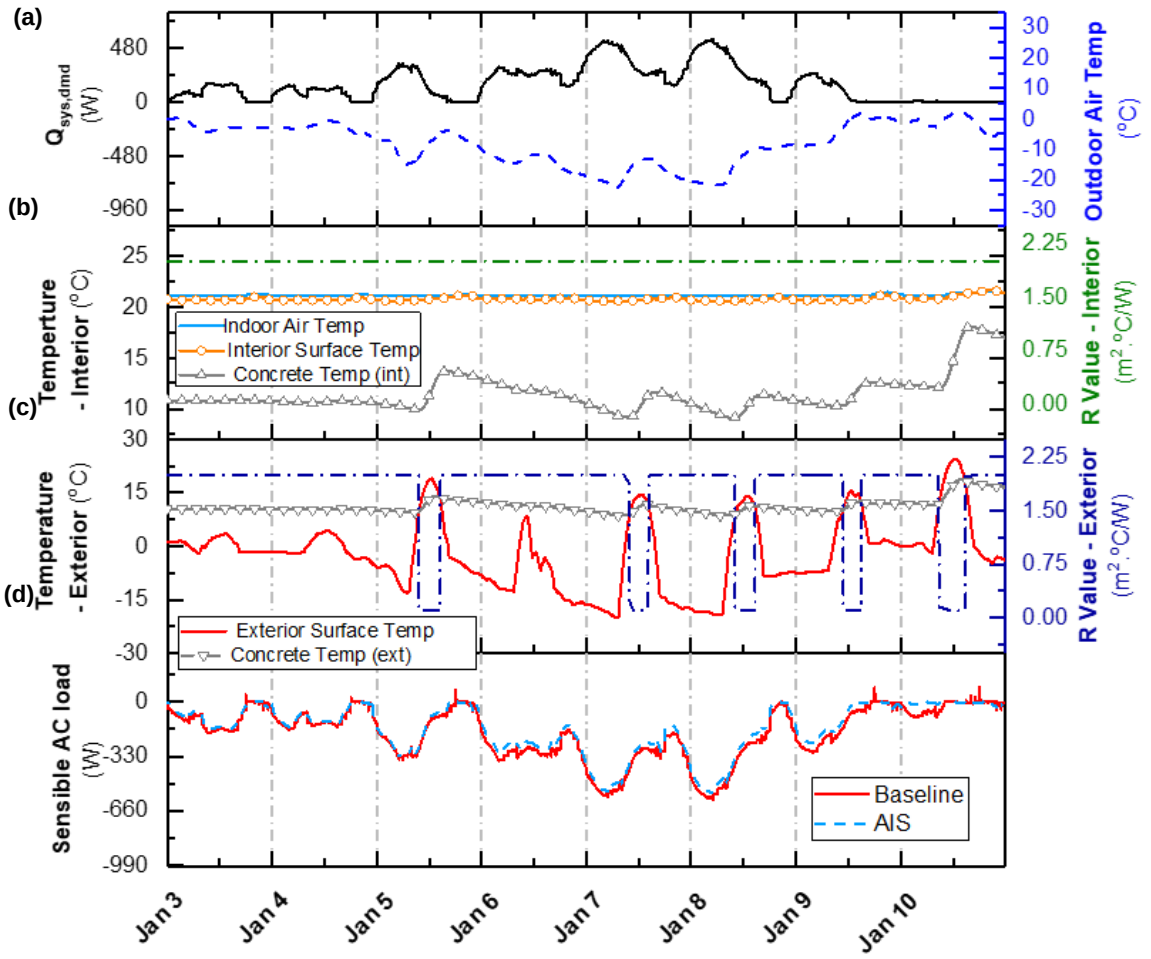


Figure 3.4 Thermal behavior of RBE in a typical heating season (January, Chicago, IL): (a) outdoor air temperature and the system output demand to reach the setpoint, $Q_{sys,dmd}$; (b) interior AIS R-value setting and indoor air, interior surface, and concrete temperatures; (c) exterior AIS R-value setting, exterior surface and concrete temperatures; (d) comparison of sensible AC load for RBE and baseline cases

In a heating dominant case where the exterior surface temperature is mostly lower

than the heating setpoint, RBE provides limited (if at all) energy-saving potential. This is consistent with prior studies (Menyhart and Krarti, 2017; Rupp and Krarti, 2019).

3.2.2.2. Cooling season

Figure 3.5 shows the thermal behavior and operation of the interior and exterior AISs for the RBE wall during the cooling season, where a summer week (July 10^{th} – 16^{th}) in Chicago, IL is selected to illustrate how the RBE responds to the changes in the outdoor environment. As indicated in **Figure 3.5** (a), the outdoor air temperature fluctuates around the AC set point, whereas the exterior surface temperature is mostly higher than the setpoint (23.9 °C) due to solar irradiation during the daytime. **Figure 3.5** (b) shows that when the temperature of concrete thermal mass is higher than the indoor air temperature, the interior AIS is at a low thermal conductivity (high thermal resistance). Whereas, when the temperature of concrete interior surface is lower than the indoor air temperature, the concrete layer provides the potential to absorb the unwanted heat from the indoor space. In that case, the controller first makes a determination if cooling from the HVAC is needed ($Q^{j}_{sys,dmd} < 0$) and then the thermal resistance of interior AIS is adjusted according to Equation (3.8) to allow just enough heat flow to compensate for the AC demand. Since in the summer (July), cooling is required for most hours with relatively high AC demand ($Q^{j}_{sys,dmd}$), the interior AIS remains at R_{low} for most of the time when free ambient cooling is available. This is different from the system behavior during transitional seasons as will be shown in the following section.

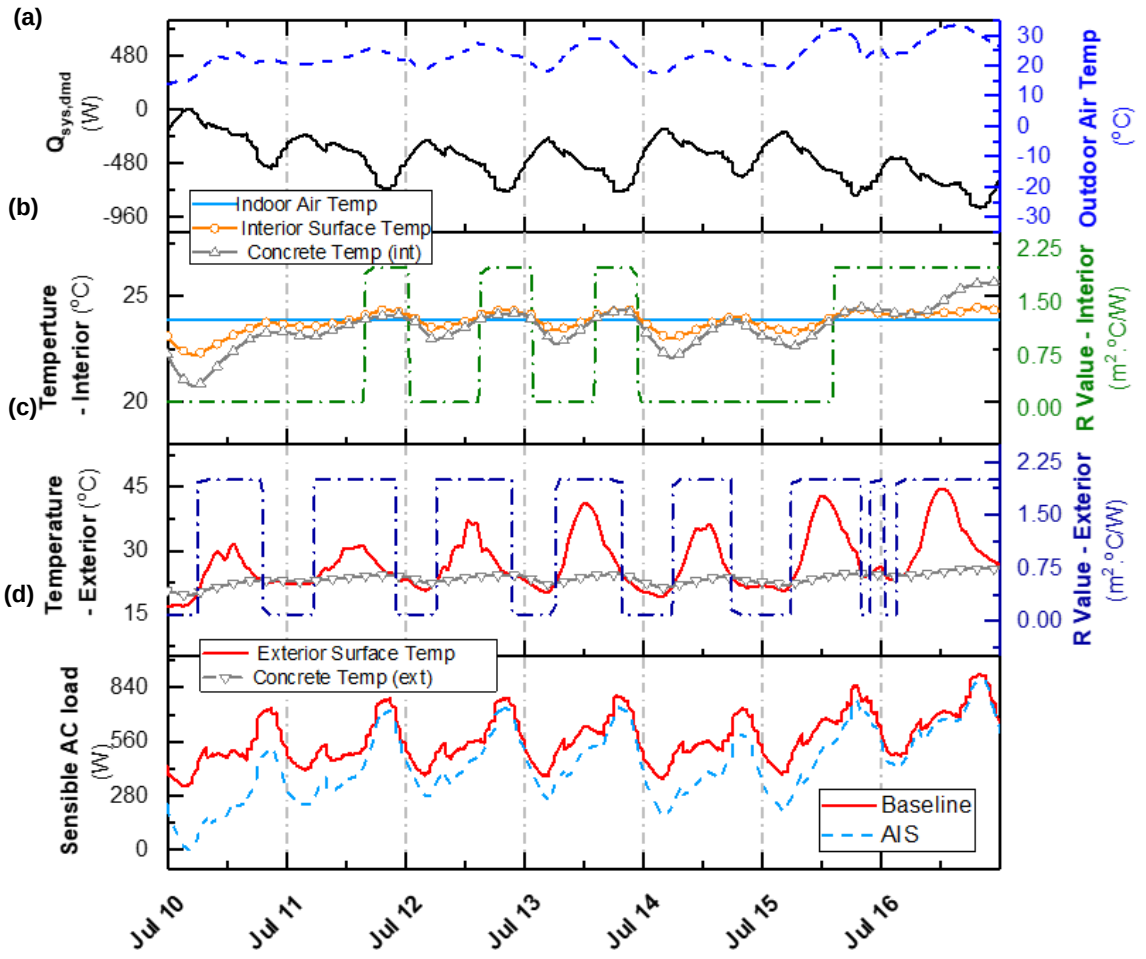


Figure 3.5 Thermal behavior of RBE in a typical cooling season (July, Chicago, IL): (a) outdoor air temperature and the system output demand to reach the setpoint, $Q_{sys,dmd}$; (b) interior AIS RSI-value setting and indoor air, interior surface, and concrete temperatures; (c) exterior AIS RSI-value setting, exterior surface, and concrete temperatures; (d) comparison of sensible AC load for RBE and baseline cases

As shown in **Figure 3.5** (c), when the exterior surface temperature is higher than the concrete layer, the thermal resistance of the exterior AIS is set to R_{high} to

cut off the undesired heat flow into the thermal mass layer; whereas when the exterior surface temperature is lower than the concrete layer, the thermal resistance of the exterior AIS is set to R_{low} to dissipate the unwanted heat stored in the thermal mass during the cool hours (from midnight to early morning). In July, the exterior surface temperature of exterior AIS is mostly higher than the concrete temperature, providing limited free ambient cooling. **Figure 3.5** (d) presents the comparison of the sensible AC load between RBE and baseline cases, where the RBE reduces energy consumption by 20% during the hot summer month (July) in Chicago, IL.

3.2.2.3. Transitional season

Figure 3.6 shows the thermal behavior and AIS settings for the RBE during a transitional season, where a representative week (April 16th – 22nd) in Chicago, IL was presented to illustrate how the dynamic RBE utilizes natural heating/cooling from the outdoor environment to reduce AC load. During the simulated period, cooling demand (see **Figure 3.6** (a)) dominates ($Q^{j}_{sys,dmd} < 0$ and sensible AC load > 0) from April 16th to April 19th. Because of the relatively high outdoor air temperature (19℃-31℃) from April 16th to April 18th, the system demand was similar to that during the cooling season. In response, the interior AISs behaved as a thermal switch with its thermal resistance setting to R_{low} when the interior concrete temperature was lower than the indoor air temperature during early mornings.

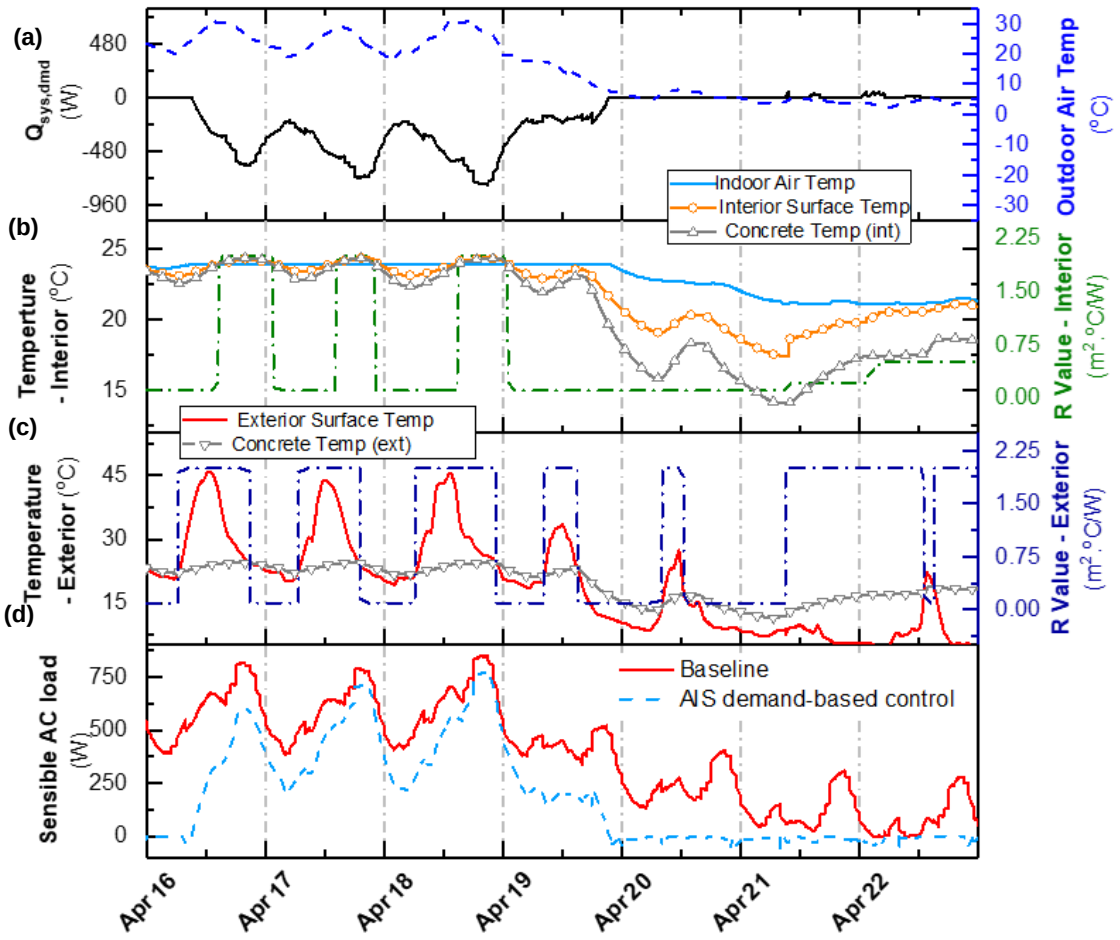


Figure 3.6 Thermal behavior of RBE in a typical transitional season (April, Chicago, IL): (a) outdoor air temperature and the system output demand to reach the setpoint, $Q_{sys,dmd}$; (b) interior AIS RSI-value setting and indoor air, interior surface, and concrete temperatures; (c) exterior AIS RSI-value setting, exterior surface and concrete temperatures; (d) comparison of sensible AC load for RBE and baseline cases

The exterior AIS was also set to R_{low} to provide passive cooling during nights and early mornings to dissipate the unwanted heat stored in the thermal mass,

see **Figure 3.6** (c). As the outdoor air temperature gradually decreased from April 19th, both exterior and interior AISs were set to R_{low} to help dissipate the undesired heat. Consequently, AC load with RBE was largely reduced compared with the baseline, see **Figure 3.6** (d). During April 20th-21st, due to the passive cooling provided by the RBE, the indoor air temperature decreased to values between the dual setpoints, and AC system demand $Q^{j}_{sys,dmd}$ stayed around zero. As a result, the interior AIS remained inactive during this time. As the indoor air temperature is getting close to the heating setpoint, the controller detected the potential actions based on the gradually increased system demand (heating demand) around noon on April 21st. In response to the changes in the estimated system demand, the interior AIS gradually increased to a low level according to Equation (3.8) and maintains the system demand close to zero. During the morning on April 22nd, the projected system demand became positive again so that the interior AIS was gradually set to 0.5 Km^2/W based on Equation (3.8) and maintained the same value as the system demand reached zero. The demand-based control rule developed in this study suppresses the AC demand via sensitive detection of potential changes to maintain the sensible AC load around zero from April 20th to April 22nd as compared to the high sensible AC load of the baseline. The simulation results show that the RBEs brought approximately 75% energy savings as compared to the RSI-4 static envelope baseline in April in Chicago, IL. Also, it is worth noting that due to the demand change (from cooling to heating) during the morning on April 21st, the control of exterior AIS automatically switched mode such that exterior AIS adjusted to R_{high} when the temperature of concrete continues to decrease. This helps prevent 'overcooling' effects that would in turn increase the AC energy usage. More

detailed comparisons between the 'demand-based' control rule as proposed in this study and temperature-based control will be elaborated in the following section.

3.2.2.4. Comparison with temperature-based control

In this section, the performance of the proposed demand-based control method for RBE is compared with temperature-based control rules. It was found in the previous work (Kishore *et al.*, 2021) that during transitional seasons, temperature-based control rules without a secondary temperature constraint tend to cause overcooling/overheating, especially in the case of AIS working together with a thermal mass. For example, during October in Chicago, IL, the baseline case (i.e., static envelope) requires mostly cooling due to the internal loads and relatively mild outdoor temperature. However, the application of the temperature-based controller without a secondary temperature restriction leads to "over-cooling" during days when night temperatures are low (e.g., Oct 7^{th} – 9^{th}, and Oct. 13^{th} – 21^{st}), see **Figure 3.7** (a). To prevent overcooling/overheating, some previous research proposed to apply a 'secondary rule' to regulate the temperature of the thermal mass (Kishore *et al.*, 2021) – e.g., during cooling seasons, if the concrete temperature falls below a threshold value $T_{th,cl}$, the exterior AIS is set to R_{high} in order to prevent overcooling.

Figure 3.7 presents the thermal behavior (R setting) of RBEs controlled by different control rules, where **Figure 3.7** (a) shows the temperature-based control without overcooling prevention in comparison with the cases with secondary temperature constraints (i.e., $T_{th,cl}$=10℃, 16℃, and 22℃).

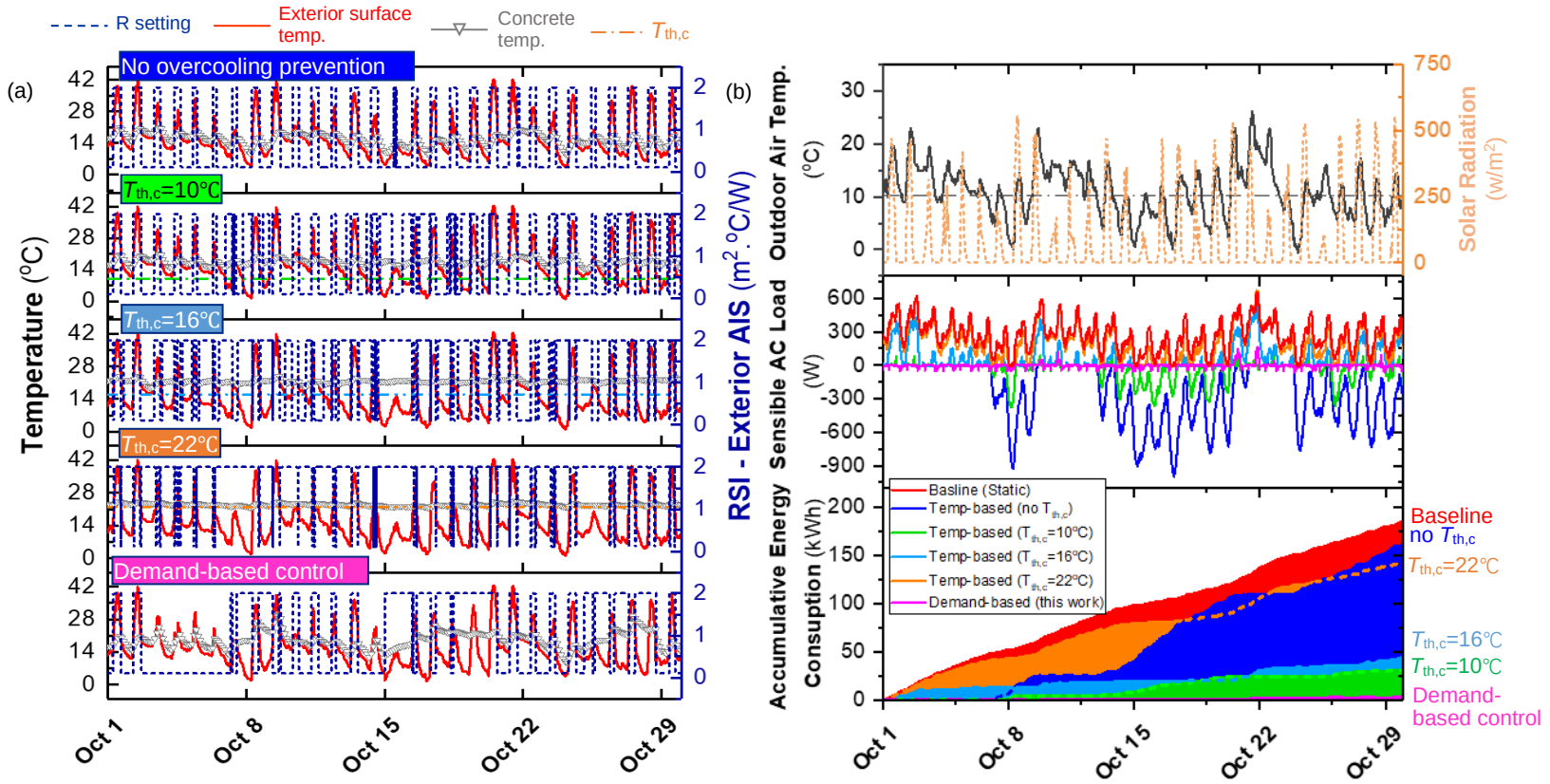


Figure 3.7 Comparison of RBE thermal behavior under demand-based control and temperature-based control

The temperature of the thermal mass is regulated within a certain range by limiting the exterior surface temperature – i.e., when the exterior surface temperature of the envelope falls below $T_{th,cl}$, the exterior AIS is set to R_{high}. While effective, a major limitation of this controller is that the system performance (e.g., energy-saving potential) is highly dependent on the prescribed $T_{th,cl}$, whose 'optimal' value varies dramatically based on the building configuration (e.g., internal load, AC setpoint, etc.), specific weather condition, and even the system design. This is demonstrated in **Figure 3.7** (b), where it can be seen that the energy savings were maximized when $T_{th,cl}$ is between 10-16℃ for October in Chicago, IL. Note that the optimal value of $T_{th,cl}$ leading to maximum saving potential varies month-to-month and is different for each climate zone. Therefore, the design of temperature rule controllers relies on high-fidelity case analysis which is not always available. On the other hand, the proposed demand-based controller regulates AIS behaviors based on projected cooling/heating demand (i.e., Equation (3.4)). When the projected AC load is low, the actions of AIS are limited to automatically prevent overheating or overcooling from occurring, see **Figure 3.7** (a). When the thermal mass temperature deviates too much from the desired cooling/heating temperature, the estimated AC demand will become non-zero to automatically trigger the action of AISs. This ensures the thermal mass stores and releases thermal energy just "as needed" and do not rely on a prescribed temperature constraint for control. Note that Equation (3.4) 'project' heating/cooling demand from AC based on current state of the building (i.e., measure surface, air temperatures, the estimated internal

load, and infiltration based on the occupancy schedule) and does not rely on a model to predict energy demand (as opposed to 'model predictive control, or MPC (Cui *et al.*, 2022)'), which greatly simplifies the controller formulation. Moreover, this strategy triggered by system demand, as outlined in CHAPTER FOUR, reduces unnecessary actuation of AIS. This is advantageous as compared to most existing temperature-driven control rules by providing effective 'on-demand' shedding of AC load while reducing the operational energy and maintenance requirement at the same time.

3.2.3 Energy-saving potential

Figure 3.8 shows the monthly and annual energy consumption from the AC cooling/heating (including sensible load and latent load) of the analyzed thermal zone located in Miami, Phoenix, San Francisco, Albuquerque, Chicago, and Minneapolis, which are in ASHRAE climate zones 1A, 2B, 3C, 4B, 5A, and 6A-7, respectively. The energy-saving potentials of the RBE with the two different control rules – i.e., temperature-based control (with $T_{th,cl}$=16℃ and $T_{th,h}$=30℃ based on the prior analysis performed by Kishore et al. (Kishore *et al.*, 2021)) and demand-based control, are also compared. The simulation results indicate that AC load was significantly reduced by the RBEs in most thermal zones regardless of the controller used. The RBE is demonstrated to be very effective in reducing AC load in climate zones with relatively mild climates and during transitional reasons – e.g., over 90% energy savings can be achieved in San Francisco or during winter months of Albuquerque, see **Figure 3.8** (a); whereas RBE has limited saving potential for hot summers or cold winters when the outdoor temperature is constantly above or below the indoor temperatures (e.g., summer of Miami or winter of Minneapolis).

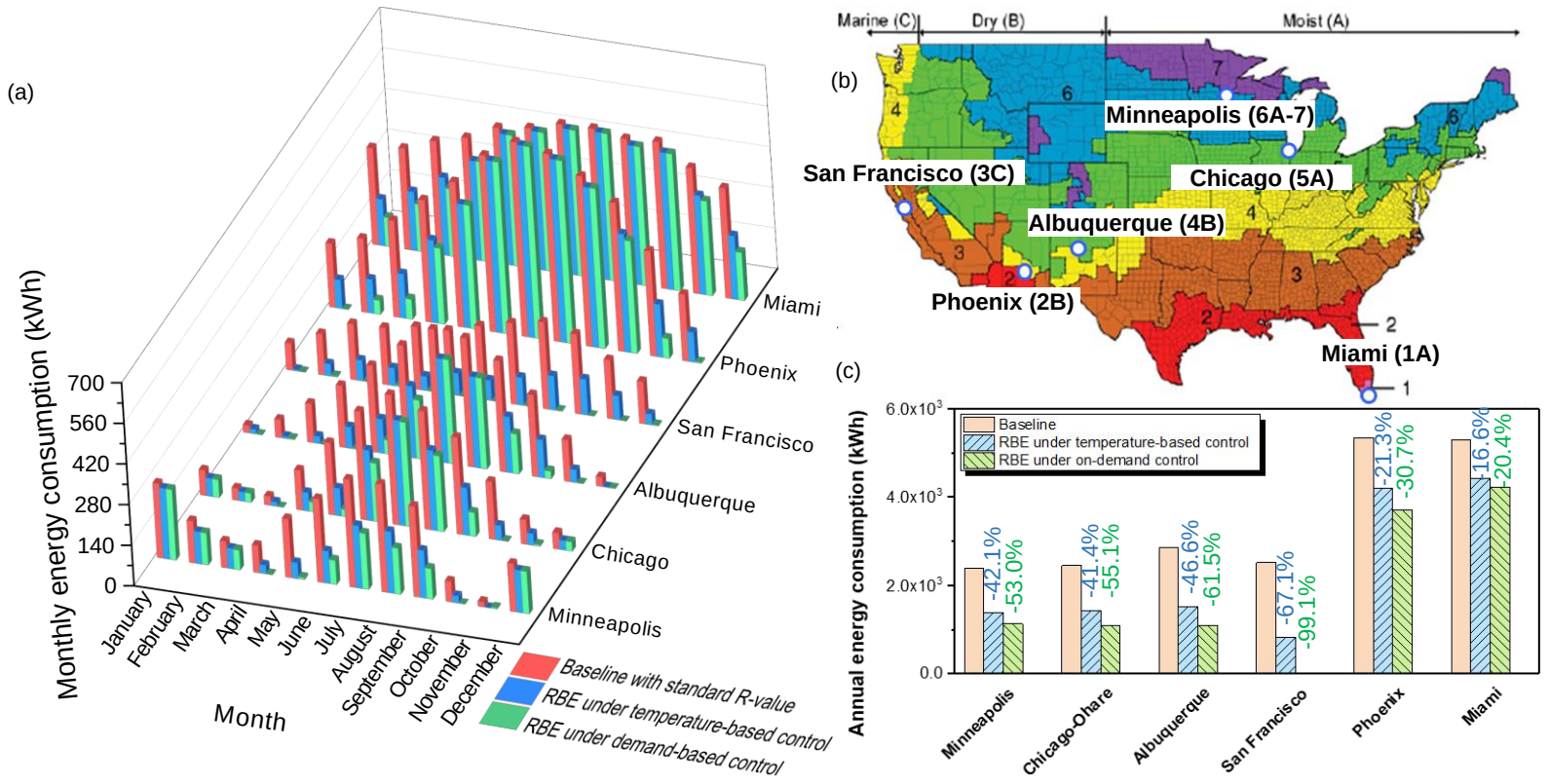


Figure 3.8 (a) Monthly energy consumption of the residential thermal zone (b) Climate classification of the six representative cities analyzed (c) Annual energy consumption compared for the static envelope baseline, RBE with temperature-based control, and RBE with demand-based control

This trend is consistent with results presented in previous studies (Antretter and Boudreaux, 2019). Overall, the simulation results show that the RBE with AIS under demand-based control provided up to 32.0% higher energy savings than the one under temperature-based control. The higher saving potential brought by the demand-based control rule is more evident in climate zones with mild climates or during transitional seasons. This is due to the high diurnal and monthly temperature fluctuations that lead to overcooling or overheating as discussed in previous sections.

3.2.4 Thermal comfort performance

In addition, the thermal comfort performance was also calculated for the baseline and RBE cases under both temperature-based control and demand-based control. **Error! Not a valid bookmark self-reference.** presents the annual Long-term Percentage of Dissatisfied (LPD) for these three cases in the 6 representative cities. The simulation results indicate that RBE can maintain satisfactory thermal comfort performance while providing energy savings. The RBE using demand-based control provides higher LPD reductions as compared to those using temperature-based control, especially in regions with relatively mild climates (i.e., San Francisco).

3.2.5 Operation of AIS and design implications

Figure 3.9 (a) presents the time histories of RSI-value of the AISs during a meteorological year under demand-based control. During the hot summer months (i.e., May – October) in Miami, the interior AIS mostly stays at R_{high} to minimize the undesirable heat flowing into the indoor space while the exterior AIS still goes through daily transitions to dissipate the heat stored in the thermal mass during evening cooler hours.

Table 3.1 The annual LPD (%) of the residential thermal zone in different scenarios

	Miami (1A)	Phoenix (2B)	San Francisco (3C)	Albuquerque (4B)	Chicago (5A)	Minneapolis (6A-7)
Baseline	9.19	7.54	8.08	6.98	7.88	8.00
RBE under temperature-based control	8.98 (-2.2%)	7.38 (-2.1%)	7.79 (-3.6%)	6.85 (-1.9%)	7.50 (-4.9%)	7.73 (-3.3%)
RBE under demand-based control	8.83 (-3.9%)	7.05 (-6.4%)	5.89 (-27.1%)	6.57 (-5.9%)	7.14 (-9.4%)	7.37 (-7.9%)

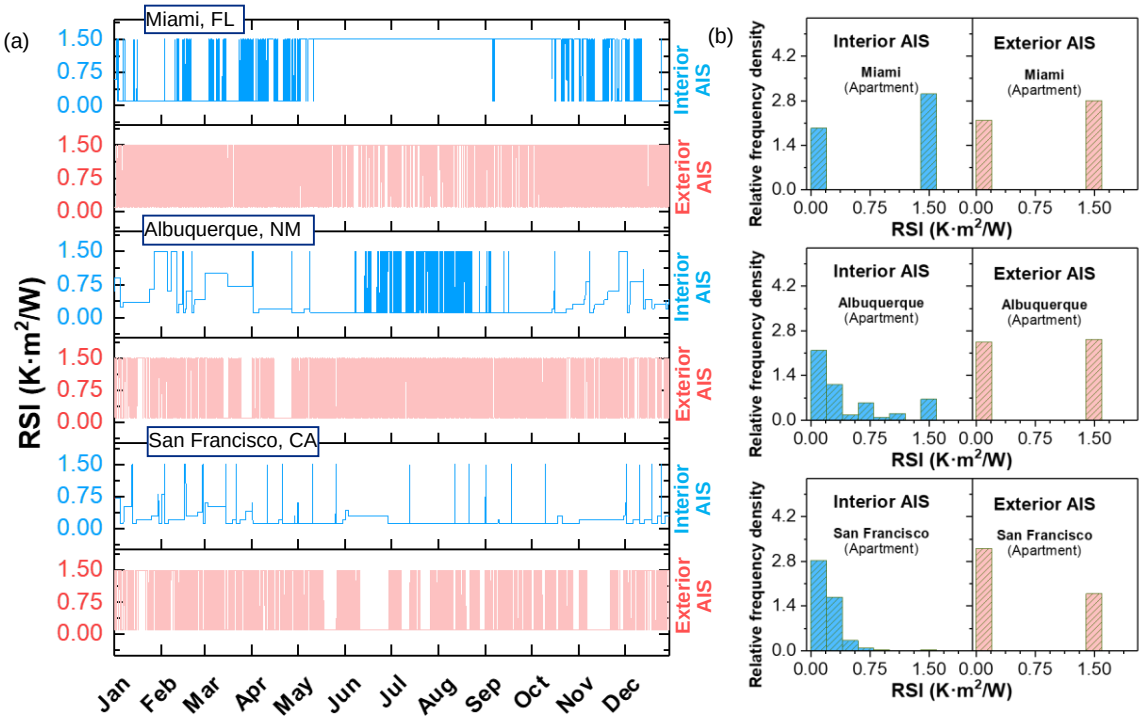


Figure 3.9 (a) Whole-year time history of RSI setting for both the interior and exterior AIS for Miami, Albuquerque, and San Francisco; (b) Relative frequency density distribution of the RSI-values

For Albuquerque, the interior AIS hovered mostly at lower insulation levels during winter and traditional seasons to utilize passive heating/cooling and reduce AC load. In regions with mild climates like San Francisco, the interior AIS mostly stayed at very low insulation levels.

Figure 3.9 (b) presents the relative (time) frequency density distribution of the RSI-value of both interior and exterior AIS for three climate zones – Miami (1A), Albuquerque (4B), and San Francisco (3C). It can be seen that for Miami, the interior and exterior AISs mostly switch between the highest and lowest RSI-values R_{low} and R_{high} throughout the year and they rarely stay at intermediate RSI-value. This indicates that for regions with predominantly hot or cold seasons, the AIS that switches between R_{low} and R_{high}, sometimes referred to as a "binary thermal switch" (Mumme and James, 2020), could yield 'near-optimal' performance.

Whereas for areas with longer transitional seasons (e.g., Albuquerque), AISs that can 'gradually' change their thermal resistance can provide higher energy-saving potential. It also can be observed from the results that for areas with mild climates (e.g., San Francisco), only a relatively low interior insulation level is needed – i.e., the RSI-value of interior AIS stayed mostly <0.5 Km^2/W throughout the year, therefore, the RBE designed with only exterior AIS may provide satisfactory energy performance. The results of thermal insulation duration distribution can help to determine the suitable AIS type and required insulation level for AIS design in different climate zones.

3.3 Conclusions

In this study, an easy-to-implement yet flexible ‘demand-based’ control rule is formulated based on demand analysis to project the ‘desired’ thermal resistance of the AIS layers such that it beneficially utilizes the heat storage or precooling of the thermal mass to reduce AC load. The thermal network model described in CHAPTER TWO is established for RBEs with integrated AIS and high thermal mass to perform whole building energy simulations. The control rule is formulated by first estimating AC demand from estimated internal gains, and infiltration, as well as measured surface temperatures and air temperatures at certain time steps. Then the desired thermal resistance of AIS is calculated based on the estimated AC demand and temperatures of the thermal mass and indoor air. The key findings of the study in this chapter are summarized as the following:

- In comparison to temperature-based control strategies in prior studies, the demand-based control rule formulated herein has achieved significantly higher energy-saving potential. During transitional seasons, the temperature-based controller tends to cause overheating or overcooling of the thermal mass which largely limits the energy-saving potential of RBEs; whereas the demand-based controller ensures that the AISs just release “as needed” thermal energy and do not rely on prescribed temperature constraints for control. For regions with mild climates, e.g., San Francisco, the demand-based control reduces the AC energy consumption by over 90%. The RBEs also bring thermal comfort improvement, especially for regions with mild climate conditions (e.g., 27.1% LPD reduction in San Francisco, CA).

- A thermal network model with high computational efficiency is established for RBEs with integrated AISs and high thermal mass. The thermal performance (e.g., temperature responses and energy consumptions) matches closely with those obtained by EnergyPlus simulations. The higher efficiency model is important to reduce computational costs for further studies that employ AI-based or online learning control.
- The integrated high thermal mass-AIS RBE has significant potential to reduce the energy consumption of buildings located in most climate zones. In particular, the case study had shown 20.4%, 30.7%, 99.1%, 61.5%, 55.1, and 53.0% heating/cooling energy use reductions for Miami (1A), Phoenix (2B), San Francisco (3C), Albuquerque (4B), Chicago (5A), and Minneapolis (6A-7), respectively. The responses from AISs help charge and discharge the thermal mass and provide compensating heat flow to offset the AC load. In general, the energy-saving potential of RBE is greater during transitional seasons and in regions with mild climates where the diurnal temperature fluctuates around the AC set points.
- The analysis of whole-year AIS operation across different climate zones can provide guidance for AIS design. It was found that for regions with predominantly hot or cold climates, the use of a "two-step" thermal switch would yield satisfactory thermal performance; whereas for regions with long transitional seasons, AISs that can gradually change their thermal resistance can provide higher energy-saving potential. In addition, for regions with mild climates (e.g., San Francisco), RBE

with only exterior AIS (the interior side is not insulated) can provide satisfactory performance.

In spite of the promising performance of the rule-based control based on the knowledge of the physical system, it will take higher costs for controller formulation with more complex systems. As a result, data-driven approaches including reinforcement learning control worth further investigation as they do not rely on physical models, which will be elaborated in CHAPTER FOUR.

CHAPTER FOUR
MODEL-FREE ONLINE REINFORCED LEARNING CONTROL FOR RBE

Given the limitations of rule-based controllers and model predictive controllers, this chapter proposes an efficient model-free control strategy using deep reinforced learning for an AIS-integrated RBE system to fully utilize the synthesis of AIS with dynamic thermal properties and sensible thermal storage. Instead of finding optimal control sequence based on system identification through detailed model formulation and calibration (e.g., MPC methods), this study aims to develop a data-driven MFORL controller that can directly capture the relation between optimal control rules and dynamic building system behavior equipped with the RBE through online learning. To evaluate the performance of the MFORL controller in improving building thermal performance via AIS-integrated RBE, case studies were performed in representative weather conditions in Chicago, IL, the US for the RBE composed of a concrete thermal mass sandwiched between the exterior AIS and a gypsum layer. To provide more insights into the synergy mechanisms of AIS and sensible thermal energy storage by smart adaptation of MFRL, the analysis results were compared to those under simple temperature-based control and demand-based control. The temperature-based control is derived simply using surface temperatures as control variables to regulate the behavior of the active insulation system. The demand-based controller is developed based on a high-fidelity AC load prediction model. The MFORL controller and training settings are carefully designed to guarantee robust performance with stale

convergence during training. Relevant implications are elaborated and discussed. The MFORL controller design implications.

4.1 Methods

To develop a reliable model-free online reinforcement learning (MFORL) controller for real-time operation and investigate the learning behavior and performance of the agent for the case that analyzes the building energy performance with RBE, the study was conducted in four phases: problem formulation, control strategy design, offline pretraining, and online deployment. Firstly, the components of the model-free reinforcement learning (MFRL) controller and online training and control strategy with pre-training were designed. The parameter settings for the controller were designed based on parametric pre-analysis through offline training. With these delicately selected parameter settings, the online control strategy was deployed using a co-simulation testbed in representative seasonal periods to assess the online training performance and the robustness of the pre-trained agent. The thermal performance improvement by the RBE under MFORL control was evaluated through comparison with those under different rule-based control strategies.

4.1.1 Problem formulation

The problem to be solved by reinforcement learning is normally defined as a Markov Decision Process (MDP), which is generally represented as a tuple (S, A, P, R), i.e. state, action, transition probability, and reward function as presented in **Figure 4.1**.

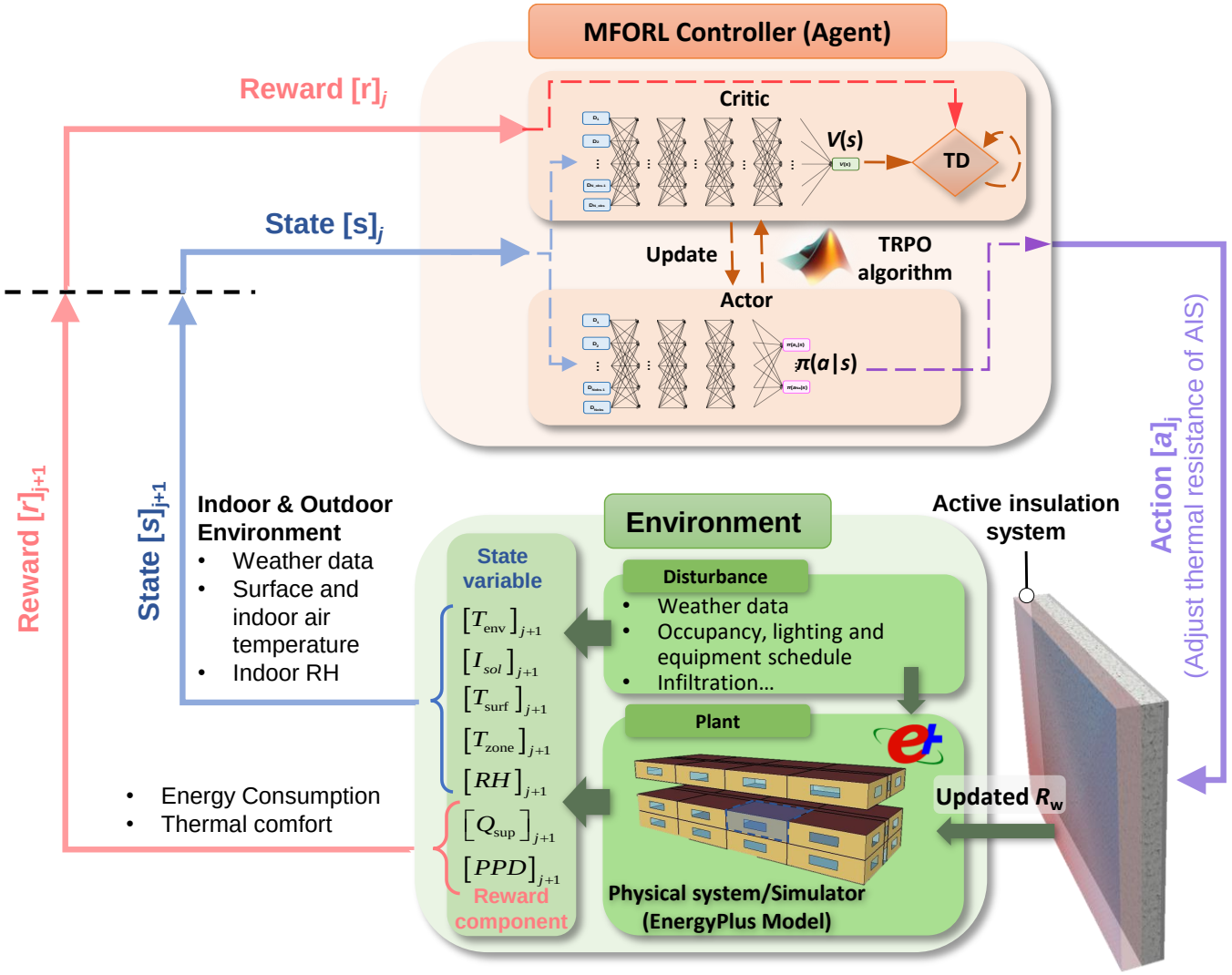


Figure 4.1 Schematic for model-free online reinforced learning framework for RBE

In the problem, the environment provides all the available data including weather conditions and all the indices representing building behaviors, e.g., surface temperature and AC load for training and control, which is mathematically represented by transition probability and reward function. Together with these elements, the environment and controller/agent comprise the basics of the whole problem. To formulate the controller framework, the controller components are designed with the following considerations.

(1) Action (A)

Action is the decision generated by the controller in response to the disturbances and outputs from the plant for the prescribed goals. For RBE, the selection of control variables for RBE is based on the configurations of the RBE for modulation, i.e., the action can be thermal properties of the walls, e.g., thermal insulation, solar reflectance, visual transmittance, etc. In this case study, where the building attains energy efficiency through modulating the dynamic thermal properties of the RBE with AIS, the only control variable a is the R-value of the exterior AIS. Action space $\mathcal{A}$ contains all the possible control actions that can be taken by the agent. At a specific time, the action is selected from the action space, i.e., $a \in \mathcal{A}$, which is constrained between $R_{\min}$ and $R_{\max}$. For the discrete action, proper action space size is required for control performance and computation cost efficiency, since small action space sizes will undermine the training performance while large action space sizes will lead to high computation costs. Moreover, the lower and upper limits of the action space should be properly selected to study the demand for the R-value of the exterior AIS under different weather conditions given compliance with ASHRAE-90.1 (ASHRAE, 2019) and availability.

(2) State (S)

The state *s* is the designated description of the environment and provides the key characteristics for the agent to identify the environment. The state space $\boldsymbol{S}$ is a selected set of variables related to the environment which enables the agent to learn the optimal control policy to achieve the maximum reward. Hence the state variables should be properly selected since unnecessary states may induce the curse of dimensionality and insufficient features cannot attain satisfactory performance regardless of efficient algorithms. Based on related studies of feature selection for building energy prediction (Sun, Haghighat and Fung, 2020; Khalil *et al.*, 2022) and pre-analysis, only 10 state variables including RBE surface temperatures $\left[T_{\text{surf}}\right]$, outdoor temperatures $\left[T_{\text{env}}\right]$, solar radiation $\left[I_{sol}\right]$, indoor air temperature $\left[T_{\text{zone}}\right]$, and relative humidity $\left[RH\right]$ are selected among diverse alternative indices to constitute the state space with a tradeoff between performance and cost in this AIS controller formulation.

(3) Reward function (R)

The reward function is used to map the state and action to the rewards. In this study, the objective of the agent is to minimize energy consumption while maintaining the thermal comfort performance of the indoor space within a desired range through taking real-time actions. Therefore, the reward function contains the components concerning energy consumption and thermal comfort. In other words, the reward function should be designed to ensure high sensitivity to the changes in the observations of the system. In addition, for RBE control, the action stability also should be considered given operator maintenance cost. There are several related indices available for representing energy consumption and

thermal comfort performance so that alternative indices were tested to represent these two components, i.e., normalized sensible AC load, normalized AC supply heating/cooling rate, Predicted Percentage of Dissatisfied (PPD), and Long-term Percentage of Dissatisfied (LPD). To improve the performance of the critic, different forms of alternative indices for the reward function were also studied in the parametric pre-analysis to find which one is more sensitive to changes in the observations. The implementation results in parametric pre-analysis show that the refined reward function of normalized mean AC supply heating/cooling rate $\bar{Q}_{\text{sup}}^{k}$ and LPD^{k} within the k^{th} control step defined in Equation (4.1) exhibits good training performance. The third component in the reward function is designed to decrease the difference between adjacent actions in case of fast switching during the control to reduce the maintenance cost of the operator.

$$r^{k} = -\left\{\eta_1\left(\bar{Q}_{\text{sup}}^{k}\right)^2 + \eta_2\left(LPD^{k}\right)^2 + \eta_3\left|R_w^{k} - R_w^{k-1}\right|\right\} \tag{4.1}$$

Where R_w^{k} is the R-value of exterior AIS at the k^{th} control step; η_1, η_2, and η_3 are the weights for the components of the reward function.

(4) Transition probability (P) and environment

In the MDP, the transition function maps the transition from state s_k at k^{th} time step to s_{k+1} with action a_k and under the disturbances d_k.

$$s_{k+1} = f\left(s_k, a_k, d_k\right) \tag{4.2}$$

Trajectory r, i.e., the sequence of states (s_1, s_2, … s_N) and actions (a_1, a_2, … a_N), is determined by the transition probability $p\left(s_{k+1}|s_k, a_k\right)$ and the policy $\pi\left(a_k|s_k\right)$.The transition probability predicts how the environment will evolve from k^{th} time step to the

next time step, which is represented by the mathematical formulas in Equation (4.3). The reward function maps the immediate reward $r(a_k, s_k)$ by taking action a_k at state s_k for the agent. Based on the characteristics of the environment, i.e. transition probability $p(s_{k+1}|s_k, a_k)$ and the reward function $r(a_k, s_k)$, the goal of the agent is to explore the optimal control policy with the highest expectation of accumulative rewards $E_{\Gamma\, p(\Gamma)}\left[\sum_k r(a_k, s_k)\right]$.

$$p(s_1, a_1, \cdots s_N, a_N) = p(s_k)\prod_{k=1}^{N}\pi(a_k|s_k)p(s_{k+1}|s_k, a_k) \tag{4.3}$$

In this study for AIS control, the environment including the plant (the building system with AIS) and all the disturbances (e.g., the surface and air temperatures, and human activity) provides all the available indices representing building behaviors for selected real-time sensed states of $\{S|\, T_{\text{env}}, I_{sol}, T_{\text{surf}}, T_{\text{zone}}, RH\}$ and reward $r(a, s)$ defined in Equation (4.1) to train the controller/agent to generate optimal actions for R-value settings of AIS to reduce energy consumption and improve the thermal comfort through online learning.

In terms of online control and implementation, the building system (plant) and disturbances are characterized by a virtual environment for feasibility analysis of the MFORL controller before application in real buildings. For the online training, the plant, i.e., the building with AIS for experience generation is represented by the commercial simulation tool EnergyPlus which is commonly used for building energy simulation to study the thermal behavior of RBEs with dynamic thermal properties shown in **Figure 4.1**.

In regard to the offline training, a thermal network model based on a finite difference approach was developed as the plant in the simulated environment to capture the possible responses of the building with AIS, see **Figure 4.2**. This model was validated through comparison with EnergyPlus (version 9.6.0) simulation results for a single-room house integrated with AIS and high thermal mass. The simulation results indicate acceptable accuracy of the thermal network model with high computational efficiency. More details of the model formulation and validation results can be found in the previous work of the authors (He, Zhou and Fahimi, 2022). This simulated environment is developed using the Simulink based on this thermal network model, to provide training data for offline training.

(5) Agent

In this study, the agent is expected to generate an optimal control sequence to change the thermal properties of RBEs to reduce energy consumption and improve thermal comfort in the building at the same time via real-time computation. A policy $\pi\left(a|s\right)$ is a distribution of actions over given states. It defines the behavior of an agent through showing how to act in different states. The policy is the stochastic probability of taking an action, as presented in Equation (4.4). The goal of the agent is to find the optimal policy given a state.

$$\pi\left(a|s\right)=p\left(a_k=a|s_k=s\right) \tag{4.4}$$

RL algorithms for computing optimal policy mainly include Dynamic programming (DP) and Temporal Difference (TD) methods. DP methods are generally used for model-based control. TD methods learn directly from interactions with the environment without the knowledge of the models. TD methods can be divided into on-policy and off-policy methods for model-free control.

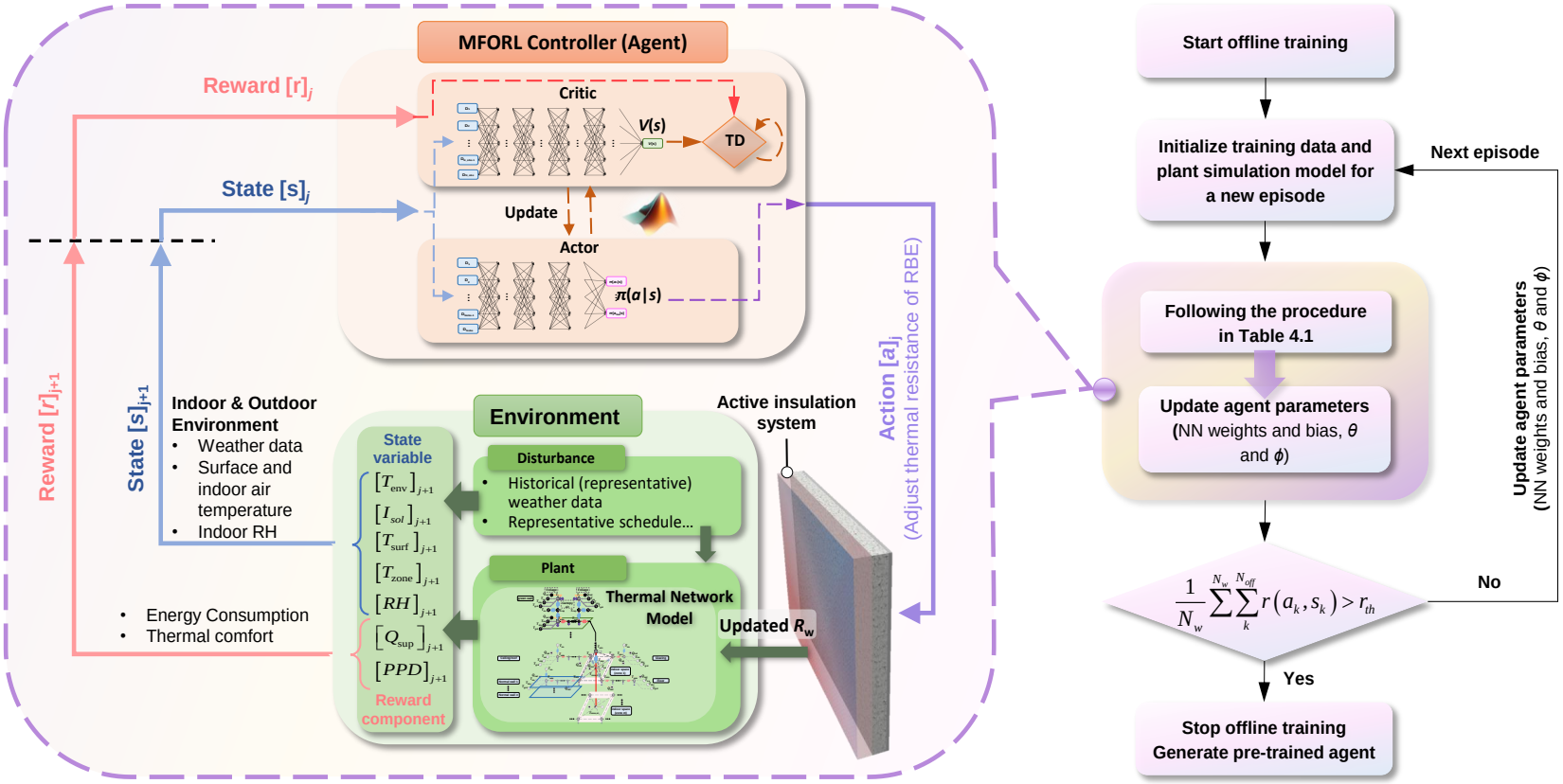


Figure 4.2 Schematic for offline training framework using MFRL for the RBE

In general, there are three MFRL methods to find optimal policies, namely, policy gradient/policy based, value-based, and actor-critic approaches. Policy based methods can handle stochastic policies effectively, but they may suffer from high variance during training, leading to slow convergence and poor sample efficiency. Value-based methods can be more sample-efficient and stable during training while they are more computationally expensive. In this case, actor-critic methods combine elements of policy based and value-based methods to address their limitations. Specifically, the actor-critic controller consists of two neural networks, i.e., the policy-based actor and the value-based critic. Similar to the practice of optimal adaptive control, the actor adjusts its parameters and learns to generate optimal policy based on the feedback from the critic which evaluates the performance of the actor through learning to estimate the value function of the current state. Accordingly, actor-critic methods can efficiently adapt to uncertain and changing environments through online learning.

As **Figure 4.1** and **Figure 4.2** show, for the MFRL controller with the on-policy method, the agent learns to update the policy through interaction with the environment, during which the actor generates actions based on the previous policy and applies them to the environment/control system throughout a specified horizon (experience horizon (Mathworks, 2022)) to generate new experience. After updating its policies based on learning from new experience during the current experience horizon, the agent completes the interaction and proceeds to the next experience horizon through repeated practice. Specifically, during j^{th} experience horizon shown in **Figure 4.1** and **Figure 4.2**, with the

newly measured experience including R-value of the AIS ($[a]_j$, i.e. $\left(a_{(j-1)N_h+1},\cdots a_{jN_h}\right)$), states ($[s]_j$, i.e. $\left(s_{(j-1)N_h+1},\cdots s_{jN_h}\right)$ including the outdoor temperatures $\left[T_{env}\right]_j$, the solar radiation $\left[I_{sol}\right]_j$, surface and indoor air temperatures $\left[T_{zone}\right]_j$, indoor air relative humidity $\left[RH\right]_j$,) and indices for reward components (e.g. thermal comfort index $\left[PPD\right]_j$ and AC supply heating/cooling rate $\left[Q_{sup}\right]_j$) and rewards ($[r]_j$, i.e. $\left(r_{(j-1)N_h+1},\cdots r_{jN_h}\right)$) through interaction with the environment, the critic identifies that action with predicted value for the current j^{th} experience horizon (N_h steps) of state and action pair. Meanwhile, the critic uses the rewards from the environment and the error to determine the prediction accuracy and update itself for a better prediction. The actor also updates itself through feedback from the critic and learns to generate the correct actions $[a]_{j+1}$ for the next interaction (j+1th experience horizon). Following the above practice, the controller collects experience, updates itself, and then moves forward to complete the whole duration, which is designated as running one episode in simulation analysis for online training and implementation, as presented in **Figure 4.1**. Given it may require long-duration training data with similar daily characteristics, it is not applicable in real systems, to generate a mature agent through online training in various scenarios. Therefore, pre-trained agents are commonly utilized to guarantee stable control performance, whose hyperparameter settings and NN settings are obtained through offline training analysis. As indicated in **Figure 4.2**, for each offline training under a specific set of parameter settings, it runs repeatedly (i.e., multiple episodes) the training practice aforementioned using selected historical weather data to generate a refined NN parameter setting. Through parametric pre-analysis of offline training with

different parameter settings, the optimal agent settings are selected for initialization in online training deployment.

(6) ANN architecture

In this study, the actor and the critic are represented by artificial neural networks, as shown in **Figure 4.3**. The node number of the input layer is set as the state space size and the number of the output layer for the actor is set as the size of the action space. To design the artificial neural networks, the number of hidden layers, hidden layer node size n_{ly} and activation functions should be properly selected. The simulation results show that low hidden layer node size and low hidden layer number are not sufficient for the ANNs to find good policies while large hidden layer node size and high hidden layer number with more clues make it difficult to find optimal policies, which leads to higher computation cost and low thermal performance. In order to improve the control performance and computation efficiency, parametric pre-analysis of the ANN architecture was conducted in offline training tests to determine the number of hidden layers, hidden layer node size n_{ly} and activation functions to attain a trade-off between training performance and computation efficiency. The training results show that the normalized input can improve the training performance of the agent with the same ANN architecture. The pre-analysis indicates that the critic with four hidden layers and the actor with three hidden layers, obtained high training performance using normalized inputs when node size parameter nly equals 10. The ANNs with Rectified Linear Unit (ReLU) activation function performed better than those with Clipped Rectified Linear Unit (Clipped ReLU) activation function and Tanh activation function.

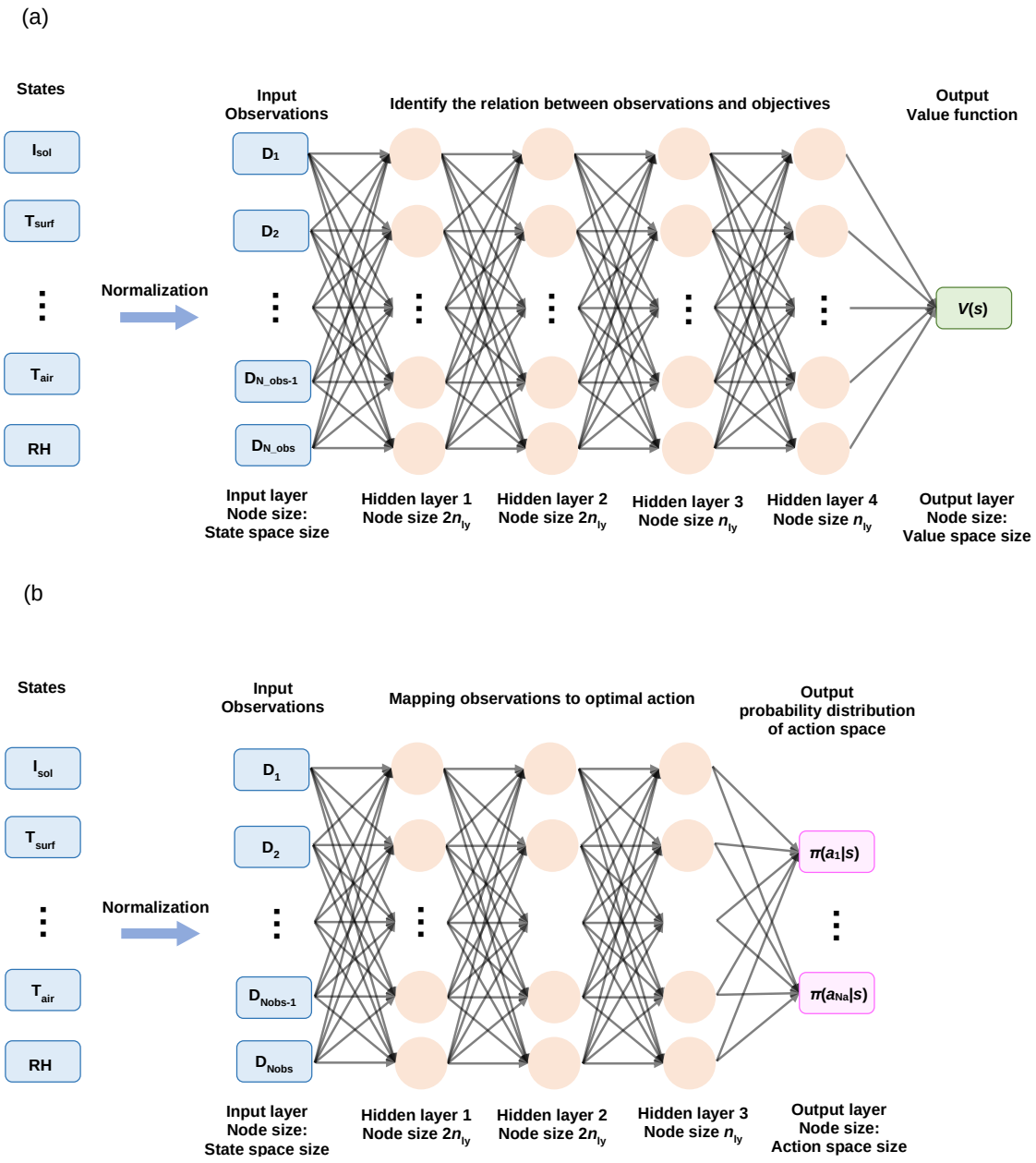


Figure 4.3 Schematic for ANN architecture of (a) the critic and (b) the actor

(7) Hyperparameters

To provide observations for the agent through interaction with the simulation environment during each experience horizon, the states are collected after every sample time (control time step); and the agent is updated based on the experience collected during the experience horizon. Parametric pre-analysis was performed to determine the proper sample time and experience horizon since small control steps lead to high maintenance costs while large control steps cannot provide sufficient observations for training. The analysis indicates that a sample time (T_s) of one hour and an experience horizon (T_h) of 12 or 24 hours strike a good balance between the training performance and instrumentation cost with low sample frequency.

4.1.2 Trust Region Policy Optimization (TRPO) algorithm

Among diverse actor-critic methods, Trust Region Policy Optimization (TRPO) algorithm obtains a trade-off between performance and training costs. TRPO is an on-policy method that improves policy gradient methods with a monotonic improvement guarantee (Schulman *et al.*, 2015, 2016). During the training using traditional policy gradient methods, large policy changes leading to performance collapse in some scenarios (Schulman *et al.*, 2015) . TRPO addresses this issue by introducing a trust region constraint. The trust region restricts the size of policy updates to prevent too far deviation between the new policy and the old policy. Consequently, TRPO achieves more stable and smoother learning with improved sample efficiency. Therefore, the actor-critic controller/agent using Trust Region Policy Optimization (TRPO) algorithm (Schulman *et al.*, 2015, 2016; Mnih *et al.*, 2016) is adopted in this study for online control of AIS with discrete action-state space.

TRPO algorithm tries to minimize the loss function related to the reward for a specific policy $\pi_j\left(a_i\left|s_i;\theta_j\right.\right)$ (Equation (4.5)) instead of the reward for a policy.

$$L\left(\theta_j\right)=\underset{\Gamma\sim\pi_{\theta_j}}{E}\left[\frac{\pi_j\left(a_i\left|s_i;\theta_j\right.\right)}{\pi_{j-1}\left(a_i\left|s_i;\theta_{j-1}\right.\right)}\right]D_i \tag{4.5}$$

where D_i is an advantage function; $\pi_j\left(a_i\left|s_i;\theta_j\right.\right)$ is the probability of taking action a_i at j^{th} experience horizon following the current policy.

To promote agent exploration, an entropy loss term $\omega\mathcal{H}_i\left(s_i,\theta_j\right)$ is added to the loss function. Thus, the optimization is modified to minimize the following loss functions.

$$L_{act}\left(\theta_j\right)=-\frac{1}{M}\sum_{i=1}^{M}\left[\frac{\pi_j\left(a_i\left|s_i;\theta_j\right.\right)}{\pi_{j-1}\left(a_i\left|s_i;\theta_{j-1}\right.\right)}D_i+\omega\mathcal{H}_i\left(s_i,\theta_j\right)\right] \tag{4.6}$$

$$\mathcal{H}_i\left(s_i,\theta_j\right)=-\sum_{i=1}^{N_a}\pi\left(a_i\left|s_i;\theta_j\right.\right)\ln\pi\left(a_i\left|s_i;\theta_j\right.\right) \tag{4.7}$$

$$L_{critic}\left(\phi_j\right)=-\frac{1}{M}\sum_{i=1}^{M}\left[G_i-V(s_i;\phi_j)\right]^2 \tag{4.8}$$

where M is the mini-batch size; w is the entropy loss weight; N_a is the action space size; G_i is the return function.

In this study, discrete action space is used and the entropy $\omega\mathcal{H}_i\left(s_i,\theta_j\right)$ is expressed as Equation (4.7). The actor parameters are updated based on the learning of the critic through minimizing the loss function defined in Equation (4.8). The minimization of $L_{act}\left(\theta_j\right)$ is subjected to the constraint:

$$\frac{1}{M}\sum_{i=1}^{M} D_{KL}\left(\theta_{j-1}, \theta_j, s_i\right) \le \delta \tag{4.9}$$

Where $D_{KL}\left(\theta_{j-1}, \theta_j, s_i\right)$ is the Kullback-Leibler (KL) divergence between the old policy and current policy; δ is the limit for D_{KL}.

Consequently, with the constraint for KL-divergence, the policy is iteratively updated over a trust region around the most recent policy and kept close to the current policy, which effectively prevents significant performance drops as compared to standard policy gradient methods. The logic for TRPO algorithm is summarized in **Table 4.1**.

4.1.3 Online control framework with pretraining

Prior studies of deep reinforced learning (Morales, 2020) indicate that it takes a certain amount of trials of search for small-scale deep neural network models to grok specialized problems and extract the desired rules from the solution space. According to pre-analysis in different scenarios, although the agent can efficiently identify the environmental characteristics and learn to switch the actions to beneficial trends rapidly to attain satisfactory performance solely based on online measured states without pre-training in some representative scenarios (e.g., those under mild weather conditions or during transitional seasons), the agent may not get abundant experience to maintain satisfactory sensitivity to all the possible modes combining different weather conditions, building types, and internal gains during online training leading to delayed beneficial responses for complex real systems. Therefore, pre-leaned experiences can help the agent identify the changing modes with limited online training experience and make instant decisions for smooth operations.

Table 4.1 TRPO algorithm logic

Initialize the hyperparameter: learning rate, the discount factor Initialize the NN parameter: θ and ϕ for actor $\boldsymbol{\pi}(a\|s;\theta)$ and critic $\boldsymbol{V_L}(s;\phi)$ Initialize environment: initial state of disturbances and plant	**Initialization**
for each episode iteration **do**	
for j^{th} Experience Horizon [$(j$-1)N_h+1th - jN_h^{th} step]	
Sample actions $[a]_j$ by the actor	**Interaction with environment**
Collect probability $\boldsymbol{\pi}(a\|s;\theta)$	**Implementation**
Execute actions	**Experience collection**
Generate experiences of N_h steps under the current policy: action $[a]_j$, state $[s]_j$, and reward $[r]_j$	
Compute the return function $[G]_j$	
for each learning epoch **do**	**Learning from collected**
Sample a random mini-batch data set of size M from the current set of experiences.	**experience**
Update ϕ by minimizing L_{critic}	**Online training and updating**
Update θ by minimizing L_{actor}	
end for	
end for	
end for	

To guarantee instant actuation and robust performance with low computation costs and controller complexity, an online training and control strategy with pre-training is applied for deployment. Before online implementation, offline pre-training is performed as shown in **Figure 4.2**, where a mathematical model, i.e., the thermal network model is adopted to represent the plant behavior in the target environment. Specifically, to achieve robust pre-trained agents, the training weather data should be properly selected with high daily fluctuations in temperature or with obvious seasonal characteristics (e.g., heating, cooling, and transitional). In this study, a specific set of typical meteorological year 3 (TMY3) weather data was adopted as the training disturbances for the offline training. Following the procedure presented in **Figure 4.2**, with fixed hypermeters in **Table 4.1**, the training inputs for disturbances and the simulation plant model are initialized for a new episode, the agent parameters, i.e., NN parameters (weights and bias) and key parameters θ and ϕ of actor $\boldsymbol{\pi}(a|s;\theta)$ and critic $\boldsymbol{V}(s;\phi)$ are initialized using the values learned from the previous episode. It keeps running the iteration, i.e., multiple episodes of the training practice described in Section 4.1.1 and 4.1.2 using the same disturbances, during which the agent parameters are refined, and the agent gradually learns to utilize the benefits of the outdoor environment via AIS correctly. Consequently, it stops the offline training when the moving average episode reward (Morales, 2020) $\frac{1}{N_w}\sum^{N_w}\sum_{k}^{N_{off}} r\left(a_k, s_k\right)$ within the designated window (with the length of N_w) reaches the prescribed threshold r_{th} to guarantee stable convergence. Based on the experience obtained in different scenarios the agent is

pre-learned how to map the observations to the actions under different weather modes for initialization in online training.

As indicated in the flowchart for online control with pre-training in **Figure 4.4**, when the pre-trained agent is applied at the beginning of the first experience horizon/execution horizon (Zeng, Augenbroe and Chen, 2022) (the time horizon over which the control sequence is implemented), the agent is initialized with parameters (e.g., NN parameters, θ and ϕ) attained from offline training so that the actor generates the actions based on the policy trained by representative experience. As the controller completes the operation for the first execution horizon, the agent collects the experience generated during the current execution horizon (i.e., experience horizon) as the training data for online training. The executed results and the updated agent parameters are saved as the initial conditions for online training and implementation of the next execution horizon. As a result, the agent generates actions using the updated policy from the most recent experience horizon to keep the agent sensitive to the changes in outdoor and indoor environments.

The control action generated by the actor largely depends on whether the observations of the current state and the reward function can help the agent with proper parameter settings to identify the correlation among outdoor weather disturbances, dynamic thermal properties of envelopes, and indoor thermal response efficiently. In addition, the model complexity of the agent also has a high impact on the training performance and deployment costs (e.g., the hidden layer number and NN node size).

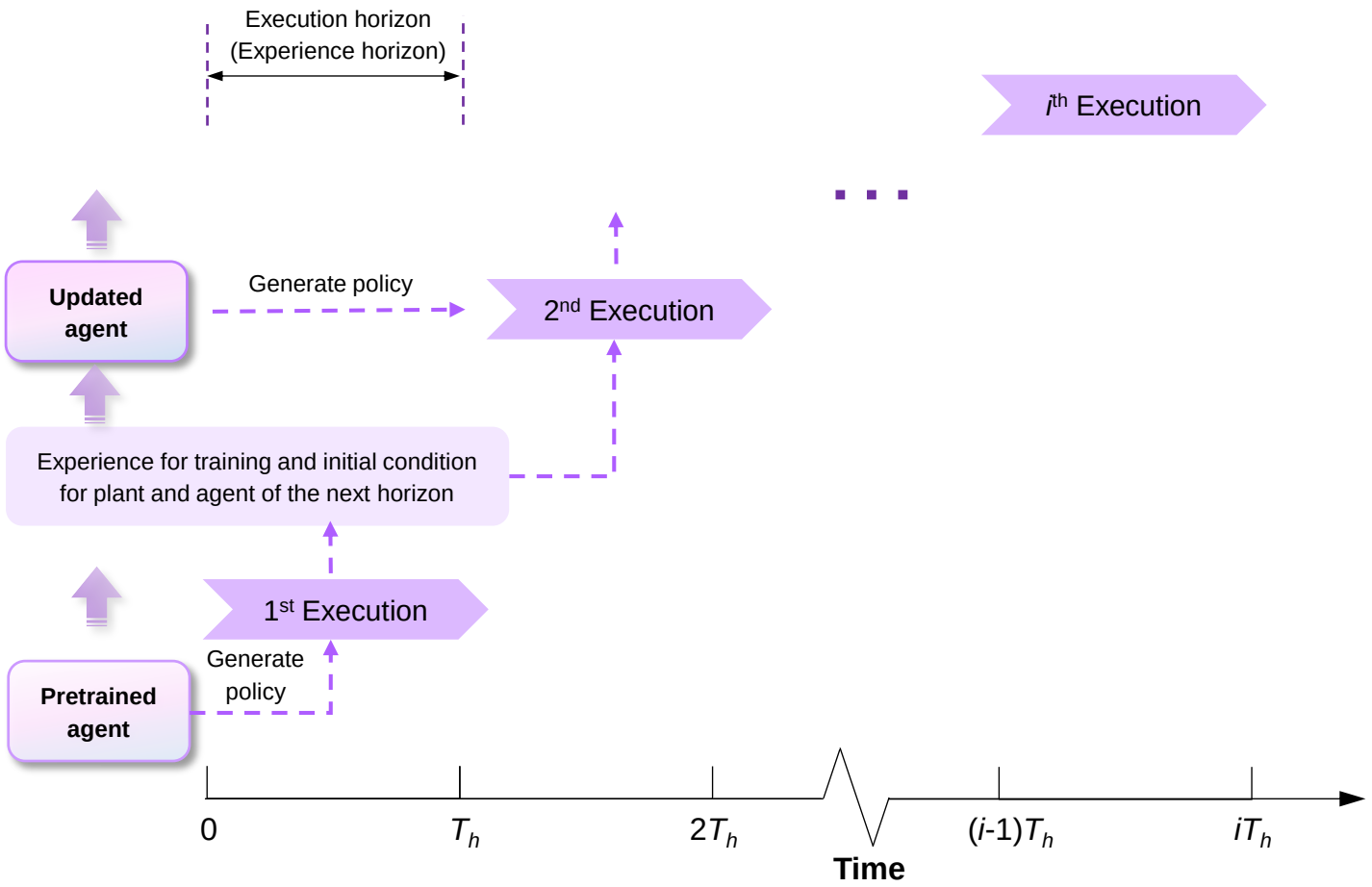


Figure 4.4 Schematic for online training with pretraining

During each experience horizon, the experience is collected after every sample time (control time step) to provide observations to update the agent through interaction with the environment. Sample time and experience horizon should be properly selected since small sample time sizes lead to high instrumentational maintenance and computation costs while large control steps cannot provide sufficient observations for training. To provide the optimal design for the MFORL controller with low complexity, high learning performance and computation efficiency, and low training complexity, parametric pre-analysis through offline training was performed using different settings of sample time, experience horizon duration, ANN architecture, action space, state variable, and training data size, with the results elaborated and discussed in Section 4.2.

The RBE thermal behavior and building energy performance generated under the controller with pretraining using the observations of weather data and system behavior will be analyzed to investigate its potential for performance improvement as compared to those under simple temperature-based control and demand-based control.

4.1.4 Case studies

4.1.4.1 Co-simulation framework for MFORL control of RBE

In this research, a co-simulation of the building with AIS was performed to testify the performance of the MFORL controller with the framework presented in **Figure 4.1**. The co-simulation platform consists of the data input layer, control layer, data exchange layer, and simulation layer. The data input layer generates the monitored data and schedules for the control and simulation layers. The MFORL controller in the control layer generates the optimal control values (R-value of AIS) based on multi-objective optimization at each control step through online training by MATLAB. The simulation layer serves as the plant

to generate the building's thermal behavior. The data exchange layer is used for data communication and implementation synchronization between the controller and the plant. In this layer, the data exchange platform was established by MLEP Co-simulation Toolbox (Dostal and Baumelt, 2019) using Building Controls Virtual Test Bed (BCVTB) (Wetter, 2011). Once the control sequence is implemented in the simulation layer for the plant, the responses of the building with RBE (e.g., $T_{\text{env}}, I_{sol}, T_{\text{surf}}, T_{\text{zone}}, RH, Q_{\text{sup}}$ and LPD) are transferred back to the MFORL controller via the data exchange layer. In response to the feedback from the simulation layer, the MFORL agent updates its parameters (e.g., NN parameters, θ and ϕ) for implementation in the next control step. The whole co-simulation framework is packaged in the Simulink environment and executed by MATLAB script automatically.

4.1.4.2 Simulation details

To study the thermal behavior of the AIS-integrated RBE using different control strategies and learning performance of the MFORL controller, co-simulation case studies were conducted for a 13 m (L) × 8m (W) ×3.05 m (H) exterior thermal zone extracted from an intermediate floor of an apartment building. This thermal zone consists of five internal walls and one exterior wall which can be the baseline with static thermal properties or RBE as shown in **Figure 4.5**. All the internal walls are assumed to be adiabatic (Jin, Favoino and Overend, 2017). The RBE is composed of a concrete (thermal mass) layer sandwiched between an exterior opaque AIS and an interior gypsum layer. The baseline exterior wall, where a concrete mass layer is sandwiched between a rigid foam insulation panel and a gypsum layer, is designed with the same layout and overall thermal mass as the RBE case. The R-value of exterior AIS is tunable to improve the indoor environment in response to

the dynamic outdoor environment. The thermal resistance of exterior AIS varies between the lower limit R_{min} (0.1 Km^2/W) and the upper limit R_{max} (2.3 Km^2/W), based on the reference range reported in prior research (Menyhart and Krarti, 2017; ASHRAE, 2019; Mumme and James, 2020; Juaristi *et al.*, 2021). The overall R-value of the static baseline is set the same as maximum thermal resistance of the RBE. The window-to-wall ratio is 15% for the exterior wall. The indoor air temperature was controlled by HVAC with dual setpoints of 21.1-23.9℃. Some other simulation parameters considered include occupant activities, lighting, equipment schedules, and infiltration level as listed in **Figure 4.5**. The Predicted Mean Vote (PMV) and Predicted Percentage of Dissatisfied (PPD) based on Frager's model (ISO, 2005) are used to evaluate the thermal comfort-time performance of the building. The Long-term Percentage of Dissatisfied (LPD) is used to assess occupants' long-term thermal comfort (Carlucci, 2013). Typical meteorological year 3 (TMY3) weather data of Chicago (ASHRAE climate zone 5A), IL with different seasonal characteristics were adopted for the offline pre-training and online deployment.

Three control strategies, i.e., a simple temperature-based control, demand-based control, and MFORL control are applied for the RBE cases. The controller aims to generate beneficial control sequences for the R-value of exterior AIS to reduce energy consumption and improve thermal comfort at the same time. The thermal performance improvement for the baseline by the RBE using these three control strategies in three representative periods in Chicago, IL are compared to assess the learning performance and robustness of the online control strategy using a pre-trained agent.

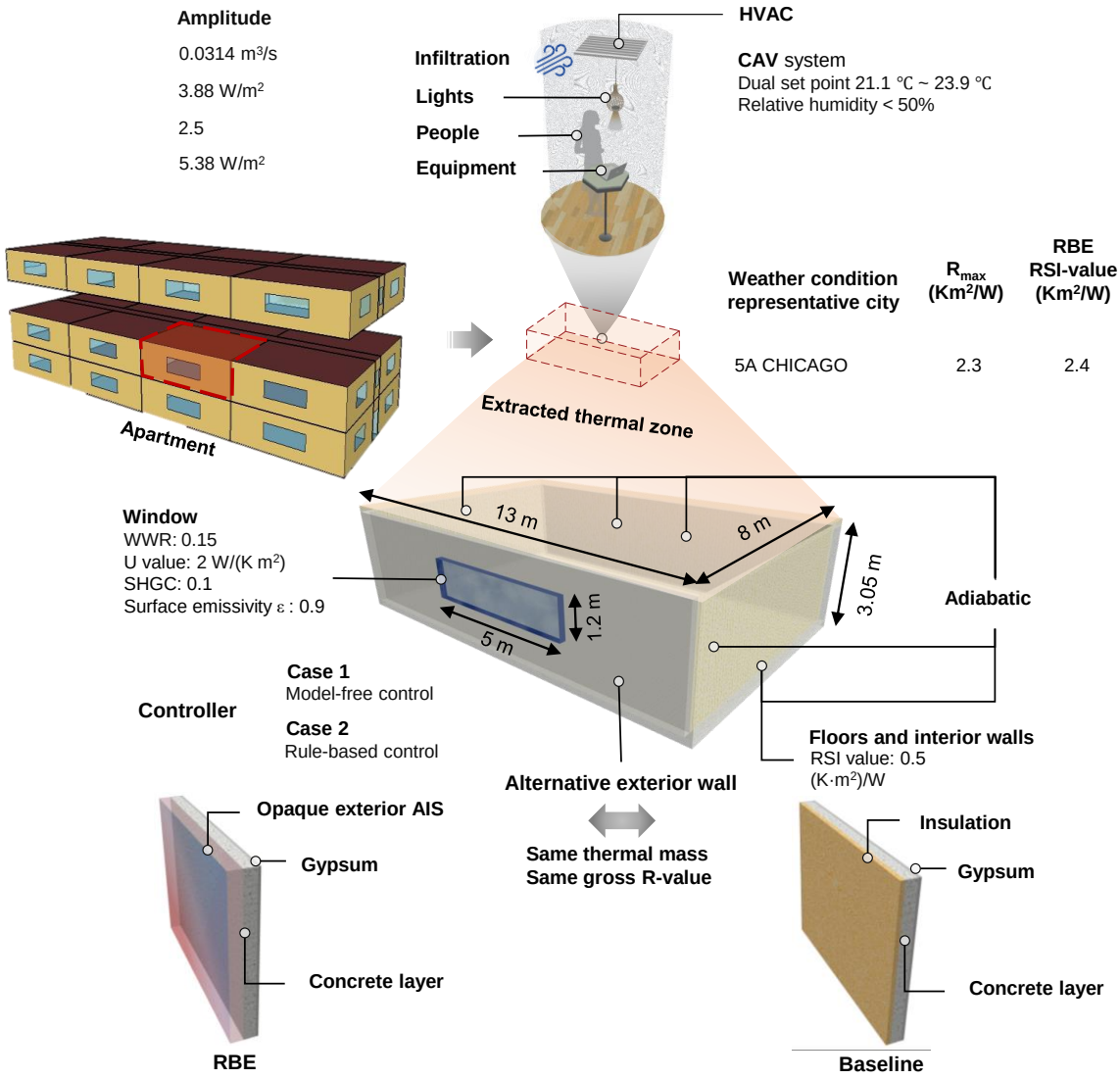


Figure 4.5 Simulation details of the case studies

4.1.4.3 Rule-based control for training performance evaluation

To evaluate the performance of the MFRL controller, its thermal performance improvement was compared with that under rule-based control, i.e., simple temperature-based control and demand-based control.

(1) Simple temperature-based control

As shown in **Figure 4.6** on Page 133, for the exterior AIS^{b}_{ext} that can change the thermal resistance (R-value) between two values ('on-and-off mode') such as those presented in previous studies (Park, Srubar and Krarti, 2015; Menyhart and Krarti, 2017), a simple temperature-based control logic similar to the one in the previous work (Kishore *et al.*, 2021) is applied as the following:

(1) Under heating mode, when the exterior surface temperature is higher than the interior surface temperature at k^{th} time step ($T^k_{ex_surf} > T^k_{in_surf}$) and exterior surface temperature is lower than the secondary temperature constraint $T_{th,ht}$ in case of overheating effect, the R-value of AIS^{b}_{ext}, R^k_w , is set to R_{min} to facilitate heat flow to charge the concrete thermal mass; otherwise if $T^k_{ex_surf} < T^k_{in_surf}$ or $T^k_{ex_surf} > T_{th,h}$, R^k_w is set to R_{max}. (2) Under cooling mode, when the exterior surface temperature is lower than the interior surface temperature at k^{th} time step ($T^k_{ex_surf} < T^k_{in_surf}$) and exterior surface temperature is higher than the secondary temperature constraint $T_{th,cl}$ in case of overcooling effect, R^k_w is set to R_{min} to help to dissipate the undesirable heat stored in the concrete layer to the outdoor environment, whereas when $T^k_{ex_surf} > T^k_{in_surf}$ or $T^k_{ex_surf} < T_{th,c}$, R^k_w is set to R_{max}.

In this case study, the threshold values for the secondary temperature restriction are set as $T_{th,cl}$=16℃ and $T_{th,ht}$=26℃ based on prior research (Kishore *et al.*, 2021) to modulate the temperature of the thermal mass to avoid overcooling/overheating.

(2) Demand-based control

The demand-based control rule for AIS^{b}_{ext} follows the logic described in Section 3.1.1. In the co-simulation with EnergyPlus, the predicted AC load is calculated using the accurate physics-based model in EnergyPlus based on sensed data with much larger size than those required for the operation of MFORL controller.

4.2 Offline pretraining

4.2.1 Offline training results

With the selected training settings illustrated in Section 4.1, offline pre-training was performed for the case elaborated in Section 4.1.4. using representative weather data. The training processes and performance comparison for one of typical scenarios are presented in **Figure 4.7**. **Figure 4.7** (a) presents a typical offline training process of episode rewards reaching stable convergence. The episode reward initially fluctuates at low values as the agent explores potential solutions in different directions. Gradually, the episode reward increases as the agent optimizes its actions in the trust region (Schulman *et al.*, 2015) based on past training experience. The offline pre-training stops when high-level moving average episode rewards $\frac{1}{N_w}\sum^{N_w}\sum_{k}^{N_{off}} r\left(a_k, s_k\right)$ stabilize within a designated window to ensure robust pre-trained agents.

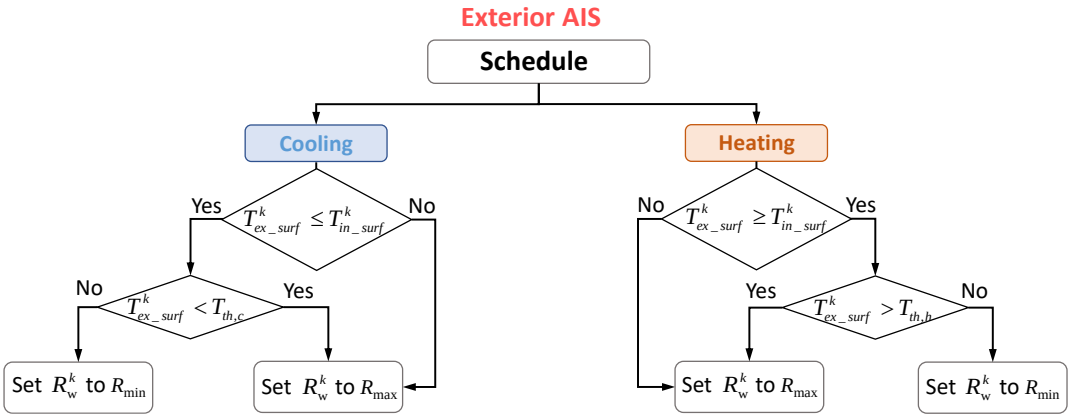


Figure 4.6 Control logic of simple temperature-based control for the AIS-integrated RBE

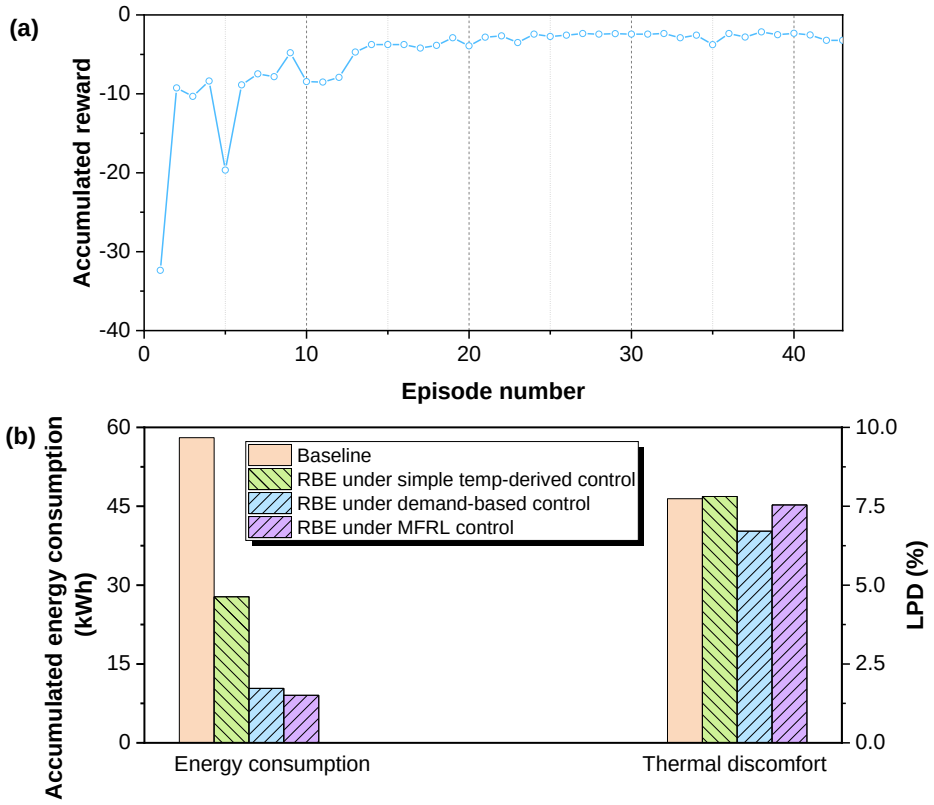


Figure 4.7 (a) Offline training episode reward in a typical training process (b) Comparisons of accumulated energy consumption and LPD among baseline and RBE cases under rule-based control and MFRL control by offline training

The simulation results by EnergyPlus for the baseline and RBE cases using a simple temperature-based controller, demand-based controller, and the agent from offline training are summarized in **Figure 4.7** (b). The RBE controlled by the MFRL agent provides the highest energy savings among the three RBE cases while maintaining improved thermal comfort for the baseline. The satisfactory performance with a balance between conflicting objectives (Jin, Favoino and Overend, 2017; Halhoul Merabet *et al.*, 2021) of energy efficiency and thermal comfort highlights the reliability of offline training performance and the proper selection of key parameters to obtain robust performance. The demand-based controller based on a high-fidelity AC load prediction model and monitoring massive data obtains higher energy-saving potential than the simple temperature-based controller. Although MFRL controller provides slightly lower thermal comfort improvement than the demand-based controller, it achieves a trade-off between performance and deployment costs with lower costs of controller formulation and instrumentation.

4.2.2 Implications for controller design and offline pre-training

The pre-analysis shows that the agent with an action space size of 10 obtained a good balance between training performance and computation efficiency. This is consistent with the findings in prior studies (Rupp and Krarti, 2019; He, Zhou and Fahimi, 2022), showcasing the advantage of AISs with continuous thermal resistance changes for higher energy savings than those with binary thermal switches. In the pre-analysis, the number of state variables was reduced from over 20 alternative features to 10. The dimension reduction in state space leads to controller complexity reduction and training acceleration (Wang and Hong, 2020). This substantially cuts down the cost of instrumentation and

maintenance for the controller as compared to the high-fidelity cases monitoring massive data.

Studies on the relation between generalization performance and training data (Power *et al.*, 2022) suggest that smaller datasets increase training costs for generalization. Similarly, the offline training results demonstrate that the RL agent efficiently grasps specific control rules using the training data with similar characteristics during adjacent experience horizons to ensure sufficient learning experience. This adds to the difficulty in training data design and induces large training data size. As a result, achieving a single small-scale pre-trained agent fully compatible with all patterns with solutions in diverse/opposite directions becomes highly computationally demanding. To attain a trade-off between robustness and training costs, the complicated problem of learning response to all the weather patterns is decomposed into pre-training the small-scale agents under several representative patterns, respectively (Wang and Hong, 2020). This allows efficient adaptation and fine-tuning of the agent during online learning and control. Thus, only small-scale ANNs and training data are required, significantly enhancing the training performance with low computation complexity.

To improve the efficiency during training the agent to respond to different weather patterns, the training weather data should include characteristics of a specific pattern with some noise or fluctuations. These environment perturbations promote exploration and advance robustness to uncertainties. In view of these requirements, customized designed weather data and historical weather data were applied in the pre-analysis. The training results indicate that the pre-trained agents using TMY3 data exhibit superior adaptability

and sensitivity to fluctuating weather conditions with more uncertainties than those trained using customized data. In prior studies on RL control for building energy efficiency and indoor environment improvement, large training data (30 days to 30 years) were required for offline pre-training to obtain satisfactory performance (Wang and Hong, 2020). In this study, the pre-analysis results using different weather data sizes show that 1-day or 3-day training data are unabundant for the small-scale agent in this study to find optimal policies. Satisfactory training performance is attained using only 7-day or 8-day training data, which are adopted as the offline training data size to reach stable convergence. The small training data size significantly reduced pre-training costs for deployment.

Moreover, the offline training using thermal network models as the plant takes only 1/32-1/21 computation time of those using commercial software (e.g., EnergyPlus) per episode. This substantial reduction in computational costs demonstrates the superior efficiency of the thermal network model and its potential in improving training performance and other AI-based control studies.

4.3 Evaluation of MFORL control

To assess the online adaptation and performance improvement potential of the MFORL controller with pre-training, online co-simulation analyses were performed for three representative scenarios in Chicago, IL using the case details described in Section 4.1.4. To analyze the differences in the thermal performance and operation modes between rule-based control and MFORL control for the RBE with AIS when applied to residential buildings, weather conditions, R-value settings, daily temperatures, AC load, energy use as well as PPD profiles are presented during representative days to evaluate the

contributions to indoor environment improvement. Analyses of different scenarios under representative weather conditions are presented in **Figure 4.8**, **Figure 4.9** and **Figure 4.10** with the detailed results of: (a) outdoor air temperature and solar radiation; (b) exterior AIS R-value setting and indoor air, interior and exterior surface temperatures under simple temperature-based control; (c) exterior AIS R-value setting and indoor air, interior and exterior surface temperatures under MFORL control; and comparisons among baseline and RBE cases under simple temperature-based control, demand-based control, and MFORL control in the performance of: (d) AC load (e) PPD (f) energy consumption.

4.3.1 Heating season

During cold winter, two-week (February 9th–22nd) representative data in Chicago, IL are chosen to study how the MFORL controller responds to the highly fluctuated outdoor environment. Relevant weather conditions are plotted in **Figure 4.8** (a) showing the fluctuated outdoor air temperature with a big range of 27°C and high variations in peak solar radiation. The thermal behavior of the RBE and AIS operations under rule-based control and MFORL control during the typical heating season are presented in **Figure 4.8** (b)-(f). During winter months, the AC is operated under heating mode for most days. **Figure 4.8** (b) indicates that the exterior surface temperature of RBE was lower than the interior surface temperature during most of this period. The thermal resistance of the exterior AIS under simple temperature-based control therefore, mostly remained as R_{max} to reduce the heat loss from the indoor space.

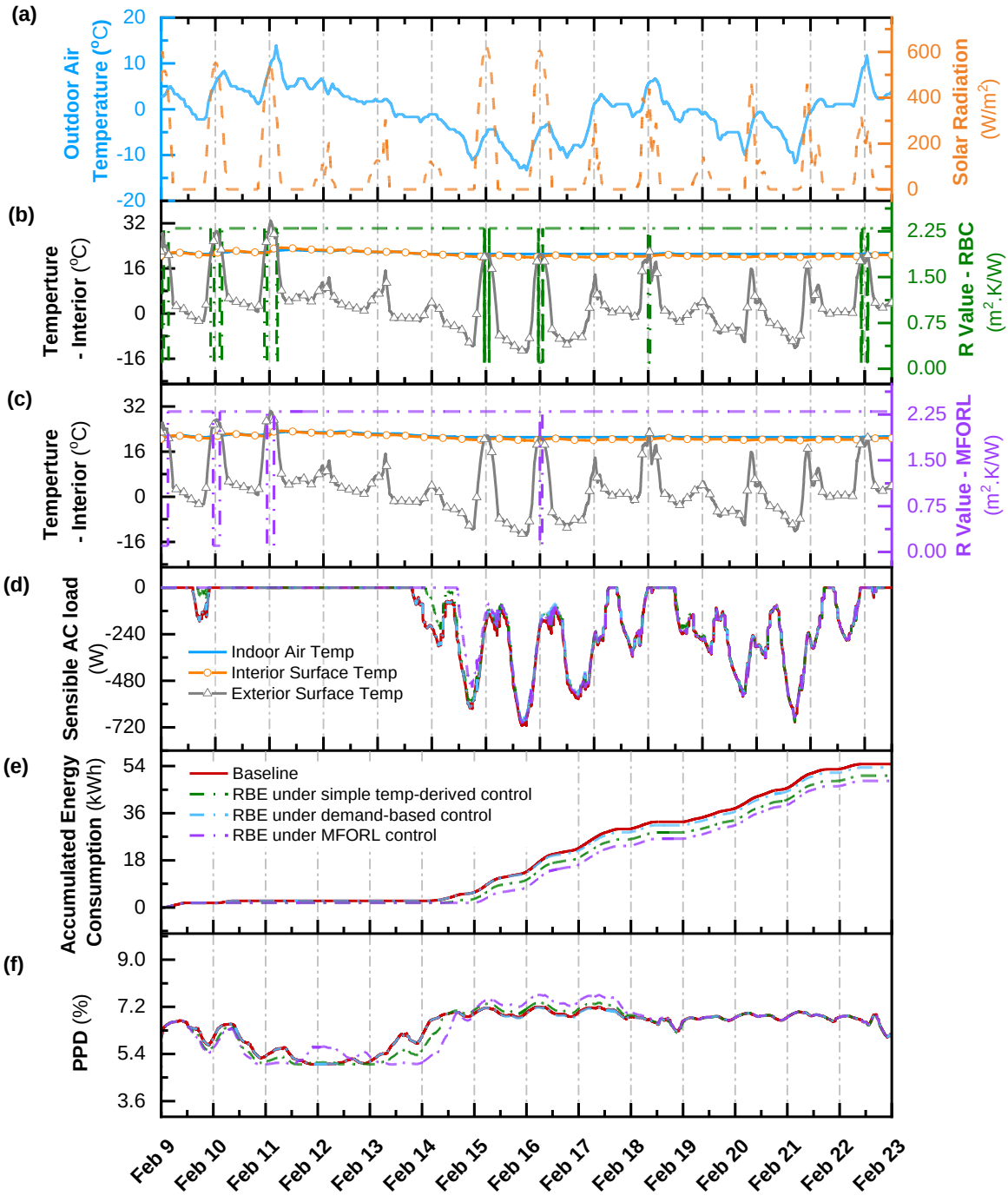


Figure 4.8 Thermal behavior of RBE cases and baseline in a typical heating season (February, Chicago, IL).

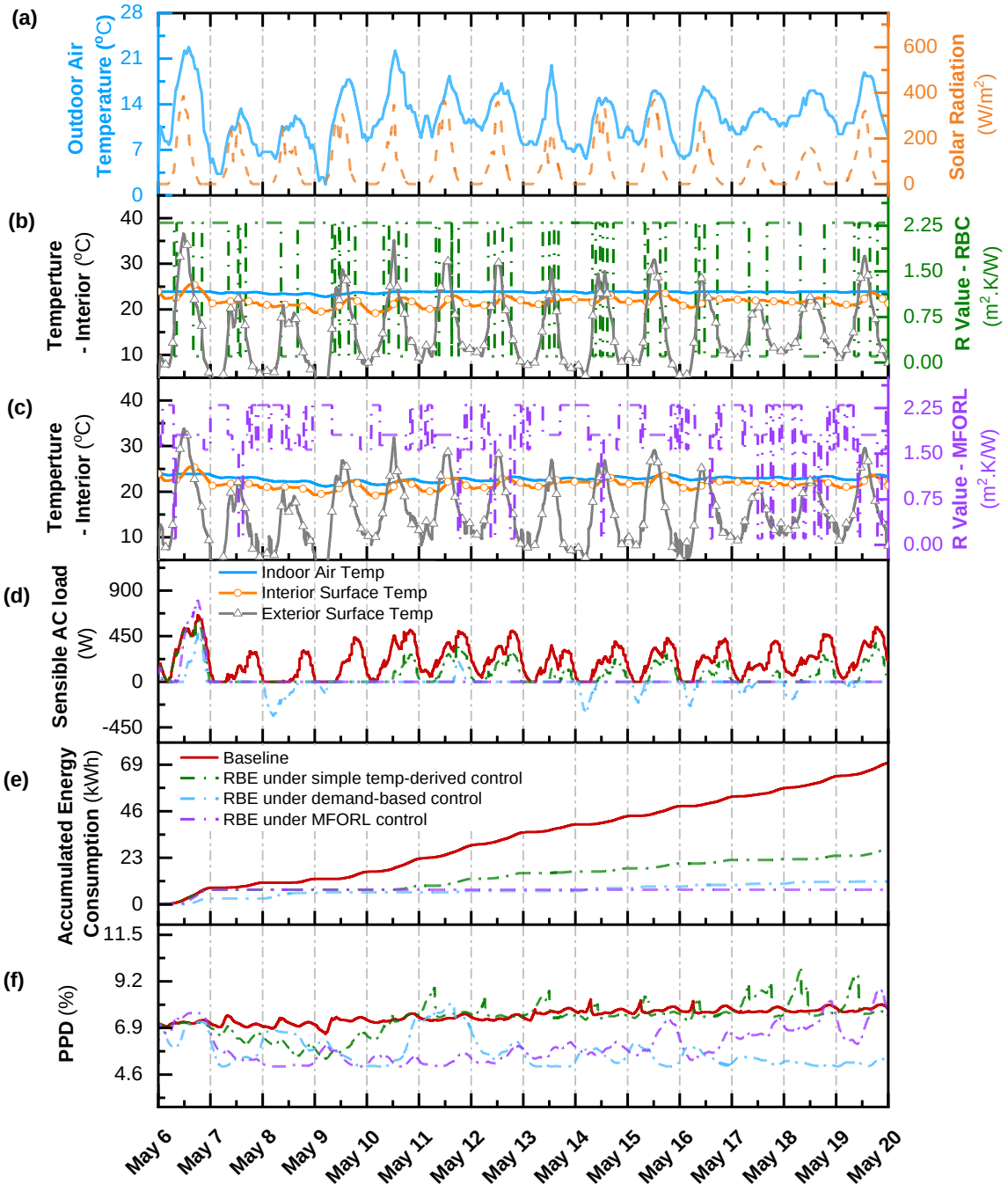


Figure 4.9 Thermal behavior of RBE cases and baseline in a typical transitional season (May, Chicago, IL)

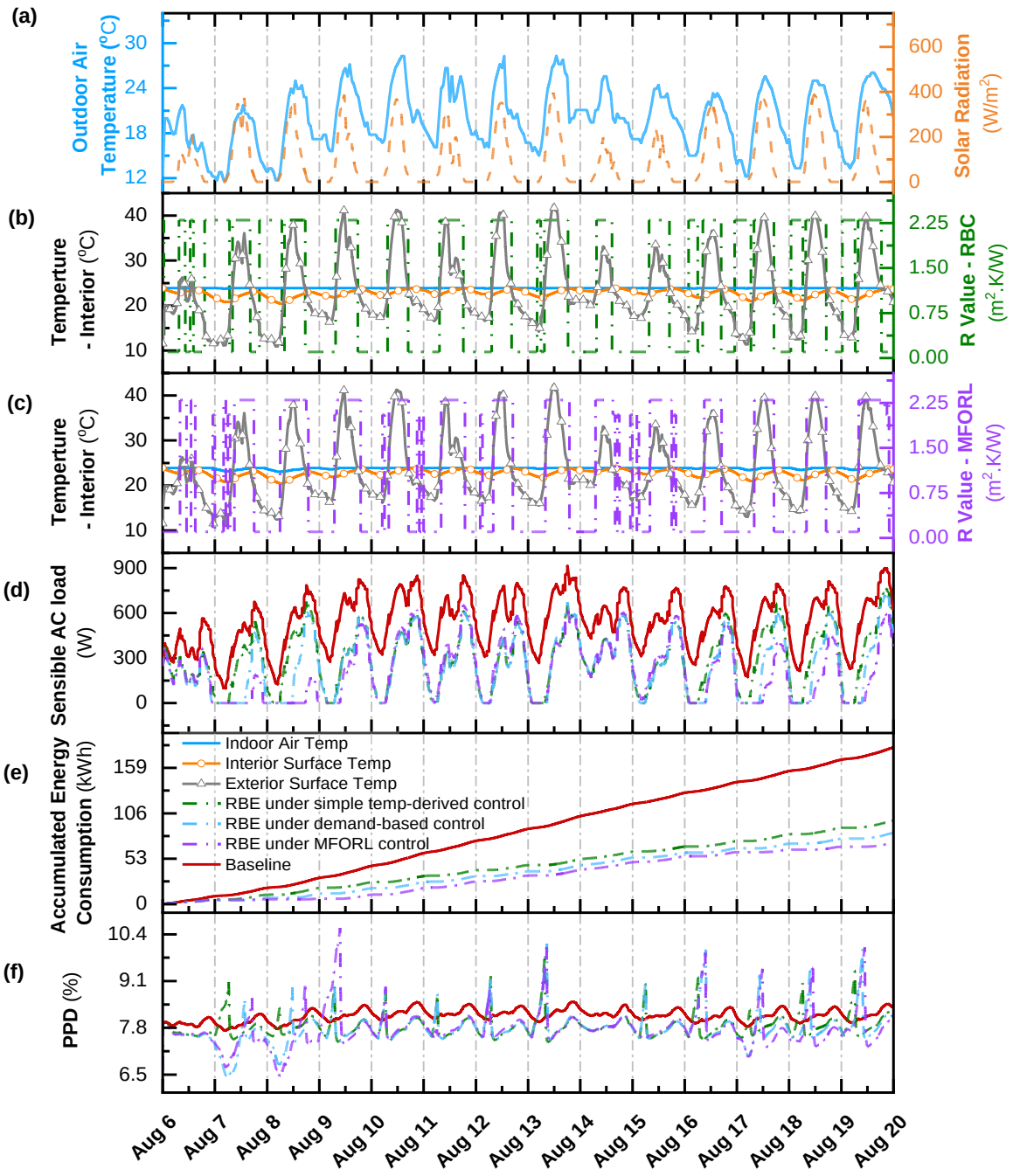


Figure 4.10 Thermal behavior of RBE cases and baseline in a typical cooling season (August, Chicago, IL)

While as **Figure 4.8** (c) shows, the exterior AIS under MFORL control switched between R_{min} and R_{max} with a longer duration at low thermal resistance (R_{min}) during the first three days when the outdoor air temperature and solar radiation were high to harvest more heat into indoor space. Consequently, the indoor space temperatures were maintained at higher levels and the AC load of the RBE case under MFORL control was still kept around zero during the second and the sixth days as compared to the increasing AC loads of the other two cases, see **Figure 4.8** (d). This superior performance during the initial stage of the deployment implies the benefits of pre-training to improve the performance of online control.

Additionally, the R-value settings exterior AIS transited from on-and-off mode during the first three days to remaining mostly at R_{max} during the following days when sharp decreases occurred in outdoor air temperatures and solar radiation. This demonstrates the MFORL controller's flexible adaptability to large variations in changing environments through online learning to fully utilize AIS charging indoor space in heating seasons. Similar to the trend of AC load reduction, the RBE under MFORL control obtained higher energy savings (11.8%) than those under simple temperature-based control (8.2%) and demand-based control (2.4%), as shown in **Figure 4.8** (e).

The demand-based control sequence is determined based on the accurate prediction of AC load using the detailed physics-based model of EnergyPlus based on monitoring more features than those required for MFORL control. However, the demand-based controller provides lower energy use reduction than the simple temperature-based control in this scenario. This demonstrates that a high-fidelity model not necessarily attains better

performance while end-to-end online learning using several sensed indices with global optimization by MFORL controller is more efficient and cost-effective for controller formulation and deployment. Furthermore, the RBE under MFORL control attained good thermal comfort with lower PPD simultaneously in comparison with the baseline, as presented in **Figure 4.8** (f).

The R-value schedules generated by the MFORL controller also switched less frequently than those by the simple temperature-based controller. This reduces unnecessary actuation of AIS and obtains a trade-off between thermal performance and maintenance cost. This demonstrates the crucial role of the refined reward function in guaranteeing learning performance and stable operation.

4.3.2 Transitional season

Figure 4.9 shows the thermal behavior and R-value settings of the AIS-integrated RBE using different controllers during a transitional season. Two representative weeks (May 6^{th} – 19^{th}) in Chicago, IL with high variations in peak temperatures and daily temperature ranges presented in **Figure 4.9** (a), are selected to investigate how AIS makes full use of beneficial passive cooling via MFORL controller.

As **Figure 4.9** (b) - (e) show, the exterior AIS switched frequently to utilize passive cooling and effectively reduced the energy consumption under the simple temperature-based control with a secondary temperature constraint (i.e., $T_{th,c}$=16 ℃) to prevent overcooling. However, the RBE energy performance using this simple temperature-based controller is highly dependent on the prescribed secondary temperature constraint $T_{th,c}$. It has a limitation of various optimal values in different scenarios demonstrated in the

previous work (He, Zhou and Fahimi, 2022) and impedes its applicability in multiple weather conditions throughout a year.

In contrast, the thermal resistance of the exterior AIS under data-driven MFORL control flexibly switched among multiple intermediate values to fully take advantage of cooling thermal energy from the outdoor environment. Therefore, the reduced interior surface and indoor air temperatures provided higher AC load reduction, see **Figure 4.9** (c) and (d). Meanwhile, the exterior AIS was restrained with less duration at low thermal resistance (R_{min}) under MFORL control to prevent overcooling. Consequently, the indoor air temperature was maintained as low-level values within the dual setpoints without too much deviation. In response, the heat flow from the outdoor environment was controlled precisely by the MFORL controller as the desired values to offset the AC load. Accordingly, the AC load was drastically reduced through online learning during the first day and maintained around zero during the rest 13 days as compared to those under rule-based control and baseline as shown in **Figure 4.9** (d). Although the MFORL agent did not have enough experience initially and showed similar performance to the rule-based controllers during the first day, it quickly adjusted its parameters based on the learning experience of the first day to fully leveraged the strengths of AIS. In consequence, the energy use was maintained around zero on the fifth day with similar weather characteristics to those of the first day.

As indicated in **Figure 4.9** (e), the RBE case under MFORL control provides much higher energy savings (89.7% energy consumption reduction) than those under simple temperature-based control (61.3% energy consumption reduction) and demand-based

control (83.9%). Moreover, the RBE under MFORL control and demand-based control exhibits substantial thermal comfort improvement with much lower PPD in comparison with the one under simple temperature-based control, as demonstrated in **Figure 4.9** (f).

The R-value settings of exterior AIS under MFORL control in transitional seasons also indicate that the high-level R-value is not necessarily required for mild weather conditions. The exterior AIS R-value under MFORL control was just slightly lower than that under simple temperature-based control with on-and-off mode between R_{min} and R_{max} while obtaining better thermal performance with lower operation cost. The R-value schedules varying among different values within the prescribed range implies the intelligent modulation of the indoor thermal environment and wise actuation regulation by the MFORL controller with flexible updating in the R-value schedules as the online training moves forward when new changes occur in the outdoor and indoor environment. These phenomena also demonstrate the advantages of the AIS that changes its R-value continuously or with multiple steps in improving RBE thermal performance, which is consistent with the finding in previous works (Rupp and Krarti, 2019; He, Zhou and Fahimi, 2022).

4.3.3 Cooling season

In terms of the scenario in cooling seasons, two representative weeks (August 6th – 19th) during summer in Chicago, IL, are selected to study the performance of AIS-integrated RBE under MFORL control. **Figure 4.10** presents the simulated thermal behavior and exterior AIS R-value settings for the AIS-integrated RBE wall using different control methods during the cooling season.

As **Figure 4.10** (a) presents, from August 10th to August 16th, the outdoor air temperature remained at a high level during the daytime so that the exterior AIS under simple temperature-based control switched between R_{max} and R_{min} to insulate outdoor unwanted heat, see **Figure 4.10** (b). The exterior AIS under MFORL control exhibited similar practice for the R-value settings during most of this period as shown in **Figure 4.10** (c). As a result, no obvious difference was observed in the AC load reduction during these 7 days between the RBE cases under different control logics, according to **Figure 4.10** (d). While during the rest time of these two weeks, exterior AIS was set to R_{min} in time under MFORL control to exploit the beneficial cooling effect from the outdoor environment and dissipate more redundant energy stored in the concrete layer opportunely under the cooler environment in the early morning, in comparison with the RBE cases under rule-based control. Therefore, the RBE case under MFORL control provides higher AC load reduction during this period than those under rule-based control, as presented in **Figure 4.10** (d).

Consequently, this contributes to higher energy consumption reduction (60.8%) by the RBE using the MFORL controller compared with the RBE cases using the simple temperature-based controller (46.5%) and demand-based control (54.5%), as demonstrated in **Figure 4.10** (e). Similar to the behavior in the previous scenario, the RBE case under MFORL control attains higher thermal comfort improvement along with promising energy performance as compared to the other two cases, according to the PPD profiles shown in **Figure 4.10** (f). Hence, the RBE under MFORL control allows more flexible charging and discharging of the thermal storage layer to provide higher energy savings and thermal comfort improvement than the cases using the rule-based controllers.

In addition, the long-term thermal comfort performance was also calculated for the baseline and RBE cases under both rule-based control and MFORL control. **Figure 4.11** (a) and (b) summarize the energy consumption and the long-term percentage of dissatisfied (LPD) in these three representative scenarios in Chicago, IL. The simulation results indicate that the MFORL controller provides the highest energy savings among AIS-integrated RBE cases in different seasons while maintaining satisfactory thermal comfort improvement. The AIS-integrated RBE cases under MFORL control bring 0.2% - 19.6% LPD reduction, which are higher than those using rule-based controllers, especially in the transitional seasons and cooling seasons. This showcases a good balance between the conflicting optimization objectives of energy savings and thermal comfort improvement by the MFORL controller.

4.4 Conclusions

In this study, a comprehensive MFORL training and control strategy using TRPO algorithm is proposed for climate-adaptive buildings with an AIS-integrated RBE. The MFORL controller adjusts the thermal resistance of RBE to attain energy savings and thermal comfort improvement solely based on several monitored indices without closed-form knowledge/detailed modeling of the sophisticated systems.

An MFORL control framework using a co-simulation testbed is developed to implement the control strategies and evaluate the training performance. To guarantee robust online control performance and obtain a trade-off between controller complexity and deployment costs, the pre-trained agent is applied in the case studies of the RBE consisting of exterior AIS and sensible energy storage under MFORL control.

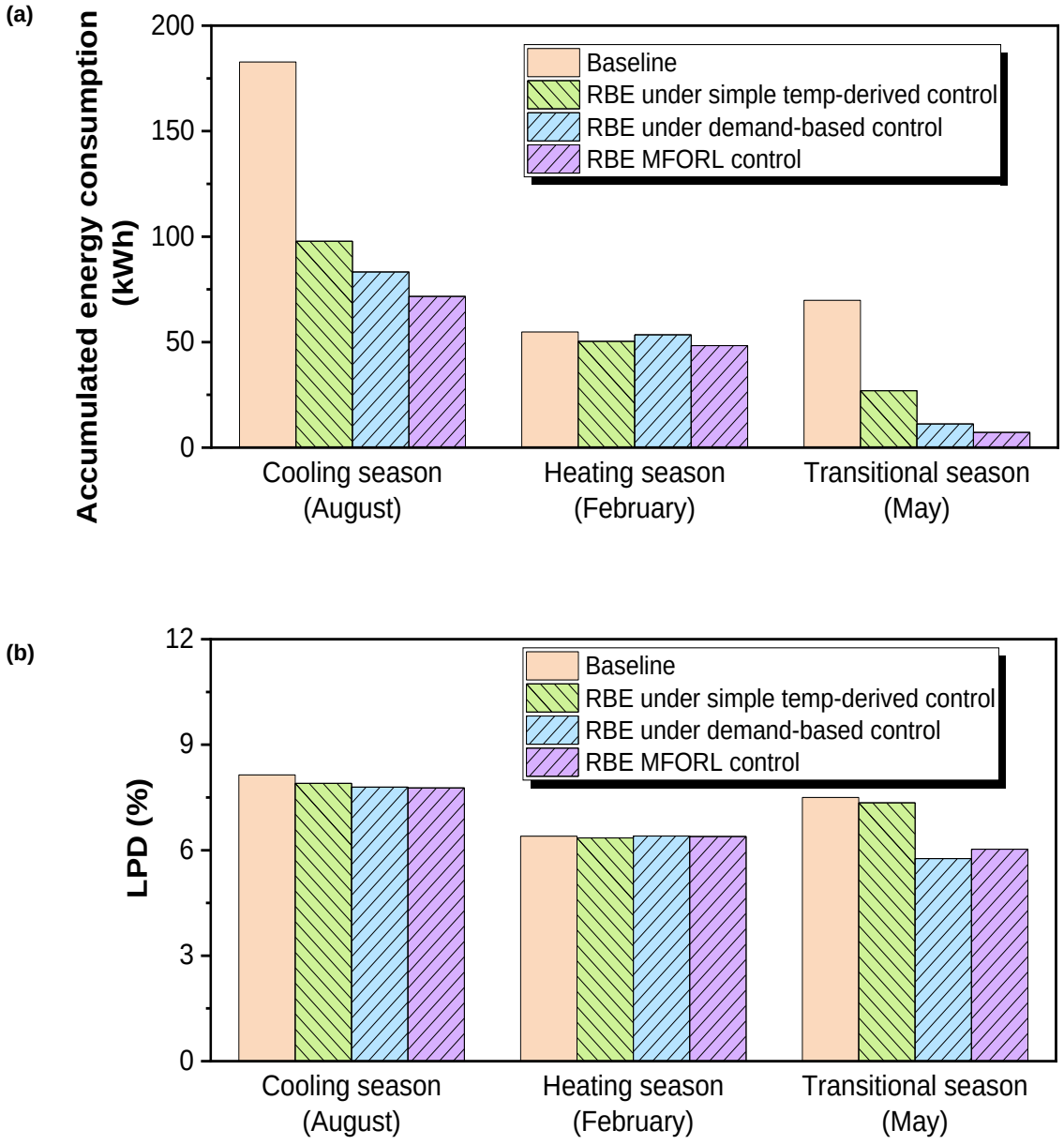


Figure 4.11 Comparisons among baseline and RBE cases under simple temperature-based control, demand-based control, and MFORL control in the performance of: (a) accumulated energy consumption (b) LPD

The simulation results exhibit intelligent and flexible responses of the MFORL controller based on efficient online learning with superior performance improvement as compared to the RBE cases under simple temperature-based control and demand-based control using high-fidelity model and much more sensed data. The crucial findings according to the case studies are summarized below:

- The case studies of representative scenarios in Chicago, IL show that the MFORL controller provides higher energy consumption reduction (11.8% in winter, 89.7% in transitional season, and 60.8% in summer) by the AIS-integrated RBE for the baseline as compared to the simple temperature-based controller (8.2% in winter, 61.3% in transitional season and 46.5% in summer) and demand-based controller (2.4% in winter, 83.9% in transitional season and 54.5% in summer) and maintains higher thermal comfort improvement (0.2% - 19.6% LPD reduction for the baseline) than rule-based controllers in most scenarios simultaneously. This demonstrates a good balance between the conflicting optimization objectives of energy savings and thermal comfort improvement by the MFORL controller.
- The control sequence generated by the MFORL controller demonstrates its high online learning performance for intelligent modulation of the indoor environment and adaptation to new changes occurring in environment. Its wise actuations of R-value settings fully leverage the AIS that changes its R-value continuously/with multiple steps in the synthesis of RBE to charge and discharge indoor space in time.

Moreover, the MFORL controller prevents unnecessary AIS triggering, which improves cost savings for both system operation and maintenance.

- The MFORL controller is carefully designed with efficient pre-training settings. The general MFORL control framework developed in this research yields promising performance, which can be extended to other cases with complex thermal mechanisms while substantially reducing controller design and deployment costs.
- The pre-analysis for controller design and training indicates that deep neural networks with multiple hidden layers, proper node size (n_{ly} equaling 10) and normalized inputs are necessary for learning optimal policies and complex RBE system behavior. The actor-critic approach based on TRPO algorithm is selected for performance improvement and computation efficiency. The refined reward function that decreases the difference between adjacent actions obtains promising energy performance while maintaining stable operation. The agent with the action space size of 10 with good performance indicates the strengths of AIS that changes the R-value with multiple steps. The reduced state space with only 10 selected state variables among many available indices prompts controller complexity reduction. This enables the small-scale agent to learn how to map optimal actions in response to different weather conditions with low computation costs. In addition, the settings of one-hour sample time and half-day or one-day experience horizon are applied. These significantly cut down the cost of online computation, instrumentation, and maintenance as compared to the high-fidelity controllers that require monitoring

massive data to attain similar performance with much higher costs for calibration before application.

- A thermal network model with high computational efficiency is constructed for offline pre-training. The analysis results show that the computation time of offline training per episode using the thermal network model is 1/32-1/21 of that using commercial software e.g., EnergyPlus, which demonstrates the prominent benefits provided by the thermal network model for offline training with low computation cost and its significant role in ensuring efficient training performance and further AI-based applications.
- The agent learns the optimal control rules effectively using the training data with similar characteristics during adjacent experience horizons. Hence, utilization of the pre-trained agent trained under several representative patterns can substantially reduce the training data design difficulty and computation complexity to provide sufficient experience for online learning compared with the practice of training a single agent that is fully compatible with all the representative patterns leading to high design and computation costs. Furthermore, the agent obtains good training performance and stable convergence using only 7-day or 8-day training data. The training data size much smaller than those used in prior studies allows cost-effective offline pre-training for deployment.

Some limitations and future investigations of the current study include:

- The MFORL controller in the case studies relies on abundant pre-training experience to guarantee robust performance in all scenarios. Thus, it is worthwhile

to further investigate the online training and control strategies without pre-training. For instance, it can integrate online control and system identification using machine learning-based methods. The system identification model as the plant of the simulated environment will increase training experience and overcome the limited trials during online training for real physical systems under unintended disturbances. This will serve as a zero-shot learning controller applied in any scenario with a good balance between computation efficiency and generalization.

- To provide deeper insight into the mechanisms that how the building energy performance is affected by the RBE behavior, and the underlying optimal control rules, further research is required for developing explainable artificial intelligence (XAI) framework such as physics-informed methods to give implications for RBE design and control.

CHAPTER FIVE
INTEGRATION WITH OTHER TECHNIQUES

To further explore the potential of AIS in improving the performance of RBE and maximize the benefits of existing self-adaptive functional modules or active techniques, multiple case studies are performed in this chapter including the scenarios integrating AIS and dynamic glazing/shading or evaporative cooling techniques. In terms of the applications of AIS integrated with dynamic glazing/shading, simulation case studies were performed for the one integrating with AIS and a dynamic shading system (DSS) using thermal network models. In particular, for the case of integration with AIS and evaporating cooling, a biomimetic mesoporous synthetic foam (or BMSF), is developed as a representative evaporative cooling technique for building roofs, which has been demonstrated effective for surface cooling through experimental studies conducted in different scenarios. Moreover, a thermal network model was developed and validated with experimental calibration for BMSF layers. With this model, simulation case studies were performed to quantify the energy-saving potential and thermal comfort performance of the cases integrating AIS and BMSF.

5.1 RBE with AIS and dynamic glazing/shading

5.1.1 Configuration and method

For the areas in cold climate zones, not only high insulation is required in winter, but passive solar gain is also beneficial (Bianco *et al.*, 2017) and desired to charge the internal thermal mass for energy use reduction. Thus, the exterior

dynamic glazing/shading (Al-Masrani and Al-Obaidi, 2019) (e.g., controllable louver) can provide more advantages for the high thermal mass-AIS integrated systems by passing through sunlight to charge the thermal mass when needed, see **Figure 5.1**. Consequently, in this chapter, case studies are performed to investigate the performance of the RBE composed of a high thermal mass sandwiched between an exterior dynamic glazing/shading and an interior AIS and study how AIS improves the potential of integration with solar harvest by smart modulation. To construct this configuration, the dynamic glazing/shading can be achieved by the techniques described in Section 1.3.1.3, and methods summarized in Section 1.3.1.1 can be adopted for the AISs.

5.1.2 Model of dynamic glazing/shading

For the envelope assembly with dynamic glazing/shading as shown in **Figure 5.1**, radiative heat flow can be modulated to leverage the beneficial heat from, e.g., passive solar gain. The heat balance equation for the exterior surface node of a dynamic glazing/shading device is the same as Equation (2.27), where the item $Q_{1,sw}^{j}$ can be expressed as:

$$Q_{1,sw}^{j} = \alpha_1^{j} I_{s,1}^{\downarrow,j} A_1 \tag{5.1}$$

where α_1^{j} is changeable solar absorptance at j^{th} time step when the device with tunable solar absorptance is adopted.

The heat balance equation for the interfacial node between the exterior dynamic glazing/shading and the adjacent concrete – i.e., node 2 in **Figure 5.1**, can be expressed as:

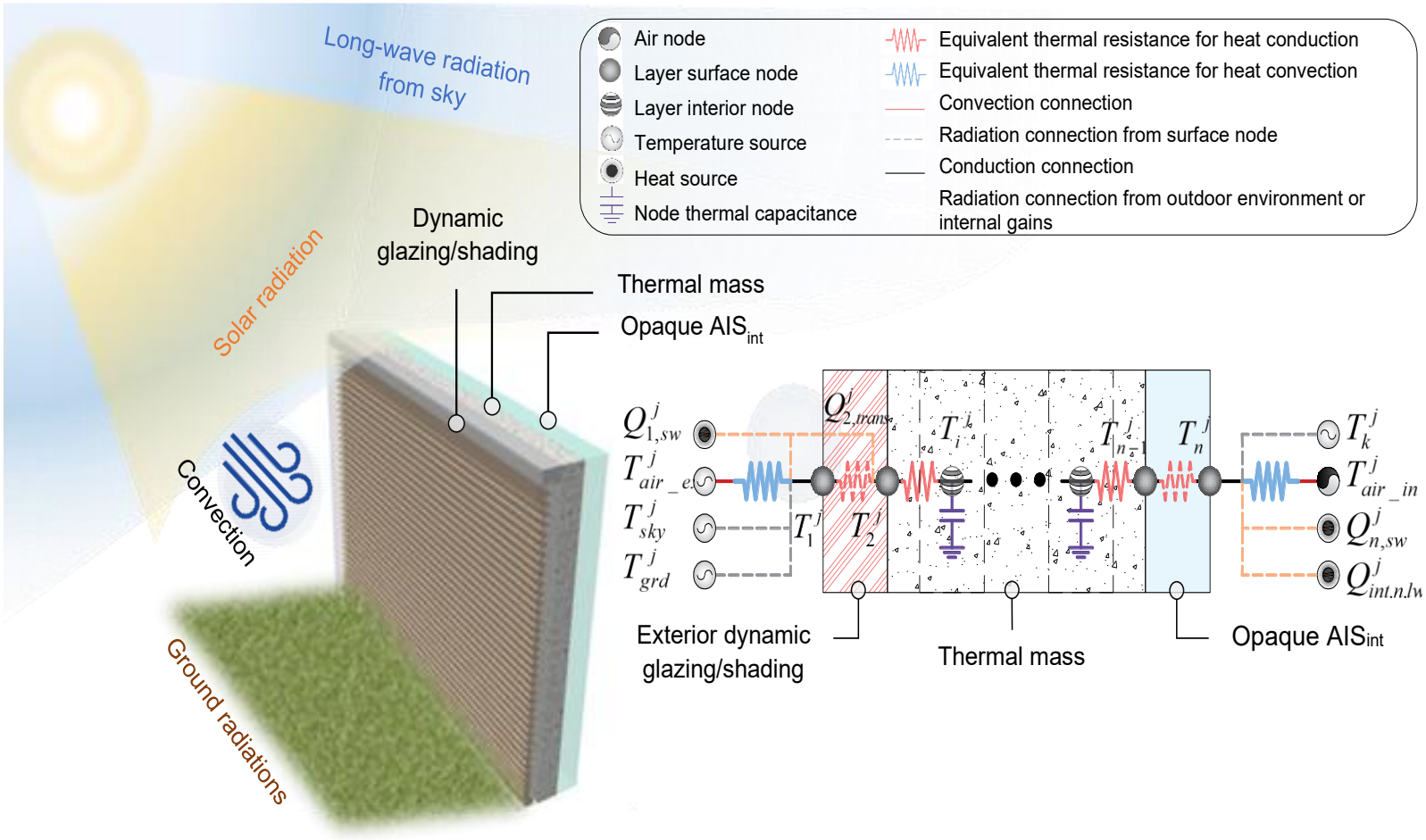


Figure 5.1 Schematic for the node scheme of synthesis of mass wall and exterior dynamic glazing/shading and interior AIS

$$C_2^j T_2^{j+1} = C_2^j T_2^j + H_{1,2}^j T_1^j + H_{3,2}^j T_3^j - \left(H_{1,2}^j + H_{3,2}^j\right) T_2^j + Q_{2,trans}^j \quad (5.2)$$

$$Q_{2,trans}^j = \tau_{1,,2}^j I_{s,1}^{\downarrow,j} A_2 \left[\alpha_2 + \left(1-\alpha_2\right)\alpha_1\right] \quad (5.3)$$

where $Q_{2,trans}^j$ is time-varying radiative heat transmitted through the dynamic glazing/shading with changeable transmittance $\tau_{1,,2}^j$ at j^{th} time step; α_2 is solar absorptance of the exterior concrete wall surface.

5.1.3 Control strategies

For envelope assemblies with a dynamic shading device (one with variable transmittance and constant insulation) as the exterior layer shown in **Figure 5.1**, the control rules are presented in **Figure 5.2**. The solar transmittance $\tau_{1,,2}^j$ of the dynamic glazing/shading is set to maximum when the indoor air temperature exceeds the cooling setpoint or prescribed threshold, otherwise the solar transmittance $\tau_{1,,2}^j$ is set to minimum or kept as previous control sequence under the corresponding criterion presented in **Figure 5.2**. The interior AIS followed the control rule prescribed in Section 3.1.1.

5.1.4 Thermal performance of the building with AIS and DSS

5.1.4.1 Simulation details

To study the thermal behavior and energy-saving potential of the RBE with dynamic shading, a thermal zone extracted from an apartment building was applied in this case study. Two representative RBEs were studied– i.e., Case 1 is a concrete (thermal mass) layer sandwiched between an exterior static insulation and an interior AIS, and Case 2 is a concrete (thermal mass) layer with an insulated exterior dynamic shading system (DSS) and an interior AIS as shown in **Figure 5.3**.

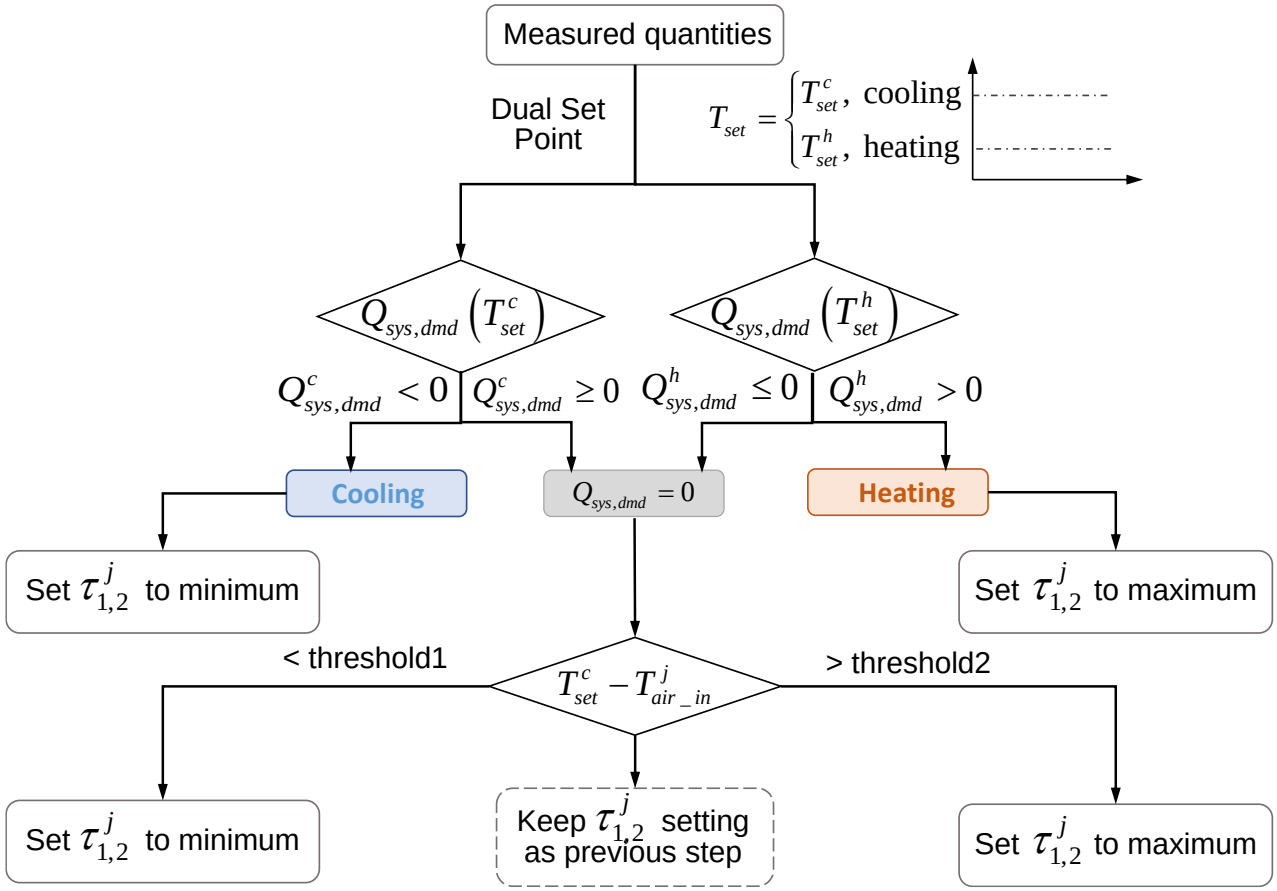


Figure 5.2 Control rule for exterior dynamic shading systems

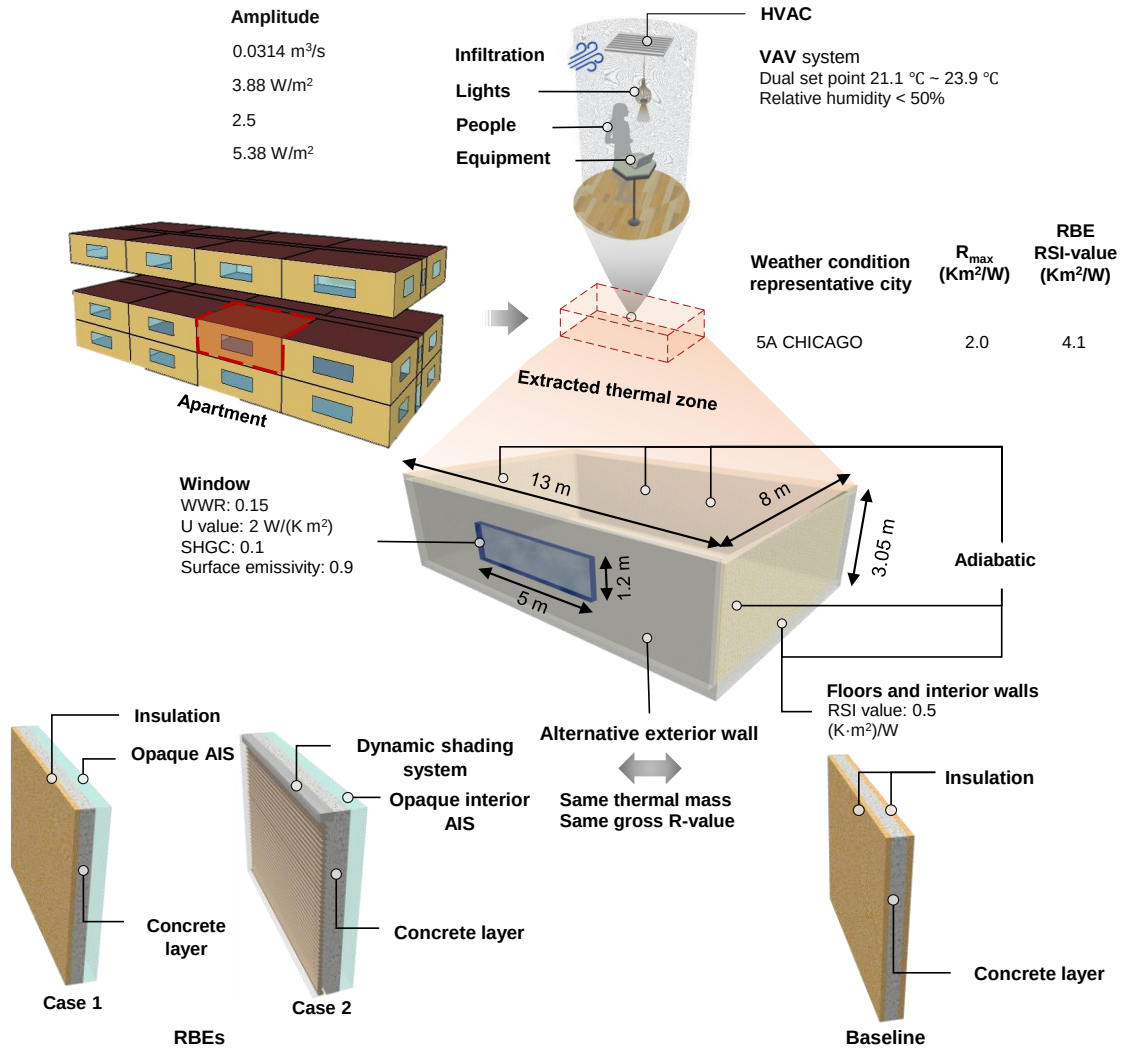


Figure 5.3 Simulation details for buildings with a baseline roof and the RBEs with DSS

The insulation level of DSS was selected based on the climate zone where the building is situated, as shown in **Figure 5.3**. The RBEs were also compared with the baseline exterior wall made of one concrete panel (mass layer) and two rigid foam insulation panels (no-mass layer) with the same overall thermal mass and maximum insulation. Typical meteorological year 3 (TMY3) weather data of Chicago, IL (ASHRAE climate zone 5A) were used for the simulation. The RSI-value range of interior AIS is assumed to be R_{low} (0.1 Km^2/W) to R_{high} (2 Km^2/W).

For the RBE integrated with a dynamic shading system (Case 2), the DSS was controlled by the simple rule prescribed in Section 5.1.1. The interior AIS followed the control rule prescribed in Section 3.1.1. The whole building simulation model was built as a thermal network based on heat and moisture balance equations described in CHAPTER TWO. In the numerical computation, long-wave radiation was linearized using the same method as detailed in (Deardorff, 1978). Moreover, the simple glazing model (Berkeley *et al.*, 2019) was used for all windows in the building model.

5.1.4.2 Thermal behavior

Figure 5.4 and **Figure 5.5** present the thermal behavior of the different RBEs compared with baseline during heating seasons and cooling seasons, respectively, which indicates that the RBE with a dynamic shading system exhibits obviously different behavior in various scenarios. Seven days' (January 3rd–10th) data in Chicago, IL (ASHRAE climate zone 5A) are arbitrarily chosen to illustrate the thermal behavior and AIS operations of the RBE with an exterior static insulation and an interior AIS, and the one with an exterior insulated DSS and an interior AIS during the heating season.

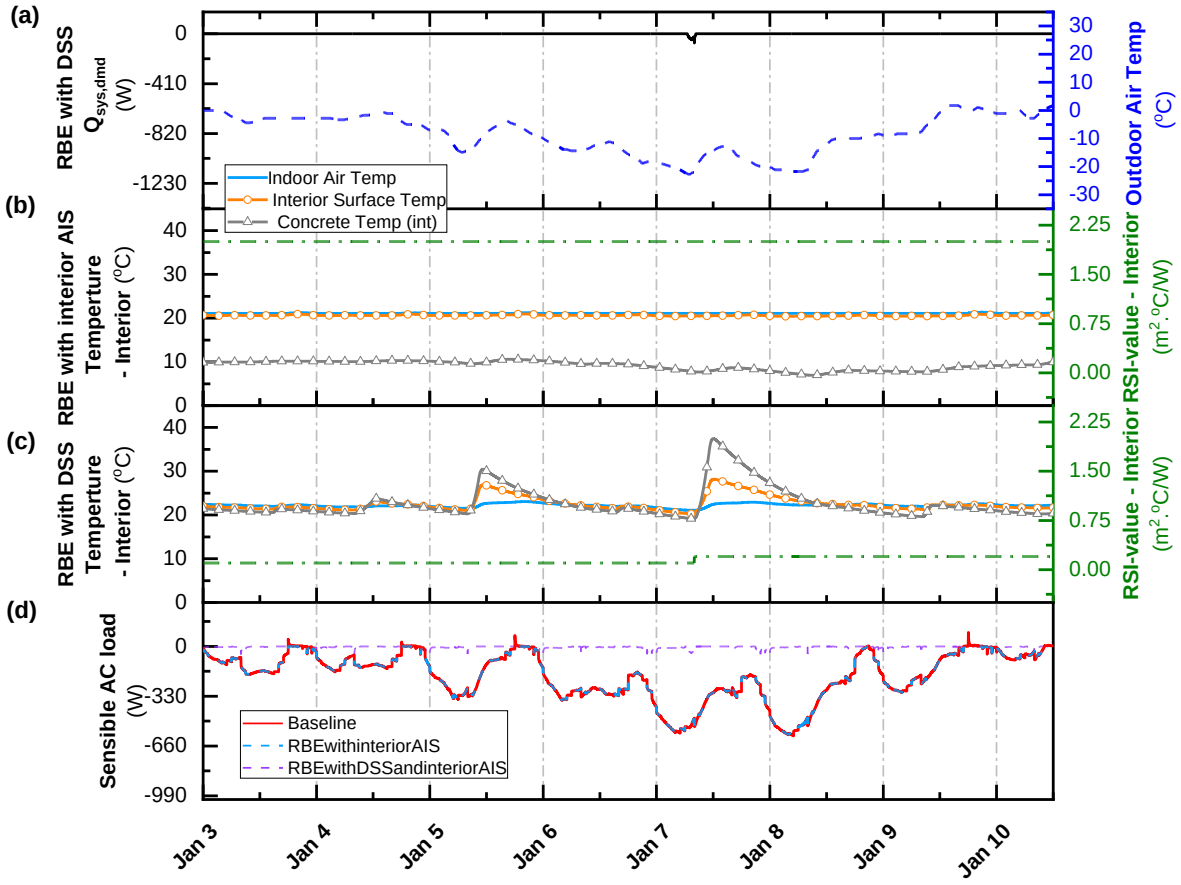


Figure 5.4 Thermal behavior of RBE in a typical heating season (January, Chicago, IL): (a) outdoor air temperature and the system output demand to reach the setpoint, $Q_{sys,dmd}$ of the thermal zone with DSS; (b) interior AIS R-value setting and indoor air, interior surface and concrete temperatures of the thermal zone with an exterior static insulation and an interior AIS; (c) interior AIS R-value setting and indoor air, interior surface and concrete temperatures of the thermal zone with DSS and AIS; (d) comparison of sensible AC load for different RBEs and baseline cases

As **Figure 5.4** (a) shows, due to the increased solar heat gain within the concrete layer from the exterior dynamic shading system so that the estimated system output demand $Q^{j}_{sys,dmd}$ to reach the setpoint of the thermal zone with the exterior insulated DSS, was maintained close to zero. Meanwhile, the concrete surface temperature of the concrete thermal mass and indoor air temperature of the RBE with DSS were much higher than the ones of the RBE with an exterior static insulation and an interior AIS, through the comparison shown between **Figure 5.4** (b) and (c). Accordingly, the thermal resistance (RSI-value) of the interior AIS for the RBE with DSS remained at a low level to provide heating flow into the indoor space since the temperature of concrete thermal mass was higher than the indoor air temperature during this period. In contrast, the interior AIS of RBE with exterior static insulation and an interior AIS was set to R_{high} to minimize the heat loss from the indoor space. During the daytime, RBE with dynamic shading not only insulated heat loss through outdoor space but also harvested much more solar heat to charge the concrete thermal mass, Therefore, the concrete surface temperature of RBE with DSS reached up to 35 °C under this accumulated heat, which mitigated the limitation of opaque AIS and consequently provided substantial AC load reduction. As a result, shown in **Figure 5.4** (d), the sensible AC load of the case with DSS was almost zero during most of this period. The sequence of sensible AC load for the three cases during winter days in Chicago were: baseline = RBE with exterior static insulation and interior AIS > RBE with insulated exterior DSS and interior AIS.

However, during the cooling seasons (July 10^{th}–16^{th}) with larger weather condition variation presented in **Figure 5.5** (a), Both the RBE cases presented similar behavior in R-value settings of interior AIS, i.e., the interior AIS remained at the maximum during most of the period such that the sensible AC load of the RBE cases were close to that of the baseline.

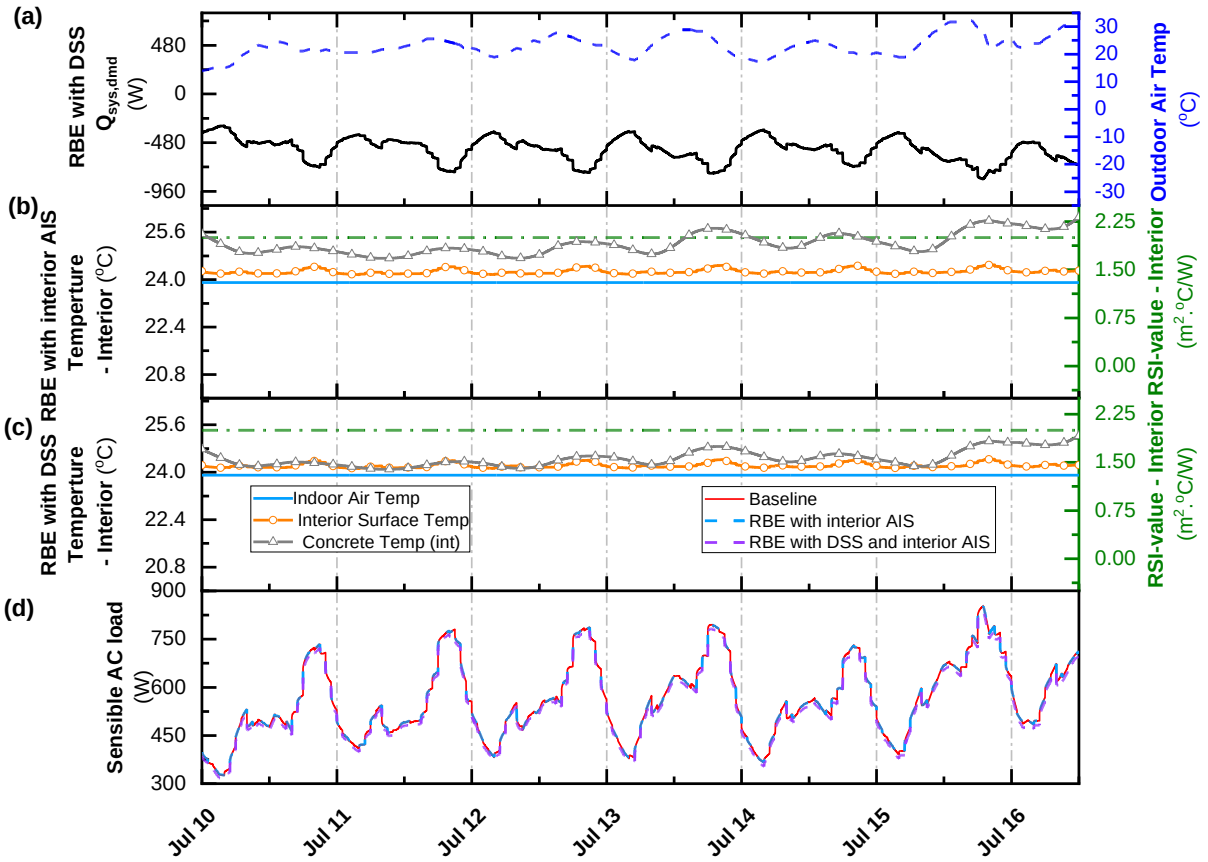


Figure 5.5 Thermal behavior of RBE in a typical cooling season (June, Chicago, IL): (a) outdoor air temperature and the system output demand to reach the setpoint, $Q_{sys,dmd}$ of the thermal zone with DSS; (b) interior AIS R-value setting and indoor air, interior surface and concrete temperatures of the thermal zone with an exterior static insulation and an interior AIS; (c) interior AIS R-value setting and indoor air, interior surface and concrete temperatures of the thermal zone with DSS and AIS; (d) comparison of sensible AC load for different RBEs and baseline cases

Given the static exterior insulation of the RBE, the redundant heat generated from the indoor space cannot be dissipated in time as the exterior AIS does. In other words, the interior AIS of the RBE with DSS maintained at a high level to insulate heat from the outdoor environment since exterior DSS with static R-value undermined outdoor beneficial cooling effect for heat dissipation from concrete thermal mass when desired, as shown in **Figure 5.5** (b) and **Figure 5.5** (c). The simulated sensible AC load shows that the solar radiation-induced load cut down by exterior DSS with static insulation was marginal. Therefore, as **Figure 5.5** (d) presents, the advantage of exterior DSS is limited and cannot provide as much AC load reduction as the exterior AIS with a flexible thermal switch does during summer days.

5.1.4.3 Energy-saving potential and thermal comfort performance

Figure 5.6 (a) shows the monthly energy consumption of the analyzed thermal zone located in Chicago. The RBE with exterior DSS brought promising energy-saving potential under cold weather conditions from January to March and December (e.g. 91.5% energy use reduction in January in Chicago), which was much higher than the counterpart by RBE with an exterior static insulation and an interior AIS, whereas its static insulation impeded redundant heat dissipation within the concrete layer during the rest time of the year when the variable insulation switching between the maximum R-value and minimum R-value of AIS was required to charge and discharge the concrete layer. Therefore, the energy consumption reduction by RBE with an exterior insulated DSS and an interior AIS was slightly higher than the one by RBE with an exterior static insulation and an interior AIS during summer in Chicago.

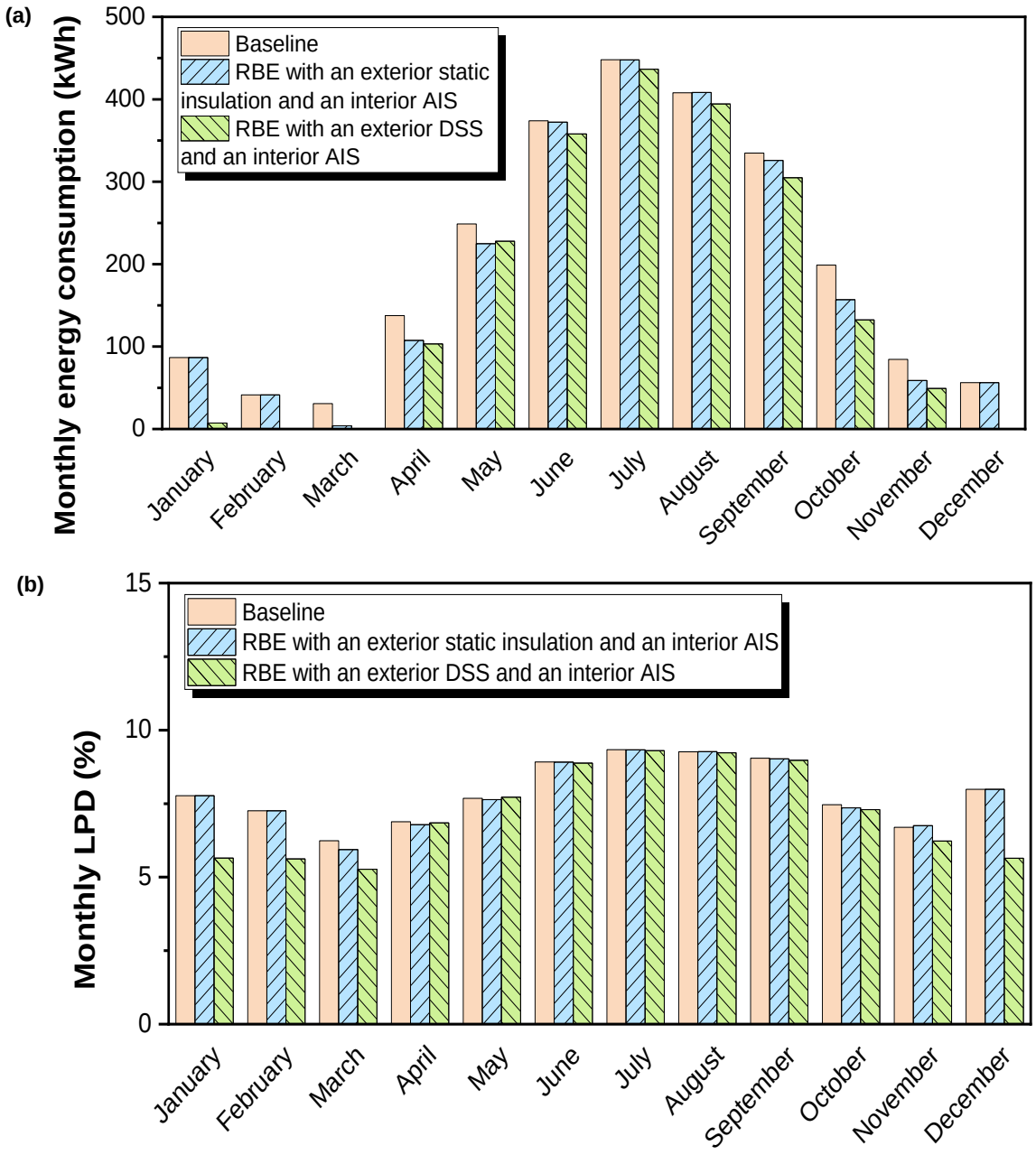


Figure 5.6 (a) Monthly energy consumption of the residential thermal zone with baseline envelope and with different RBEs (b) Monthly LPD of the residential thermal zone with baseline envelope and with different RBEs

In conclusion, the annual energy consumption reduction by RBE with an exterior insulated DSS and an interior AIS (17.8%) was still higher than the one by RBE with an exterior static insulation and an interior AIS (6.5%). Furthermore, as presented in **Figure 5.6** (b), the RBE with insulated DSS and interior AIS also provided significantly higher thermal comfort improvement under relatively cool or cold conditions (e.g. January to March and November to December) in comparison with the one with an exterior static insulation and an interior AIS, which is similar to the behavior of energy performance of different cases. The sequence of annual LPD of the different cases in Chicago was: baseline (7.88%) > RBE with an exterior static insulation and an interior AIS (7.84%) > RBE with an exterior insulated DSS and an interior AIS (7.23%).

5.2 RBE with AIS and evaporative cooling

Due to its direct exposure to solar radiation, the building roof alone can be responsible for up to about 50% of the thermal load in single or two-story buildings (Nahar, Sharma and Purohit, 2003). Therefore, regulating heat gains of building roofs is of interest to both academia and industry. In the past two decades, different evaporative cooling techniques, such as roof shading (Kumar and Kaushik, 2005), increasing the insulation and thickness (thermal mass) (Al-Sanea, Zedan and Al-Hussain, 2012), green roofs via roof vegetating (Shafique, Kim and Rafiq, 2018), and blue roofs (e.g., roof spray (Nayak, Hagishima and Tanimoto, 2020) and roof ponds (Sharifi and Yamagata, 2015)), have been explored. However, most of the techniques developed so far require the installation of complicated plumbing (pump) systems or the use of non-durable surface materials such as

hydrogel (Rotzetter *et al.*, 2012), which would inevitably increase the maintenance costs of building roof systems and may cause issues like water leakage (roof ponds) and microbial growth. Moreover, few existing approaches to date simultaneously have the properties of high cooling efficiency, long durability (e.g. resistance to thermal cycling and UV irradiation), and low cost (Cuce and Riffat, 2016). To overcome these challenges, a biomimetic mesoporous synthetic foam (or BMSF), is developed herein as an evaporative cooling layer for building roofs, which is validated through experimental studies in different scenarios in the author's work (He *et al.*, 2022). The study in the author's work also indicates that evaporative cooling techniques with low insulation can provide substantial benefits in energy savings in summer with high internal gains while they may bring marginal advantages or even adverse effects in winter with low internal gains. To this end, as **Figure 5.7** presents, AIS is applied in this case to leverage its flexible regulation of heat transfer through envelopes and maximize the synthesis benefits with evaporative cooling techniques, where the roof is equipped with an exterior evaporative cooling layer and an interior AIS. Case studies are performed to investigate the energy and thermal comfort performance of the building integrating AIS and evaporative cooling techniques.

5.2.1 Configuration and method

In this chapter, the BMSF layer is adopted as a representative evaporative cooling technique in the following case studies. The evaporation rate from the BMSF flat panel was tested very close to that of an open water surface, leading to a high cooling effect for AC load reduction.

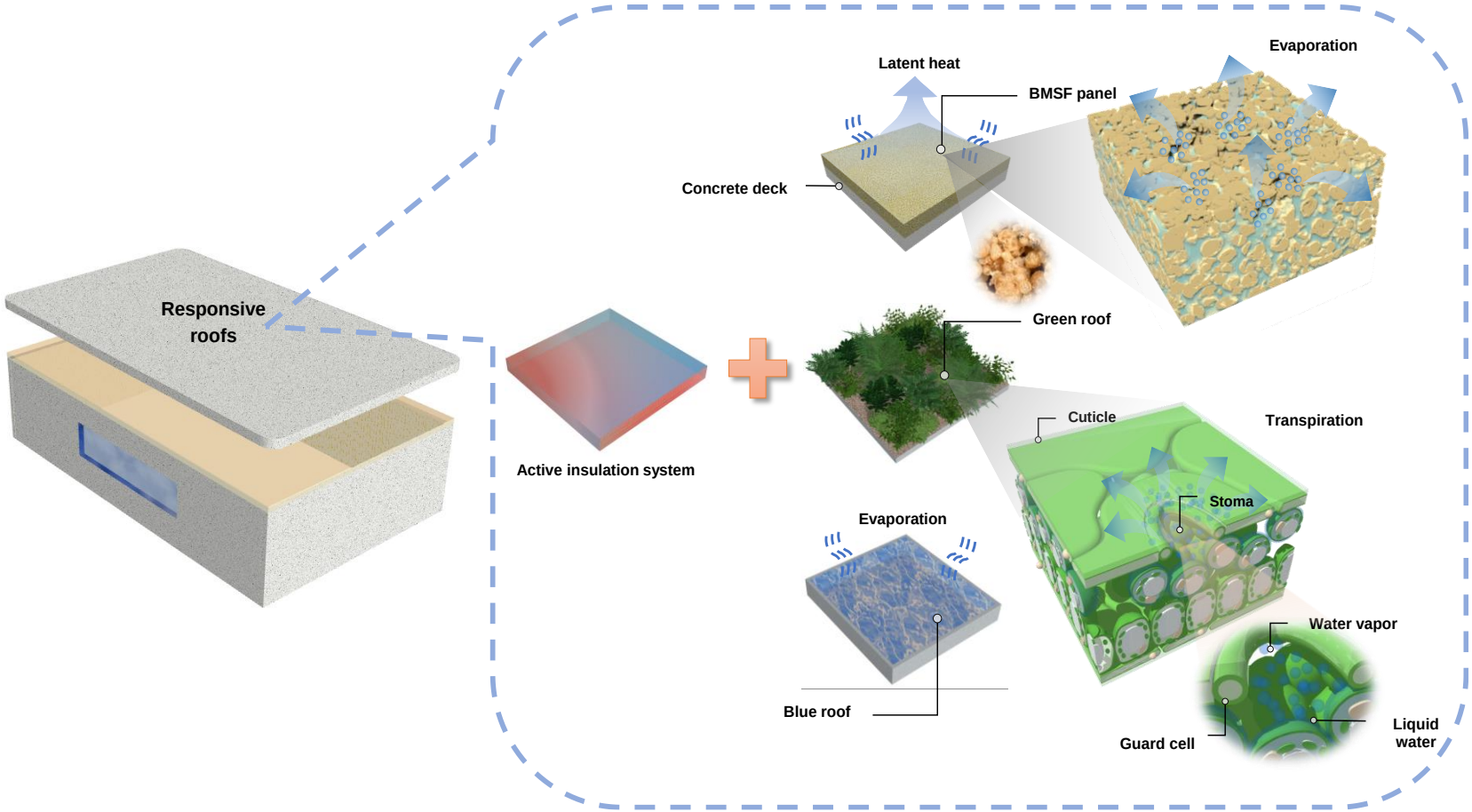


Figure 5.7 Schematic for responsive roofs integrated with AIS and evaporative cooling techniques

The thermal behavior of this BMSF is investigated through material tests to provide reference thermal properties (He *et al.*, 2022) for later simulation in case studies in Section 5.2.4. The evaporative cooling performance of the BMSF layer is validated through experimental studies for concrete roofs in different scenarios in the author's work (He *et al.*, 2022) to test the cooling effectiveness of BMSF for building roof cooling applications with a scaled-down concrete roof panel model tested in conjunction with one equipped with BMSF cooling panels. The results demonstrated the promising cooling performance of BMSF – i.e., the surface temperature was reduced by 12.5℃ in comparison with the baseline concrete roof, and heat flux flowing through the concrete panel was reduced by nearly 65% in comparison with the concrete baseline panel.

In nature, plants and animals are autonomously adaptive to the changing ambient environment (e.g., temperature, relative humidity) through transpiration and perspiration of water, which has one of the highest latent heats among various fluids. Inspired by the passive biological cooling process, several self-adaptive cooling technologies related to bio-inspired artificial skins have been reported, including superabsorbent polymer (i.e., hydrogel) based building skin (Cui *et al.*, 2016), and thermochromic reflective coatings (Berardi, Garai and Morselli, 2020). In comparison with inorganic materials, hydrogels are generally less durable and are susceptible to UV deterioration and wet-dry cycling, which may hinder their long-term application as building surfaces. Typically, animals with large bodies tend to retain more heat due to their relatively small ratio of surface area to body volume for heat dissipation. The remarkable cooling ability of certain animal skins like those of the African elephant (Loxodonta) stems from the morphology enabled moisture

absorption and evaporative cooling. Recent studies discovered that an intricate network of crevices adorns the skin surface of the African bush elephant. These micrometer-wide channels enhance the effectiveness of thermal regulation (by water retention), as well as protection against parasites and intense solar radiation (Martins *et al.*, 2018). Inspired by its hierarchical functional structures, a biomimetic 'hydro-foam', namely biomimetic mesoporous synthetic foam (or BMSF), is developed herein as an evaporative cooling layer for building roofs. The microstructure of the evaporative layer was inspired by the morphological features of certain animal skin driving the water transport and storage to enable evaporative cooling on elephant skin surfaces using an industrial byproduct – fly ash cenospheres (FAC). FAC are hollow aluminosilicate hollow microspheres that are produced as a byproduct during the coal combustion process. It is featured by low bulk density (400-900 kg/m^3) and is nearly spherical in shape with highly selectable particle size distributions – from several micrometers to several hundreds of micrometers in diameter (Brooks, Zhou and Hanna, 2018; Zhou and Brooks, 2019) as shown in **Figure 5.8** on Page 170. In addition, FAC surfaces are mostly hydrophilic and have large interior cavity spaces (over 80% by volume) for water storage if needed. The hydrophilic surface of FAC also promotes wicking and capillary water transport within the BMSF material, which helps water to evenly distribute across the entire evaporation surface (Zhou *et al.*, 2017). These features make FAC an ideal material to produce low-cost inorganic synthetic foam, which resembles the keratinous skin of African elephants. The mesoporous synthetic foam is formed by a 'minimal-contact' process developed by the authors (Brooks, Zhou and Hanna, 2018; Zhou and Brooks, 2019), where micro-size FACs are bonded through drying a clay-

water suspension before it is sintered into an inorganic synthetic foam with over 95% interconnected pores. Thus, the foam layer can be effectively used to store rainwater (Wanphen and Nagano, 2009; Zhang *et al.*, 2018) and roof run-offs for prolonged evaporative cooling. The material developed herein also has other advantages such as being lightweight and low-cost as compared to superabsorbent polymers and traditional porous materials used for roof cooling (Wanphen and Nagano, 2009; Karamanis, 2015; Shokri Kuehni *et al.*, 2016). In addition, since the material is made from sintered inorganic minerals, it is not susceptible to UV-induced degradation.

5.2.2 Model of biomimetic mesoporous synthetic foam (BMSF)

A thermal network model is developed to simulate the thermal behavior of building roofs covered with BMSF panels. The heat transfer equations were established by the heat balance within each finite volume represented by the thermal nodes shown in **Figure 5.9**.

The heat balance at the exterior surface node of the BMSF panel considers effects due to convective heat exchange, heat conduction, short-wave radiation, $Q_{i,sw,b}$, long-wave radiation, $Q_{i,lw,b}$ and latent heat from evaporation, $Q_{i,lat,b}$, which can be expressed as:

$$\int_{V_{i,b}} \rho_b c_{p,b} dV_{i,b} \frac{dT_{i,b}}{dt} = H_{i,b}^{air_ex}\left(T_{air_ex} - T_{i,b}\right) + H_{i,b}^{i-1} T_{i-1} + H_{i,b}^{i+1} T_{i+1} - \left(H_{i,b}^{i-1} + H_{i,b}^{i+1}\right) T_{i,b} + Q_{i,sw,b} + Q_{i,lw,b} + Q_{i,lat,b} \tag{5.4}$$

$$Q_{i,sw,b} = \bar{\alpha}_{i,b} I_s^{\downarrow} A_{i,b} \tag{5.5}$$

$$Q_{i,lw,b} = \left[F_i^{sky}\left(T_{sky,abs}^4 - T_{i,abs,b}^4\right) + F_i^{grd}\left(T_{grd,abs}^4 - T_{i,abs,b}^4\right) + F_i^{air_ex}\left(T_{air_ex,abs}^4 - T_{i,abs,b}^4\right)\right] \cdot \sigma \varepsilon_{i,b} A_{i,b} + \sum_k \sigma \varepsilon_{i,b} F_i^k \left(T_{k,abs}^4 - T_{i,abs,b}^4\right) A_k \tag{5.6}$$

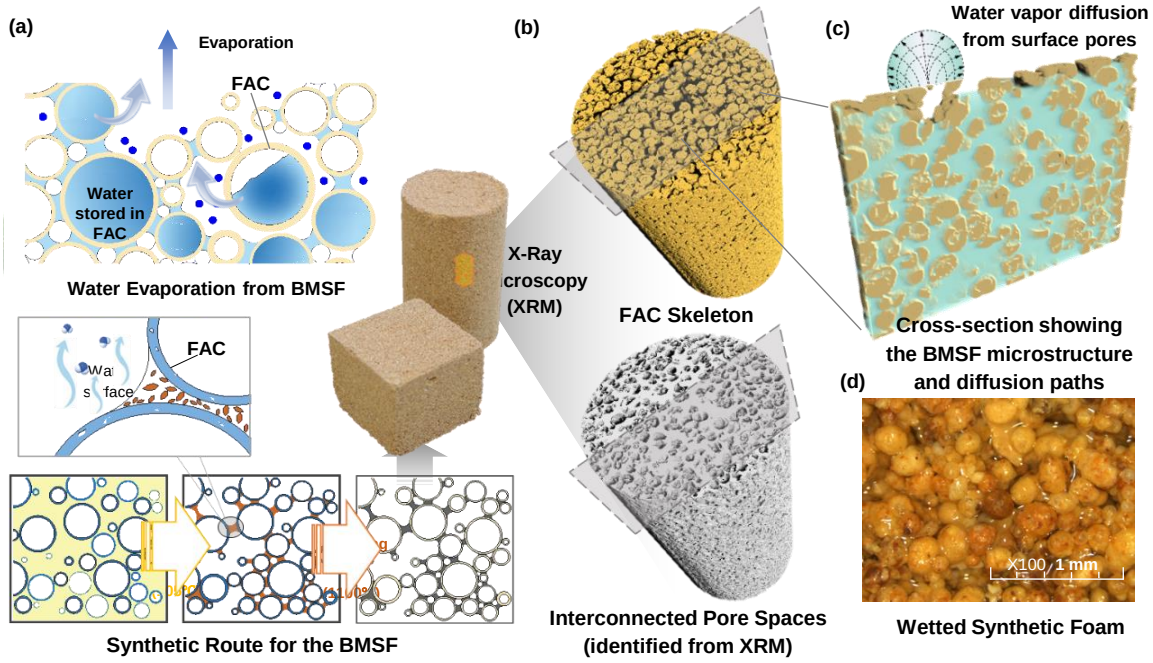


Figure 5.8 Schematic showing BMSF (a) the wetting and evaporation mechanism; (b) sintering process and microstructure of BMSF; (c) perceived evaporation mechanism; and (d) optical micro-image showing the wetted BMSF

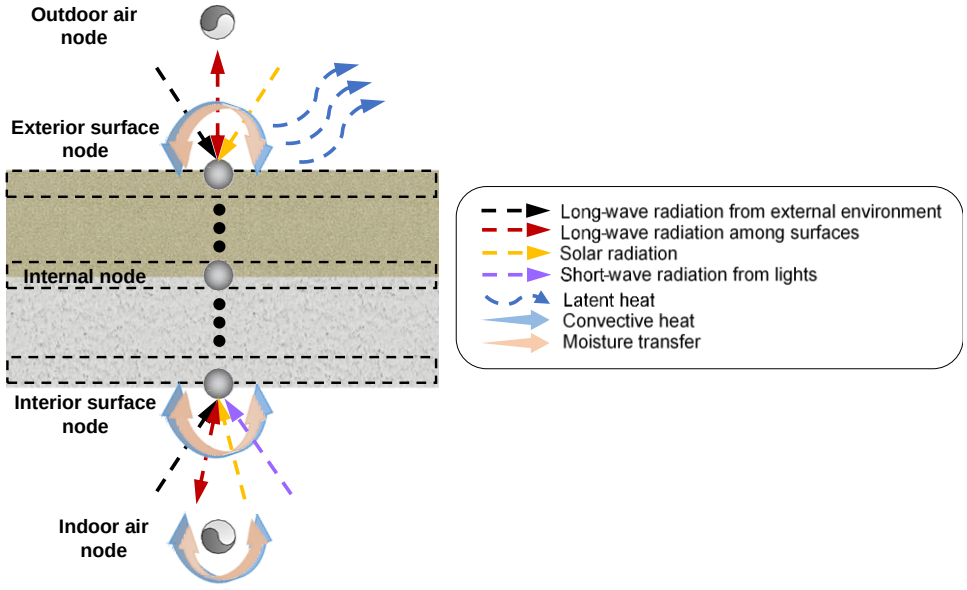


Figure 5.9 Thermal network model of the concrete roof covered with BMSF panel

$$Q_{i,lat,b} = q_w h_{i,m,b}^{air_ex}(u_{i,b} - u_{air_ex})A_{i,b} \tag{5.7}$$

$$h_{i,m,b}^{air_ex} = \frac{h_{i,c,b}^{air_ex}}{\rho_{air_ex} c_{p,air_ex}} Le^{-\frac{2}{3}} \tag{5.8}$$

$$h_{i,c,b}^{air_ex} = 6.47 + 6.806 v_{ex} \tag{5.9}$$

where $H_{i,b}^{air_ex}$ is heat transfer coefficient between outdoor air and BMSF surface node *i*; $\bar{\alpha}_{i,b}$ is solar absorptance of the BMSF surface; q_w is latent heat per unit mass of water evaporation; $h_{i,m,b}^{air_ex}$ is surface mass transfer coefficient between outdoor air and BMSF surface node *i*; $h_{i,c,b}^{air_ex}$ is surface heat transfer coefficient between outdoor air and BMSF surface node *i;* The classic empirical formula adopted in ASHRAE/DOE-2 model (Yazdanian.Mehrangiz, 1994; Palyvos, 2008) in Equation (5.6) is used for surface heat transfer coefficient calculation; *Le* is the Lewis number – a dimensionless number defined as the ratio of thermal diffusivity to mass diffusivity(Kloppers and Kröger, 2005); v_{ex} is air velocity. In this research, a continuous water supply (dripping pipe) was provided to maintain the BMSF panel under saturated conditions. A water barrier was placed between the BMSF panel and the concrete roof to prevent moisture transfer between the BMSF layer and the adjacent concrete layer, thus only heat conduction takes place at the interface between BMSF and the concrete roof substrate.

Moreover, this thermal network model developed is calibrated as compared to the experimental results (He *et al.*, 2022), which is adopted in the simulations to study the responsive roofs' contribution to performance improvement for buildings in Section 5.2.4.

5.2.3 Control strategies

In this research, the water supply is only available in summer using dripping pipes to maintain the BMSF panel under saturated conditions The interior AIS followed the control rule prescribed in Section 3.1.1.

5.2.4 Thermal performance of the building with AIS and evaporative cooling

The simulation analysis in the author's work (He *et al.*, 2022) of RBE with BMSF evaporative cooling panel shows that the RBE with low insulation level can provide substantial energy consumption reduction in summer for the case with relatively high internal gains. However, it may also lead to adverse effects in winter once the internal gains become lower. To this end, a responsive roof consisting of a concrete layer sandwiched between an exterior BMSF evaporative cooling panel and an interior AIS is analyzed to investigate its potential for performance improvement as compared to the case.

5.2.4.1 Simulation details

To investigate the thermal behavior and quantify the energy-saving potential of building roofs equipped with the BMSF evaporative cooling panel, case studies were conducted using the case of a single-story commercial building through comparisons between baseline roofs and BMSF roofs, see **Figure 5.10**. For the case studies, three types of building roofs were analyzed, i.e. the baseline concrete roof with standard *R*-value ($R = 4.55(\mathrm{K \cdot m^2})/\mathrm{W}$) according to the specification of ASHRAE 90.1 (Edition *et al.*, 2013), the concrete roof with BMSF evaporative cooling panel, and the roof composed of a concrete decking sandwiched between an exterior BMSF evaporative cooling panel and an interior AIS. For the roof case with only a BMSF panel, two scenarios of different roof insulations were designed to study the effects of BMSF under different insulation levels with different weather conditions.

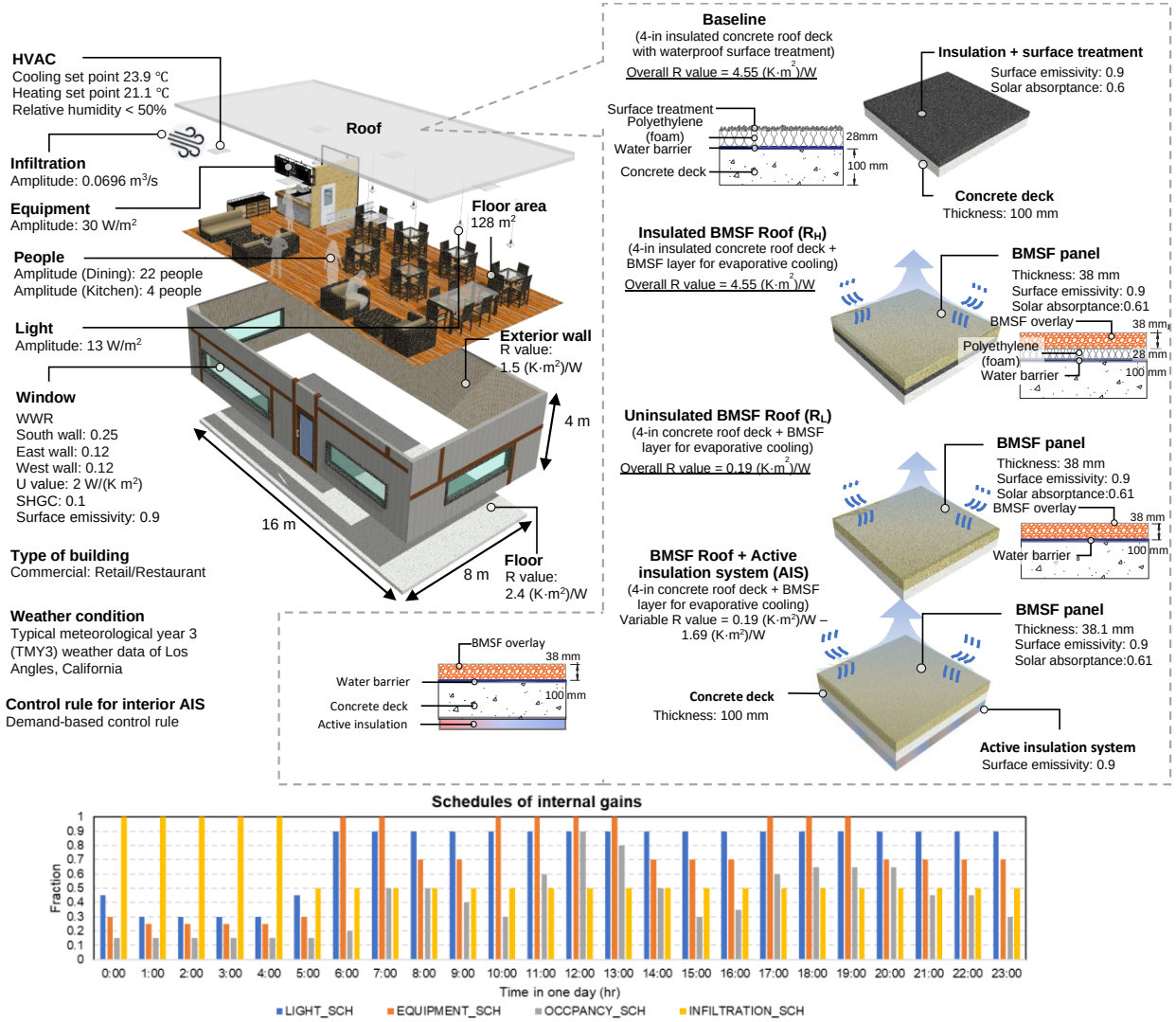


Figure 5.10 Simulation details for buildings with a baseline roof and the ones with BMSF and AIS

The case R_H has standard R-value (R = 4.55(K·m^2)/W) according to the specification of ASHRAE 90.1 (Edition *et al.*, 2013); another case R_L was designed as a BMSF and concrete only roof with no additional insulation (R = 0.29(K·m^2)/W). The purpose of case R_L was to demonstrate that in certain scenarios (e.g., buildings with high internal load), low thermal resistance building envelopes can augment the cooling effect of evaporative cooling surfaces. The R-value of the interior AIS varied between R_{low} and R_{high}, which was designed to study the performance improvement by the synthesis of AIS and BMSF evaporative cooling panel, see **Figure 5.10**. To analyze the impact of the upper limit of variable thermal resistance on the energy performance of the roof with AIS, two scenarios, i.e., an intermediate upper limit (R_{high}= 2 (K·m^2)/W) and a high upper limit (R_{high}= 4.35 (K·m^2)/W) that have the same overall thermal resistance as the baseline with standard insulation were applied in the case studies.

In the case study, material properties (density, thermal conductivity, specific heat, solar absorptance,) parameters used for the calculation of surface mass transfer coefficient and surface heat transfer coefficient for BMSF panel and concrete are assumed the same as the measured values presented in the author's work (He *et al.*, 2022) and formulas presented in Section 5.2.2. The building dimensions are 16 m (L) × 8m (W) ×4 m (H) and the mean window-to-wall ratio is 12.3% for the exterior walls. Other simulation parameters including occupant activities, lighting, equipment, and infiltration are enlisted in **Figure 5.10**. It was assumed that the long-wave absorptance and long-wave emissivity are equal for all wall surfaces. Typical meteorological year 3 (TMY3) weather data of Los Angles, California was used for the simulation. Water supply was

only available in summer (June to August) since the building has low cooling demands in winter. The indoor air temperature was controlled by HVAC by dual setpoint within the temperature range of 21.1-23.9℃. The whole building simulation model was built as a thermal network based on heat and moisture balance equations described in CHAPTER TWO. In the numerical computation, long-wave radiation was linearized using the same method as detailed in (Deardorff, 1978). Moreover, the simple glazing model (Berkeley *et al.*, 2019) was used for all windows in the building model.

5.2.4.2 Thermal behavior

Building energy simulation and thermal comfort analyses were performed for the cafeteria equipped with the baseline roof, the BMSF roofs, and the responsive roofs composed of BMSF and AIS during representative winter and summer days in Los Angles, California.

Figure 5.11 and **Figure 5.12** present the thermal behavior of BMSF evaporative cooling roofs with different insulation levels, the roof equipped with BMSF and interior AIS and baseline during one representative summer week (June 17th - June 23nd) and, one representative winter week (January 8th - January 14th). during which the behavior of different roofs varied under different weather conditions. As **Figure 5.11** (c) shows, the exterior roof surface temperature was greatly reduced by the BMSF panel in comparison with that of the baseline due to shading and the evaporative cooling effects from the BMSF panel. For the case study scenarios, the surface temperature of the baseline concrete roof with standard *R*-value (R_H) reaches around 53℃ in summer, whereas it remained around 30℃ for the other cases with BMSF evaporative cooling panel. This is consistent with the experimental observations in the author's previous work (He *et al.*, 2022).

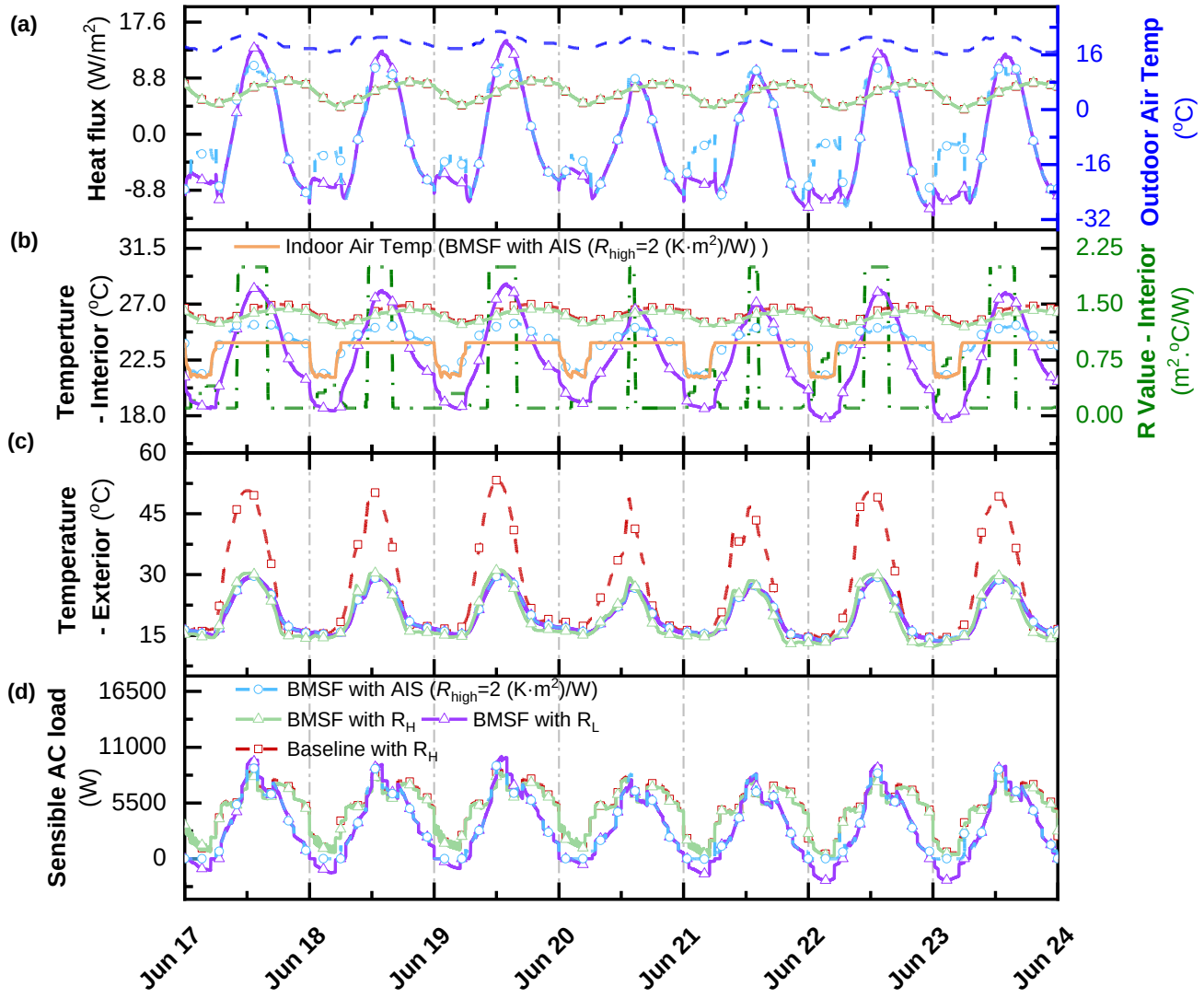


Figure 5.11 Thermal behavior of evaporative cooling roof composed of BMSF and AIS compared with baseline in a summer week (June, Los Angeles, CA): (a) outdoor air temperature and heat flux; (b) interior AIS R-value setting and indoor air, interior surface, and exterior surface temperatures; (c) exterior surface temperatures (d) comparison of sensible AC load for baseline roof and the BMSF roof with and without AIS

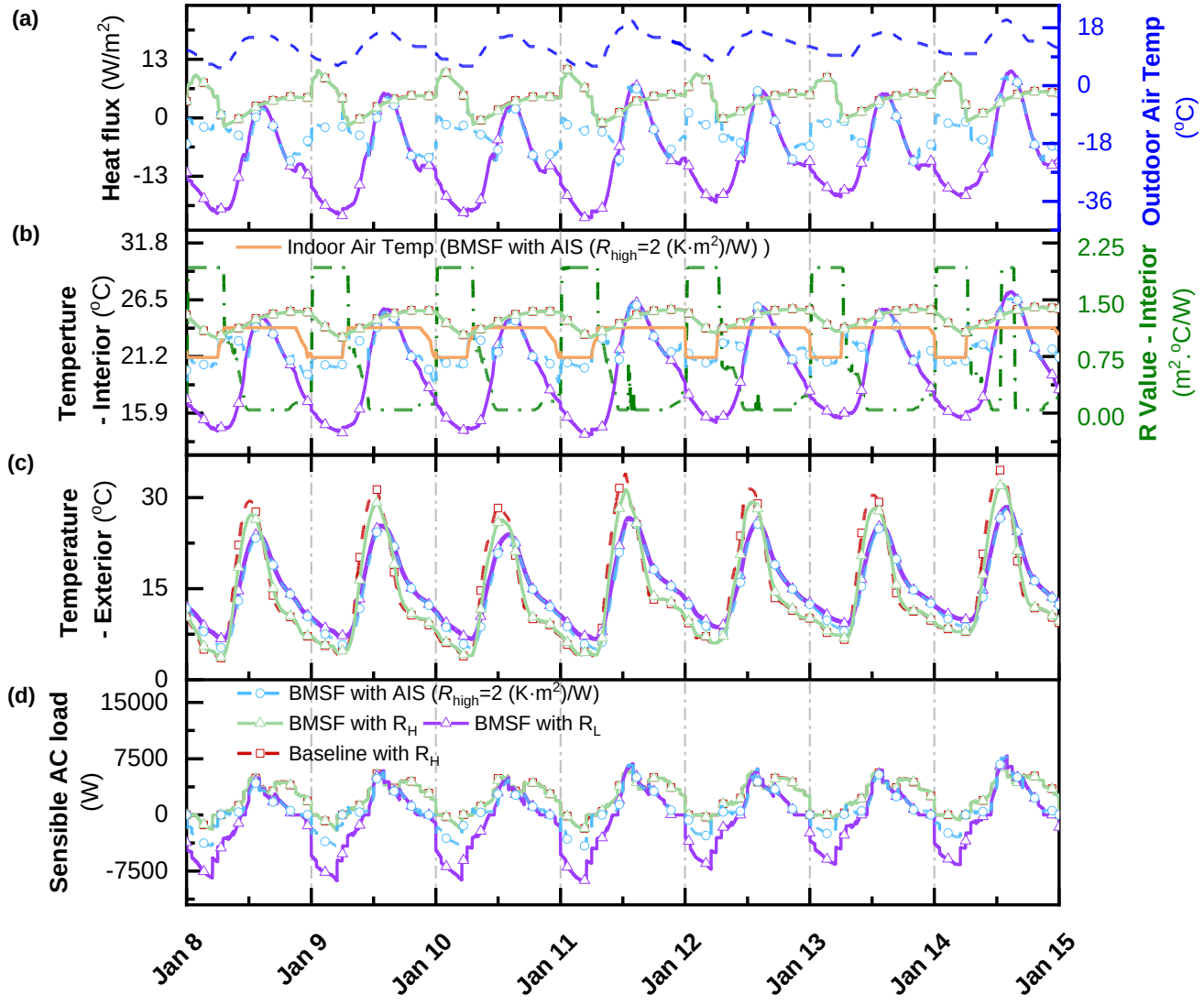


Figure 5.12 Thermal behavior of the evaporative cooling roof composed of BMSF and AIS compared with baseline in a winter week (January, Los Angeles, CA): (a) outdoor air temperature and heat flux; (b) interior AIS R-value setting and indoor air, interior surface, and exterior surface temperatures; (c) exterior surface temperatures (d) comparison of sensible AC load for baseline roof and the BMSF roof with and without AIS

In addition, no obvious difference was observed in the exterior surface temperature between the BMSF roofs with and without AIS in summer. It is noted that due to the high internal load level of a cafeteria during the daytime and the relatively mild outdoor temperature, high insulation building envelopes may act adversely and lead to high energy consumption for the HVAC system – i.e., most of the unwanted heat from internal loads (i.e., occupants, equipment, and lighting) must be cooled by HVAC. In this case, evaporative cooling can effectively reduce the cooling load by allowing the unwanted heat flowing from the indoor space to the outdoor environment. Therefore, for this case study, a low-insulated case (R_L) is examined where the uninsulated building roof can maximize the cooling effect from the evaporative cooling surface as compared to the BMSF case with standard insulation shown in **Figure 5.11** (d). Despite the benefits of effective heat transfer by BMSF case with low insulation, as shown in **Figure 5.11** (b) and **Figure 5.12** (b), it may also induce overcooling issues at night and higher interior surface temperature than the baseline during the period with peak internal load when the evaporative cooling effect is limited. Consequently, AIS complements the limitations of static insulation in these scenarios. When the interior surface temperature increased to the peak value at during the daytime, the R-value of interior AIS was set to maximum to insulate the unwanted heat from the outdoor environment shown in **Figure 5.11** (b) so that the AC load of the case with interior AIS was reduced compared with the BMSF roof without interior AIS. While the R-value of interior AIS was tuned to the intermediate level at night to prevent overcooling effects in summer, which provided substantial AC load reduction as compared to the BMSF roof without interior AIS. In contrast, as **Figure 5.12** (b) presents, during cold

winter nights, the interior AIS was set to maximum to insulate the undesired cold heat flow from the outdoor environment and switched gradually to a low level to offset the internal load as the indoor air transited from heating mode to cooling mode during the daytime. Similar behavior of the heat flux modulation is presented in **Figure 5.11** (a) and **Figure 5.12** (a). Therefore, interior AIS overcomes the limitation of the BMSF in the scenarios of lower internal gains level. Since the cooling mode dominated during most of the summer week, the BMSF roof with AIS provided considerably higher AC load reduction than the BMSF cooling roof in winter according to the comparison between **Figure 5.11** (d) and **Figure 5.12** (d).

5.2.4.3 Energy-saving potential and thermal comfort performance

Figure 5.13 presents the comparison of AC loads of the studied case with different roof designs -i.e., insulated concrete baseline (R_H), concrete + BMSF + low-level insulation (R_L), and concrete + BMSF + interior AIS. **Figure 5.13** (a) presents monthly mean AC loads for buildings with both the baseline roof and BMSF roofs with different roof designs. The sequence of monthly mean AC load for the different cases in Los Angles were: baseline > BMSF roof with standard insulation > BMSF roof with low insulation > BMSF roof with interior AIS (R_{high}= 2 (K·m^2)/W) > BMSF roof with interior AIS (R_{high}= 4.35 (K·m^2)/W), during which no obvious difference in AC load reduction was found between the one by the BMSF roof with standard insulation (1.5%) and the one by the BMSF roof with low insulation (5.0%) in winter. Whereas in summer, the BMSF roof with low insulation provides much a higher energy-saving potential (31.9% AC load reduction) than the BMSF roof with standard insulation (4.5% AC load reduction).

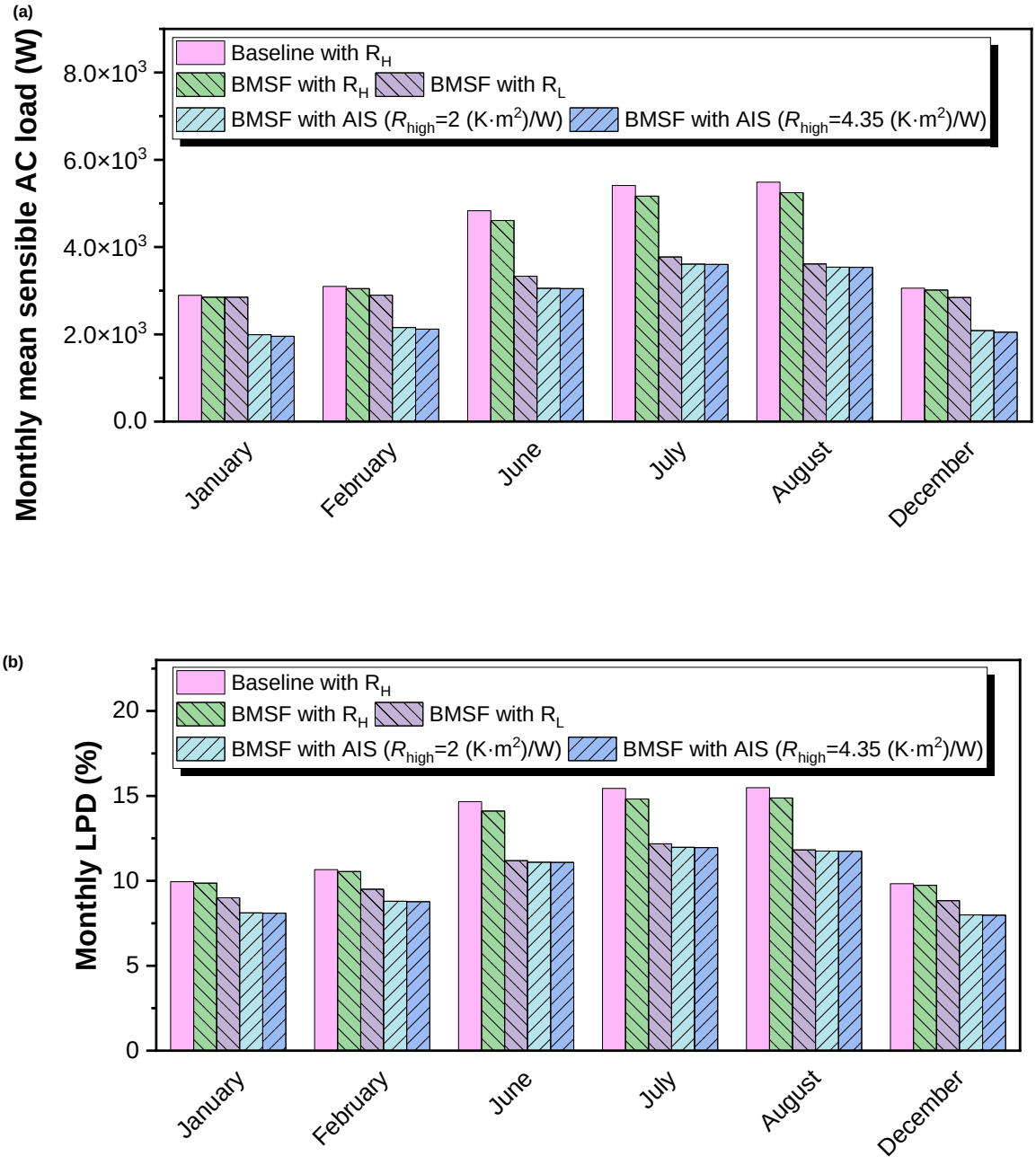


Figure 5.13 Energy performance of the building installed with baseline, BMSF roof and BMSF roof with AIS: (a) Monthly mean AC load and (b) Monthly LPD

For buildings in mild climates and with high internal loads, more energy savings can stem from reducing the roof insulation to augment the cooling effects of the evaporative BMSF roof, which consequently leads to lower interior surface temperatures. As a result, the AC load can be effectively shed by evaporative cooling from the BMSF roof during the summer days. High roof insulation in this case hinders the beneficial heat flow from the indoor space to the cooling surfaces.

As shown in **Figure 5.11** (a) and **Figure 5.12** (a), the AC load reduction for the BMSF roof with standard insulation is very minimal. Therefore, in cases when internal gains are substantial, lower roof insulation (R_L) is beneficial to the reduction of AC load.

The simulation results show that in summer, there was a slight difference in AC load reduction between the one by the BMSF roof with low roof insulation (31.9%) and the one by the BMSF roof with interior AIS (R_{high}= 2 (K·m^2)/W) (35.1%); while in winter BMSF roof with interior AIS (R_{high}= 2 (K·m^2)/W) provided substantially higher AC load reduction (31.8%.) as compared to the BMSF roof with the lower roof insulation (5.0%). In other words, with regard to the comparison of AC load reduction with the BMSF roof, the BMSF roof with interior AIS presented significantly higher energy-saving potential in winter and limited benefits in summer for the cases with high internal gains, which indicates that high insulation is required under cold conditions and only low insulation enables considerable cooling effect into indoor space from the outdoor environment in summer. Therefore, these phenomena imply that the crucial advantages of heat flow modulation enabled by variable insulation of AIS during seasonal periods, which especially

maximizes the benefits through synthesis with other functional modules (e.g., evaporative cooling).

The AC load reduction by the AIS with a high R-value upper limit (R_{high}= 4.35 (K·m^2)/W) (35.2% AC load reduction in summer and 32.4% AC load reduction in winter) is marginal as compared to the one by the AIS with intermediate R-value upper limit (R_{high}= 2 (K·m^2)/W). To this end, the promising performance of the BMSF roof with AIS also demonstrates that AIS with intermediate insulation fulfills the requirement for performance improvement, which significantly reduces the construction cost of the high R-value limit suggested by the ASHRAE standards for envelopes with static thermal insulation.

Figure 5.13 (b) presents the corresponding monthly long-term percentage of dissatisfied (LPD). Similar to the trend of AC load reduction, the sequence of annual LPD of the different cases in Los Angles were: baseline (12.69%) > BMSF roof with standard insulation (12.35%) > BMSF roof with low insulation RBE (10.43%) > BMSF roof with interior AIS (R_{high}= 2 (K·m^2)/W) (9.97%) > BMSF roof with interior AIS (R_{high}= 4.35 (K·m^2)/W) (9.95%). BMSF roof with interior AIS shows higher thermal comfort improvement potential during representative winter and summer months.

Despite its energy-saving potential, it is well known that evaporative cooling systems need water for cooling, which may be partially compensated by rainwater precipitated on the roof surface (Spanaki, Tsoutsos and Kolokotsa, 2011). The water demands of the BMSF with R_H and R_L are 475.7 kg/m^2 and 501.1 kg/m^2, respectively. The rainwater available for utilization is 362.0 kg/m^2 according to historical weather data from NOAA's National Weather Service for the Los Angeles, CA area, such that only a fraction

of the water demand needs to be compensated by freshwater support (or reuse of greywater generated from buildings). In addition, with well-designed control and optimization (e.g., water supply can be shut off when cooling demand is low), the water demand may be further reduced – the controller design for the water supply system falls outside the scope of this study.

5.3 Conclusions

In this chapter, case studies of RBEs integrating an interior AIS and an exterior dynamic shading system (DSS) or evaporative cooling techniques are conducted to extensively explore the potential of AIS. The main contributions and findings are summarized below:

- A low-cost, biomimetic inorganic synthetic foam material, namely BMSF, was developed and demonstrated for building surface cooling. The BMSF material is made from an abundant industrial byproduct – i.e., fly ash cenospheres, through a minimal contact method developed by the authors. The material is low-cost and can be mass-produced for large-scale building applications. Microstructural analysis (i.e., X-ray microtopography and scanning electron microscopy) revealed that the microstructure of the BMSF resembles that of the keratinous skin of elephants and certain desert lizards, where the hydrophilic surface and hollow cavity structure of BSMF enable water to be transported and stored effectively within the material through capillary actions. The thermophysical properties of BMSF were characterized and a series of controlled drying/evaporation experiments were

conducted on BMSF panels under various combinations of temperature and relative humidity to quantify the drying behavior and evaporation rate of the material.

- A calibrated thermal network model with good agreements with the experimental results, was utilized for simulation analyses of evaporative cooling roofs composed of the BMSF layer, where a case study was conducted on a single-story cafeteria in Los Angeles, California (climate zone 3B) under insulation levels to quantify the energy-saving potential and thermal comfort improvement. In addition, the roof consisting of an exterior BMSF layer and an interior AIS was also analyzed for the performance improvement potential of AIS. The simulation results show that the BMSF roof with standard insulation (R= 4.55($K \cdot m^2$)/W) provides limited energy-saving potential (4.5% AC load reduction compared with baseline with standard insulation level in summer) as the high thermal resistance of roof insulation cut off heat flow from the evaporative surface and therefore limits the benefit of evaporative cooling. The building roofs equipped with BMSF with low thermal resistance may provide substantial energy savings (31.9% AC load reduction compared with baseline with standard insulation level in summer) and thermal comfort improvement (22.8% LPD reduction compared with baseline with standard insulation level) for buildings in the mild climate and with high internal loads. Moreover, the building roof composed of an exterior BMSF layer, and an interior AIS presents more flexible behavior to avoid over cooling effect as compared to the previous BMSF cases, which consequently leads to higher energy savings (35.1% AC load reduction in summer) and thermal comfort improvement (23.6%

LPD reduction), especially in winter (31.1% AC load reduction by BMSF with AIS as compared to 5.0% AC load reduction by the BMSF case with low insulation) under cool or cold conditions at nights. The AC load reduction by the AIS with a high R-value upper limit (R_{high}= 4.35 (K·m^2)/W) is marginal as compared to the one by the AIS with an intermediate R-value upper limit (R_{high}= 2 (K·m^2)/W). The promising performance of the BMSF roof with AIS also demonstrates that AIS with intermediate insulation fulfills the requirement for performance improvement, which significantly reduces the construction cost of the high R-value limit suggested by the ASHRAE standards for envelopes with static thermal insulation.

- The RBE integrating AIS and DSS shows superior energy performance (17.8% annual energy consumption reduction) under cold weather conditions as compared to the baseline and the RBE case composed of a concrete (thermal mass) layer sandwiched between an exterior static insulation and an interior AIS (6.5% annual energy consumption reduction), while presents marginal advantages in the scenarios with mild weather conditions.

These results imply that more research is required for the integration of AIS and other functional modules to fully leverage the benefits from outdoor and indoor space for constructing Net-zero energy buildings and maintaining an eco-friendly environment.

CHAPTER SIX
CONCLUSIONS AND RECOMMENDATIONS

This chapter concludes the studies by summarizing the main objectives of the dissertation. What follows is the discussion of the essential findings related to the case studies. The innovative contributions of this dissertation are presented. Finally, it also reviews the limitations of the studies and proposes topics for future research.

6.1 Conclusions

Responsive building envelopes (RBEs) represent a promising and evolving paradigm of building envelope technologies that will facilitate the co-evolutionary interaction between the buildings, the inhabitants, and the environment. The research and development of environmentally responsive building envelopes are still in their early stages where numerous technological, economic, and implementation challenges are yet to be overcome. The potential of responsive building envelope technologies to improve building energy efficiency and improve thermal comfort is well demonstrated. Meanwhile, recent decades have witnessed dramatic advances in the precision and reliability of sensors and actuators with falling prices. These technological developments are providing unprecedented opportunities to embed programmable components into building envelopes to further enhance their performance. However, despite these promising trends, many adaptive façade technologies remain designed for, and used in, single architectural projects. The widespread commercialization of RBEs for either new or existing buildings is still limited.

With the majority of our current building stock being obsolete and energy inefficient, the development of adaptive facades for building retrofitting may have a faster and more significant reduction potential on energy use and greenhouse gas emissions than strategies that solely focus on new buildings. In this research, it thereby tries to develop a deep insight into the mechanisms of RBE behavior and formulate an intelligent control framework for different RBEs. Based on the simulation case studies of different RBEs and experimental analysis with theoretical calibration, the performance of multiple RBEs and their applicability are analyzed and evaluated for design implications.

According to the previous research and studies performed in this dissertation, the key findings and original contributions of the dissertation are summarized below:

- Widely applicable thermal network models based on the finite difference method are developed for various self-adaptive building envelopes with experimental calibration and RBEs validated through comparisons with EnergyPlus simulation results with a good agreement. The thermal network model with high computational efficiency is also constructed for offline pretraining of the model-free controller. The analysis results show that offline training using the thermal network model takes much lower computation time than that using commercial software e.g., EnergyPlus, which demonstrates that the thermal network model is significant to reduce computational costs for studies that employ AI-based online learning control.
- A versatile computational framework that can flexibly integrate multiple control strategies (e.g., white box/forward/physics-derived and black box/reverse/model-free methods) and buildings with diverse functional modules is established to perform

building energy analyses, validation/experimental calibration, offline training, and online training and control/co-simulation implementation for design and control implications of buildings with RBEs.

- An easy-to-implement yet flexible demand-based control strategy is proposed for RBEs based on demand analysis to project the 'desired' thermal resistance of the RBE composed of active insulation systems (AISs) to provide on-demand heat flow. The traditional temperature-based control strategies published in many previous studies tend to lead to overheating or overcooling during transitional seasons when applied to RBEs with high thermal mass or other forms of thermal energy storage (TES), which largely limits the energy-saving potential of RBEs. In contrast, the proposed demand-based control has achieved significantly higher energy-saving potential and thermal comfort and guaranteed the system performance by modulating thermal energy stored in the thermal mass and releasing on-demand heat into/from the building envelope by calculating the desired R-value of the AIS based on the projected AC demands. This approach does not rely on a prescribed temperature constraint and overcomes the limitations of overcooling/overheating. The proposed demand-based control rule fully leverages the advantages of AISs that are designed to change their thermal properties continuously, as opposed to the two-stage 'on-and-off' control. Meanwhile, this control strategy also avoids unnecessary triggering of AISs, which reduces both operational and maintenance costs of the systems.
- A model-free online reinforced learning control (MFORL) framework using a co-simulation testbed is developed for the RBE consisting of AIS and sensible energy

storage. It is indicated that the model-free online reinforced learning controller provides higher energy savings and thermal comfort improvement as compared to those under simple temperature-based rule-based control and demand-based control. This demonstrates a good balance between the conflicting optimization objectives of energy savings and thermal comfort improvement by the MFORL controller. The control sequence generated by the MFORL controller implies intelligent modulation of the indoor environment and wise actuation with flexible adaptation to new changes occurring in the environment. Moreover, the MFORL controller prevents unnecessary AIS triggering, which improves cost savings for both system operation and maintenance.

- An efficient online control strategy with pretraining is proposed to guarantee robust performance and low training costs. The MFORL controller is properly constructed with thoughtful consideration of action and state space selection, artificial neural networks (ANNs) architecture design, reward function design, agent algorithm selection, etc. through parametric pre-analysis. The MFORL controller design and implications for offline training are elaborated. The actor-critic approach based on the TRPO algorithm is selected with a trade-off between performance and computation efficiency. The analysis results indicate that deep neural networks with multiple hidden layers, proper node size, and normalized inputs are necessary for learning optimal policies and complex RBE system behavior. The refined reward function that decreases the difference between adjacent actions obtains promising energy performance while maintaining stable operation. The agent with the action space size of 10 indicates the strengths of AIS that changes the R-value with multiple steps. The reduced state space with only several state

variables among many available indices prompts controller complexity reduction. This enables the small-scale agent to learn how to map optimal actions in response to different weather conditions with low computation costs. In addition, the settings of one-hour sample time and half-day or one-day experience horizon are applied. These significantly cut down the cost of online computation, instrumentation, and maintenance as compared to the high-fidelity controllers that require monitoring massive data to attain similar performance with much higher costs for calibration before application.

- The agent learns the optimal control rules effectively using the training data with similar characteristics during adjacent experience horizons. Hence, utilization of the pre-trained agent trained under several representative patterns can substantially reduce the training data design difficulty and computation complexity to provide sufficient experience for online learning compared with the practice of training a single agent that is fully compatible with all the representative patterns leading to high design and computation costs. Furthermore, the agent obtains good training performance and stable convergence using only 7-day or 8-day training data. The training data size much smaller than those used in prior studies allows cost-effective offline pre-training for deployment.
- The case studies on different types of buildings with diverse RBEs in multiple climate zones were performed to evaluate their performance and applicability in different scenarios. The analyses results demonstrate that thermal mass-AIS integrated RBE provides noticeably superior energy performance. AIS is effective in regulating the charging and discharging of thermal energy stored in thermal masses to provide as-needed compensating heat flow to offset the AC load. Detailed case studies carried out

in six climate zones in the US show that the integrated high thermal mass-AIS RBE has significant potential to reduce the energy consumption of buildings located in most climate zones. Generally, the energy-saving potential of this RBE is greater during transitional seasons and in regions with a mild climate where the diurnal temperature fluctuates around the AC set points.

- Analysis of whole-year AIS operation across different climate zones can provide guidance for AIS design. It was found that in regions with predominantly hot or cold climates, the use of a "two-step" thermal switch would yield satisfactory thermal performance; whereas in regions with long transitional seasons, AISs that gradually change their thermal resistance can provide higher energy-saving potential. In addition, for regions with mild climates (e.g., San Francisco), RBE with only exterior AIS (i.e., the interior side is not insulated) can provide satisfactory performance.
- Case studies of RBE integrating AIS and self-adaptive/active modules using calibrated thermal network models are performed. The simulation results of a responsive roof consisting of a concrete layer sandwiched between an exterior biomimetic mesoporous synthetic foam (or BMSF) evaporative cooling panel and an interior AIS indicate that this integration provides higher energy-saving potential and improved thermal comfort as compared to the cases only with evaporative cooling techniques or high insulations. Moreover, the AIS effectively prevents overcooling impact on the cases with passive cooling techniques. Another simulation case study for the RBE composed of a concrete layer sandwiched between an exterior dynamic shading system (DSS) and an interior AIS was performed. The results show that RBE with exterior DSS under cold weather

conditions brings promising energy-saving potential, which was much higher than the counterpart by RBE with an exterior static insulation and an interior AIS. However, its static insulation impedes redundant heat dissipation within the concrete layer during the rest time of the year with marginal benefits in summer.

6.2 Recommendations

The studies conducted in this dissertation have identified some limitations and brought to light interesting topics as the following that are worth further investigation to facilitate the extensive commercialization of RBEs:

- Development of materials, especially those that enable passive and autonomous responses of building envelopes and that focus on obtaining a higher 'switching ratio' while meeting the requirements for conventional building insulation is still much desired.
- Future development of RBEs should focus on technologies or products that can be easily integrated into a wide range of existing building types, especially those integrating AIS and other active or passive techniques. With regard to the RBE with evaporative cooling, it is worth noting that this cooling system in general consumes a large amount of water, which may be compensated by rainwater collection or the reuse of greywater in buildings. The water management aspects and durability of the BMSF material are not included in this study, which is suggested for future research on the integration of AIS and evaporative cooling roof with active water supply control.
- The MFORL controller in the case studies relies on abundant pre-training experience to guarantee robust performance in all scenarios. Thus, it is worthwhile to further investigate the online training and control strategies without pre-training. For instance, it

can integrate online control and system identification using machine learning-based methods. The system identification model as the plant of the simulated environment will increase training experience and overcome the limited trials during online training for real physical systems under unintended disturbances. This will serve as a zero-shot learning controller applied in any scenario with a good balance between computation efficiency and generalization.

- To provide deeper insight into the mechanisms that how the building energy performance is affected by the RBE behavior, and the underlying optimal control rules, further research is required for developing explainable artificial intelligence (XAI) framework such as physics-informed methods to give implications for RBE design and control.
- The case studies performed in this dissertation focus on the scenarios of a single thermal zone. Control strategies and design optimizations for RBE implementation in multi-thermal zone buildings (e.g., distributed control strategies with a decentralized law) are needed for future studies.
- Further investigations may involve designs or mechanisms that arise from human-centered design. RBE controls can be oriented towards multiple objectives including grid flexibility, air quality, and daylighting performance, other than focusing on energy efficiency and thermal comfort. In addition, occupancy behavior can be integrated as part of RBE control.

REFERENCES

ADVANCED RESEARCH PROJECTS AGENCY – ENERGY (ARPA-E) U.S. DEPARTMENT OF ENERGY (2014) *DELIVERING EFFICIENT LOCAL THERMAL AMENITIES (DELTA),DE-FOA-0001127*.

Al-Masrani, S. M. and Al-Obaidi, K. M. (2019) 'Dynamic shading systems: A review of design parameters, platforms and evaluation strategies', *Automation in Construction*. Elsevier, 102(January), pp. 195–216. doi: 10.1016/j.autcon.2019.01.014.

Al-Sanea, S. A., Zedan, M. F. and Al-Hussain, S. N. (2012) 'Effect of thermal mass on performance of insulated building walls and the concept of energy savings potential', *Applied Energy*. Elsevier Ltd, 89(1), pp. 430–442. doi: 10.1016/j.apenergy.2011.08.009.

Amir Tabadkani , Saeed Banihashemi, M. R. H. (2018) 'Daylighting and visual comfort of oriental sun responsive skins.pdf'.

Angayarkanni, S. A. and Philip, J. (2015) 'Review on thermal properties of nanofluids: Recent developments', *Advances in Colloid and Interface Science*. Elsevier B.V., 225, pp. 146–176. doi: 10.1016/j.cis.2015.08.014.

Antretter, F. and Boudreaux, P. (2019) 'Assessing the Potential of Active Insulation Systems to Reduce Energy Consumption and Enhance Electrical Grid Services', *2019 Buildings XIV International Conference*, pp. 12–15.

Artmann, N., Manz, H. and Heiselberg, P. (2007) 'Climatic potential for passive cooling of buildings by night-time ventilation in Europe', *Applied Energy*, 84(2), pp. 187–201. doi: 10.1016/j.apenergy.2006.05.004.

ASHRAE (2019) *ANSI/ASHRAE/IEC Standard 90.1-2019: Energy Standard for Buildings Except Low-Rise Residential Buildings.*

Athienitis, A. and Brien, W. O. (2015) *Modeling, Design, and Optimization of Net-Zero Energy Buildings*.

Augustin, N. (2018) *Motion with Moisture Creating Passive Dynamic Envelope Systems Using the Hygroscopic Properties of Wood Veneer, University of Waterloo*. Available at: http://link.springer.com/10.1007/978-3-319-59379-1%0Ahttp://dx.doi.org/10.1016/B978-0-12-420070-8.00002-7%0Ahttp://dx.doi.org/10.1016/j.ab.2015.03.024%0Ahttps://doi.org/10.1080/07352689.2018.1441103%0Ahttp://www.chile.bmw-motorrad.cl/sync/showroom/lam/es/.

Baldi, S. *et al.* (2015) 'Model-based and model-free "plug-and-play" building energy efficient control', *Applied Energy*, 154, pp. 829–841. doi: 10.1016/j.apenergy.2015.05.081.

Beites, S. (2013) 'Morphological behavior of shape memory polymers toward a deployable, adaptive architecture', *ACADIA 2013: Adaptive Architecture - Proceedings of the 33rd Annual Conference of the Association for Computer Aided Design in Architecture*, pp. 121–128.

Belzer, D. B., Scott, M. J. and Sands, R. D. (1996) 'Climate Change Impacts on U.S. Commercial Building Energy Consumption: An Analysis Using Sample Survey Data', *Energy Sources*, 18(February 2015), pp. 177–201. doi: 10.1080/00908319608908758.

Benson, David K., Potter, T. F. and Tracy, C. E. (1994) 'Design of a variable-conductance vacuum insulation', *SAE Technical Papers*, 103(1994), pp. 176–181. doi:

10.4271/940315.

Benson, David K, Potter, T. F. and Tracy, C. E. (1994) ‘Design of a Variable - Conductance Vacuum Insulation’, *Journal of Materials and Manufacturing*, 103–5, pp. 88–95. doi: 10.4271/940315.Thomas.

Berardi, U., Garai, M. and Morselli, T. (2020) ‘Preparation and assessment of the potential energy savings of thermochromic and cool coatings considering inter-building effects’, *Solar Energy*. Elsevier Ltd, 209(August), pp. 493–504. doi: 10.1016/j.solener.2020.09.015.

Berge, A. *et al.* (2015) ‘Effect from a Variable U-Value in Adaptive Building Components with Controlled Internal Air Pressure’, *Energy Procedia*. Elsevier B.V., 78, pp. 376–381. doi: 10.1016/j.egypro.2015.11.677.

Berkeley L, Ridge OAK, Ut-battelle MBY, For A, Energy S, Or D, et al. (2019) *EnergyPlusTM Version 8.9.0 Documentation Input Output Reference*.

Berkeley, L. *et al.* (2019) *EnergyPlus™ Version 8.9.0 Documentation Engineering Reference*.

Bianco, L. *et al.* (2017) ‘Responsive glazing systems: Characterisation methods and winter performance’, *Solar Energy*. Elsevier Ltd, 155, pp. 372–387. doi: 10.1016/j.solener.2017.06.029.

Biloria, N. and Sumini, V. (2009) ‘Performative Building Skin Systems: A Morphogenomic Approach towards Developing Real-Time Adaptive Building Skin Systems’, *International Journal of Architectural Computing*, 7(4), pp. 643–675. doi: 10.1260/1478-0771.7.4.643.

Biyik, E. and Kahraman, A. (2019) ‘A predictive control strategy for optimal management of peak load, thermal comfort, energy storage and renewables in multi-zone buildings’, *Journal of Building Engineering*. Elsevier Ltd, 25(June), p. 100826. doi: 10.1016/j.jobe.2019.100826.

Bodach, S., Lang, W. and Hamhaber, J. (2014) ‘Climate responsive building design strategies of vernacular architecture in Nepal’, *Energy and Buildings*. Elsevier B.V., 81, pp. 227–242. doi: 10.1016/j.enbuild.2014.06.022.

Boris Belousov, Hany Abdulsamad, Pascal Klink, Simone Parisi, J. P. (2021) *Reinforcement Learning—Algorithms and Applications, Studies in Computational Intelligence*. Springer. doi: 10.1007/978-3-030-41188-6_10.

Brigham, J. (2015) *Collaborative Research : Adaptive and Reconfigurable Tiles for Building Surfaces, NSF*.

Brooks, A. L., Zhou, H. and Hanna, D. (2018) ‘Comparative study of the mechanical and thermal properties of lightweight cementitious composites’, *Construction and Building Materials*. Elsevier Ltd, 159, pp. 316–328. doi: 10.1016/j.conbuildmat.2017.10.102.

Brunner, S. *et al.* (2014) ‘Vacuum insulation panels for building applications - Continuous challenges and developments’, *Energy and Buildings*. Elsevier B.V., 85, pp. 592–596. doi: 10.1016/j.enbuild.2014.09.016.

Brunner, S. and Wakili, K. G. (2014) ‘Hints for an additional aging factor regarding the thermal performance of vacuum insulation panels with pyrogenic silica core’, *Vacuum*. Elsevier Ltd, 100, pp. 4–6. doi: 10.1016/j.vacuum.2013.07.033.

Bursill, M. J., O’Brien, L. and Beausoleil-Morrison, I. (2020) ‘Multi-zone field study of

rule extraction control to simplify implementation of predictive control to reduce building energy use', *Energy and Buildings*. Elsevier B.V., 222, p. 110056. doi: 10.1016/j.enbuild.2020.110056.

Cabeza, L. F. *et al.* (2017) 'Thermochemical energy storage by consecutive reactions for higher efficient concentrated solar power plants (CSP): Proof of concept', *Applied Energy*. Elsevier Ltd, 185, pp. 836–845. doi: 10.1016/j.apenergy.2016.10.093.

Carlucci, F. (2021) 'A review of smart and responsive building technologies and their classifications', *Future Cities and Environment*, 7(1), pp. 1–12. doi: 10.5334/fce.123.

Carlucci, S. (2013) *Thermal Comfort Assessment of Buildings*. Springer Milan Heidelberg New York Dordrecht London. doi: 10.1007/978-88-470-5238-3.

Casini, M. (2018) 'Active dynamic windows for buildings: A review', *Renewable Energy*. Elsevier Ltd, 119, pp. 923–934. doi: 10.1016/j.renene.2017.12.049.

Cheng, V., Ng, E. and Givoni, B. (2005) 'Effect of envelope colour and thermal mass on indoor temperatures in hot humid climate', *Solar Energy*, 78(4 SPEC. ISS.), pp. 528–534. doi: 10.1016/j.solener.2004.05.005.

Claros-marfil, L. J. *et al.* (2014) 'Active and passive PCM walls simulation – a new TRNSYS PCM-Type', *1st International Congress on research in Construction and Architectural Technologies*, (June).

Council, N. F. R. (2013) 'National Fenestration Rating Council Incorporated NFRC 700-2013[E1A1] Product Certification Program'.

Cuce, P. M. and Riffat, S. (2016) 'A state of the art review of evaporative cooling systems for building applications', *Renewable and Sustainable Energy Reviews*. Elsevier,

54, pp. 1240–1249. doi: 10.1016/j.rser.2015.10.066.

Cui, B. *et al.* (2022) 'Model predictive control for active insulation in building envelopes', *Energy and Buildings*. Elsevier B.V., 267, p. 112108. doi: 10.1016/j.enbuild.2022.112108.

Cui, H. and Overend, M. (2019) 'A review of heat transfer characteristics of switchable insulation technologies for thermally adaptive building envelopes', *Energy and Buildings*. Elsevier B.V., 199, pp. 427–444. doi: 10.1016/j.enbuild.2019.07.004.

Cui, S. *et al.* (2016) 'Bio-inspired effective and regenerable building cooling using tough hydrogels', *Applied Energy*. Elsevier Ltd, 168, pp. 332–339. doi: 10.1016/j.apenergy.2016.01.058.

Das, Sarit K., Stephen U. Choi, Wenhua Yu, and T. P. (2007) *Nanofluids: science and technology*. John Wiley & Sons, Inc.

Deardorff, J. W. (1978) 'Efficient prediction of ground surface temperature and moisture, with inclusion of a layer of vegetation', *Journal of Geophysical Research*, 83(C4), p. 1889. doi: 10.1029/jc083ic04p01889.

Decker, M. (2013) 'Emergent Futures: Nanotechology and Emergent Materials in Architecture', *Conference of Tectonics of Teaching: Building Technology Educators Society (BTES)*, (January 2013).

DeForest, N. *et al.* (2017) 'A comparative energy analysis of three electrochromic glazing technologies in commercial and residential buildings', *Applied Energy*. Elsevier Ltd, 192, pp. 95–109. doi: 10.1016/j.apenergy.2017.02.007.

Dehwah, A. H. A. and Krarti, M. (2020) 'Impact of switchable roof insulation on energy

performance of US residential buildings', *Building and Environment*. Elsevier Ltd, 177(March), p. 106882. doi: 10.1016/j.buildenv.2020.106882.

Delalat, F., Ranjbar, M. and Salamati, H. (2016) 'Blue colloidal nanoparticles of molybdenum oxide by simple anodizing method: decolorization by PdCl2 and observation of in-liquid gasochromic coloration', *Solar Energy Materials and Solar Cells*. Elsevier, 144, pp. 165–172. doi: 10.1016/j.solmat.2015.08.038.

Deru, M. *et al.* (2011) 'U.S. Department of Energy commercial reference building models of the national building stock', *Publications (E)*, (February 2011), pp. 1–118. Available at: http://digitalscholarship.unlv.edu/renew_pubs/44.

Dewidar, K.M, Mohamed, N.M., Ashour, Y. . *et al.* (2013) 'Living Skins: A New Concept of Self Active Building Envelope Regulating Systems', *SB13 Dubai*, pp. 1–8. Available at: https://www.irbnet.de/daten/iconda/CIB_DC26849.pdf.

Dincer, I. and Rosen, M. A. (2013) *Exergy Analysis of Thermal Energy Storage Systems*, *Exergy*. doi: 10.1016/b978-0-08-097089-9.00009-7.

Dols, W. S. and Polidoro, B. J. (2020) 'CONTAM User Guide and Program Documentation Version 3.4', *National Institute of Standards and Technology*, p. 330. Available at: https://doi.org/10.6028/NIST.TN.1887r1%0Ahttps://nvlpubs.nist.gov/nistpubs/TechnicalNotes/NIST.TN.1887r1.pdf.

Dostal, J. and Baumelt, T. (2019) 'Model predictive control for buildings with active one-pipe hydronic heating', *E3S Web of Conferences*, 111(201 9), pp. 1–8. doi: 10.1051/e3sconf/201911104050.

E. Mitrofanova, A. Rathee, and P. S. (2014) ‘Hydroceramic Digital Matter - Intelligent Contructions’.

Eapen, J. *et al.* (2010) ‘The classical nature of thermal conduction in nanofluids’, *Journal of Heat Transfer*, 132(10), pp. 1–14. doi: 10.1115/1.4001304.

Edition, S. I. *et al.* (2013) *ANSI/ASHRAE/IES Standard 90.1-2013 Energy standard for buildings except low-rise residential buildings (SI Edition), ASHRAE Standard*.

Elsarrag, E., Al-Horr, Y. and Imbabi, M. S. E. (2012) ‘Improving building fabric energy efficiency in hot-humid climates using dynamic insulation’, *Building Simulation*, 5(2), pp. 127–134. doi: 10.1007/s12273-012-0067-6.

Faghri, A. (1995) *Heat pipe science and technology*. Global Digital Press.

Favoino, F., Jin, Q. and Overend, M. (2017) ‘Design and control optimisation of adaptive insulation systems for office buildings. Part 1: Adaptive technologies and simulation framework’, *Energy*. Elsevier Ltd, 127, pp. 301–309. doi: 10.1016/j.energy.2017.03.083.

Frank, T. (2005) ‘Climate change impacts on building heating and cooling energy demand in Switzerland’, *Energy and Buildings*, 37(11 SPEC. ISS.), pp. 1175–1185. doi: 10.1016/j.enbuild.2005.06.019.

Fraternali, F., De Chiara, E. and Skelton, R. E. (2015) ‘On the use of tensegrity structures for kinetic solar facades of smart buildings’, *Smart Materials and Structures*. IOP Publishing, 24(10). doi: 10.1088/0964-1726/24/10/105032.

Gholamzadehmir, M. *et al.* (2020) ‘Adaptive-predictive control strategy for HVAC systems in smart buildings – A review’, *Sustainable Cities and Society*. Elsevier Ltd, 63(November 2019). doi: 10.1016/j.scs.2020.102480.

Goia, F. *et al.* (2010) ‘Towards an Active, Responsive, and Solar Building Envelope’, *Journal of Green Building*, 5(4), pp. 121–136. doi: 10.3992/jgb.5.4.121.

Goubran, S. *et al.* (2017) ‘Comparing methods of modeling air infiltration through building entrances and their impact on building energy simulations’, *Energy and Buildings*. Elsevier B.V., 138, pp. 579–590. doi: 10.1016/j.enbuild.2016.12.071.

Gracia, A. de (2019) ‘Dynamic building envelope with PCM for cooling purposes – Proof of concept’, *Applied Energy*. Elsevier, 235(November 2018), pp. 1245–1253. doi: 10.1016/j.apenergy.2018.11.061.

Hammad, F. and Abu-Hijleh, B. (2010) ‘The energy savings potential of using dynamic external louvers in an office building’, *Energy and Buildings*. Elsevier B.V., 42(10), pp. 1888–1895. doi: 10.1016/j.enbuild.2010.05.024.

Han, M. *et al.* (2018) ‘A review of reinforcement learning methodologies on control systems for building energy A review of reinforcement learning methodologies on control systems for building energy’, *Working papers in transport, tourism, information technology and microdata analysis*, pp. 1–26. Available at: http://www.diva-portal.org/smash/get/diva2:1221058/FULLTEXT01.pdf.

Harris, C. B. (2019) *Grid-interactive Efficient Buildings Technical Report Series: Windows and Opaque Envelope*. Available at: https://www1.eere.energy.gov/buildings/pdfs/75387.pdf%0Ahttps://www.nrel.gov/docs/fy20osti/75387.pdf.

He, Y. *et al.* (2020) ‘Energy-saving potential of 3D printed concrete building with integrated living wall’, *Energy and Buildings*. Elsevier B.V., 222, p. 110110. doi:

10.1016/j.enbuild.2020.110110.

He, Y. *et al.* (2022) ‘Towards building homeostasis through a durable biomimetic synthetic foam for building surface evaporative cooling’, *Journal of Building Engineering*. Elsevier Ltd, 385(November 2022), p. 135626. doi: 10.1016/j.jclepro.2022.135626.

He, Y., Zhou, H. and Fahimi, F. (2022) ‘Modeling and demand-based control of responsive building envelope with integrated thermal mass and active thermal insulations’, *Energy and Buildings*. Elsevier B.V., 276, p. 112495. doi: 10.1016/j.enbuild.2022.112495.

Holmes, M. J. and Hacker, J. N. (2007) ‘Climate change, thermal comfort and energy: Meeting the design challenges of the 21st century’, *Energy and Buildings*, 39(7), pp. 802–814. doi: 10.1016/j.enbuild.2007.02.009.

Hosseini, S. M. *et al.* (2019) ‘A morphological approach for kinetic façade design process to improve visual and thermal comfort: Review’, *Building and Environment*. Elsevier, 153(March 2019), pp. 186–204. doi: 10.1016/j.buildenv.2019.02.040.

I. Ayala Castro, M. Manosong, and Y. C. C. (2017) ‘Water-Driven Breathing Skin’. Srchitecture of Catalonia.

IEA (2022) *Buildings*. Available at: https://www.iea.org/reports/buildings.

Iffa, E. *et al.* (2022) ‘Performance evaluation of a dynamic wall integrated with active insulation and thermal energy storage systems’, *Journal of Energy Storage*. Elsevier Ltd, 46(May 2021), p. 103815. doi: 10.1016/j.est.2021.103815.

Ihm, P., Nemri, A. and Krarti, M. (2009) ‘Estimation of lighting energy savings from

daylighting', *Building and Environment*, 44(3), pp. 509–514. doi: 10.1016/j.buildenv.2008.04.016.

ISO (2005) 'ISO 7730: Ergonomics of the thermal environment Analytical determination and interpretation of thermal comfort using calculation of the PMV and PPD indices and local thermal comfort criteria', *Management*, 3, pp. 605–615. doi: 10.1016/j.soildyn.2004.11.005.

J.S.E.M. Svensson and C.G. Granqvist (1985) 'ELECTROCHROMIC COATINGS FOR "SMART WINDOWS"', *Solar Energy Materials*, 12(6), pp. 391–402. Available at: http://www.cylaw.org/nomoi/enop/non-ind/1985_1_111/full.html.

Jang, S. P. and Choi, S. U. S. (2004) 'Role of Brownian motion in the enhanced thermal conductivity of nanofluids', *Applied Physics Letters*, 84(21), pp. 4316–4318. doi: 10.1063/1.1756684.

Jin, Q., Favoino, F. and Overend, M. (2017) 'Design and control optimisation of adaptive insulation systems for office buildings. Part 2: A parametric study for a temperate climate', *Energy*. Elsevier Ltd, 127, pp. 634–649. doi: 10.1016/j.energy.2017.03.096.

Joe, J. *et al.* (2013) 'Load characteristics and operation strategies of building integrated with multi-story double skin facade', *Energy and Buildings*. Elsevier B.V., 60, pp. 185–198. doi: 10.1016/j.enbuild.2013.01.015.

Jong-Jin Kim and Jin Woo Moon (2009) 'IMPACT OF INSULATION ON BUILDING ENERGY CONSUMPTION', in *Eleventh International IBPSA Conference*, pp. 674–680.

Juaristi, M. *et al.* (2021) 'Adaptive opaque façades and their potential to reduce thermal energy use in residential buildings: A simulation-based evaluation', *Journal of Building*

Physics. doi: 10.1177/17442591211045418.

Kalnæs, S. E. and Jelle, B. P. (2014) 'Vacuum insulation panel products: A state-of-the-art review and future research pathways', *Applied Energy*, 116(7465), pp. 355–375. doi: 10.1016/j.apenergy.2013.11.032.

Karamanis, D. (2015) *Solar cooling with hydrophilic porous materials for reducing building cooling needs, Eco-efficient Materials for Mitigating Building Cooling Needs: Design, Properties and Applications*. Elsevier Ltd. doi: 10.1016/B978-1-78242-380-5.00010-8.

Kim, D. and Braun, J. E. (2015) 'A general approach for generating reduced-order models for large multi-zone buildings', *Journal of Building Performance Simulation*, 8(6), pp. 435–448. doi: 10.1080/19401493.2014.977952.

Kimber, M., Clark, W. W. and Schaefer, L. (2014) 'Conceptual analysis and design of a partitioned multifunctional smart insulation', *Applied Energy*. Elsevier Ltd, 114, pp. 310–319. doi: 10.1016/j.apenergy.2013.09.067.

Kirkegaard, P. H. and Worre Foged, I. (2011) 'Development and Evaluation of a Responsive Building Envelope Development and Evaluation of a Responsive Building Envelope', in *International Adaptive Architecture Conference*. London, pp. 1–9.

Kishore, R. A. *et al.* (2021) 'Enhancing building energy performance by effectively using phase change material and dynamic insulation in walls', *Applied Energy*. Elsevier Ltd, 283(November 2020), p. 116306. doi: 10.1016/j.apenergy.2020.116306.

Kloppers, J. C. and Kröger, D. G. (2005) 'The Lewis factor and its influence on the performance prediction of wet-cooling towers', *International Journal of Thermal*

Sciences, 44(9), pp. 879–884. doi: 10.1016/j.ijthermalsci.2005.03.006.

Krarti, M., Erickson, P. M. and Hillman, T. C. (2005) 'A simplified method to estimate energy savings of artificial lighting use from daylighting', *Building and Environment*, 40(6), pp. 747–754. doi: 10.1016/j.buildenv.2004.08.007.

Krielaart, M. A. R., Vermeer, C. H. and Vanapalli, S. (2015) 'Compact flat-panel gas-gap heat switch operating at 295 K', *Review of Scientific Instruments*, 86(11), pp. 1–7. doi: 10.1063/1.4936356.

Krietemeyer, B., Andow, B. and Dyson, A. (2015) 'A computational design framework supporting human interaction with environmentally-responsive building envelopes', *International Journal of Architectural Computing*, 13(1), pp. 1–24. doi: 10.1260/1478-0771.13.1.1.

Krietemeyer, E. a and Dyson, A. H. (2011) 'Electropolymeric Technology for Dynamic Building Envelopes', pp. 75–83. Available at: https://www.google.co.id/url?sa=t&rct=j&q=&esrc=s&source=web&cd=1&cad=rja&uact=8&ved=0CBwQFjAA&url=http://cumincad.architexturez.net/system/files/pdf/acadiaregional2011_008.content.pdf&ei=02BIVZjcKYLauQSC3YDgDg&usg=AFQjCNFiy77X04p0AXGxfGHaGcSeVdlgnw&sig2=.

Krzaczek, M. and Kowalczuk, Z. (2011) 'Thermal Barrier as a technique of indirect heating and cooling for residential buildings', *Energy and Buildings*. Elsevier B.V., 43(4), pp. 823–837. doi: 10.1016/j.enbuild.2010.12.002.

Kumar, R. and Kaushik, S. C. (2005) 'Performance evaluation of green roof and shading for thermal protection of buildings', *Building and Environment*, 40(11), pp. 1505–1511.

doi: 10.1016/j.buildenv.2004.11.015.

L. Roth (2015) ‘Hydromembrane’. Institute for advanced architecture of Catalonia.

Lee, E. S. *et al.* (2013) *A post-occupancy monitored evaluation of the dimmable lighting, automated shading, and underfloor air distribution system in The New York Times Building, Berkeley National Laboratory*.

Lehmann, B., Dorer, V. and Koschenz, M. (2007) ‘Application range of thermally activated building systems tabs’, *Energy and Buildings*, 39(5), pp. 593–598. doi: 10.1016/j.enbuild.2006.09.009.

Li, Z. and Zhang, J. (2021) ‘Study on the distributed model predictive control for multi-zone buildings in personalized heating’, *Energy and Buildings*. Elsevier, 231, p. 110627. doi: 10.1016/j.enbuild.2020.110627.

Liu, S. and Henze, G. P. (2006) ‘Experimental analysis of simulated reinforcement learning control for active and passive building thermal storage inventory: Part 2: Results and analysis’, *Energy and Buildings*, 38(2), pp. 148–161. doi: 10.1016/j.enbuild.2005.06.001.

Liu, Y. *et al.* (1999) ‘High strain rate deformation of martensitic NiTi shape memory alloy’, *Scripta Materialia*, 41(1), pp. 89–95. doi: 10.1016/S1359-6462(99)00058-5.

Loonen, R. *et al.* (2015) ‘Design for façade adaptability: Towards a unified and systematic characterization’, *10th Conference on Advanced Building Skins*, (2015), pp. 1284–1294.

Loonen, R. C. G. M. *et al.* (2013) ‘Climate adaptive building shells: State-of-the-art and future challenges’, *Renewable and Sustainable Energy Reviews*, 25, pp. 483–493. doi:

10.1016/j.rser.2013.04.016.

Loonen, R. C. G. M. (2015) ‘Bio-inspired Adaptive Building Skins’, in Pacheco Torgal, F. et al. (eds) *Biotechnologies and Biomimetics for Civil Engineering*. Springer, pp. 115–134.

Loonen, R. C. G. M. *et al.* (2017) ‘Review of current status, requirements and opportunities for building performance simulation of adaptive facades†’, *Journal of Building Performance Simulation*, 10(2), pp. 205–223. doi: 10.1080/19401493.2016.1152303.

Loonen, R. C. G. M., Hoes, P. and Hensen, J. L. . (2014) ‘Performance prediction of buildings with responsive building elements: Challenges and solutions’, *Proceedings of building simulation and optimization*, (June), pp. 1–8. Available at: https://pure.tue.nl/ws/portalfiles/portal/3992582/392669136570421.pdf.

Ma, J., Qin, S. J. and Salsbury, T. (2014) ‘Application of economic MPC to the energy and demand minimization of a commercial building’, *Journal of Process Control*. Elsevier Ltd, 24(8), pp. 1282–1291. doi: 10.1016/j.jprocont.2014.06.011.

Ma, P., Wang, L. S. and Guo, N. (2015) ‘Energy storage and heat extraction - From thermally activated building systems (TABS) to thermally homeostatic buildings’, *Renewable and Sustainable Energy Reviews*. Elsevier, 45, pp. 677–685. doi: 10.1016/j.rser.2015.02.017.

El Mankibi, M. *et al.* (2015) ‘Numerical modeling of thermal behaviors of active multi-layer living wall’, *Energy and Buildings*. Elsevier B.V., 106, pp. 96–110. doi: 10.1016/j.enbuild.2015.06.084.

Marshall, M. T. (2015) ‘Bi-directional thermo-hygroscopic facades: Feasibility for liquid desiccant thermal walls to provide cooling in a small-office building’, *ARCC 2015 Conference. FUTURE of Architectural Research*, (April 2015), pp. 45–56.

Martins, A. F. *et al.* (2018) ‘Locally-curved geometry generates bending cracks in the African elephant skin’, *Nature Communications*. Springer US, 9(1), pp. 1–8. doi: 10.1038/s41467-018-06257-3.

Masoso, O. T. and Grobler, L. J. (2010) ‘The dark side of occupants’ behaviour on building energy use’, *Energy and Buildings*, 42(2), pp. 173–177. doi: 10.1016/j.enbuild.2009.08.009.

Mehrizi-Sani, A. (2017) ‘Distributed Control Techniques in Microgrids’, in *Microgrid: Advanced Control Methods and Renewable Energy System Integration*, pp. 43–62. doi: 10.1016/B978-0-08-101753-1.00002-4.

Meng, H. and Li, G. (2013) ‘Reversible switching transitions of stimuli-responsive shape changing polymers’, *Journal of Materials Chemistry A*, 1(27), pp. 7838–7865. doi: 10.1039/c3ta10716g.

Menyhart, K. and Krarti, M. (2017) ‘Potential energy savings from deployment of Dynamic Insulation Materials for US residential buildings’, *Building and Environment*. Elsevier Ltd, 114, pp. 203–218. doi: 10.1016/j.buildenv.2016.12.009.

Michailidis, I. T. *et al.* (2018) ‘Energy-efficient HVAC management using cooperative, self-trained, control agents: A real-life German building case study’, *Applied Energy*. Elsevier, 211(October 2017), pp. 113–125. doi: 10.1016/j.apenergy.2017.11.046.

Ministerial, G. and Forum, E. (2011) ‘Hygroscopic climatic modulated boundaries: a

strategy for differenti-ated performance using a natural circulative and energy captive build-ing envelope in hot and moisture rich laden air environments', 2(1), pp. 41–53.

Mnih, V. *et al.* (2016) 'Asynchronous methods for deep reinforcement learning', *33rd International Conference on Machine Learning, ICML 2016*, 4, pp. 2850–2869.

Monetti, V. *et al.* (2015) 'Calibration of building energy simulation models based on optimization: A case study', *Energy Procedia*. Elsevier B.V., 78, pp. 2971–2976. doi: 10.1016/j.egypro.2015.11.693.

Moroşan, P. D. *et al.* (2010) 'Building temperature regulation using a distributed model predictive control', *Energy and Buildings*, 42(9), pp. 1445–1452. doi: 10.1016/j.enbuild.2010.03.014.

Mumme, S. and James, N. (2020) 'Smart and Efficient Building Envelopes : Thermal Switches and Thermal Storage for Energy Savings and Load Flexibility', *ASHRAE Transactions*, 126(2), pp. 140–148.

Nahar, N. M., Sharma, P. and Purohit, M. M. (2003) 'Performance of different passive techniques for cooling of buildings in arid regions', *Building and Environment*, 38(1), pp. 109–116. doi: 10.1016/S0360-1323(02)00029-X.

Navarro, L. *et al.* (2015) 'PCM incorporation in a concrete core slab as a thermal storage and supply system: Proof of concept', *Energy and Buildings*. Elsevier B.V., 103, pp. 70–82. doi: 10.1016/j.enbuild.2015.06.028.

Navarro, L. *et al.* (2016) 'Thermal energy storage in building integrated thermal systems: A review. Part 1. active storage systems', *Renewable Energy*, 88, pp. 526–547. doi: 10.1016/j.renene.2015.11.040.

Nayak, A. ketan, Hagishima, A. and Tanimoto, J. (2020) 'A simplified numerical model for evaporative cooling by water spray over roof surfaces', *Applied Thermal Engineering*. Elsevier, 165(October 2019), p. 114514. doi: 10.1016/j.applthermaleng.2019.114514.

Ogwezi, B. *et al.* (2013) 'Development of a passive and adaptable façade element for humidity control', *Technologies for Sustainable Built Environments (TSBE)*, p. 7. Available at: https://www.reading.ac.uk/web/files/tsbe/Ogwezi_TSBE_Conference_Poster_2013.pdf.

Palyvos, J. A. (2008) 'A survey of wind convection coefficient correlations for building envelope energy systems' modeling', *Applied Thermal Engineering*, 28(8–9), pp. 801–808. doi: 10.1016/j.applthermaleng.2007.12.005.

Park, B. and Krarti, M. (2016) 'Energy performance analysis of variable reflectivity envelope systems for commercial buildings', *Energy and Buildings*. Elsevier B.V., 124, pp. 88–98. doi: 10.1016/j.enbuild.2016.04.070.

Park, B., Srubar, W. V. and Krarti, M. (2015) 'Energy performance analysis of variable thermal resistance envelopes in residential buildings', *Energy and Buildings*. Elsevier B.V., 103, pp. 317–325. doi: 10.1016/j.enbuild.2015.06.061.

Pesenti, M. *et al.* (2015) 'Kinetic Solar Skin: A Responsive Folding Technique', *Energy Procedia*. Elsevier B.V., 70, pp. 661–672. doi: 10.1016/j.egypro.2015.02.174.

Pflug, T. *et al.* (2015) 'Closed translucent façade elements with switchable U-value - A novel option for energy management via the facade', *Energy and Buildings*. Elsevier B.V., 86, pp. 66–73. doi: 10.1016/j.enbuild.2014.09.082.

Pflug, T. *et al.* (2017) 'Potential analysis of a new removable insulation system', *Energy*

and Buildings. Elsevier B.V., 154, pp. 391–403. doi: 10.1016/j.enbuild.2017.08.033.

Pflug, T. *et al.* (2018) 'Modeling of facade elements with switchable U-value', *Energy and Buildings*. Elsevier B.V., 164, pp. 1–13. doi: 10.1016/j.enbuild.2017.12.044.

Philip, J., Shima, P. D. and Raj, B. (2008) 'Nanofluid with tunable thermal properties', *Applied Physics Letters*, 92(4), pp. 1–4. doi: 10.1063/1.2838304.

Pinto, G. *et al.* (2021) 'Coordinated energy management for a cluster of buildings through deep reinforcement learning', *Energy*, 229. doi: 10.1016/j.energy.2021.120725.

Pujadas-Gispert, E. *et al.* (2020) 'Design, construction, and thermal performance evaluation of an innovative bio-based ventilated façade', *Frontiers of Architectural Research*. Elsevier Ltd, 9(3), pp. 681–696. doi: 10.1016/j.foar.2020.02.003.

Ramesh, T., Prakash, R. and Shukla, K. K. (2010) 'Life cycle energy analysis of buildings: An overview', *Energy and Buildings*, 42(10), pp. 1592–1600. doi: 10.1016/j.enbuild.2010.05.007.

Reichert, S., Menges, A. and Correa, D. (2015) 'Meteorosensitive architecture: Biomimetic building skins based on materially embedded and hygroscopically enabled responsiveness', *CAD Computer Aided Design*. Elsevier Ltd, 60, pp. 50–69. doi: 10.1016/j.cad.2014.02.010.

Reilly, A. and Kinnane, O. (2017) 'The impact of thermal mass on building energy consumption', *Applied Energy*. Elsevier Ltd, 198, pp. 108–121. doi: 10.1016/j.apenergy.2017.04.024.

Rotzetter, A. C. C. *et al.* (2012) 'Thermoresponsive polymer induced sweating surfaces as an efficient way to passively cool buildings', *Advanced Materials*, 24(39), pp. 5352–

5356. doi: 10.1002/adma.201202574.

Rupp, S. and Krarti, M. (2019) ‘Analysis of multi-step control strategies for dynamic insulation systems’, *Energy and Buildings*. Elsevier B.V., 204. doi: 10.1016/j.enbuild.2019.109459.

Rybkowski, Z. *et al.* (2015) *EAGER : Interaction of Smart Materials for Transparent , Self - regulating Building Skins*, *NSF*.

Sadineni, S. B., Madala, S. and Boehm, R. F. (2011) ‘Passive building energy savings: A review of building envelope components’, *Renewable and Sustainable Energy Reviews*, 15(8), pp. 3617–3631. doi: 10.1016/j.rser.2011.07.014.

Santos-Herrero, J. M., Lopez-Guede, J. M. and Flores-Abascal, I. (2021) ‘Modeling, simulation and control tools for nZEB: A state-of-the-art review’, *Renewable and Sustainable Energy Reviews*. Elsevier Ltd, 142, p. 110851. doi: 10.1016/j.rser.2021.110851.

Schulman, J. *et al.* (2015) ‘Trust region policy optimization’, *32nd International Conference on Machine Learning, ICML 2015*, 3, pp. 1889–1897.

Schulman, J. *et al.* (2016) ‘High-dimensional continuous control using generalized advantage estimation’, *4th International Conference on Learning Representations, ICLR 2016 - Conference Track Proceedings*, pp. 1–14.

Scott, M. J., Wrench, L. E. and Hadley, D. L. (1994) ‘Effects of Climate Change on Commercial Building Energy Demand’, *Energy Sources*, 16, pp. 317–332. doi: 10.1080/00908319408909081.

Sepehri, A. and Pavlak, G. S. (2023) ‘Evaluating optimal control of active insulation and

HVAC systems in residential buildings', *Energy and Buildings*. Elsevier B.V., 281, p. 112728. doi: 10.1016/j.enbuild.2022.112728.

Shafique, M., Kim, R. and Rafiq, M. (2018) 'Green roof benefits, opportunities and challenges – A review', *Renewable and Sustainable Energy Reviews*, 90(April 2017), pp. 757–773. doi: 10.1016/j.rser.2018.04.006.

Shaikh, P. H. *et al.* (2014) 'A review on optimized control systems for building energy and comfort management of smart sustainable buildings', *Renewable and Sustainable Energy Reviews*. Elsevier, 34, pp. 409–429. doi: 10.1016/j.rser.2014.03.027.

Sharifi, A. and Yamagata, Y. (2015) 'Roof ponds as passive heating and cooling systems: A systematic review', *Applied Energy*. Elsevier Ltd, 160(December), pp. 336–357. doi: 10.1016/j.apenergy.2015.09.061.

Shekar, V. and Krarti, M. (2017) 'Control strategies for dynamic insulation materials applied to commercial buildings', *Energy and Buildings*. Elsevier B.V., 154, pp. 305–320. doi: 10.1016/j.enbuild.2017.08.084.

Shian, S. and Clarke, D. R. (2016) 'Electrically tunable window device', *Optics Letters*, 41(6), p. 1289. doi: 10.1364/ol.41.001289.

Shokri Kuehni, S. M. S. *et al.* (2016) 'Roof cooling by direct evaporation from a porous layer', *Energy and Buildings*. Elsevier B.V., 127, pp. 521–528. doi: 10.1016/j.enbuild.2016.06.019.

Simfukwe, J. *et al.* (2017) 'Superporous Intelligent Hydrogels for Environmentally Adaptive Building Skins', *MRS Advances*, 357(May), pp. 1–8. doi: 10.1557/adv.201.

Simmler, H. and Brunner, S. (2005) 'Vacuum insulation panels for building application:

Basic properties, aging mechanisms and service life', *Energy and Buildings*, 37(11 SPEC. ISS.), pp. 1122–1131. doi: 10.1016/j.enbuild.2005.06.015.

Smith, S. I. and Lasch, C. (2016) 'Machine Learning Integration for Adaptive Building Envelopes: An Experimental Framework for Intelligent Adaptive Control', in *Proceedings of the 36th Annual Conference of the Association for Computer Aided Design in Architecture (ACADIA)*, pp. 98–105. doi: 10.52842/conf.acadia.2016.098.

Spanaki, A., Tsoutsos, T. and Kolokotsa, D. (2011) 'On the selection and design of the proper roof pond variant for passive cooling purposes', *Renewable and Sustainable Energy Reviews*. Elsevier Ltd, 15(8), pp. 3523–3533. doi: 10.1016/j.rser.2011.05.007.

Stadler, I. and Sterner, M. (2018) *Urban Energy Storage and Sector Coupling*. 2nd edn, *Urban Energy Transition*. 2nd edn. Elsevier Ltd. doi: 10.1016/b978-0-08-102074-6.00026-7.

Stec, W. J. and Paassen, a. H. C. V (2005) 'Symbiosis of the double skin facade with the HVAC system', *Energy and Buildings*, 37(5), pp. 461–469. doi: 10.1016/j.enbuild.2004.08.007.

Sun, L. *et al.* (2012) 'Stimulus-responsive shape memory materials: A review', *Materials and Design*. Elsevier Ltd, 33(1), pp. 577–640. doi: 10.1016/j.matdes.2011.04.065.

Sung, D. (2016) 'A New Look at Building Facades as Infrastructure', *Engineering*. THE AUTHORS, 2(1), pp. 63–68. doi: 10.1016/J.ENG.2016.01.008.

Sung, D. K. (2010) 'Skin Deep: Making Building Skins Breathe with Smart Thermo bimetals, Where Do You Stand', in *Proceedings of the 2011 ACSA National Conference*. Washington, DC: ACSA Press, pp. 145–152.

Tang, Y. *et al.* (2017) ‘Programmable Kiri-Kirigami Metamaterials’, *Advanced Materials*, 29(10), pp. 1–9. doi: 10.1002/adma.201604262.

Taveres-Cachat, E. *et al.* (2019) ‘Responsive building envelope concepts in zero emission neighborhoods and smart cities - A roadmap to implementation’, *Building and Environment*. Elsevier, 149(December 2018), pp. 446–457. doi: 10.1016/j.buildenv.2018.12.045.

Theodore L. Bergman, Frank P. Incropera, David P. DeWitt, A. S. L. (2011) *Fundamentals of heat and mass transfer*. Seventh Ed. John Wiley & Sons, Inc.

Thuot, K. W. and Andersen, M. (2011) ‘A Novel Louver System for Increasing Daylight Usage in Buildings’, in *Conference on Passive and Low Energy Architecture*. Louvain-la-Neuve, pp. 1–6.

Tomko, J. A. *et al.* (2018) ‘Tunable thermal transport and reversible thermal conductivity switching in topologically networked bio-inspired materials’, *Nature Nanotechnology*. Springer US, 13(10), pp. 959–964. doi: 10.1038/s41565-018-0227-7.

Trubiano, F. (2013) *Design and Construction of High-Performance Homes, Public Works*. Edited by F. Trubiano.

Valitabar, M. *et al.* (2018) ‘Design optimum responsive façade based on visual comfort and energy performance’, *CAADRIA 2018 - 23rd International Conference on Computer-Aided Architectural Design Research in Asia: Learning, Prototyping and Adapting*, 2, pp. 93–102.

Varga, S., Oliveira, A. C. and Afonso, C. F. (2002) ‘Characterisation of thermal diode panels for use in the cooling season in buildings’, *Energy and Buildings*, 34(3), pp. 227–

235. doi: 10.1016/S0378-7788(01)00090-1.

Velikov K, T. G. (2013) ‘Responsive Building Envelopes : Characteristics and Evolving Paradigms’, in *Design and Construction of High-Performance Homes*, pp. 75–92.

Villegas, J. E., Gutiérrez, J. and Colorado, H. (2020) ‘Active materials for adaptive building envelopes: a review’, *J. Mater. Environ. Sci*, 2020(6), pp. 988–1009. Available at: http://www.jmaterenvironsci.com.

Wan, K. K. W. *et al.* (2012) ‘Impact of climate change on building energy use in different climate zones and mitigation and adaptation implications’, *Applied Energy*. Elsevier Ltd, 97, pp. 274–282. doi: 10.1016/j.apenergy.2011.11.048.

Wang, J., Beltrán, L. O. and Kim, J. (2012) ‘From static to kinetic: A review of acclimated kinetic building envelopes’, *World Renewable Energy Forum, WREF 2012, Including World Renewable Energy Congress XII and Colorado Renewable Energy Society (CRES) Annual Conferen*, 5, pp. 4022–4029.

Wang, X., Chen, D. and Ren, Z. (2010) ‘Assessment of climate change impact on residential building heating and cooling energy requirement in Australia’, *Building and Environment*. Elsevier Ltd, 45(7), pp. 1663–1682. doi: 10.1016/j.buildenv.2010.01.022.

Wang, Z. and Hong, T. (2020) ‘Reinforcement learning for building controls: The opportunities and challenges’, *Applied Energy*. Elsevier, 269(May), p. 115036. doi: 10.1016/j.apenergy.2020.115036.

Wanphen, S. and Nagano, K. (2009) ‘Experimental study of the performance of porous materials to moderate the roof surface temperature by its evaporative cooling effect’, *Building and Environment*, 44(2), pp. 338–351. doi: 10.1016/j.buildenv.2008.03.012.

Wetter, M. (2011) ‘Co-simulation of building energy and control systems with the building controls virtual test bed’, *Journal of Building Performance Simulation*, 4(3), pp. 185–203. doi: 10.1080/19401493.2010.518631.

Wigginton, M. and Harris, J. (2002) *Intelligent Skins, Elsevier*.

Wu, Z. *et al.* (2014) ‘a Comparative Study on Thermal Conductivity and Rheology Properties of Alumina and Multi-Walled Carbon Nanotube Nanofluids’, *Frontiers in Heat and Mass Transfer*, 5(December). doi: 10.5098/hmt.5.18.

Xu, X. and Dessel, S. Van (2008) ‘Evaluation of an Active Building Envelope window-system’, *Building and Environment*, 43(11), pp. 1785–1791. doi: 10.1016/j.buildenv.2007.10.013.

Xu, X., Dessel, S. Van and Messac, A. (2007) ‘Study of the performance of thermoelectric modules for use in active building envelopes’, *Building and Environment*, 42(3), pp. 1489–1502. doi: 10.1016/j.buildenv.2005.12.021.

Yan Feng (2005) *A User’s Guide to Vacuum Technology [Book Review], IEEE Circuits and Devices Magazine*. doi: 10.1109/mcd.2005.1438817.

Yazdanian.Mehrangiz, and J. H. K. (1994) ‘Measurement of the exterior convective film coefficient for windows in low-rise buildings’, *ASHRAE Transactions*, 100(1), pp. 1087–1096.

Yoon, Y. R. and Moon, H. J. (2019) ‘Performance based thermal comfort control (PTCC) using deep reinforcement learning for space cooling’, *Energy and Buildings*. Elsevier B.V., 203. doi: 10.1016/j.enbuild.2019.109420.

Yu, Z. *et al.* (2011) ‘A systematic procedure to study the influence of occupant behavior

on building energy consumption', *Energy and Buildings*. Elsevier B.V., 43(6), pp. 1409–1417. doi: 10.1016/j.enbuild.2011.02.002.

Zawidzki, M. (2015) 'Dynamic shading of a building envelope based on rotating polarized film system controlled by one-dimensional cellular automata in regular tessellations (triangular, square and hexagonal)', *Advanced Engineering Informatics*. Elsevier Ltd, 29(1), pp. 87–100. doi: 10.1016/j.aei.2014.09.008.

Zhang, L. *et al.* (2018) 'Impact of post-rainfall evaporation from porous roof tiles on building cooling load in subtropical China', *Applied Thermal Engineering*. Elsevier, 142(July), pp. 391–400. doi: 10.1016/j.applthermaleng.2018.07.033.

Zheng, Z. and Wang, N. (2002) 'Model-free control based on neural networks', *Proceedings of 2002 International Conference on Machine Learning and Cybernetics*, 4(November), pp. 2180–2183. doi: 10.1109/icmlc.2002.1175425.

Zhou, H. and Brooks, A. L. (2019) 'Thermal and mechanical properties of structural lightweight concrete containing lightweight aggregates and fly-ash cenospheres', *Construction and Building Materials*. Elsevier Ltd, 198, pp. 512–526. doi: 10.1016/j.conbuildmat.2018.11.074.

Zhou, T. *et al.* (2017) 'Hydrophilic Sponges for Leaf-Inspired Continuous Pumping of Liquids', *Advanced Science*, 4(6). doi: 10.1002/advs.201700028.

Zohuri, B. (2011) *Heat Pipe Design and Technology, Heat Pipe Design and Technology*. doi: 10.1201/b10806.

APPENDIX

Nomenclature	
a	Action
A	Area [m^2]
$\mathcal{A}$	Action space
AIS	Active insulation system
AOF	Adaptive opaque façade
c_p	Specific heat [J/(kg·K)]
C	Heat capacity of node [J/K]
CV-RMSE	Coefficient of variation of the root mean square error
C	Advantage function
D_{KL}	Kullback-Leibler (KL) divergence
DIMs	Dynamic insulation materials
E	Heat from energy source [J]
F	View factor [—]
G	Return function
GA	Genetic algorithm
GEB	Grid interactive efficient building
h	Specific enthalpy [J/kg]
h_c	Surface heat transfer coefficient [m/s]
h_m	Surface mass transfer coefficient [m/s]
H	Heat transfer coefficient [W/K]
$\mathcal{H}$	Entropy loss
HVAC	Heating Ventilation and Air Conditioning
$I_s^{\downarrow}$	Solar radiation incident [W/m^2]
J	Diffusive mass flux [kg/m^2]
L	Loss function
Le	Lewis number [—]
LPD	Long-term Percentage of Dissatisfied [%]
m	Mass [kg]
M	Mini-batch size
MPC	Model-predictive control
n_{ly}	Parameter of ANN hidden layer node size
N	Number of steps/episodes/nodes/inputs/outputs
Net ZEB	Net-zero energy building
NMBE	Normalized mean bias error
p	Transition probability

PCM	Phase change material
PMV	Predicted mean vote [—]
PPD	Predicted percentage of dissatisfied [%]
q_{PCM}	Latent heat generated during phase change per unit mass [W/kg]
q_v	Heat rate [W/m^3]
q_w	latent heat per unit mass of water evaporation [W/kg]
Q	Heat transfer rate [W]
r	Reward
R/R_w	Thermal resistance [(K·m^2)/W]
RBE	Responsive building envelope
RH	Relative humidity
RSI	Thermal resistance with SI unit [(K·m^2)/W]
s	State
$\mathcal{S}$	State space
$SHGC$	Solar heat gain coefficient [—]
t	Time [s]
T	Temperature [°C]
TES	Thermal energy storage
TMY3	Typical meteorological year 3 weather data
T_h	Experience horizon
T_s	Sample time
u	Moisture content [kg/m^3]
U	Thermal transmittance [W/(m^2·K)]
v_{ex}	Air velocity [m/s]
V	Differential control volume or finite control volume [m^3]
V_L	Value function
W	Water mass [kg]
WWR	Window-to-wall ratio [—]
3R2C	Three resistors and two capacitors
Greek symbols	
α	Solar absorptance [—]
δ	Limit for D_{KL}
ε	Surface emissivity [—]
η	Weight for the components of the reward function [—]
θ	Parameter of actor
κ	Discount factor
λ	Heat conductivity [W/(m·K)]
π	Policy
ρ	Density [kg/m^3]
σ	Stephan-Boltzmann constant [W/(m^2·K^4)]

τ	Surface reflectance [—]
Γ	Trajectory
ϕ	Parameter of critic [—]
ω	Entropy loss weight
Subscripts and superscripts	
a	Air
air_in	Indoor air
abs	Thermodynamic temperature
air_ex	Outdoor air
b	Biomimetic mesoporous synthetic foam layer
c	Concrete
cl	Cooling
des	Desired value
dmd	Demand
env	Outdoor environment
f	Foliage layer
grd	Ground (long-wave radiation)
ht	Heating
high	Upper limit
inf	Infiltration
int	Internal gains
lat	Latent heat
low	Lower limit
lw	Long-wave radiation
max	minimum
min	maximum
off	Offline training horizon
sat	Saturated state
set	Set point
sky	Sky (long-wave radiation)
surf	Surface (wall, floor, or ceiling)
sup	Air conditioner supply air for space heating/cooling
sw	Short-wave radiation
sys	Air conditioning system
th	Threshold value
v	vapor
w	Wall layer
zone	Thermal zone air

VITA

Yawen He was born in China. She received her BS in Civil Engineering from Southeast University in 2014 and MEng in Architectural and Civil Engineering from Tongji University in 2017, respectively. She was enrolled as a graduate research assistant in 2018 for pursuing her Ph.D. and her study focuses on modeling, design, and control of energy-efficient and environmentally responsive building envelope systems. She will attain her Doctor of Philosophy in Civil Engineering in August 2023.